



universität  
wien

# DISSERTATION

Titel der Dissertation

Pore gating of potassium channels and its relevance for  
drug effects

verfasst von

Mag. pharm. Tobias Linder

angestrebter akademischer Grad

Doktor der Naturwissenschaften (Dr. rer. nat.)

Wien, 2014

Studienkennzahl lt. Studienblatt:

A 791 449

Dissertationsgebiet lt. Studienblatt:

Pharmazie

Betreut von:

Mag. Dr. Anna Weinzinger, Univ.-Prof. Mag. Dr. Gerhard Ecker



K<sup>+</sup> channels are involved in virtually all physiological processes and adopt critical roles in diverse events such as neuronal signaling, muscle contraction, cardiac action potential regulation, and hormone secretion. Thus, it is not surprising that malfunction of K<sup>+</sup> channels can have a wide-spread disruptive impact on the homeostasis of the human body. With severe diseases such as cardiac arrhythmias, diabetes, and cancer linked to K<sup>+</sup> channels, these membrane proteins are subject of extensive research to unravel their functional properties and develop future drugs. While the function of K<sup>+</sup> channels and their involvement in the ionic currents of cells are well studied by electrophysiological experiments, the atomistic details of transitions between conformations allowing and preventing ion flow, called gating, still lack important insights. Crystal structures of ion channels mark a major breakthrough in our understanding of channel architecture and have provided elementary information of the conformations that ion channels can adopt in different channel states. However, as ion channels are highly dynamical proteins, knowledge of the local and global conformational changes during gating on an atomistic level is of extraordinary interest. In particular, it was shown that a plethora of drugs targeting K<sup>+</sup> channels are crucially dependent on channel gating to develop their blocking potency emphasizing the importance of detailed knowledge of channel dynamics.

Comprehensive studies on three different K<sup>+</sup> channels, the prototypical bacterial K<sup>+</sup> channel KcsA, the bacterial inward rectifier K<sup>+</sup> channel KirBac1.1, and the human Kv channel hERG, were performed to shed light on the gating dynamics of K<sup>+</sup> channels and to identify channel specific structural rearrangements. Molecular dynamics simulations and two-electrode voltage clamp experiments revealed that aromatic amino acids adopt crucial roles in gating by unlocking channels from a specific state (F114 in KcsA), by forming the pore gate (F146 in KirBac1.1) and by shaping the drug binding site (Y652 and F656 in hERG). Specifically, studies on the hERG channel disclosed the important role of F656 for drug trapping which is characterized by the drug's retention in its binding site upon channel closure. While F656 is a key binding determinant of hERG blockers, it might also serve as physical barrier for drug dissociation. In case of KcsA and KirBac1.1, energy calculations allowed the investigation of the energy landscape of channel gating and correlations of structural rearrangements to energy changes. Gating studies on KirBac1.1 focused on the coupling between the transmembrane and the cytoplasmic domains and revealed that the communication between these two domains operates bidirectionally. Summarizing, this thesis provides novel insights into channel specific movements during pore gating. Although the three investigated channels share similar global gating rearrangements in terms of transmembrane domain movements, they exhibit uniquely fine-tuned local gating changes at the amino acid level.



Kaliumkanäle sind nahezu an allen physiologischen Prozessen beteiligt und nehmen eine Schlüsselrolle in zahlreichen Vorgängen, wie zum Beispiel bei der Signalweiterleitung in Nerven, bei Muskelkontraktionen, bei der Regulation des Aktionspotentials des Herzens, oder bei der Freisetzung von Hormonen, ein. Daher ist es nicht verwunderlich, dass Fehlfunktionen dieser Kanäle weitreichende Folgen auf die Homöostase des menschlichen Körpers haben können. Schwerwiegende Krankheiten wie zum Beispiel Herzrhythmusstörungen, Diabetes mellitus und Krebs stehen in Zusammenhang mit  $K^+$  Kanälen. Aus diesem Grund sind diese Membranproteine das Forschungsobjekt zahlreicher Studien um ihre Funktionsweise zu entschlüsseln und zukünftige Medikamente zu entwickeln. Während die Beteiligung von  $K^+$  Kanälen am Ionenfluss von Zellen mittels elektrophysiologischen Experimenten gründlich untersucht wurde, sind Einblicke in die Übergänge zwischen Kanalkonformationen, die Ionenfluss erlauben und verhindern, dem sogenannten „Gating“, auf atomarer Ebene nach wie vor verwehrt. Die Entschlüsselung der Kristallstrukturen von Ionenkanälen stellt einen entscheidenden Durchbruch in unserem Verständnis der Kanalarchitektur dar und hat elementare Informationen der Konformationen, die Ionenkanäle in unterschiedlichen Zuständen einnehmen können, geliefert. Da diese Kanäle aber hochdynamische Proteine sind, sind genaue Kenntnisse der lokalen und globalen Konformationsänderungen von entscheidender Bedeutung. Insbesondere wurde gezeigt, dass die Wirkung von zahlreichen Medikamenten, die an  $K^+$  Kanälen angreifen, vom Kanalzustand abhängt. Dieser Umstand zeigt die Wichtigkeit der detaillierten Untersuchung des dynamischen Verhaltens von diesen Kanälen weiter auf.

Die hierin durchgeführten Studien an drei unterschiedlichen Kanälen, dem prototypischen bakteriellen  $K^+$  Kanal KcsA, dem bakteriellen inwärts gerichteten  $K^+$  Kanal KirBac1.1 und an dem humanen, spannungsabhängigen  $K^+$  Kanal hERG, untersuchen die Gatingdynamik von  $K^+$  Kanälen und identifizieren kanalspezifische strukturelle Veränderungen während dieses Prozesses. Moleküldynamiksimulationen und two-electrode voltage clamp Experimente zeigten, dass aromatische Aminosäuren eine entscheidende Rolle im Kanal gating spielen, indem sie Kanäle aus einem bestimmten Zustand freigeben (F114 in KcsA), die Kanalpforte bilden (F146 in KirBac1.1) und die Bindungstasche von Wirkstoffen formen (Y652 und F656 in hERG). Speziell die Studien am hERG Kanal offenbarten die wichtige Funktion von F656 für das „drug trapping“ Phänomen, welches durch den Wirkstoffeinschluss in der Bindetasche während der Schließbewegung des Kanals charakterisiert ist. Neben der Rolle von F656 als einer der wichtigsten Bindungs determinanten von hERG blockierenden Wirkstoffen, könnte es auch als physikalische Barriere die Dissoziation von Wirkstoffen während des Schließens verhindern. In Studien an KcsA und KirBac1.1 ermöglichten Energieberechnungen die Untersuchung der Energieprofile von Kanal gating und die Korrelation von Konformationsänderungen mit Energieänderungen. Gatinguntersuchungen

## Zusammenfassung

an KirBac1.1 zeigten, dass die Bewegungen des transmembranären und der intrazellulären Domäne aneinander gekoppelt sind und die Kommunikation zwischen den beiden Domänen von bidirektionaler Natur ist. Diese Dissertation verschafft neuartige Einsichten in die Kanalspezifischen Bewegungen während des Gatings. Obwohl die drei untersuchten Kanäle ähnliche globale Gatingbewegungen der transmembranären Domänen aufweisen, sind deren lokale Bewegungen der Aminosäuren von präzise abgestimmter und hoch spezifischer Art.

First and foremost, I would like to express my sincerest gratitude to my supervisor Dr. Anna Weinzinger for all her support, encouragement and advice during my thesis. Her dedication to science and her deep motivation to reveal and understand protein dynamics was not only a great driving force for the realization of this thesis but was also very inspiring and incentive. She always took the time for fruitful discussions which I usually left full of new ideas and eager to try them out. In her group, she provided an atmosphere of communication and discussion in whose science feels vitally alive.

I would like to thank Univ.-Prof. Gerhard Ecker and Univ.-Prof. Steffen Hering for providing the financial basis of my thesis which allowed me to completely focus on my scientific work. Additionally, their expertise in computational ligand-based approaches and electrophysiology recordings helped to pursue interdisciplinary approaches in several projects.

I thank my colleagues Song Ke and Eva-Maria Zangerl for the great atmosphere in our office where we shared a lot of good laughs, extraordinarily good cakes, and had many stimulating discussions about our scientific work and life in general. The mutual support was essential to believe in the guiding principle of every thesis: "Hang in there!" I thank all my colleagues of the Department of Pharmacology and Toxicology and of the Doctoral program MolTag for many unforgettable nights and enjoyable retreats and conferences.

I am very grateful for a research stay at Bert de Groot's group at the Max Planck Institute for Biophysical Chemistry in Göttingen where I was able to acquire in-depth knowledge of energy calculation methods of protein systems. Especially, I thank David Köpfer for introducing me to scientific programming which was a great help in analyzing complex simulation data. Additionally, their expertise in cluster computing specialized for MD simulations and their generosity in sharing their knowledge, special thanks to Martin Fechner, helped me to establish a high performance computer in our lab.

I would also like to thank Michael Sanguinetti at the University of Utah for the opportunity to join his group for two months to acquire extensive knowledge of the hERG channel physiology and electrophysiological recordings. It was a marvelous pleasure to discuss scientific questions from his biophysical and my structural way of thinking. It was very impressive and inspiring to work in his lab.

I want to thank my family for their support. Especially Christoph und Sarina for innumerable hilarious weekends in Vienna which helped to clear one's mind.

Most of all, I want to thank my wife Nadine for all her love and support during my thesis. Her advice in every situation in life and her belief in me was key to pursue my goals and accomplish three years of intensive scientific research.



1	Introduction .....	1
1.1	Ion channels .....	1
1.2	K <sup>+</sup> channels .....	1
1.2.1	General structure of K <sup>+</sup> channels .....	4
1.2.2	Pore gating of K <sup>+</sup> channels .....	6
1.3	hERG channels.....	7
1.3.1	Physiological and pathophysiological role.....	7
1.3.2	Gating of hERG channels .....	9
1.3.3	Structure of hERG channels .....	11
1.3.4	Drug block of hERG channels.....	14
1.3.5	Drug trapping.....	16
1.4	Kir channels.....	16
1.4.1	Physiological and pathophysiological role.....	17
1.4.1.1	Classical Kir channels (Kir2.x).....	18
1.4.1.2	G-protein-gated Kir channels (K <sub>G</sub> or Kir3.x).....	19
1.4.1.3	ATP-sensitive K <sup>+</sup> channel (K <sub>ATP</sub> or Kir6.x).....	20
1.4.1.4	K <sup>+</sup> -transport channels (Kir1.1, Kir4.x, Kir5.1, and Kir7.1).....	22
1.4.2	Structural basis of Kir channel gating.....	24
1.4.2.1	Prokaryotic vs. eukaryotic Kir channel gating .....	27
2	Methods.....	29
2.1	MD simulations .....	29
2.1.1	Principal components analysis and essential dynamics simulations .....	31
2.1.2	Umbrella sampling .....	32
2.2	Two-electrode voltage clamp .....	32
3	Motivation .....	35
4	Results .....	37
4.1	Probing the energy landscape of activation gating of the bacterial potassium channel KcsA.....	37

## Table of Contents

4.2	Molecular dynamics simulations of KirBac1.1 mutants reveal global gating changes of Kir channels.....	49
4.3	Structural insights into trapping and dissociation of small molecules in K <sup>+</sup> channels .....	72
4.4	Drug trapping in hERG channels – an experimental approach.....	107
5	Discussion .....	115
6	References .....	121
7	Curriculum Vitae .....	150

ACh	acetylcholine
CBND	cyclic-nucleotide-binding domain
CCD	cortical collecting duct
CHO	Chinese hamster ovary
CHI	congenital hyperinsulinism
CTD	cytoplasmic domain
DCT	distal convoluted tubule
DTT	dithiothreitol
ECG	electrocardiogram
$E_K$	equilibrium potential of $K^+$
ED	essential dynamics
GPCR	G protein-coupled receptor
HBC	helix bundle crossing
hERG	human ether-a-go-go related gene
Kir	inwardly rectifying $K^+$
KirBac	bacterial Kir
Kv	voltage-gated $K^+$
MD	molecular dynamics
NBD	nucleotide binding domain
ND	neonatal diabetes
NDP	nucleoside diphosphate
NKCC	$Na^+-K^+-2Cl^-$ cotransporter
PIP2	phosphatidylinositol-4,5-bisphosphate
SF	selectivity filter
SU	subunit
SVD	snowflake vitreoretinal degeneration
SUR	sulfonylurea receptor
TAL	thick ascending limb of the loop of Henle
TBA	tetrabutylammonium
tbHO <sub>2</sub>	tert-butyl hydroperoxid
TdP	Torsade de pointes
TEVC	two-electrode voltage clamp
TLC	thin layer chromatography
TM	transmembrane
VSD	voltage sensor domain
PAS	Per-Arnt-Sim
PCA	principle component analysis

## Abbreviations

P-helix	pore helix
WHAM	weighted histogram analysis method
WT	wild type

# 1 Introduction

## 1.1 Ion channels

Throughout the biological kingdom, cells are separated from their environment by lipid membranes. While the barrier function of membranes is essential to maintain homeostasis and the structure of cells, it also prevents substrate exchange with the environment.<sup>1</sup> Especially ion exchange between the intracellular and extracellular side and vice versa is crucial to allow communication between cells and initiate intracellular signaling pathways. This task is mediated by membrane embedded proteins, the ion channels. While this general concept appears to be fairly simple, their regulation by specific triggers, their diverse response, and their selectivity for different ions render ion channels powerful and high specific signaling proteins present in virtually all living cells. They are involved in signal transduction in the nervous system, control hormone and neurotransmitter release, and regulate the cardiac action potential and muscle contraction.

The two aspects of ion channels, gating by specific triggers and ion selectivity, are used to classify ion channels. Ion channels are divided into voltage-gated<sup>2</sup> and ligand-gated<sup>3-5</sup> ion channels as well as into channels with completely different structural properties like aquaporins. According to the permeating ion, ion channels are grouped into sodium, calcium, potassium, non-selective cation, chloride and other anion channels.<sup>6-8</sup> A comprehensive overview of ion channel groups was recently published by Alexander et al.<sup>9</sup>

## 1.2 K<sup>+</sup> channels

With more than 70 different genes encoding K<sup>+</sup> channels in the human genome, K<sup>+</sup> channels are the largest and most diverse group of ion channels.<sup>8</sup> Among this group, the voltage-gated K<sup>+</sup> (Kv) channels comprise the largest family.<sup>10</sup> Kv channels play a crucial role in electrically excitable cells such as neurons and myocytes by responding to the transmembrane voltage. They set the resting membrane potential, repolarize the cells during the falling phase of the action potential and thereby facilitate the termination of action potentials.<sup>11</sup> It is their role in the cardiac action potential that has attracted the attention of a whole scientific community focusing on a unique Kv channel which is extensively studied in this thesis and described in more detail in chapter 1.3 (page 7). In electrically unexcitable cells such as lymphocytes, Kv channels control the resting potential and prevent cells from depolarization.<sup>12</sup> In addition, Kv channels are involved in the transepithelial K<sup>+</sup> transport in several tissues such as the kidney<sup>13</sup> and the auditory cochlea.<sup>14</sup>

Inwardly rectifying K<sup>+</sup> (Kir) channels also contribute to the resting membrane potential and the transepithelial K<sup>+</sup> transport.<sup>13</sup> Kir channels play an essential role in the insulin secretion of pancreatic beta cells.<sup>15,16</sup> These channels were termed inwardly rectifying because of their ability to conduct K<sup>+</sup> ions inward more readily than outward. Although Kir channels are not gated by the transmembrane voltage, the membrane potential still contributes to their function. At depolarizing potentials, these channels are blocked by intracellular Mg<sup>2+</sup> and polyamines, thereby impeding outward K<sup>+</sup> flow. Kir channels are regulated by many different cellular factors such as ATP, intracellular pH, and lipids.<sup>17-19</sup>

Beside these two K<sup>+</sup> channel families, channels that are activated by Ca<sup>2+</sup>, Na<sup>+</sup>, or Cl<sup>-</sup> (K<sub>Ca</sub>),<sup>20</sup> modulated by cyclic nucleotides (CNG and HCN),<sup>4,21,22</sup> or formed by two pores (K<sub>2P</sub>)<sup>23,24</sup> can conduct K<sup>+</sup> ions, but are not subject of this thesis and therefore will not be discussed further. A phylogenetic tree, shown in Figure 1, illustrates the relations of K<sup>+</sup> conducting channels based on the amino acid sequence of the channel pores.

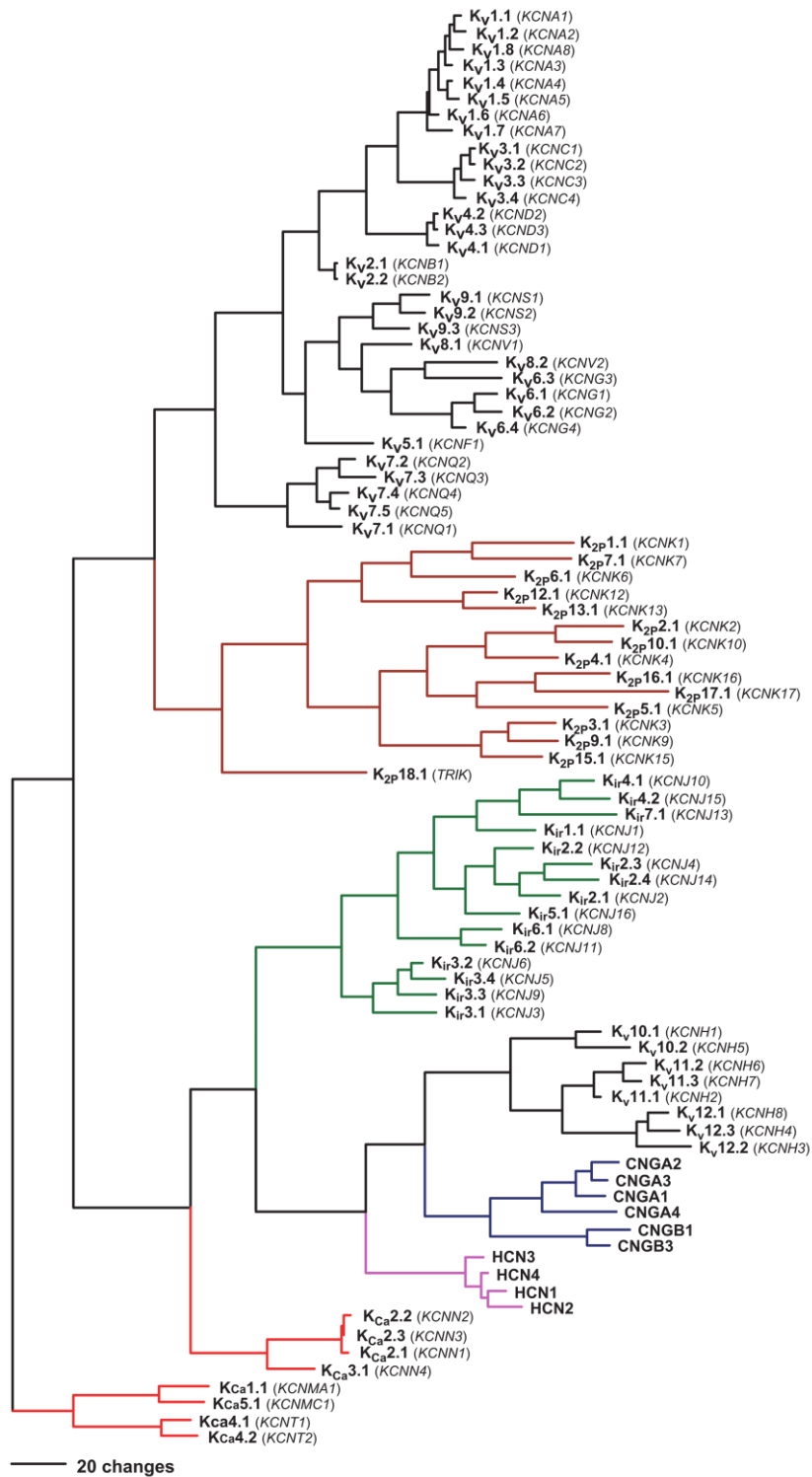


**Figure 1. Phylogenetic relation of K<sup>+</sup> channels.** The consensus tree was inferred by analyzing the amino acid sequence of the pore domains. The horizontal scale bar corresponds to the number of amino acid changes needed to explain differences in the protein sequence. The vertical branch length is not exact. Modified from Yu et al.<sup>10</sup>

### 1.2.1 General structure of K<sup>+</sup> channels

K<sup>+</sup> channels are composed of four homologous subunits (SU) that assemble to form a central ion conducting pore. Each SU consists of transmembrane (TM)  $\alpha$  helices whose number varies among K<sup>+</sup> channel families. While Kv channels possess six consecutively numbered TM segments per SU, Kir channels comprise of two TM helices, termed TM1 and TM2. These two helices are analogous in structure and function to the last two TM helices of Kv channels, called S5 and S6. Helices one to four in Kv channels form the voltage sensor domain (VSD). Intracellular and extracellular domains complete the whole channel structure (Figure 2A and B).

In the absence of three dimensional information based on X-ray crystallography until the late 90s, scientists were able to derive a schematic yet remarkably accurate structural understanding of ion channels from electrophysiology studies. It was the groundbreaking work of Hodgkin and Huxley,<sup>25</sup> Armstrong,<sup>26,27</sup> and Hille<sup>11,28</sup> that provided first insights into the ion channel structure. Hille published a schematic representation in 1978 highlighting the key parts of an ion channel (Figure 2C).<sup>28</sup> On the extracellular side, the channel pore possesses a narrow site, the selectivity filter (SF), that is responsible for ion selectivity. On the intracellular site, a constriction site, the pore gate, is present which can open and close in response to specific triggers. In case of Kv channels, changes in the membrane potential are sensed by the VSD which control the gate.

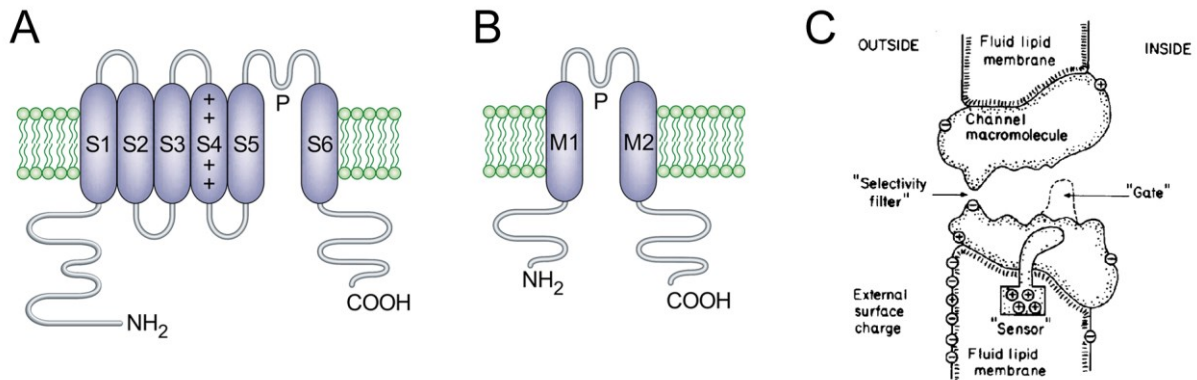


**Figure 2. Topology of K<sup>+</sup> channel SUs.** A) Topology of an individual Kv channel SU. B) Topology of a Kir channel SU. C) Schematic figure of an ion channel originally published by Hille.<sup>28</sup> Channel topology representations were modified from Goldstein et al.<sup>29</sup>

However, essential questions could not be answered by the above cited studies. First, how can K<sup>+</sup> channels discriminate with almost perfect fidelity between K<sup>+</sup> and Na<sup>+</sup> ions which exhibit almost the same size (K<sup>+</sup> is 10,000 times more permeant than Na<sup>+</sup><sup>30</sup>). Second, how can K<sup>+</sup> channels be so highly selective and at the same time display throughput rates of up to 10<sup>8</sup> ions per second,<sup>11</sup> which is close to the diffusion limit? The first crystal structure of a K<sup>+</sup>

channel by the MacKinnon lab in 1998 provided detailed structural answers to these issues.<sup>31</sup> Roderick MacKinnon was later awarded the 2003 Nobel Prize in Chemistry for his groundbreaking “structural and mechanistic studies of ion channels”.<sup>32</sup> By making use of a homotetrameric bacterial  $K^+$  channel from *Streptomyces lividans* (KcsA), they revealed that  $K^+$  channels exhibit an “inverted teepee” arrangement of the TM1 (outer helix) and TM2 (inner helix) helices which are settled around a central water filled pore, called the cavity. The four TM2 helices line the inner pore and are crossed at the intracellular side forming the closed pore gate (Figure 3A and B). On the extracellular side, the descending pore helices (P-helix) and the ascending SF are located. While the P-helix plays an important role in forming intersubunit contacts and stabilizing the SF in a conductive conformation, the SF is responsible for ion discrimination and conductance. The SF in  $K^+$  channels exhibits a common amino acid sequence of T-X-G-Y/F-G (X is any hydrophobic residue). A subsequent study has shown that the carbonyl oxygen atoms of the SF backbone form highly specific binding sites for  $K^+$  ions, termed S0-S4 (Figure 3C).<sup>33</sup> The interactions between the  $K^+$  ion and the SF backbone can compensate the energy penalty of dehydrating ions as  $K^+$  enters the SF, thus allowing high ion flux rates. This energy compensation varies among different ions species and is relative to the energy of dehydration resulting in an energy-driven selectivity.<sup>34</sup> Further crystal structures revealed that the SF binding sites are occupied by alternating  $K^+$  ions and water molecules.<sup>35</sup>  $K^+$  ions reside in the specific configurations S1-S3 or S2-S4 and transitions between these two configurations lead to  $K^+$  flux.<sup>36,37</sup>

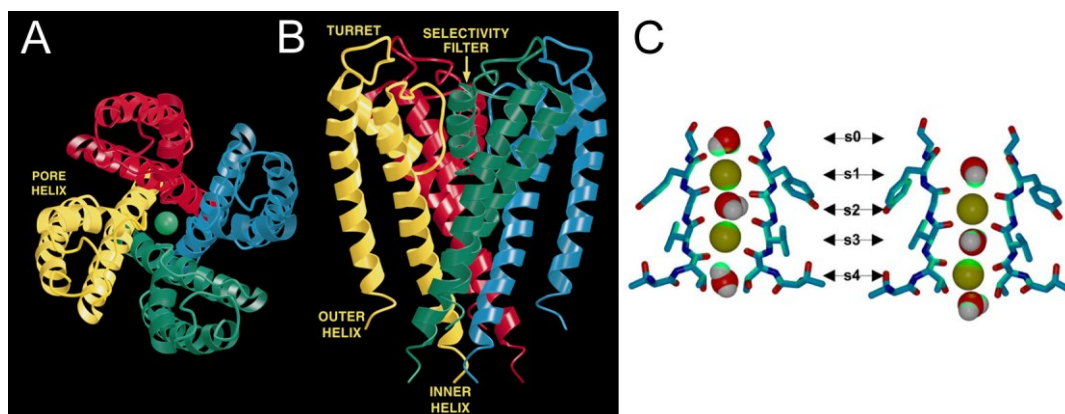


**Figure 3. Crystal structure of KcsA.** Original figures from Doyle et al.<sup>31</sup> showing the homotetrameric KcsA in top (A) and side view (B). The four SUs are represented by different colors. The green sphere illustrates an ion in the SF. C) Two distinct ion configurations S1-S3 (left) and S2-S4 (right). The SF backbone is shown as sticks. The ions and water molecules are shown as green and red spheres, respectively. Modified from Treptow and Tarek.<sup>37</sup>

### 1.2.2 Pore gating of K<sup>+</sup> channels

The functional behavior of K<sup>+</sup> channels is defined by two coupled mechanisms: activation and inactivation gating. Activation is associated with a large motion of the inner TM2 helices as observed in several activated, open state crystal structures of K<sup>+</sup> channels (e.g. KcsA,<sup>38</sup> MthK,<sup>39</sup> KvAP,<sup>40</sup> Kv1.2,<sup>41</sup> and KirBac3.1<sup>42</sup>) and characterized spectroscopically in KcsA.<sup>43–46</sup> In the open state, the inner TM2 helices are splayed apart leading to a sufficient gate opening to allow ion passage (Figure 4A). Dependent on the K<sup>+</sup> channel species, this splaying is caused by bending of the TM2 helices at either a glycine hinge or a Pro-X-Pro motif. The importance of this glycine hinge or the Pro-X-Pro motif for specific ion channels was demonstrated by mutational studies which led to drastically altered gating properties.<sup>47–50</sup>

Inactivation, more specifically C-type inactivation, originates from conformational changes in the SF and is highly modulated by permeant ions.<sup>51–53</sup> Accordingly, crystal structures of KcsA in high and low K<sup>+</sup> concentrations identified rotameric changes of the SF backbone which lead to the constriction of the permeation pathway and is thought to represent the inactivated SF state (Figure 4B).<sup>33</sup> As the SF sequence is conserved among K<sup>+</sup> channels and the KcsA pore can substitute for the pore of other K<sup>+</sup> channels, it is believed that the inactivation mechanism is conserved in all K<sup>+</sup> channels.<sup>54</sup> Recent structures by Cuello et al. with an open gate and an inactivated SF revealed coupling between inactivation and pore gating.<sup>38,55</sup> The presence of two functional mechanisms and crystal structures in each state<sup>33,38</sup> have led to the description of a four state model (Figure 4C). In this model, the pore gate is either open or closed and the SF is either conductive or inactivated.

Beside these general gating properties which are valid for most of the K<sup>+</sup> channels, each channel species exhibits its unique gating features. These specificities will be described in more detail in the corresponding chapters of the herein studied K<sup>+</sup> channels.

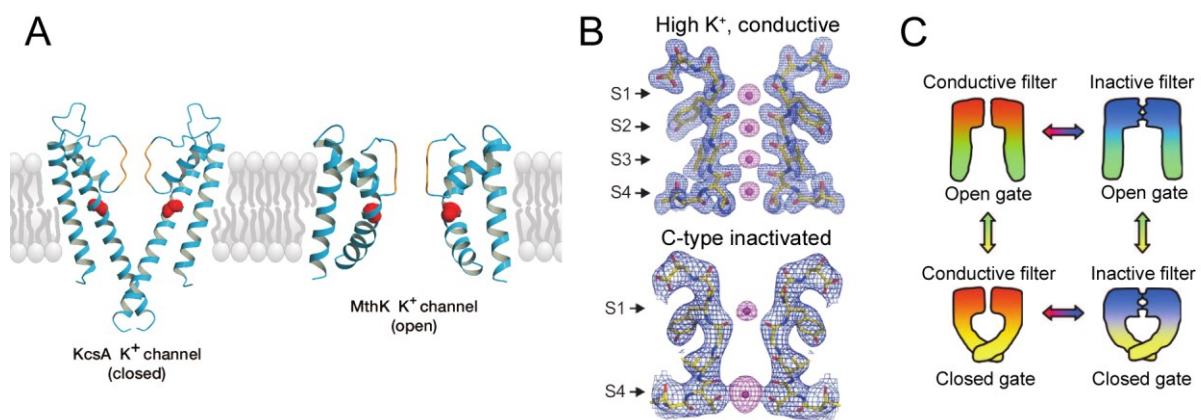


**Figure 4. Gating of K<sup>+</sup> channels.** A) Closed (KcsA) and open (MthK) conformations of K<sup>+</sup> channels. For clarity, only the two opposing SUs are shown. The glycine hinge is marked by red spheres. The

SF is colored orange. Figure from Yu et al.<sup>10</sup> B) Top: Electron density map of the conductive SF crystallized in high  $K^+$  concentration. Bottom: The electron density map of an inactivated SF. Electron density of  $K^+$  ions is shown as a magenta grid sphere. The two opposing SUs are shown. Figure from Cuello et al.<sup>38</sup> C) Depiction of the four functional states in  $K^+$  channels. Figure from Ostmeyer et al.<sup>56</sup>

### 1.3 hERG channels

The human ether-a-go-go related gene (hERG, *KCNH2*)<sup>57</sup> encodes the pore forming domain of a delayed rectifier Kv channel which is termed hERG channel or Kv11.1 channel. The important role of the hERG channel became evident when inherited mutations in *KCNH2* were found to cause a dramatic prolongation in the cardiac action potential which is termed long QT syndrome (LQTS).<sup>58</sup> Beside *KCNH2* mutations, a plethora of structurally diverse cardiac and noncardiac drugs can induce LQTS by either directly blocking the hERG channel<sup>59,60</sup> or disrupting channel trafficking to the surface.<sup>61–63</sup> LQTS predisposes individuals to arrhythmia and can result in sudden death.<sup>64–66</sup> Due to this severe potential side effect of drugs, several medications were withdrawn from the market or their use was heavily restricted.<sup>67–69</sup> Thus, great effort is directed toward a better understanding of the functionality of the hERG channel and its interaction with drugs.

#### 1.3.1 Physiological and pathophysiological role

hERG channels are expressed in a wide range of tissues, including specific brain regions,<sup>70</sup> smooth muscle cells of the gastrointestinal and genitourinary tracts,<sup>71–73</sup> and pancreatic beta cells.<sup>74</sup> However, the highest expression levels of hERG occur in the heart and this is where the function of hERG channels is best understood.

The action potential of ventricular myocytes derives its shape from a sophisticated chronology of ionic current through channels of various species (Figure 5A). Activation of the  $Na^+$  channel Nav1.5 leads to an inward  $Na^+$  current ( $I_{Na}$ ) triggering a rapid depolarization of membrane. Repolarization is much slower and can be divided into three phases. In phase 1, a transient  $K^+$  outward current ( $I_{to}$ ) causes a short and partial repolarization. The subsequent slower repolarization phase is called the plateau during which an inward  $Ca^{2+}$  current occurs. The duration of the plateau is caused by delayed rectifier  $K^+$  channels which activate slowly and/or carry low  $K^+$  currents during this phase. It was the seminal work of Noble and Tsien<sup>75,76</sup> as well as Sanguinetti and Jurkiewicz<sup>77</sup> that showed that two different  $K^+$  currents ( $I_{Kr}$  and  $I_{Ks}$ ) of two distinct channels define the length of the plateau phase (see Nattel<sup>78</sup> for a review). This prolonged repolarization phase is crucial to allow sufficient  $Ca^{2+}$  entry into the

myocyte for an optimal cardiac contraction. Termination of the action potential (phase 3) is mainly caused by the rapid delayed rectifier  $K^+$  current ( $I_{Kr}$ ) conducted by hERG channels.<sup>79–81</sup> Therefore, it is the proper function of the hERG channels that defines the length of an action potential. Not surprisingly, altered hERG channel function can have drastic effects on the cardiac action potential.

The most prominent disorder induced by the hERG channel is LQTS. In LQTS, partial or complete loss of hERG channel function, either caused by mutations in *KCNH2* or channel block by drugs, reduces the  $I_{Kr}$  thereby leading to a prolonged action potential (Figure 5B top). This prolongation is seen in a body surface electrocardiogram (ECG) by measuring the QT interval which represents the time between depolarization (QRS) and repolarization (T wave) of the ventricles (Figure 5B bottom). This observation of the prolonged QT interval led to the name of LQTS and was first described in an ECG by Anton Jervell and Fred Lange-Nielsen in 1957.<sup>82</sup> The delayed repolarization of the ventricles greatly increases the risk of life-threatening cardiac arrhythmia which occurs in a unique form called “torsade de pointes” (TdP).<sup>83,84</sup> TdP is characterized by ECG traces that twist around the isoelectric line (Figure 5C). TdP can either return to a normal heart rhythm or result in lethal ventricular fibrillation.

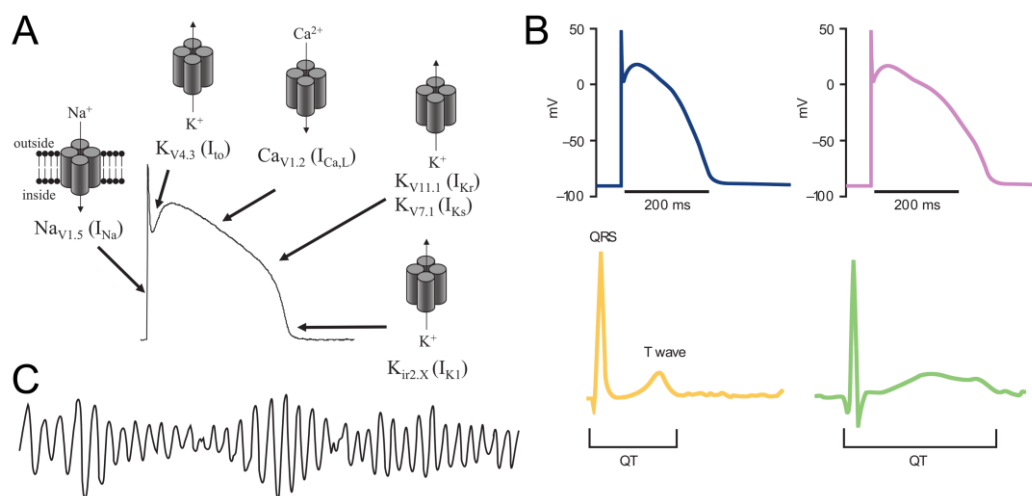


**Figure 5. Action potential of the heart.** A) Different ion channels are activated in distinct action potential phases. Figure from Pollard et al.<sup>85</sup> B) top: Normal (blue) and prolonged (pink, reduced hERG current by 80%) action potential of a ventricular myocyte. Bottom: Normal (yellow) and pathological ECG trace with a prolonged QT interval (green). C) ECG trace of a TdP arrhythmia. B and C were modified from Sanguinetti et al.<sup>86</sup>

While the first description of LQTS was accompanied by deafness and, as found out later,<sup>87</sup> caused by mutations in the  $I_{Ks}$  carrying channel Kv7.1, another LQTS was identified in families by Romano<sup>88</sup> and Ward<sup>89</sup> in the 60s without any hearing deficit. This form of LQTS is considerably more common and was linked to mutations in the hERG  $K^+$  channel encoding

gene *KCNH2*, beside other gene mutations.<sup>58,86</sup> More than 290 LQTS-associated mutations in *KCNH2* were described (<http://www.fsm.it/cardmoc/>). Most of the hERG mutations result either in premature termination of *KCNH2* transcription or misfolding of the SUs and disruption of trafficking of hERG channels to the cell surface.<sup>90–92</sup> Misfolded proteins are retained in the endoplasmic reticulum and are degraded by the ubiquitin-proteasome pathway.<sup>93</sup> Additionally, mutations can affect the gating properties of hERG K<sup>+</sup> channels (described in chapter 1.3.2, page 9) leading to a reduced or complete loss of I<sub>Kr</sub>.

In 2004, mutations in *KCNH2* were identified<sup>94</sup> that lead to a shortened QT interval which is a characteristic of the short QT syndrome (SQTS).<sup>95,96</sup> These mutations express the hERG channel mutant N588K which exhibits reduced inactivation and thus greater current during the plateau phase of the cardiac action potential. Due to the shorter repolarization phase, cardiac myocytes are more prone to premature excitation resulting in ventricular fibrillation and potentially in sudden cardiac death. The fact that both increase and decrease of channel function can cause lethal arrhythmia underlines the importance of a precisely balanced channel expression for normal cardiac activity.

In recent years, there is accumulating evidence that the hERG channel plays a role in cancer.<sup>97</sup> Differential expression patterns of hERG were found in numerous cancer cell lines including neuronal,<sup>98,99</sup> leukemic,<sup>98,100</sup> lung,<sup>98,101</sup> colorectal,<sup>102</sup> and breast tissue.<sup>103,104</sup> A functional effect of hERG channels in cancer was first demonstrated by Smith et al.<sup>100</sup> showing that block of hERG channels reduces the rate of cell proliferation. Additionally, hERG channels are involved in tumor cell migration<sup>102</sup> and adhesion-dependent signaling.<sup>105</sup> These findings indicate that hERG channel might serve as a possible target for anticancer drugs. However, given the cardiac side effects of hERG channel blockers, there are strong drawbacks in the use of such drugs. Comprehensive reviews of hERG induced diseases, so called channelopathies, were published recently.<sup>106,107</sup>

### **1.3.2 Gating of hERG channels**

The unusual gating properties render the hERG channel essential for the delayed K<sup>+</sup> current in cardiac repolarization. hERG channels exist in closed, open, or inactivated conformation. As other Kv channels, they exhibit a VSD domain with positively charged lysine and arginine residues located in the S4 helix which sense the membrane potential (Figure 2, page 3). Upon depolarization of the cell membrane, the S4 helix perform an upward movement (see next chapter) and triggers opening of the pore gate via electromechanical coupling.<sup>108</sup> This S4 movement was shown to happen relatively slowly<sup>109,110</sup> and accounts for the slow activation kinetics of the hERG channel.<sup>111</sup> After

depolarization, activated hERG channels immediately inactivate which happens about 100 times faster than activation (Figure 6). Due to this fast inactivation transition, the  $K^+$  current occurring at depolarized potentials is very limited, leading to the prolonged plateau of the action potential (Figure 6B and C).<sup>112–114</sup> As repolarization begins at the end of the plateau phase, hERG channels recover rapidly and deactivate slowly resulting in the typical “hooked” tail currents (Figure 6B).<sup>115</sup> This  $K^+$  current passed through the hERG channel is responsible for the phase 3 repolarization of the cardiac action potential. Due to the slow closing kinetics, hERG channels remain open for considerable time after reaching the resting membrane potential. Since the resting potential is close to the  $K^+$  reversal potential, there is limited current passed through hERG channels. However, the open hERG channels render the cardiac muscle refractory to premature excitation. If a premature beat occurs shortly after repolarization, depolarization of the myocyte will be antagonized by a large increase in hERG current and thereby prevent re-entrant arrhythmia (Figure 6C).<sup>116</sup> Consequently, reduced hERG channel function caused by mutations renders affected individuals more vulnerable to arrhythmias initiated by premature beats (see previous chapter).

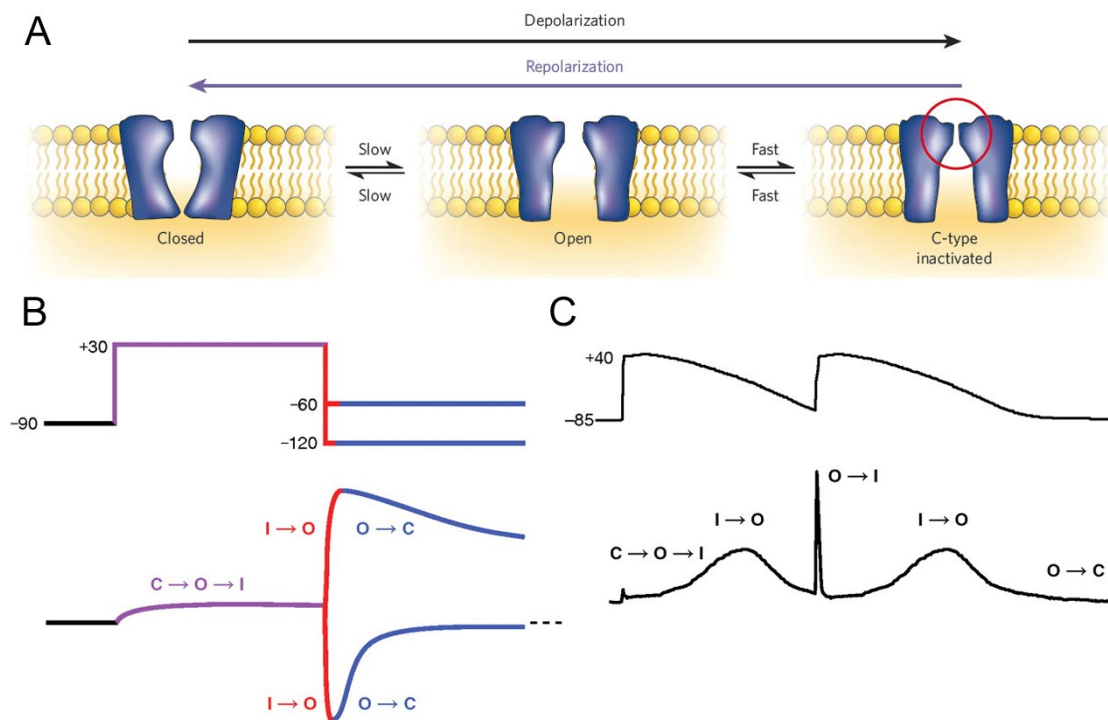


**Figure 6. Gating of hERG channels.** A) Schematic representation of state transition during de- and repolarization. C-type inactivation is caused by SF constriction (red circle). Figure from Sanguinetti et al.<sup>86</sup> B) Current traces during a two-step voltage protocol shown on top. At a depolarization step to 30 mV, channels are activated and rapidly inactivated (magenta). Subsequent repolarization to -60 mV (above  $K^+$  reversal potential, outward current) or -120 mV (below  $K^+$  reversal potential, inward current) leads to recovery from the inactivated state (red). Fast recovery and slow deactivation result in the typical “hooked” tail current (blue). C) hERG channel currents recorded in CHO cells in response to an

action potential waveform. During repolarization of the first action potential waveform, hERG current increases due to recovery from inactivation. Subsequent current decrease is caused by the reduction of electrochemical driving force for  $K^+$  outward current; however, hERG channels remain open. Premature depolarization results in a large current through open hERG channels before they rapidly inactivate. Figure from Vandenberg et al.<sup>107</sup>

### 1.3.3 Structure of hERG channels

As mentioned before, hERG channels consist of four SUs that coassemble to form an ion permeating pore. While it was initially thought that hERG channels comprise only of the hERG 1a isoform and form a homotetrameric channel,<sup>117</sup> it was shown that the native hERG current in cardiac tissue is conducted by a heterotetramer with the hERG 1b isoform, which lacks the N-terminal part.<sup>118,119</sup> Independent of the isoform, each SU comprises 6 TM spanning helices which are consecutively numbered S1 to S6 and are separated into two functionally distinct domains (Figure 7A). TM helices S1 to S4 form the VSD with positive charges on S4 that respond to changes in the membrane potential. How these S4 movements occur has been hotly debated over the last decades.<sup>120,121</sup> Most probable, the S4 moves up and down in a helical screw motion<sup>122</sup> in a groove formed by the S1 to S3 helices. It was the seminal work of Jensen et al.<sup>123</sup> that confirmed a helical screw motion in a Kv channel and provided atomistic insights by employing long time scale molecular dynamics (MD) simulations of up to 350  $\mu$ s. However, in case of hERG, the S4 appears to be loosely packed in the VSD as mutations of the charged residues to the bulky, hydrophobic amino acid Trp are well tolerated.<sup>124</sup> Nevertheless, salt bridge formation between the positive charges of S4 and negatively charged amino acids of S1 to S3 appears to be important for stabilization of the VSD in different channel states.<sup>125</sup> VSD movement is transmitted to the pore domain, which is formed by the S5 and S6 helices, via interactions of the S4-S5 linker with the cytoplasmic ends of the S6 helices.<sup>108,126,127</sup> It was shown that this S4-S5 linker is an amphipathic  $\alpha$  helix and contributes to the slow deactivation kinetics of hERG.<sup>128,129</sup> The S6 helices form a water filled cavity and, depending on the straight or bended conformation, define if the gate is closed or open. In contrast to other Kv channels,<sup>47–50</sup> glycine hinges in hERG do not appear to be a prerequisite for channel opening.<sup>130</sup> The cavity of hERG is shaped by the S6 conformation and the orientation of cavity facing amino acids in S6 and the bottom of the SF. Especially, the two aromatic amino acids, Y652 and F656, located on S6 can have dramatic effects on the cavity shape and thereby alter the drug binding orientation in the cavity as we were able to show in a recent study.<sup>131</sup> Y652 and F656 and their conformational changes upon gating are subject of a comprehensive study of this thesis (see chapter 4.3, page 72).

In the hERG channel, the SF is formed by the S624-V625-G626-F627-G628 sequence and it is this region where inactivation basically occurs. This fact was demonstrated by several mutational studies. Smith et al. showed that the double mutant S631C-G628C completely lacks inactivation.<sup>113</sup> The important role of S631 was further emphasized by Schönherr et al. showing that replacement with an alanine also abolishes inactivation.<sup>114</sup> A subsequent study, however, revealed that this is not completely true; instead, S631A shifts the inactivation by +102 mV.<sup>132</sup> Interestingly, this alanine is equivalent to the residue in the non-inactivating Kv10.1. In a subsequent study by Herzberg et al.,<sup>133</sup> introduction of the P-helix and SF from hERG into the Kv10.1 resulted in an inactivating Kv10.1 channel underlining the essential role of these two regions for inactivation. As already pointed out by them and also shown by Ficker et al.,<sup>134</sup> the point mutation of S620 on the P-helix of hERG to the corresponding threonine in Kv10.1 was sufficient to eliminate inactivation. Molecular insights into the role of these inactivation eliminating mutations were provided by Stansfeld et al. using a homology model of the hERG channel.<sup>135</sup> S620T and S631C-G628C stabilized the carbonyl oxygen of Y627 in the S0 ion binding site forming orientation (see chapter 1.2.1, page 4) while in wild type (WT) simulations regular flips were observed which disrupted the S0 K<sup>+</sup> binding site. This stabilization of the SF is thought to be caused by an increased hydrogen bond network between the SF and the P-helix mediated by a water molecule. Interestingly, such a water molecule on the backside of the SF was also observed in a crystal structure of KcsA<sup>136</sup> and a recent MD simulation study on KcsA has further highlighted the important role of water molecules on inactivation.<sup>56</sup> The study of Stansfeld et al. suggests that the water molecule in hERG bridges interactions between S620 and N629. This is supported by the fact that the equivalent residues in KcsA, E71 and D80, are crucial for inactivation in KcsA.<sup>137,138</sup>

Between the S5 and the P-helix, the hERG channel exhibits an extraordinary long linker (approximately 40 residues in hERG compared to 12-15 residues typically in Kv channels). Cysteine scanning and NMR studies revealed that the middle part of this linker forms an amphiphilic helical structure, the turret helix.<sup>139,140</sup> Interestingly, the secondary structure of this linker appears to be very flexible as the helical structure was only observed in membrane mimicking micelles.<sup>140</sup> This is further supported by Jiang et al. suggesting that the linker can switch between a helical and a loop structure depending on a hydrophobic or hydrophilic environment.<sup>141</sup> Further, mutations of the turret helix led to disruption of inactivation suggesting that the turret helix contributes to the unusual fast inactivation in hERG.<sup>139,142,143</sup> Although the mechanism is not well understood, it is clear that this linker is of great importance for inactivation and might represent a key component for the exceptional fast inactivation in hERG.

The hERG N-terminus is formed by the intracellular Per-Arnt-Sim (PAS) domain and a preceding N-terminal cap.<sup>144</sup> It was shown that both, PAS<sup>114,144,145</sup> and the N-terminal cap,<sup>146,147</sup> are important for the slow deactivation kinetics. Recently, Ke et al. revealed that the N-terminal cap is also essential for the PAS domain stability and in further consequence channel trafficking.<sup>148</sup> On the C-terminus, hERG exhibit a cyclic-nucleotide-binding domain (cNBD). However, binding of cAMP to the cNBD had only a minor effect on channel gating suggesting that cyclic-nucleotide binding is not the major purpose of the cNBD in hERG.<sup>149</sup> Indeed, Gustina and Trudeau have shown that deletion of the cNBD resulted in rapid deactivation kinetics comparable to the deleted PAS domain channel.<sup>150</sup> By using hERG constructs with/without PAS and/or cNBD, they proposed that the slow deactivation kinetics in hERG occur due to interactions between the PAS domain and cNBD.

In the absence of hERG crystal structures, tremendous efforts have been directed towards the generation of reliable and predictive hERG homology models.<sup>151–159</sup> These homology models mostly rely on crystal structures of KcsA, MthK and KvAP and focus on the pore domain of the hERG channel since most drugs bind in the cavity inside the channel. Due to the lack of a template for the turret helix, the linker between S5 and P-helix is often modelled as a short loop. While there is a broad consensus on the sequence alignment of the S6 helix, the alignments vary in the S5 region. A comprehensive study by Stary et al.<sup>157</sup> validated several alignments and proposed a consensus model of the hERG channel pore (Figure 7B). This model is used throughout our studies.

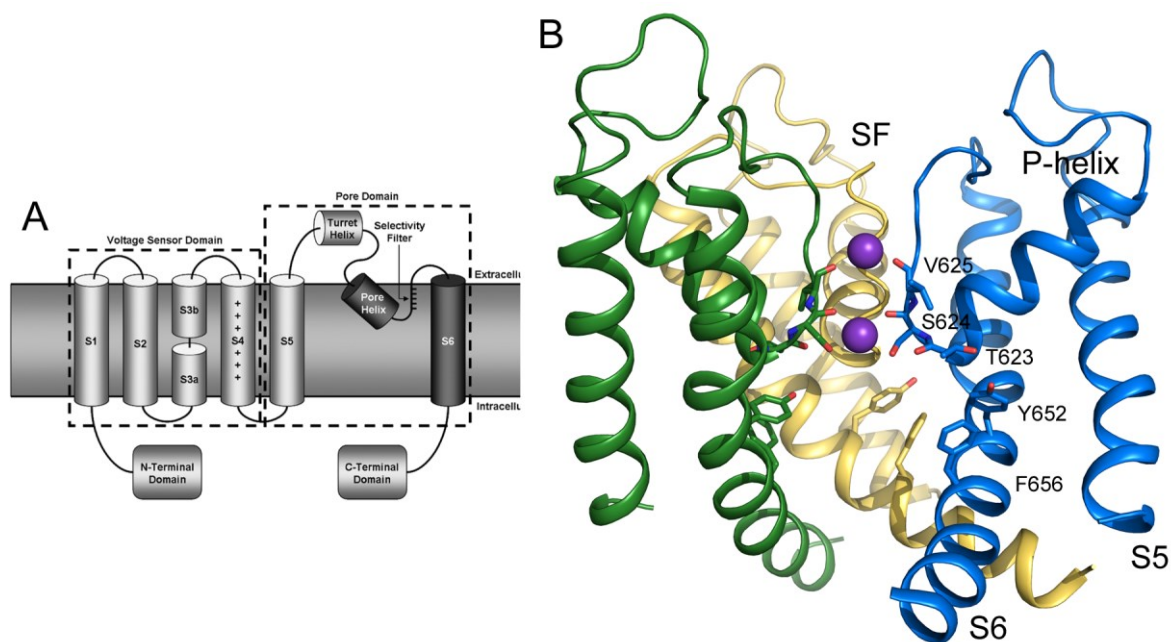


**Figure 7. hERG channel structure.** A) TM topology of an individual hERG SU. Used from Stansfeld et al.<sup>135</sup> B) Consensus homology model of the hERG pore domain. 3 of the 4 SUs are shown and

colored blue, yellow, and green. Amino acids that form the drug binding site are shown as sticks. K<sup>+</sup> ions are represented as magenta spheres.

### 1.3.4 Drug block of hERG channels

In clinical practice, LQTS is most commonly observed in patients taking drugs that block the hERG K<sup>+</sup> channel. Obviously, this effect can be caused by antiarrhythmic drugs, such as dofetilide, ibutilide, sotalol, and amiodarone, blocking the K<sup>+</sup> current during phase 3 of repolarization (class III antiarrhythmic drugs).<sup>160</sup> TdP induced by these drugs is a relatively frequent side effect, affecting up to 12.5 % of patients treated with ibutilide for example.<sup>161</sup> Beside antiarrhythmic drugs, LQTS and TdP were reported for a variety of non-cardiac drugs with diverse chemical entities including antihistamines (e.g. terfenadine), psychiatric (e.g. haloperidol and thioridazine), antimicrobial (e.g. erythromycin), prokinetic (e.g. cisapride), and antimalarial drugs (e.g. pentamidine and halofantrine). Although TdP occurs rarely by the administration of non-cardiac drugs (1 out of 120,000 patients treated with cisapride for example),<sup>162</sup> this risk is intolerable for medications that are used to treat non-life-threatening diseases such as allergies. Consequently, several drugs such as terfenadine and cisapride were withdrawn from the market or had their use heavily restricted by regulatory agencies. It has now become a standard procedure to screen drug candidates for their hERG blocking capacity as laid out by the ICH guideline S7B.<sup>163</sup> However, as hERG is blocked by a plethora of drug classes and chemical entities, it is still a major challenge to reliably predict hERG blocking potency during drug development.<sup>67,107,164,165</sup>

Nonetheless, substantial progress has been made in identifying the drug binding site in hERG. Starting in 2000, alanine scanning mutagenesis was employed to measure the contribution of a native amino acid on drug binding.<sup>166</sup> Since then, this method is extensively applied on different hERG blockers and identified key amino acids that are commonly important for hERG blockers. They include T623, S624, and V625 from the bottom of the SF and the two aromatic amino acids Y652 and F656 located on the S6 helices (Figure 7B).<sup>166–177</sup> All these amino acids, except V625, line the hERG cavity which was identified as the consensus binding site for most hERG blockers. Interestingly, the location of two aromatic amino acids on the S6 helix is quite unique among Kv channels.<sup>178</sup> The presence of 8 aromatic amino acids lining the cavity allows numerous  $\pi$ - $\pi$  or cation- $\pi$  as well as hydrophobic interactions and might account for the promiscuity of hERG channel block. However, the non-inactivating Kv10.1 channel also possesses tyrosine and phenylalanine residues in analogous positions but is less sensitive to drug block.<sup>133,179</sup> This suggests that inactivation might contribute to high-affinity block. Indeed, introducing inactivation into Kv10.1

increased the channel's sensitivity to drug block<sup>133,179</sup> and inactivation impaired hERG channel can reduce drug sensitivity.<sup>134,167</sup> However, this is not generally valid as not all drugs are affected by inactivation impaired hERG channels,<sup>180,181</sup> increased inactivation can still reduce sensitivity to block,<sup>166,182</sup> and the reduced sensitivity is relatively minor to Y652 and F656 mutations.<sup>183,184</sup> This suggests that binding to the predominant inactivated state is not essentially critical and may vary among different blockers.<sup>184</sup> The seminal work of Chen et al.<sup>185</sup> proposed that conformational changes of Y652 and F656 occur during inactivation and thereby change the drug binding site.

While there is no clear picture regarding the dependence of block on inactivation, it is well known that most hERG blockers require an open pore gate to gain access to the cavity.<sup>168,174,186,187</sup> It was also shown that channels can close in the presence of a drug in the cavity. This phenomenon, referred to as trapping, will be described in more detail in the following chapter 1.3.5.

Beside drug-induced LQTS caused by direct block of hERG channel, drugs can also influence the hERG channel density on the cell membrane and thereby decrease K<sup>+</sup> current during cardiac repolarization.<sup>188</sup> Several drugs, including arsenic trioxide,<sup>189</sup> pentamidine,<sup>61,190</sup> and probucol,<sup>191</sup> were identified which can reduce trafficking of hERG channels to the cell membrane. These drugs disrupt trafficking without direct channel block. Interestingly, other compounds such as fluoxetine and ketoconazole acutely block hERG channels and reduce the amount of hERG protein at the cell surface by long-term exposure.<sup>192,193</sup> These two effects could be separated by mutating F656 which abolished channel block but did not affect impaired trafficking. This suggests that these drugs might also act on alternative binding sites of the channel<sup>194</sup> or target distinct pathways that regulate hERG protein trafficking.<sup>195</sup> Conversely, hERG blocking compounds can also rescue trafficking defective mutant channels and thereby act as so called pharmacological chaperones. This effect was shown for several drugs including astemizole, cisapride, and terfenadine.<sup>196–198</sup> This rescue is thought to be caused by binding of the drugs to the inner cavity of the channel pore soon after assembly of the channel tetramers in the endoplasmic reticulum. This leads to the stabilization of protein structures and thereby prevents degradation of the protein. However, while these pharmacological chaperones rescue trafficking to the cell membrane, they are hERG blockers by nature which ultimately do not increase K<sup>+</sup> current during the repolarization phase. Therefore, attempts have been made to separate these two effects.<sup>198</sup> In a recent study, we used pentamidine as a model drug to identify chemical key features for drug-induced trafficking defects. Additionally, the relation between correction of drug-induced trafficking defects and hERG channel block was studied by using dofetilide and derivatives.<sup>199</sup> This might facilitate the design of non-blocking correctors for trafficking

defective hERG proteins. Although the mechanism of action of altered trafficking by drugs is not well understood, it is important to consider altered trafficking as an alternative pathway for drug-induced LQTS during drug development. Especially since conventional screening methods for hERG channel block may not detect a decrease in current by this mechanism.<sup>107</sup>

### 1.3.5 Drug trapping

It was shown for several hERG blockers that recovery from block in the cavity occurs relatively slowly.<sup>173,174,176,187,200–202</sup> It was already suggested by Armstrong in 1971 that this slow rate of recovery may result from a blocker which is trapped in the cavity during gate closure.<sup>203</sup> Direct evidence for the trapping hypothesis was provided by Mitcheson et al.<sup>201</sup> by making use of the high affinity hERG blocker MK-499 and the point mutation D540K. The D540K channel exhibits almost WT gating behavior which means that the channel is mostly closed at a membrane potential of -90 mV and opens in response to membrane depolarization. However, the channel can also be opened by hyperpolarization to membrane potentials below -90 mV.<sup>204</sup> This unique gating behavior of D540K channels provides an excellent approach to test if drugs are present in the cavity when channels are in a closed state. While recovery from block was very slow in closed WT channels, the reopening of the D540K mutant at hyperpolarized potentials resulted in a facilitated dissociation of MK-499 indicating that the compound is trapped in the cavity. This approach was widely used to provide evidence for trapping of hERG blockers of various chemical entities.<sup>173,174,176,187</sup> Additionally, drug trapping in hERG was investigated by measuring the extent of recovery from block after a 330 s resting period in which channels are kept closed.<sup>187,202</sup> In both approaches, it remained elusive which structural descriptors of hERG blockers or specific interactions with the channel cause trapping. Therefore, we conducted MD simulations to provide atomistic insights into conformational changes occurring during drug trapping (see chapter 4.3, page 72).

## 1.4 Kir channels

The third class of  $K^+$  channels investigated in this thesis is the inward rectifier  $K^+$  channel family. Kir channels are characterized by their ability to conduct  $K^+$  inward more easily than outward, termed inward rectification. Under physiological conditions, these channels generate a large  $K^+$  current at potentials negative to the equilibrium potential of  $K^+$  ( $E_K$ ), but permit less conductance at potentials positive to  $E_K$  (Figure 10, page 28).<sup>205–208</sup> Because of this unique feature, Kir channels are involved in various key physiological processes and can

cause severe diseases (see chapter 1.4.1, page 17). Recent progress has been made in understanding the unique gating properties of Kir channels by crystallization of several mammalian and bacterial Kir channels (see chapter 1.4.2, page 24).

Kir channels are classified by their strength of rectification and their response to various triggers. The 15 identified Kir SU genes are grouped into seven subfamilies (Kir 1.x to 7.x).<sup>209</sup> These subfamilies can be categorized into four functional groups: classical Kir channels (Kir2.x), G-protein-gated Kir channels (K<sub>G</sub> or Kir3.x), ATP-sensitive K<sup>+</sup> channel (Kir6.x), and K<sup>+</sup>-transport channels (Kir1.1, Kir4.x, Kir5.1, and Kir7.1) (Figure 8).<sup>18</sup>

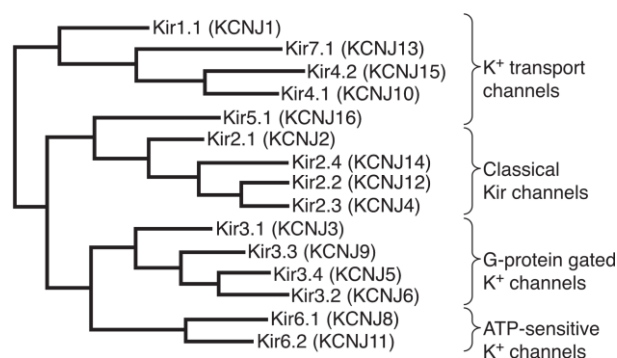


**Figure 8. Phylogenetic tree of Kir channels.** Kir channels are grouped into seven subfamilies (Kir1.x to Kir7.x) and are categorized into four functional groups. Figure from Hibino et al.<sup>18</sup>

### 1.4.1 Physiological and pathophysiological role

Kir channels are found in various distinct cell types including cardiac myocytes,<sup>205,210</sup> neurons,<sup>211–213</sup> blood cells,<sup>214</sup> and epithelial cells.<sup>215,216</sup> In the following part of this chapter, the physiological and pathophysiological roles of each functional group will be discussed separately to provide a concise yet clear overview of the widespread involvement of Kir channels. As an outline, the human Kir channelopathies are listed in Table 1.

**Table 1. Human Kir channelopathies.** Adopted from Hibino et al.<sup>18</sup> ND, not determined.

Disease	Channel	Condition
Bartter's syndrome (type II)	Kir1.1	Loss of function
Andersen's syndrome (LQT7)	Kir2.1	Loss of function
SQTS	Kir2.1	Gain of function
Generalized seizures	Kir4.1	ND
SeSAME syndrome	Kir4.1	Loss of function

congenital hyperinsulinism	SUR1, Kir6.2	Loss of function
neonatal diabetes	SUR1, Kir6.2	Gain of function
Snowflake vitreoretinal degeneration	Kir7.1	Gain of function

#### 1.4.1.1 Classical Kir channels (Kir2.x)

Classical Kir channels (Kir2.x) are responsible for  $I_{K1}$  in cardiac myocytes (Figure 5A, page 8) which is essential for the final cardiac repolarization.<sup>205,210,217</sup> Additionally, they carry a time-independent background  $K^+$  current that is responsible to retain the cardiac resting potential close to  $E_K$ . Membrane potentials more negative than  $E_K$  are corrected by an inward current and slightly increased membrane potentials are compensated by an outward current. As myocytes are depolarized, the lack of outward  $K^+$  flow through Kir2.x channels at positive membrane potentials is essential for the maintenance of the plateau phase. Interestingly, as several  $K^+$  channels including hERG and Kir2.x are important for the cardiac repolarization, the hindrance of  $K^+$  current during the plateau phase is caused by completely distinct mechanisms. This fact further emphasizes the importance of the sophisticated performance of ion channels during the cardiac action potential. When repolarization is initiated by Kv channel current, the outward current  $I_{K1}$  accelerates the final stage of cardiac repolarization. Therefore, Kir2.x channels play a crucial role in shaping the action potential by setting the resting potential, facilitating the plateau phase, and inducing late repolarization. Consequently, changes in Kir2.x channel function can lead to severe disorders. Loss-of-function mutations in the Kir2.1 encoding gene *KCNJ2*<sup>218</sup> cause Andersen's syndrome which is accompanied by cardiac arrhythmias, periodic paralysis and dysmorphic bone structure in face and fingers.<sup>219</sup> As these mutations reduce  $K^+$  current during late repolarization, the QT interval is prolonged (LQTS type 7) rendering the heart more prone to arrhythmias. Additionally, Kir2.1 malfunction might destabilize the resting cardiac potential and thereby trigger arrhythmias. Conversely, a mutation was identified in *KCNJ2* that cause SQTS.<sup>220</sup> This mutation results in the substitution of an aspartic acid to an asparagine residue at position 172 (D172N). D172, located at the C-terminal end of TM2, is crucial for the strong inward rectification characteristics of Kir2.1 (see chapter 1.4.2, page 24).<sup>220</sup> Loss of inward rectification leads to  $K^+$  current during the plateau phase and results in early repolarization.

Beside their role in the heart, Kir2.x channels are expressed in blood vessels,<sup>221</sup> neurons in the brain,<sup>222</sup> skeletal muscle<sup>218</sup> and kidney.<sup>216</sup> In blood vessels, they contribute greatly to vasodilation. Kir channels, located in the vascular endothelial cells, set the cells to a negative membrane potential which provides the driving force for  $Ca^{2+}$  flux into cells which in further consequence leads to the NO facilitated vasodilation.<sup>221,223,224</sup> In vascular smooth muscle cells, it has been suggested that Kir2.x channels contribute to vasodilation in response to an

increase in extracellular  $K^+$  concentration.<sup>225</sup> As high extracellular  $K^+$  concentrations normally cause depolarization, increased Kir conductance compensates depolarization and result in membrane hyperpolarization.<sup>226</sup>

The significance of Kir2.1 channels in muscle function is shown by the Kir2.1 deficient disease Andersen's syndrome which is accompanied by periodic paralysis. It was suggested that, due to the reduced Kir2.1 function, the resting membrane potential is shifted in the depolarizing direction. Thereby,  $Na^+$  channels are inactivated and are rendered insensitive to action potential initiation and propagation.<sup>218</sup> In the kidney, classical Kir channels are involved in  $K^+$  secretion in the cortical collecting duct (CCD) of the kidney. It was shown that apical (facing the duct lumen) and basolateral (facing the interstitial space) membranes of CCD express distinct type of Kir channels. While the apical Kir1.1 channels exhibit mild inward rectification with an intermediate conductance,<sup>216,227,228</sup> the basolateral Kir2.3 channels display strong rectification with a small conductance.<sup>216,229–231</sup> This asymmetric profile of Kir channels in epithelial cells is important to allow  $K^+$  transport from the basolateral to the apical side. Kir1.1 plays also a major role in  $Na^+$ ,  $K^+$ , and  $Cl^-$  reabsorption in the thick ascending limb of the loop of Henle (TAL) (see chapter 1.4.1.4, page 22).<sup>18,216</sup>

Interestingly, the function of classical Kir channels is influenced by the cholesterol fraction of the membrane. Application of cholesterol reduces Kir2.1 current in Chinese hamster ovary (CHO) cells and native Kir2.x current in bovine and human aortic endothelial cells.<sup>232,233</sup> Additionally, an increased plasma cholesterol level in hypercholesterolemic pigs causes reduced endothelial Kir current and depolarization of the membrane resting potential.<sup>234</sup> This suggests that the suppression of Kir channels might display an important factor in hypercholesterolemia-induced endothelial dysfunction and other vascular diseases associated with an altered lipid membrane profile.

#### **1.4.1.2 G-protein-gated Kir channels ( $K_G$ or Kir3.x)**

$K_G$  channels are regulated by G protein-coupled receptors (GPCRs). Upon agonist binding to GPCRs, the two subunits  $G_\alpha$  and  $G_{\beta\gamma}$  are separated from each other. In further consequence, the  $G_{\beta\gamma}$  subunit activates the  $K_G$  channel by binding to both N- and C-termini of the  $K_G$  channel.<sup>235–242</sup> Although  $K_G$  channels are activated only by the  $G_{\beta\gamma}$  subunit,<sup>243–247</sup> it was suggested that the  $G_\alpha$  subunit is involved in the control of channel activity.<sup>238,248,249</sup> Stimulation of GPCRs by different ligands such as dopamine,<sup>250</sup> glutamate,<sup>251,252</sup> and acetylcholine (ACh)<sup>253</sup> results in activation of  $K_G$  channels which hyperpolarizes the cells.

$K_G$  channels play an important role in the regulation of the heart beat frequency by responding to ACh release from the vagal nerve. In the sinoatrial node,<sup>254,255</sup> ACh induces  $K^+$  efflux through Kir3.1 and Kir3.4 channels and causes membrane hyperpolarization which result in slowing of the heart rate.<sup>253,256–258</sup> In the brain,  $K_G$  channels are located at presynaptic and postsynaptic membranes.<sup>259–261</sup> On the postsynaptic site,  $K_G$  channels diminish the excitability of the postsynaptic membrane by hyperpolarization.<sup>262</sup> This hyperpolarization can be triggered by several neurotransmitters such as opioid receptor agonists<sup>263,264</sup> or GABA<sub>B</sub> agonists.<sup>265</sup> Additionally, it was suggested that  $K_G$  channels are involved in drug abuse and addiction.<sup>18</sup> Kir3.x channels were also found to be located in secretory vesicles of the pituitary gland.<sup>266</sup> Beside the manifold roles of  $K_G$  channels in the heart and the brain, these channels regulate insulin and glucagon secretion in the pancreas in response to hormones and neurotransmitters. GPCR ligands such as catecholamines and somatostatin cause a  $K_G$  channel induced membrane hyperpolarization. This effect leads to a decreased insulin secretion from  $\beta$ -cells and a reduced glucagon release from  $\alpha$ -cells.<sup>267–271</sup>

#### **1.4.1.3 ATP-sensitive $K^+$ channel ( $K_{ATP}$ or Kir6.x)**

$K_{ATP}$  channels are found in pancreatic  $\beta$ -cells,<sup>272,273</sup> cardiac myocytes,<sup>274</sup> skeletal muscle,<sup>275</sup> vascular smooth muscle,<sup>276,277</sup> and neurons.<sup>278</sup> The channels are inhibited by ATP (except for channels in smooth muscle) and are activated by nucleoside diphosphates (NDPs) such as ADP.<sup>279</sup>  $K_{ATP}$  channels are comprised of four Kir channel SUs forming the channel pore and four surrounding sulfonylurea receptor (SUR) proteins.<sup>280</sup> While the Kir SUs are responsible for ATP induced inhibition, NDP binding to the SUR proteins cause activation.

The most prominent expression of  $K_{ATP}$  is found in the pancreatic insulin secreting  $\beta$ -cells. These channels consist of Kir6.2 SUs and SUR1 proteins.<sup>281</sup> By setting the membrane resting potential, they couple the blood glucose concentration to insulin secretion.<sup>282</sup> At substimulatory blood glucose levels,  $K_{ATP}$  channels are constitutively open and the steady  $K_{ATP}$  outward current maintains a hyperpolarized membrane potential. As the blood glucose level increases, enhanced glucose uptake and metabolism in  $\beta$ -cells results in an increased ATP concentration and a lowered ADP concentration. Consequently, the higher ATP concentration counteracts the ADP activatory effect and causes closure of the  $K_{ATP}$  channels which leads to depolarization of the cell membrane. The subsequent  $Ca^{2+}$  influx through activated L-type voltage-gated  $Ca^{2+}$  channels leads to insulin secretion from cell vesicles. Additionally,  $K_{ATP}$  channels appear to be involved in the hypoglycemia induced glucagon

release from  $\alpha$ -cells. However, the exact regulation by  $K_{ATP}$  channels in  $\alpha$ -cells is not fully understood yet.<sup>283–285</sup>

The key role of  $K_{ATP}$  channels in glucose metabolism implicates that improper function of Kir6.2 or SUR1 can result in severe glucose homeostasis disorders. Indeed, the majority of  $K_{ATP}$  channelopathies are linked to pancreatic  $\beta$ -cells.<sup>286–288</sup> Loss-of-function mutations cause congenital hyperinsulinism (CHI) which is characterized by a persistent and unregulated insulin secretion despite low blood glucose levels.<sup>289</sup> Shortly after birth, affected individuals present hypoglycemia which causes irreversible brain damage if untreated. In most cases, therapy is accompanied by a partial pancreatectomy. Loss-of-function mutations are either located in SUR1,<sup>290,291</sup> which account for 50 % of the cases, or in the Kir6.2 encoding gene *KCNJ11*.<sup>287,292–295</sup> These mutations can alter gating *per se*, affect the channel response to NDP, or disrupt trafficking defects to the surface membrane. Mutations in the nucleotide binding domain (NBD) of SUR1 result in an impaired response to NDP and in further consequence persistent closed  $K_{ATP}$  channels. Trafficking deficient mutations are mainly located on the SUR1 gene. Gain-of-function mutations, located either on SUR1 or on Kir6.2, cause neonatal diabetes (ND) which normally occurs in the first 6 months of life.<sup>282,287</sup> In this phenotype, the sensitivity of  $K_{ATP}$  channels to ATP is reduced. Thus, channel closure and membrane depolarization in response to high blood glucose levels is impaired.<sup>296,297</sup> Most patients with ND can be treated by sulfonylureas. These drugs bind to the SUR proteins and cause closure of the  $K_{ATP}$  channels leading to an increased insulin secretion. Therefore, sulfonylureas are also administrated in diabetes mellitus type 2. Beside hyperglycemia, around 20 % of ND patients also suffer from neurological problems such as delayed development of speech and walking, muscle hypotonia and epilepsy.<sup>298</sup> This range of symptoms is a consequence of the widespread distribution of  $K_{ATP}$  channels in the human body.

In contrast to  $K_{ATP}$  channels in the pancreatic  $\beta$ -cells, cardiac  $K_{ATP}$  channels are closed under physiological conditions due to the high intracellular ATP concentration.<sup>299,300</sup> During a cardiac metabolic insult such as an increased cardiac work load, hypoxia, or ischemia,  $K_{ATP}$  channels are activated and cause ST elevation in the ECG which is a hallmark of acute myocardial ischemia.<sup>301</sup> Interestingly, it was shown that opening of  $K_{ATP}$  channels plays a key role in ischemic preconditioning.<sup>302–304</sup> This phenomenon is characterized by the observation that a period of sublethal ischemia can profoundly protect the cardiac cells from a subsequent ischemic insult.<sup>304,305</sup> Additionally,  $K_{ATP}$  channels appear to be involved in cardiac stress adaption and maintenance of cellular functions.<sup>306–308</sup>

Opening of  $K_{ATP}$  channels in vascular smooth muscle results in membrane hyperpolarization, closure of voltage-gated  $Ca^{2+}$ -channels, and thus in relaxation of the

smooth muscle cells.<sup>309,310</sup> This effect is employed to treat hypertension and angina pectoris by  $K_{ATP}$  channel openers such as nicorandil which causes vasodilation of blood vessels.  $K_{ATP}$  channels are also expressed in the uterine myometrial smooth muscles and channel density increases during pregnancy.<sup>311,312</sup> Therefore,  $K_{ATP}$  channel openers can inhibit uterine contractions during late pregnancy. In the brain,  $K_{ATP}$  channels might play a role in excitation regulation of neurons in response to glucose, similar to that of  $\beta$ -cells.<sup>278,313</sup> Additionally, it is thought that  $K_{ATP}$  channels act as protective mediators under pathological conditions by suppressing neuronal activity during hypoxia.<sup>314–316</sup>

#### **1.4.1.4 $K^+$ -transport channels (Kir1.1, Kir4.x, Kir5.1, and Kir7.1)**

Kir1.1 was the first cloned Kir channel and was initially described as the “rat outer medullary  $K^+$  channel” which led to the commonly used abbreviation ROMK1.<sup>317</sup> It plays a major role in the electrolyte homeostasis regulation in the kidney.<sup>216</sup> More specifically, Kir1.1 channels are located in renal epithelial cells of TAL, CCD, and the distal convoluted tubule (DCT). In the TAL cells, around 25 % of the urine  $Na^+$  is reabsorbed by the  $Na^+-K^+-2Cl^-$  cotransporter (NKCC) which is located on the apical cell membrane. To maintain the activity of NKCC, Kir1.1 channels, expressed also on the apical side, conduct  $K^+$  to the lumen.<sup>13,216</sup> A  $Na^+-K^+-ATPase$  on the basolateral membrane carries reabsorbed  $Na^+$  to the interstitial space while a Kir2.3 channel maintains the  $K^+$  ion gradient. Therefore, the cooperative work of NKCC, Kir1.1,  $Na^+-K^+-ATPase$ , and Kir2.3 causes a unidirectional transport of  $Na^+$  from the urine to the interstitial space.<sup>216</sup> The positive membrane potential difference in the lumen represents the main driving force for paracellular  $Na^+$ ,  $Ca^{2+}$ , and  $Mg^{2+}$  reabsorption.<sup>216</sup> Kir1.1 channels are also critically involved in the secretion of  $K^+$  in the CCD (see chapter 1.4.1.1, page 18).<sup>18,318</sup> Mutations in the Kir1.1 encoding gene *KCNJ1*<sup>216,319–323</sup> are associated with type II Bartter’s syndrome which is an autosomal recessive renal tubulopathy. Symptoms include hypokalemia, alkalosis, renal salt wasting, and elevated renin and aldosterone blood levels.<sup>321,324,325</sup> In TAL cells, the disrupted Kir1.1 function greatly reduces the extracellular  $K^+$  concentration which is needed by NKCC for  $Na^+$  and  $Cl^-$  reabsorption. Additionally, due to the missing positive membrane potential difference in the lumen, the paracellular reabsorption of  $Na^+$  is greatly reduced. This symptomatic phenotype was confirmed by Kir1.1 knockout mice which exhibited renal  $Na^+$ ,  $Cl^-$ , and  $K^+$  wasting and hypokalemia.<sup>326,327</sup> The mechanism of hypokalemia was initially unknown since it was suggested that Kir1.1 is the major secretory pathway of  $K^+$ . Consequently, impaired Kir1.1 channel function was expected to result in hyperkalemia. A recent study shed light on this discrepancy.<sup>328</sup> In Kir1.1 knockout mice,  $K^+$  secretion by Kir1.1 in TAL cells was diminished. However,  $K^+$  secretion was maintained by

continuous  $K^+$  efflux through large-conductance  $Ca^{2+}$ -activated  $K^+$  channels in the late distal tubule leading to the observed hypokalemia in Bartter's syndrome.

Kir4.x and Kir5.1 channels are located in the kidney, stomach, cochlea and glial cells. In the kidney, apical  $Na^+$  channels in DCT cells play a major role in reabsorption of  $Na^+$ . This absorption is coupled to a basolateral  $Na^+-K^+$ -ATPase to maintain a unidirectional transport of  $Na^+$  from the lumen to the interstitial space. Basolateral Kir channels adopt a " $K^+$  recycling" function by conducting intracellular  $K^+$  to the interstitial space.<sup>216</sup> Additionally, the pH sensitivity of these channels strongly suggests that they are involved in acid-base homeostasis by pH-dependent regulation of ion transport.<sup>216,329–331</sup> In gastric parietal cells, Kir4.1 channels are expressed together with an  $H^+-K^+$ -ATPase on the apical membrane.<sup>332,333</sup> This pump secretes protons, which are essential for the production of hydrochloric acid in the stomach, in exchange for  $K^+$ .  $K^+$  efflux through Kir4.1 channels thereby maintains the activity of the  $H^+-K^+$ -ATPase by providing sufficient extracellular  $K^+$ .

The cochlea of the inner ear hosts two extracellular liquids, the perilymph and endolymph. While the ionic composition of the perilymph is similar to other extracellular liquids, the endolymph exhibits a high  $K^+$  concentration of around 150 mM and a highly positive potential of +80 mV. This potential is called the "endocochlear potential".<sup>334–336</sup> These unique properties of the endolymph are maintained by Kir4.1 and are crucial for proper audition.<sup>337</sup> In addition, the Pendred syndrome which exhibit thyroid goiter and deafness was linked to the loss of Kir4.1 channel function in the cochlea.<sup>338</sup>

In brain astrocytes and retinal Müller cells, Kir channels conduct a large  $K^+$  current to maintain the ionic and osmotic environment in the extracellular compartment.<sup>18</sup> Most importantly, they carry off  $K^+$  from regions with high  $K^+$  concentration resulting from synaptic excitation.<sup>339</sup> The rapid  $K^+$  clearance by glial cells is essential for proper synaptic function as a high concentration of  $K^+$  would result in continuous neuronal signaling. Interestingly, glial cells from patients with intractable epilepsy exhibit almost complete lack of Kir conductance,<sup>340</sup> a reduced inward rectification<sup>341</sup> and a diminished  $K^+$  clearance.<sup>342,343</sup> Additionally, patients suffering from the SeSAME syndrome, which is accompanied by seizures, deafness, ataxia, mental retardation, and electrolyte imbalance, exhibit mutations in the Kir4.1 gene.<sup>344,345</sup> The affected organs, brain, ear, and kidney, correspond to the distribution pattern of Kir4.1.

Kir7.1 channels are found in the choroid plexus epithelial cells,<sup>346</sup> in the retinal pigmented epithelia,<sup>347,348</sup> in intestinal epithelial cells,<sup>346</sup> in thyroid follicular cells,<sup>346</sup> and in renal epithelia.<sup>349,350</sup> The physiological role of Kir7.1 is unknown. However, due to the Kir7.1 presence in various epithelial cells, involvement in cellular ion transport seems likely.

Mutations in the Kir7.1 encoding gene *KCNJ13* can cause snowflake vitreoretinal degeneration (SVD). SVD is characterized as a developmental and progressive eye disease accompanied by fibrillar degeneration of the vitreous humor, early-onset cataract, snowflake-like crystalline deposits in the retina and retinal detachment.<sup>18,351</sup>

### 1.4.2 Structural basis of Kir channel gating

Kir channels comprise of four identical SUs which coassemble to form a TM domain and a cytoplasmic domain (CTD). Each SU consists of two TM spanning helices (Figure 2B, page 4) and thus exhibit similar conformations as the crystallized bacterial channels KcsA and MthK (see chapter 1.2.1, page 4). However, Kir channels have an additional helix in the TM domain which is located on the N-terminal end of TM1. This slide-helix is of amphiphilic character which strongly suggests that it runs parallel to the membrane-cytosol interface. The importance of the slide-helix for proper channel function is emphasized by the fact that mutations in this region can cause type II Bartter's syndrome and Andersen's syndrome.<sup>218,320,352–354</sup> As other K<sup>+</sup> channels, Kir channels possess a SF and a pore gate, termed helix bundle crossing (HBC) gate, which can open and close by bending of the TM2 at a glycine hinge.<sup>355</sup> In the HBC gate, several bacterial (KirBac) and mammalian Kir channels exhibit a bulky aromatic amino acid (e.g. F181 in Kir3.1 and F187 in Kir3.4, F146 in KirBac1.1, Y132 in KirBac3.1), which was proposed to act as a barrier for ion permeation. Mutations of the phenylalanine to alanine or serine led to constitutively open channels verifying the crucial role of this amino acid in closing the HBC gate.<sup>356,357</sup> Crystallization of the CTD revealed that the N- and C-termini of all four SUs form a  $\beta$ -strand rich cylinder which is characteristic for Kir channels.<sup>358–360</sup> This cylinder is mainly formed by the long C-termini of each SU while the shorter N-termini are located between adjacent C-termini. The CTD lengthens the ion permeation pathway by approximately 30 Å resulting in a total of 60 Å that needs to be passed by K<sup>+</sup> ions.<sup>358</sup> The CTD introduces another gate to the permeation pathway, the G-loop gate.<sup>359,361</sup> This gate is located on the upper part of the CTD and faces the TM domain. It was suggested that the G-loop not only contribute to channel gating but also to the inward rectification of Kir channels.<sup>359</sup> Additionally, several mutations causing Andersen's syndrome are located in the G-loop gate of Kir2.1.<sup>218,362,363</sup> The CTD is also the binding site for Kir subfamily specific triggers such as nucleotides and G proteins.<sup>235,238,241,242,364</sup>

Recent full length crystal structures of bacterial and mammalian Kir channels in open and closed conformations shed light on the arrangement of the TM domain and CTD in different channel states (Figure 10C).<sup>42,361,365–371</sup> They revealed that the CTD undergoes a rotational

movement of 23° upon channel gating and thus exists in a non-twisted and twisted conformation. Since the first observations of a twisted and non-twisted CTD occurred in the context of a closed HBC gate<sup>367</sup> and a subsequent open crystal structure exhibited only a twisted CTD,<sup>42</sup> it was suggested that the rotational movement of the CTD has to occur prior to HBC gate opening.<sup>42</sup> As this assumption is based on static conformations of KirBac channels, we set out to test this hypothesis and investigated the dynamical, sequential process of gating events by making use of MD simulations. Pore gating of Kir channels was studied on the bacterial homologue KirBac1.1 and was the subject of a comprehensive study of this thesis (see chapter 4.2, page 49). Beside the rotational movement of the CTD during gating, Clarke et al.<sup>367</sup> suggested an additional movement based on the observation of a latched and unlatched state of the CTD. In the unlatched conformation, more interactions are formed in the interface of adjacent SUs leading to tighter packing of the interface which has great implications for the polyamine effect on Kir channels (described below). The rotational movement of the CTD was proposed to be directly linked to conformational changes of the SF via the slide-helix as several crystal structures with a twisted CTD displayed a nonconductive filter.<sup>367</sup> A recent study by Bavro et al.,<sup>42</sup> however, showed that the CTD can exhibit a twisted conformation while the SF remains in an activated, conductive conformation. Thus, a possible coupling between the two distinct gates remains controversial and needs to be further investigated. The TM domain is connected to the CTD via the C-linker which exhibits positively charged amino acids. The C-linker was suggested to play a key role in communication between the two domains by forming an interaction network between the HBC gate, the slide-helix, and the G-loop.<sup>42</sup> There is overwhelming evidence that the C-linker interacts with the negatively charged phosphatidylinositol-4,5-bisphosphate (PIP2) which is essential for proper function of Kir channels.<sup>368,372–382</sup> Recently, an additional secondary binding site for nonspecific anionic phospholipids was identified on the slide-helix. Binding of phospholipids to this site was suggested to stabilize the activatory site for PIP2.<sup>383,384</sup>

Beside PIP2 and nonspecific phospholipids, Kir channel function is maintained and regulated by cholesterol. Most Kir channels have been found to partition into cholesterol-rich membrane domains and are affected by the membrane cholesterol concentrations.<sup>19,385–387</sup> Interestingly, the impact of the cholesterol concentration greatly depends on the channel type. While an increase in membrane cholesterol reduces Kir2.x current (see chapter 1.4.1.1, page 18), Kir4.x channels are inhibited by cholesterol depletion (see Levitan et al.<sup>386</sup> for a comprehensive review). A mutational study identified multiple structural determinants in the CTD, partially overlapping with the PIP2 binding site, that are crucial for Kir sensitivity to membrane cholesterol.<sup>385</sup> Additionally, it was suggested that the channel interactions with cholesterol are of specific nature rather than caused by changes in the membrane physical properties.<sup>387</sup>

Kir channels are characterized by their ability to allow inward conductance more easily than outward conductance. This effect is achieved by the physical block of Kir channels by  $Mg^{2+}$  ions and polyamines at membrane potentials more positive than the  $K^+$  reversal potential (Figure 10A).<sup>388–390</sup> Electrophysiological and mutational studies suggest that there are more than one binding site for blocking ions. The first binding site was identified in the TM2 helices of Kir2.1 and Kir1.1. While the strong rectifier Kir2.1 channel exhibits a negatively charged aspartic acid at position 172 (D172), the weakly rectifying Kir1.1 possesses a neutral asparagine at the equivalent position (N171). The mutation N171D in Kir1.1 drastically increased the rectification by an increased affinity for  $Mg^{2+}$ .<sup>391–393</sup> Moreover, D172 in Kir2.1 was shown to be essential for polyamine block.<sup>394</sup> Thus, the strength of inward rectification by  $Mg^{2+}$  and polyamines is dependent on the presence of a negatively charged residue in the TM2 helix and this site is therefore called “D/N site” or “rectification controller”. Another TM2 residue, S165, was shown to cause inward rectification in Kir2.1 by  $Mg^{2+}$  but not by polyamines.<sup>395</sup> Beside the TM binding sites, Kir channels have several negatively charged residues in the CTD which are crucially involved in  $Mg^{2+}$  and polyamine sensitivity.<sup>396–398</sup> Crystal structures of the CTD of several Kir channel revealed that these amino acids point toward the ion conducting pore and form a ring of negatively charged side chains which serve as a complimentary electrostatic match for the long, positively charged polyamines.<sup>358,359,365</sup> In a recent study on Kir2.1,<sup>399</sup> we were able to show that this electrostatic ring can be specifically targeted by drugs which do not only cause inward rectification but also inhibit inward current. By making use of a pentamidine derivative library, we identified a compound which exhibits phenyl rings on the pentamidine substructure and thereby enhance hydrophobic interactions in addition to the electrostatic contacts. Docking studies suggested that the more hydrophobic pentamidine derivative can bind stronger to the ring of the CTD which leads to the inward current inhibition.

In the crystal structures of KirBac3.1 by Clarke et al.<sup>367</sup> two separate binding pockets for the polyamine spermine were identified which are associated to the latched and unlatched CTD conformation (Figure 10B). In the latched conformation, the CTD interface of adjacent SUs forms a pocket which allows accommodation of spermine. In the unlatched conformation, the tight packing of the interface closes the pocket and spermine binds in the pore at the HBC gate which is consistent with the above described “D/N site”. This finding suggests that the unlatching movement not only participates in channel opening but also causes the release of polyamines from the interface binding pocket and makes the polyamines available for Kir channel block.

#### 1.4.2.1 Prokaryotic vs. eukaryotic Kir channel gating

Although prokaryotic and eukaryotic Kir channels are only distantly related (~ 20 % sequence identity, Figure 9), they share the same general topology and exhibit functional similarity. Both are  $K^+$  selective, blocked by  $Ba^{2+}$  and inhibited by acidic pH.<sup>400</sup> Additionally, KirBac channels resemble eukaryotic weak inward rectifiers such as Kir1.1 which are only sensitive to  $Mg^{2+}$  and polyamines when a negative charge is introduced at the “D/N site”. In KirBac1.1, inward rectification is achieved by mutating the corresponding I138 to an aspartic acid.<sup>400</sup>

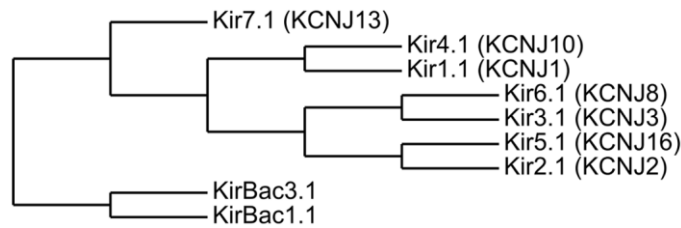


**Figure 9. Phylogenetic tree of bacterial Kir channels.** Protein sequence alignment and phylogenetic tree were generated with ClustalX.<sup>401</sup>

An important difference between bacterial and mammalian Kir channels is their response to PIP2. While PIP2 is a well-known activator in all eukaryotic Kir channels, KirBac channels are inhibited by PIP2.<sup>400,402</sup> MD simulations of PIP2 binding to KirBac1.1 and a homology model of Kir6.2 suggested that the binding sites for PIP2 are conserved in prokaryotic and eukaryotic Kir channels.<sup>382</sup> Therefore, it is unlikely that the opposing effect is caused by different binding sites. The opposing gating response rather results from structural differences in the C-linker of these channels as the C-linker in KirBac channels is shortened by three amino acids. This has important implications for the distance and consequently for the interactions between the TM domain and the CTD. These interactions might be critical for channel opening and are not present in the longer eukaryotic C-linker. However, a bound PIP2 might mediate interactions between the TM domain and the CTD, thereby facilitating channel opening. Interestingly, a PIP2 bound crystal structure of Kir2.2 revealed an upward movement of the CTD by 6 Å, leading to a tighter connection of the two domains (Figure 10D). This structural finding supports the potential mediating effect of PIP2 for channel opening in eukaryotic Kir channels.

Additionally, single channel recordings showed that the KirBac1.1 channel exhibits multiple subconductance states which are rarely seen in eukaryotic channels.<sup>400</sup> This finding might be attributed to several histidine residues that line the channel pore. These residues could be reversibly protonated, thereby causing repulsion of permeating  $K^+$  ions.<sup>400</sup> Further, KirBac1.1 possesses several positively charged amino acids in the CTD pore which might

contribute to the low conducting states. This is supported by a study of Robertson et al. showing that the CTD in KirBac1.1 is less favorable for  $K^+$  permeation compared to eukaryotic Kir channels.<sup>403</sup>

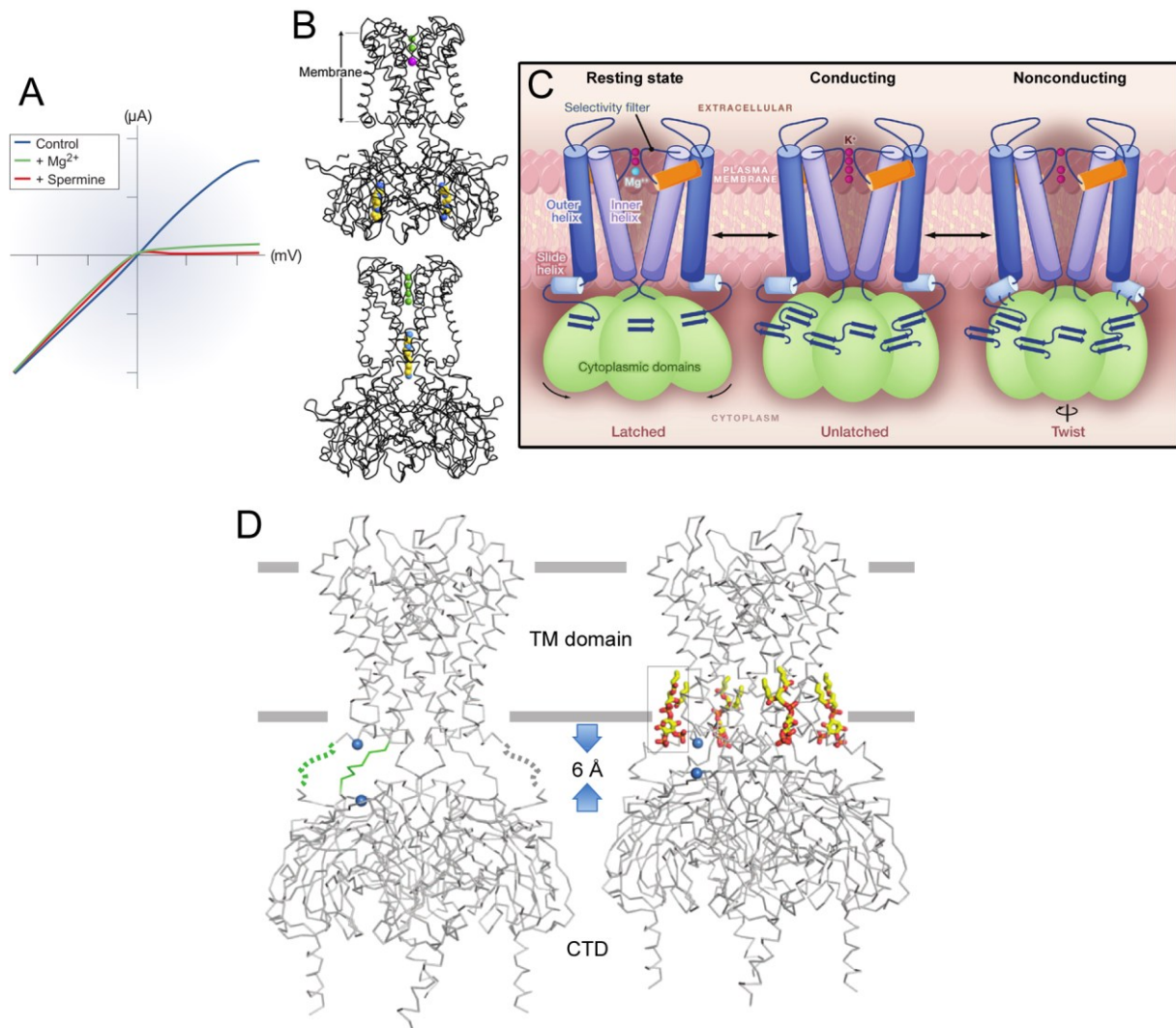


**Figure 10. Gating of Kir channels.** A) Inward rectification caused by intracellular  $Mg^{2+}$  and spermine. Modified from Bichet et al.<sup>17</sup> B) Full length crystal structure of KirBac3.1 with the CTD in latched (top) and unlatched (bottom) conformation. The C $\alpha$  trace is shown as a black coil. Spermine is represented as yellow (C atoms) and blue (N atoms) spheres. The green spheres in the SF represent  $K^+$  ions, while the magenta sphere in the upper panel illustrates a  $Ca^{2+}$  ion which blocks the SF. Figure from Clarke et al.<sup>367</sup> C) Schematic representation of Kir channel gating. Modified from Zhou et al.<sup>404</sup> D) Crystal structures of the apo- (left) and PIP2-bound (right) Kir2.2 channel. The lipid bilayer boundaries are indicated by gray bars. Four bound PIP2 molecules are shown as sticks. The CTD translates towards the TMD by 6 Å (measured between the two reference atoms highlighted as blue spheres). The green and gray dotted lines indicate unresolved structures in the crystals while the green solid line was resolved. Modified from Hansen et al.<sup>368</sup>

## 2 Methods

In this thesis, two main biophysical concepts were employed. First, theoretical approaches in terms of MD simulations were used to provide full atomistic insights into conformational changes of ion channels. More specifically, gating transitions of KcsA, hERG, and KirBac and their relation to drug binding and interactions were investigated. Second, the two-electrode voltage clamp (TEVC) technique was used for an electrophysiology study to probe the influence of drug trapping on the extent of channel closure in hERG.

### 2.1 MD simulations

MD simulation is a well-established research field of computational biophysics and has led to tremendous insights into the dynamical behavior of biochemical entities on the atomic level. Due to the impact on our understanding of the dynamics of chemical structures achieved with MD simulations, three of the most influential researchers of this field, Martin Karplus, Michael Levitt, and Arieh Warshel, received the 2013 Nobel Prize in Chemistry for “the development of multiscale models for complex chemical systems”.<sup>405</sup> The achievements, limitations, and perspectives of MD simulations were extensively reviewed and can be found elsewhere.<sup>406–409</sup> Herein, a short overview of the theoretical principles of MD simulations will be given.

MD simulations describe the time-dependent evolution of a molecular system by solving Newton’s equations of motion. The molecular system is described by a set of particles which move in response to forces interacting between them. In contrast to other approaches such as quantum mechanics where the atom nuclei and electrons are treated separately, the atoms are seen as single particles with an assigned point charge in MD simulations. Interactions between atoms are represented by potentials and related force constants and are incorporated in the force field. The force field potentials can be grouped into intramolecular short-range interactions, which occur between bonded atoms, and long-range interactions which exist between nonbonded interaction partners. The bonded interactions comprise of covalent bonds, angles, dihedral angles and improper dihedral angles. For example, the covalent bond between two atoms is described by a harmonic potential  $V = k/2(r - r_{eq})^2$ . In this equation, the force constant  $k$  and the equilibrium bond length  $r_{eq}$  depend on the involved atom types and the bond type between them. Likewise, similar equations are defined for the other types of bonded interactions. For more detailed descriptions of force field equations, the interested reader is referred to the original paper of the amber force field<sup>410</sup> and a modified version<sup>411</sup> which was employed throughout the MD simulation studies. Due

to the fact that the bonded interactions are constant and covalent bonds cannot be broken or formed during MD simulations, the usage of such force fields is limited to systems where no chemical reactions occur. Additionally, as the covalent bond length show only high frequency oscillations with low amplitude and are considered being of minor biological relevance, the covalent bond length is normally constrained to a fixed value with LINCS.<sup>412</sup> Nonbonded interactions are defined by electrostatic and van der Waals interactions and are implemented in the force fields by Coulomb and Lennard-Jones potentials, respectively. For electrostatic interactions, the charge of a system particle is crucial. The effective charges of atoms are normally determined by quantum mechanical calculations of the nuclei and the electronic wave function and, for simplicity, are approximated to point charges located on the atomic position. As the Coulomb interactions are long-range interactions, they must be calculated for all pairs of particles in the system. For systems with periodic boundary conditions, this calculation is effectively performed by the Particle Mesh Ewald method<sup>413</sup> which splits the Coulomb potential into a real space and Fourier space part in which the charges are positioned in a mesh. Periodic boundary conditions are used to minimize the edge effects which would occur in a finite system from an unnatural boundary with the vacuum outside the system. Therefore, the atoms of the system are put into a space-filling unit cell, which is surrounded by translated copies of itself in all three dimensions. Since the Lennard-Jones potential decays relatively fast over distance, plain cut offs can be defined where the van der Waals interactions became negligible.

With the initial position of the particles and assigned velocities, the forces acting on the particles are calculated by building the derivative of the potential obtained from the force field and the corresponding coordinates. By making use of Newton's second law of motion  $F = ma$  and an integrator algorithm, the positions and velocities of all atoms at the time  $t = t_0 + \Delta t$  can be calculated. The integration time step  $\Delta t$  should be shorter than the fastest motions of the system which are, beside the fixed covalent bond length, the bond-angle vibrations between carbon and hydrogen atoms. Therefore,  $\Delta t$  is usually set to 2 fs. However, by freezing the angles of hydrogens in chemical entities such as methyl groups or aromatic rings by so called virtual sites,<sup>414</sup> a larger integration time step can be chosen which leads to a higher efficiency in simulating hydrogen-rich systems such as proteins. Thus, virtual sites were adopted in MD simulations of the full length KirBac channel consisting of 1046 amino acids (see chapter 4.2, page 49).

MD simulations are usually constantly coupled to a specific temperature and pressure to reproduce the conditions that are present in biological systems. In terms of temperature coupling, this task is conducted by coupling algorithms such as the Berendsen thermostat,<sup>415</sup> the velocity rescaling thermostat,<sup>416</sup> and the Nosé-Hoover algorithm<sup>417,418</sup> which was used in

MD simulations described herein. To maintain a constant pressure, similar algorithms were developed which rescale the coordinates of a system and adjust the boundaries of the simulation unit cell. They include the Berendsen pressure coupling<sup>415</sup> and the Parrinello-Rahman pressure coupling<sup>419</sup> which was employed in our MD simulations studies.

### **2.1.1 Principal components analysis and essential dynamics simulations**

Trajectories of MD simulations provide tremendous insights into conformational changes of systems over time. However, due to the multidimensional motions of a system caused by the  $3N$  degrees of freedom ( $N$  being the number of atoms), it can be virtually impossible to identify the functionally relevant dynamics of such a system. Therefore, it is of great interest to find a lower dimensional representation of a trajectory which reveals the major collective motions. For such an approach, principle component analysis (PCA) can be employed. In PCA, a covariance matrix of the atomic fluctuations is calculated. Diagonalisation of this matrix yields a set of eigenvectors which describe the collective motions of a system. The corresponding eigenvalues describe the magnitude of the fluctuations along the eigenvectors. The eigenvectors with the largest eigenvalues represent the prominent collective motions of a system and are thus called “principal components”. Remarkably, it was shown that the main conformational changes of a system can be described by a relatively low number of eigenvectors (usually by the first few).<sup>420</sup> As these principal components could be often linked directly to protein function, they were termed “essential dynamics (ED)”<sup>420</sup> to emphasize the fact that these are the motions essential for function. Beside the advantage that PCA helps the identification of the ED of a MD trajectory, the extracted principal components can also be used to enhance, or more generally, alter sampling of the essential subspace.<sup>421–425</sup>

Therefore, the so called ED simulations can be of great importance to investigate slow functional transitions of proteins that occur on timescales which are not accessible by common computer simulation systems today. For this purpose, a system can be facilitated to move in a specific direction of the essential subspace by applying stepwise constraint forces. This approach was used in our studies to simulate  $K^+$  channel gating (see chapter 4.1, page 37 and chapter 4.3, page 72). In these studies, channel proteins were driven towards an open or closed channel state by permitting only MD steps that move the system closer to the target structure along a predefined eigenvector. It is important to note that only this predefined eigenvector in the essential subspace is biased while all other degrees of freedom are able to equilibrate. Thereby, an almost unbiased MD simulation can be obtained

from functional collective motions of a system. Additionally, the ED simulation method can be employed to prohibit a system to evolve in a specific direction or to maintain a system at a given position to extensively sample the corresponding essential subspace. The latter case allows the calculation of energy profiles of functional transitions by umbrella sampling (see next chapter). A comprehensive review of PCA and ED simulations was written by Hayward and de Groot.<sup>426</sup>

### **2.1.2 Umbrella sampling**

Umbrella sampling was introduced by Torrie and Valleau in 1977 to conduct free energy calculations by increased sampling of system transitions. For the mathematical background of this method, the reader is referred to the original paper<sup>427</sup> and the book section “Free Energy Calculations” in “Understanding Molecular Simulation” by Frenkel and Smit.<sup>428</sup> In order to achieve sufficient sampling of transitions, especially of short-lived energy barriers, an artificial biasing, usually a harmonic, potential is introduced. For good sampling, it is more efficient to use multiple umbrella windows along the transition pathway of interest, called reaction coordinate. Sampling of the transition has to occur in equilibrium as the free energy is a property of equilibrium. Therefore, for each umbrella window a certain equilibration time is discarded so that only equilibrated sampling in response to the biasing potential is taken into account. After sufficient sampling of the reaction coordinate by umbrella sampling simulations, the free energy profile can be calculated by making use of algorithms such as the weighted histogram analysis method (WHAM).<sup>429,430</sup> For a robust calculation of the free energy by WHAM, sufficient overlap of the sampling distribution of umbrella windows is essential. The idea of WHAM is to estimate the global distribution of sampling by a weighted average of the distributions of the individual windows.<sup>431</sup> Additionally, recent progress has been made in estimating the statistical errors of energy profiles calculated with WHAM.<sup>432</sup>

## **2.2 Two-electrode voltage clamp**

TEVC experiments were conducted as a visiting researcher in the laboratory of Michael C. Sanguinetti at the Nora Eccles Harrison Cardiovascular Research and Training Institute, University of Utah, USA. Using this well-established experimental setup for ion channel recordings, we set out to shed light on the drug trapping phenomenon in hERG K<sup>+</sup> channels (see chapter 4.4, page 107)

Many reviews and book chapters have been written about voltage clamp and its application.<sup>433–436</sup> In this chapter, the basic theory of TEVC will be discussed as well as the

specific methodological approach used for the hERG channel recordings. The concept of voltage clamp was first described by Cole<sup>437</sup> and Marmont<sup>438</sup> in the late 1940s by applying an internal current supplying electrode and an external electronic feedback on squid giant axons. This first approach allowed them to control the cell membrane potential. The technique was further developed by Hodgkin et al. by adding an internal voltage measuring electrode and was consequently termed “voltage clamp” by them.<sup>439</sup> This improvement allowed the control of the membrane potential and at the same time the measurement of the membrane voltage changes induced by ionic currents. For their seminal work describing how membrane currents give rise to an action potential in nerve fibres,<sup>25</sup> Hodgkin and Huxley received the Nobel Prize in Physiology or Medicine in 1963.<sup>440</sup>

Since then, the principle concept of two-electrode voltage clamp experiments remained unchanged. The first electrode, the internal voltage electrode, measures the transmembrane voltage (membrane potential) relative to an external grounding electrode. The second internal electrode, the current electrode, supplies current into the cell. Based on this setting, the membrane potential can be set to a defined holding potential or command potential. To maintain the defined command potential, TEVC uses negative feedback where the measured membrane potential is compared to the command potential. The difference is amplified by an amplifier and current is passed into the cell to set the difference between membrane potential and command potential to zero. Thus, the negative feedback of TEVC produces a current which is equal and opposite to the ionic current that is of interest in ion channel studies.

In our drug trapping investigations, the two hERG mutant channels D540C-L666C and S660C were studied by TEVC recordings in *Xenopus laevis* oocytes. *Xenopus laevis* frogs were anesthetized by immersion in 0.2 % tricaine methanesulfonate solution. The subsequently removed and dispersed ovarian lobes were placed into a  $\text{Ca}^{2+}$ -free saline solution containing type I and II collagenase (2 mg/ml each, Worthington Biochemical Corporation) and shaken for 1-1.5 hours to isolate oocytes from their follicles. The  $\text{Ca}^{2+}$ -free saline solution contained 96 mM NaCl, 2 mM KCl, 1 mM  $\text{MgCl}_2$ , and 5 mM HEPES. The pH was adjusted to 7.6 with NaOH. Selected Stage IV and V oocytes were injected with the cRNA of either D540C-L666C or S660C hERG channels. Subsequently, oocytes were incubated at 17 °C for 1-7 days in Barth's saline solution containing 88 mM NaCl, 1 mM KCl, 0.41 mM  $\text{CaCl}_2$ , 0.33 mM  $\text{Ca}(\text{NO}_3)_2$ , 1 mM  $\text{MgSO}_4$ , 2.4 mM  $\text{NaHCO}_3$ , 10 mM HEPES, and 1 mM pyruvate plus gentamycin (50 mg/l); pH was adjusted to 7.4 with NaOH.

Whole-cell hERG currents were recorded at room temperature by using the TEVC technique.<sup>441</sup> Agarose-tipped microelectrodes were prepared by filling 1-mm borosilicate pipettes with 1 % agarose dissolved in 3 M KCl and subsequent back-filling with 3 M KCl. In the presence of oxidizing and reducing agents, agar bridges of 1 % agarose in 3 M KCl were

used for the reference electrodes. Oocytes were placed in a 0.3 ml oocyte chamber (RC-1Z; Warner Instruments) and superfused with KCM211 solution that contained 98 mM NaCl, 2 mM KCl, 1 mM  $\text{CaCl}_2$ , 1 mM  $\text{MgCl}_2$ , and 5 mM HEPES, pH adjusted to 7.6 with NaOH. For disulfide bond forming and breaking experiments, tert-butyl hydroperoxid ( $\text{tbHO}_2$ ; 0.5 mM for D540C-L666C, 1 mM for S660C; Sigma-Aldrich) and 20 mM dithiothreitol (DTT; Sigma-Aldrich) were added to the KCM211 solution, respectively. A GeneClamp 500 amplifier, a Digidata 1322A data acquisition system and the pCLAMP 9 software (Molecular Devices) were used to operate command voltage steps and to record digitized current and voltage signals. For  $\text{IC}_{50}$  recordings, oocytes were voltage-clamped to a holding potential of -90 mV. 1-s test pulses to a potential of +20 mV were applied every 3 s. Tail currents were recorded at -70 mV and normalized to the current of control sweeps. The concentration-effect relationship was fitted with a Hill equation. In case of the disulfide bond forming experiments, the test pulse was set to +40 mV, as described by Ferrer et al.,<sup>127</sup> while the rest of the voltage protocol remained the same. For I-V relationship, the holding potential was set to the  $\text{K}^+$  reversal potential in the KCM211 solution of -95 mV. 2-s test pulses were applied in a range from -80 to +70 mV in 10 mV increments. Tail currents were recorded at -70 mV and normalized to the maximal tail current obtained at 70 mV. Currents were then plotted as a function of the preceding voltage step and fitted to a Boltzmann function to determine the half-point of activation ( $V_{1/2}$ ).

### 3 Motivation

Since the first description of the importance of ionic currents through channels by Hodgkin and Huxley in the 1950s,<sup>25</sup> ion channels have been subject to extensive research. Their ubiquitous expression in the human body and their involvement in virtually all physiological processes render ion channels important drug targets. While the function of ion channels is well understood from an electrophysiological point of view, the atomistic details of ion channel gating still lack important insights. Crystal structures of ion channels mark a major breakthrough in our understanding of channel architecture and have provided elementary information of the conformations that ion channels can adopt in different channel states (for a list of available crystal structures see <sup>442</sup>). However, as ion channels are highly dynamical proteins that respond to various triggers, knowledge of the local and global conformational changes during gating on an atomistic level is of particular interest. Additionally, it was shown that a plethora of drugs targeting ion channels are crucially dependent on the channel state to develop their blocking potency. As the binding site for these drugs is located within the channel cavity, the pore gate needs to be open to allow access of the drugs.<sup>186,187,200,443</sup> Based on the state dependence of drug block, the trapping phenomenon was identified in K<sup>+</sup> channels which is characterized by a slow recovery from block from the closed channel state.<sup>201,203</sup> These two observations, state dependent block and trapping, further emphasize the importance of understanding channel gating.

Herein, we investigated the gating dynamics of KcsA, hERG, and KirBac1.1 to identify channel specific differences in pore gating among K<sup>+</sup> channels. Specifically, we studied global conformational changes of the pore gate and local rearrangements of pore lining amino acids. A major challenge in these studies is the slow time course of pore gating occurring in native K<sup>+</sup> channels (usually in the ms range). To date, simulations of complex membrane proteins on such time scales are limited to special purpose computers<sup>409</sup> and were not applicable in our studies. Therefore, two different approaches were used to simulate gating. In case of KcsA and hERG (chapter 4.1, page 37 and chapter 4.3, page 72), we made use of the ED technique, described in the method section, which allows enhanced sampling of the gating transition pathway. For investigations on Kir channel gating (chapter 4.2, page 49), a point mutation was introduced in the TM2 helix which drastically increases the open probability of the channel<sup>444</sup> and enabled gating simulations on the ns time scale.

The trapping phenomenon was described for various hERG blockers (chapter 1.3.5, page 16). However, it remained elusive which structural descriptors of blockers or specific interactions with the channel cause trapping. A recent study showed that trapped drugs carry a higher pro-arrhythmic risk.<sup>445</sup> This finding further emphasizes the stringent necessity of a

detailed understanding of the trapping process. Therefore, we addressed three major questions. First, do specific amino acids in the channel cause trapping? Second, when does the drug get trapped during gate closure? And third, does the trapped drug influence the global gating movements of the channel? To probe the first question, gating simulations with a trapped compound were conducted in KcsA and hERG. Additionally, force probe MD simulations and umbrella sampling were performed to determine at which state the drug gets trapped (chapter 4.3, page 72). To study the impact of trapped drugs on the global gating behavior, the applicability of an experimental TEVC approach was probed during a research stay in the laboratory of Michael C. Sanguinetti (chapter 4.4, page 107).

## 4 Results

### 4.1 Probing the energy landscape of activation gating of the bacterial potassium channel KcsA

---

Linder T, de Groot BL, Strydom A

*PLoS Computational Biology*

2013 May 9(5), e1003058

# Probing the Energy Landscape of Activation Gating of the Bacterial Potassium Channel KcsA

Tobias Linder<sup>1</sup>, Bert L. de Groot<sup>2</sup>, Anna Stary-Weinzinger<sup>1\*</sup>

**1** Department of Pharmacology and Toxicology, University of Vienna, Vienna, Austria, **2** Computational Biomolecular Dynamics Group, Max Planck Institute for Biophysical Chemistry, Göttingen, Germany

## Abstract

The bacterial potassium channel KcsA, which has been crystallized in several conformations, offers an ideal model to investigate activation gating of ion channels. In this study, essential dynamics simulations are applied to obtain insights into the transition pathways and the energy profile of KcsA pore gating. In agreement with previous hypotheses, our simulations reveal a two phasic activation gating process. In the first phase, local structural rearrangements in TM2 are observed leading to an intermediate channel conformation, followed by large structural rearrangements leading to full opening of KcsA. Conformational changes of a highly conserved phenylalanine, F114, at the bundle crossing region are crucial for the transition from a closed to an intermediate state. 3.9  $\mu$ s umbrella sampling calculations reveal that there are two well-defined energy barriers dividing closed, intermediate, and open channel states. In agreement with mutational studies, the closed state was found to be energetically more favorable compared to the open state. Further, the simulations provide new insights into the dynamical coupling effects of F103 between the activation gate and the selectivity filter. Investigations on individual subunits support cooperativity of subunits during activation gating.

**Citation:** Linder T, de Groot BL, Stary-Weinzinger A (2013) Probing the Energy Landscape of Activation Gating of the Bacterial Potassium Channel KcsA. *PLoS Comput Biol* 9(5): e1003058. doi:10.1371/journal.pcbi.1003058

**Editor:** Emad Tajkhorshid, University of Illinois, United States of America

**Received:** November 22, 2012; **Accepted:** March 27, 2013; **Published:** May 2, 2013

**Copyright:** © 2013 Linder et al. This is an open-access article distributed under the terms of the Creative Commons Attribution License, which permits unrestricted use, distribution, and reproduction in any medium, provided the original author and source are credited.

**Funding:** This work was supported by the Austrian Science Fund (FWF; Grants P22395, W1232; <http://www.fwf.ac.at>). Tobias Linder was supported by a research fellowship 2013 from the University of Vienna. The funders had no role in study design, data collection and analysis, decision to publish, or preparation of the manuscript.

**Competing Interests:** The authors have declared that no competing interests exist.

\* E-mail: [anna.stary@univie.ac.at](mailto:anna.stary@univie.ac.at)

## Introduction

K<sup>+</sup> channels play a crucial role in a wide variety of physiological and pathophysiological processes including action potential modeling [1], cancer cell proliferation [2], and metabolic pathways mediation [3]. In the last few decades, the understanding of ion channels has increased tremendously. The Hodgkin-Huxley equations [4] provided first insights into the ion flow in nerve cells and Hille showed a comprehensive picture of the electrophysiological properties of ion channels [5]. In 1998, the first crystal structure of an ion channel, the bacterial potassium channel of *Streptomyces lividans* (KcsA), shed light on the molecular details of a K<sup>+</sup> channel [6]. The pore-forming domain of KcsA is composed of four identical subunits (SUs) which are arranged symmetrically around a channel pore. Each SU consists of two transmembrane helices, TM1 and TM2, which are connected by the P-helix and the selectivity filter (SF) (Figure 1B). While the extracellular facing SF tunes the selection of different ions and modulates inactivation, the main conformational changes regulating ion flow, are found at the TM2 helices. These motions, referred to as activation gating, are thought to involve an iris-like motion of the TM2 helices that constrict the permeation pathway at the helix bundle crossing region [7–10]. This region is believed to form the main activation gate. Starting in 1998, several different pore domain structures of KcsA in its closed state [6,11] and more recently in intermediate and open states have been solved [12]. These crystal structures provide excellent insights into different conformations of proteins; however, they feature only snapshots of dynamical proteins [13].

Therefore, the transition steps and the mechanisms of activation gating are still unknown.

A number of computational studies have been published over the last years, aiming at exploring the gating pathways of ion channels by making use of available X-ray structures as templates [14–22]. However, the lack of particular K<sup>+</sup> channels in different conformations was a limitation of previous publications. Thus, these studies had to compare crystal structures of different channels or had to rely on homology models of open structures of KcsA. With the successful crystallization of intermediate and open structures of KcsA by Cuello et al in 2010 [12], *in silico* activation gating of K<sup>+</sup> channels cannot only be readdressed, but also allowed us to calculate a complete energy profile of activation gating. The essential dynamics (ED) simulation method has been shown as a useful tool to investigate sampling of proteins in conformational space and to derive transition pathways between conformational states [23–27]. In this study, we applied ED simulations combined with umbrella sampling calculations to investigate activation gating of KcsA.

## Results/Discussion

### Stability of closed and open conformations

A prerequisite of the ED method is that the starting and target structures are of equal length and identical amino acid sequence. Thus, the KcsA crystal structures (pdb identifier: 1k4c, closed; 3fb6, intermediate; 3f7v, open) were adjusted at the N- and C-termini so that all states started from residue 29 and ended at

## Author Summary

Voltage gated ion channels are membrane embedded proteins that initiate electrical signaling upon changes in membrane potential. These channels are involved in biological key processes such as generation and propagation of nerve impulses. Mutations may lead to serious diseases such as cardiac arrhythmia, diabetes or migraines, rendering them important drug targets. The activity of ion channels is controlled by dynamic conformational changes that regulate ion flow through a central pore. This process, which involves opening and closing of the channels, is known as gating. To fully understand or to control ion channel gating, we need to unravel the underlying principles. Crystal structures, especially of K<sup>+</sup> channels, have provided excellent insights into the conformation of different channel states. However, the transition states and structural rearrangements are still unknown. Here we use molecular dynamics simulations to simulate the full transition pathway and energy landscape of gating. Our results suggest that channel gating involves local structural changes followed by global conformational changes. The importance of many of the residues identified in our simulations is supported by experimental studies. The ability to accurately simulate the gating transitions of ion channels may be beneficial for a better understanding of ion channel related diseases and drug development.

residue 118, leading to channels with four times 89 amino acids. Additionally, Q117 in the open and intermediate crystal structure was mutated to arginine to obtain the wild type structure.

Before probing the transition pathway between closed and open conformations of KcsA, the stability of the different channel states was assessed in molecular dynamics (MD) simulations. Repeated simulations (3 times 50 ns) of the structures, embedded in a lipid-bilayer membrane, were performed. The root-mean-square deviation (RMSD) of the backbone atoms without loops of all three channel states is less than 2 Å (Figure S1). The stability of the closed state is similar to previous values reported in literature [28,29]. Moreover, the RMSD of the intermediate state is comparable to the two other states with a RMSD of 1.75 Å.

## Activation gating simulated by essential dynamics

To investigate the activation pathway, the backbone atoms of closed and open structures without loops were compared by principal component analysis (PCA). The resulting eigenvector (EV) was used to enforce the transition between the two states. Thus, the ED simulation is a free MD simulation, with all coordinates equilibrating except for one coordinate that is biased to drive the gating transition. Ten opening and ten closing ED simulations, all of them lasting for 20 ns, were carried out. In the following paragraphs, results of opening simulations are explained in detail. Since similar observations were also found in the reversed direction, results for the closing runs are summarized at the end of this section and corresponding figures are shown in the supplemental material.

The conformational changes during the ED opening simulations were analyzed by monitoring the RMSD as a function of time (Figure 1A). The deviation from the target structure (open conformation, pdb identifier: 3f7v) was measured over time. The difference between the starting and target structure is 4 Å. In all ten opening ED simulations, the RMSD values steadily decreased and reached final values between 1.35 and 2.20 Å, indicating that all simulations reached the open state. Successful opening is defined by a decrease of the RMSD to approximately 2 Å

compared to the target structure. For simplicity, the average RMSD and standard deviation of the ten simulations were calculated. On average, a final RMSD of 2 Å as shown in Figure 1A was reached. The standard deviation indicates that in the first 11 ns, the RMSD values of the simulations did not vary. However, in the subsequent simulation time at which the simulations reached the target structure, the RMSD of the ten simulations showed wider distribution.

To investigate the conformational states of the end structures, the deviation of the C $\alpha$  atoms from the target structure was analyzed. An average structure of the ten ED simulations was generated which exhibits minimal RMSD (Figure 1B). This average structure revealed that ED simulations were able to reach the target structure. Figure 1B shows the color coded deviation of each C $\alpha$  atom from the open structure. As expected, the TM1 and P-helices displayed a very modest RMSD deviation of 0.05 Å to the target structure since there are no conformational changes in these regions during activation gating. In contrast, deviations up to 3 Å were found in the C-termini of the TM2 helices, which undergo large conformational changes during channel opening. Additionally, large deviations were found in the loop regions due to the high mobility of loops. Investigations on the loop region (amino acid G56) showed that mutations did not influence gating [30,31]. Thus, the loops were not investigated further.

The program HOLE [32] was used to calculate the activation gate radius profiles (Figure 2) of the backbone atoms of different channel states. In the closed conformation, the constriction of the activation gate features a diameter of 5.9 Å. In the intermediate state, the diameter of the constriction site is 8.3 Å. In the open conformation, the activation gate diameter expands to 11.8 Å. The diameter of the activation gate in the ED simulations reached 10.7 Å on average. The shape of the pore radius profile of the end structures obtained from ED simulations matched the essential features of the profile of the open crystal conformation, further indicating that the simulation derived structures adopted the open state.

The major motions of opening were also observed in the reversed direction during closing (see Figure S2). However, only seven out of ten ED simulations successfully closed (RMSD < 2.3 Å). Careful inspection revealed that the underlying reason for unsuccessful closure of three runs was partial unwinding of single TM2 helices. This observation may suggest that optimal packing of helices at the bundle crossing region is important for channel closure.

## Coupling between activation gate and SF

As described in the method section, no forces were applied to the side chains in the simulations. Hence, the simulations allowed investigations of the rotameric side chain changes coupled to gating. A phenylalanine, F103, present in the TM2 helices of KcsA, was shown to change its rotameric state upon activation gating [12,21] and affecting the SF conformation [33,34]. Therefore, the  $\chi_1$  angle dynamics in the ten ED simulations were analyzed (Figure 3A). F103 can adopt two different rotameric states which are called “up” ( $\chi_1$  angle of  $-55$  to  $-72^\circ$ ) and “down” state ( $\chi_1$  angle of  $-166$  to  $-185^\circ$ ). In the first 5 ns of the opening ED simulations, F103 was stable in the up state. Subsequently, the conformational changes of the channel allowed F103 to adopt the down state. The F103 amino acids switched from the up to the down state over the next 15 ns. In most of the cases, this change was irreversible. Once F103 was in the down state, it was not able to switch to the up state again. After 20 ns, 78% of all F103 were in the down state. To validate if the F103 rotameric changes occurred because of activation gating, dihedral

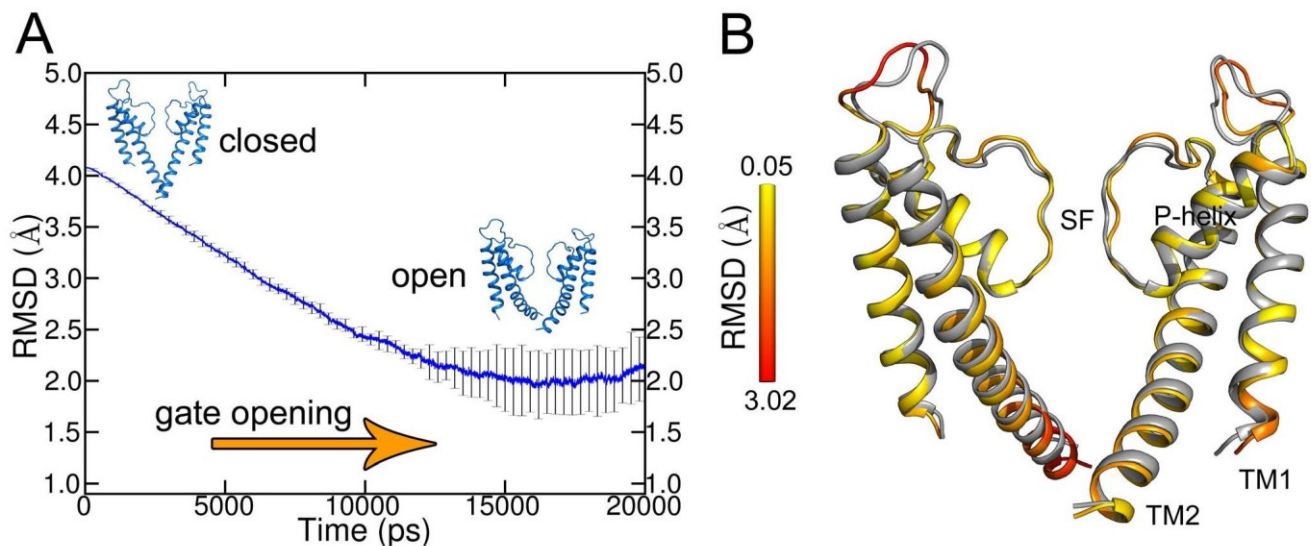


**Figure 1. RMSD analysis of ED opening simulations.** A) Average of the backbone RMSD (without loops) of ten opening ED simulations. The open crystal structure was used as reference. The standard deviation is indicated by error bars. B) Comparison of the average structure (built out of the minimal RMSD structures of the ten ED simulations; yellow to red) and the open crystal structure (gray). The RMSD of the C $\alpha$  atoms is shown as a spectrum from yellow to red. For the sake of clarity, only the two opposite SUs are shown.  
doi:10.1371/journal.pcbi.1003058.g001

angles of unbiased open and closed state MD simulations were analyzed (data not shown). In the open state, all F103 of the three 50 ns MD simulations were in the down state. In the closed conformation, F103 showed more flexibility. Initially in the up state, the F103 was able to change to the down state; however, the up state is observed more frequently. This finding is in agreement with adiabatic energy maps of Pan et al [34] and a study by Cuello et al [33]. The dynamic behavior of F103 in the closing ED simulations is shown in Figure S2. In the first 2 ns, F103 was stable in the down state. Subsequently, F103 can adopt both up and down states as expected from the energy maps of Pan et al [34].

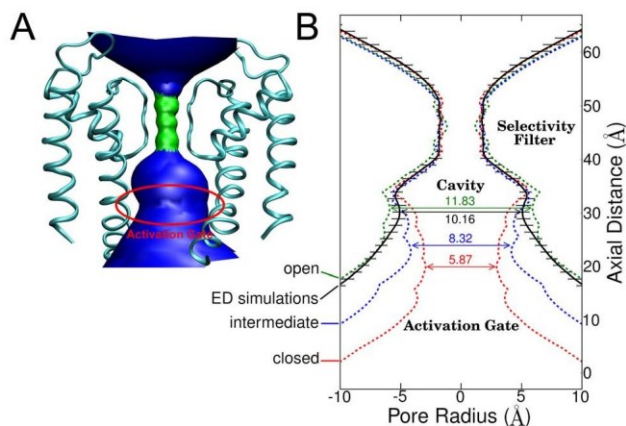


**Figure 2. Pore radius profiles derived from backbone atoms of channel states.** A) 3D representation of the pore domain depicting the HOLE profile. For the sake of clarity, only two opposing SUs are shown. B) Comparison of the profiles formed by the closed (red dashed line), intermediate (blue dashed line), and open (green dashed line) crystal structures with the average of the ten ED simulation structures (black dashed line). The subtle differences of the ED simulation structures in the activation gate region are indicated as standard deviation by error bars.  
doi:10.1371/journal.pcbi.1003058.g002

Despite different SF conformations in the closed and open crystal structures (activated vs. inactivated), the SF in all ten opening simulations did not adopt the inactivated conformation as seen in the crystal structure (pdb identifier: 3f7v; Figure 3B–E). The stability of the SF of the ED derived open conformation is further supported by a 100 ns free MD simulation, where no changes in the filter were observed. Previous studies reported that side chain

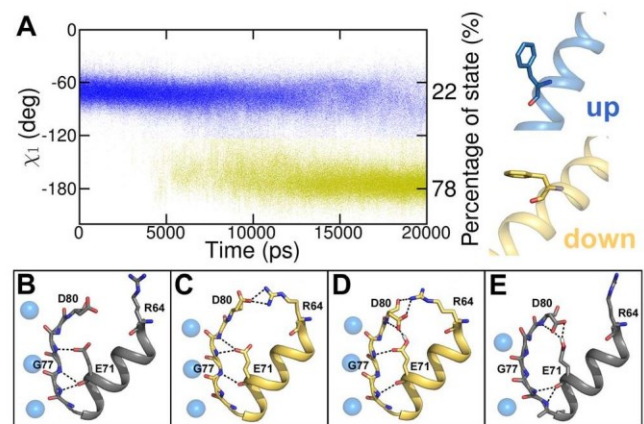


**Figure 3. Conformational changes of F103 during activation gate opening and SF conformations of channel states.** A) Analysis of  $\chi_1$  angle dynamics of F103 (in ten opening ED simulations). Changes of the F103 orientation ( $\chi_1$  angle) were measured over time. An angle of  $-70^\circ$  indicates the “up” state (blue) while an angle of  $-180^\circ$  represents the “down” state (yellow). The percentage of state was calculated from the end states at 20 ns of the ten ED simulations. B) SF and P-helix of the closed crystal structure (gray). Blue spheres represent K $^+$  ions. C) SF and P-helix at the end of the 20 ns ED simulation structure with deprotonated E71 (yellow). D) SF and P-helix at the end of the 20 ns ED simulation structure with protonated E71 (yellow). E) SF and P-helix of the open inactivated crystal structure (gray). The G77 conformation defines the SF state as it was shown by Cuello et al. [12].  
doi:10.1371/journal.pcbi.1003058.g003

hydrogen bonds between D80 and a protonated E71 promote inactivation of the SF [35–37]. Hence, we performed ED simulations with protonated E71 amino acids and analyzed the SF conformation. These simulations revealed similar conformations, irrespective of the protonation state. This conformation might be influenced by the ion occupancy in the filter. The ions were located at the most favored positions S0, S2, and S4 since the simulations started from a conductive state [38].

### Free energy profile of activation gating

Umbrella sampling was employed to investigate the free energy landscape of activation gating (Figure 4A). The ED simulation with the lowest RMSD was used for a subsequent PCA calculation and thereof the first EV was employed as reaction coordinate. MD simulations of closed, intermediate, and open states were projected onto this reaction coordinate to determine sampling regions of the crystal structures. Three main energy wells, separated by two energy barriers, were identified. The first energy well, which is sampled by the closed state, is located at  $-0.7$  to  $3.1$  nm. The intermediate state is sampled at the adjacent energy well, separated by a small energy barrier at  $4$  nm (barrier 1) from the closed state. Broad sampling of the intermediate conformation was observed, ranging from  $3.4$  to  $7.4$  nm. The subsequent large energy barrier at  $9$  nm (barrier 2) separates the open conformation from the intermediate state. The open conformation samples a relatively small energy well ranging from  $8.8$  to  $11.4$  nm. Next, we investigated the underlying structural rearrangements shaping the energy wells and barriers.

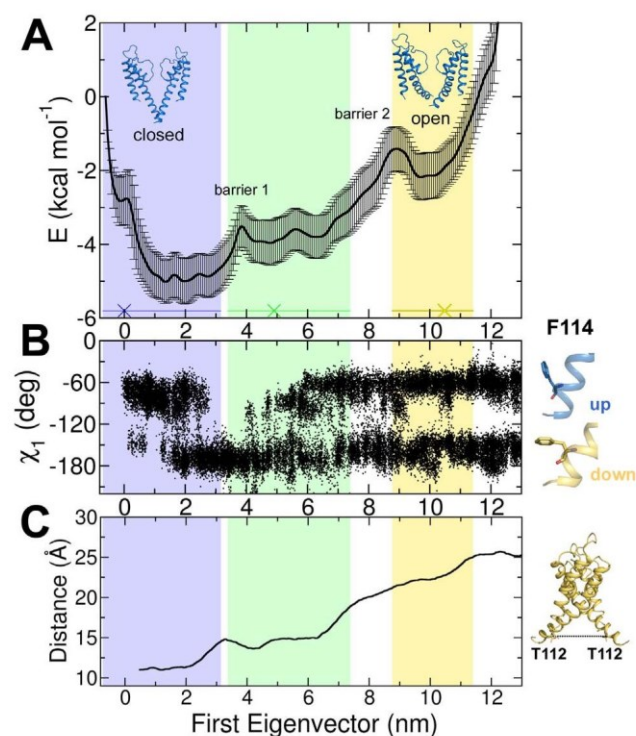


**Figure 4. Free energy profile of gate opening.** The blue, green, and yellow shades depict the sampling of the closed, intermediate, and open structures along the first EV. A) Free energy profile of the activation gate opening derived from  $3.9 \mu\text{s}$  umbrella sampling simulations. The X marks indicate the positions of the crystal structures. B)  $\chi_1$  angle dynamics of all four F114 during activation gating. C) Distance between opposite T112 as a measure of pore opening. doi:10.1371/journal.pcbi.1003058.g004

### Local structural rearrangements correspond to energy barrier 1

By analyzing the dihedral angles of all side chains, a single residue in the helix bundle crossing region was identified (F114) whose conformational changes correspond to the first energy barrier (Figure 4B). This unique rotameric pattern of F114 was observed in all ten opening ED simulation runs suggesting that this pattern was essential for activation gating (Figure 5A). In the early stage of activation gating (after  $5$  ns),  $80\%$  of all F114 changed from an up state ( $\chi_1$  angle of  $-55$  to  $-72^\circ$ ) to a down state ( $\chi_1$  angle of  $-166$  to  $-185^\circ$ ). After the change to the down state, a rigid phase from  $5$  to  $10$  ns was observed. Subsequently, F114 regained its flexibility. This suggests that the first flip of F114 and the changes in interacting amino acids may cause energy barrier 1. Consequently, interacting amino acids were analyzed in more detail. Figure 5B–E depicts residues that interact with F114 over time. Residues L110, W113, and R117 of TM2 and L105 of the adjacent TM2 helix interacting in all states are shown in green. Additional interacting amino acids in the closed state were A108, A109, and T112 of the adjacent TM2 (Figure 5B). In the rigid transition state (Figure 5C), additional interactions to V115 were observed. In the open state, interactions with T101 and S102 of the neighboring TM2 were found. When F114 occupied the down state, it was in close contact with A32 of the adjacent TM1 helix. F114 interacted with L35 (adjacent TM1 helix) independently of the rotameric state, indicating a specific interaction pattern. The importance of the F114 and adjacent amino acids is supported by experimental mutation studies (see section “relation to experimental data”).

The dynamical behavior of the F114 side chain is further supported by free MD simulations of the open and closed state. In the open state,  $75\%$  of the  $12$  F114 side chains in the MD simulations adopted the down state. Flipping between the two states occurred as a rare event, indicating that the F114 side chains showed high stability over  $50$  ns. An increased flexibility of F114 was observed in the closed state. Although  $80\%$  of the F114 side chains adopted the initial up state, flipping between the two states was observed frequently. Nevertheless, the specific rotameric pattern of F114 as seen during the ED simulations did not occur, indicating that this rotameric pattern is unique for activation gating. Additionally, these analyses showed that not only F103 but also F114 is allowed to adopt two rotameric states in the closed conformation.

### Global conformational changes of TM2 correspond to energy barrier 2

$\text{C}\alpha$ - $\text{C}\alpha$  distances between two opposite T112 residues (TM2) as a measure of activation gate opening (as proposed by Cuello et al [12]) were found to correlate with the energy barriers (Figure 4C). This measurement allows direct comparison of ED derived conformational states (closed, intermediate, and open) to the crystal structures. At the first energy barrier, an initial conformational change of the activation gate from  $12 \text{ \AA}$  to  $14 \text{ \AA}$  was observed correlating to structural rearrangements of F114. In the subsequent plateau phase of opening, a good correlation with the energy wells of the intermediate structures was observed. The second energy barrier is linked to a distance increase of  $8 \text{ \AA}$  between the two opposing T112 residues. This suggests that the second energy barrier is mainly caused by global conformational changes of TM2. To further test the significance of this two-phasic activation gate opening, the T112 distances of all ten opening ED simulations were analyzed. Again, a two-phasic gating with global conformational changes at  $4$  to  $5$  ns and at  $7.5$  to  $16$  ns was found

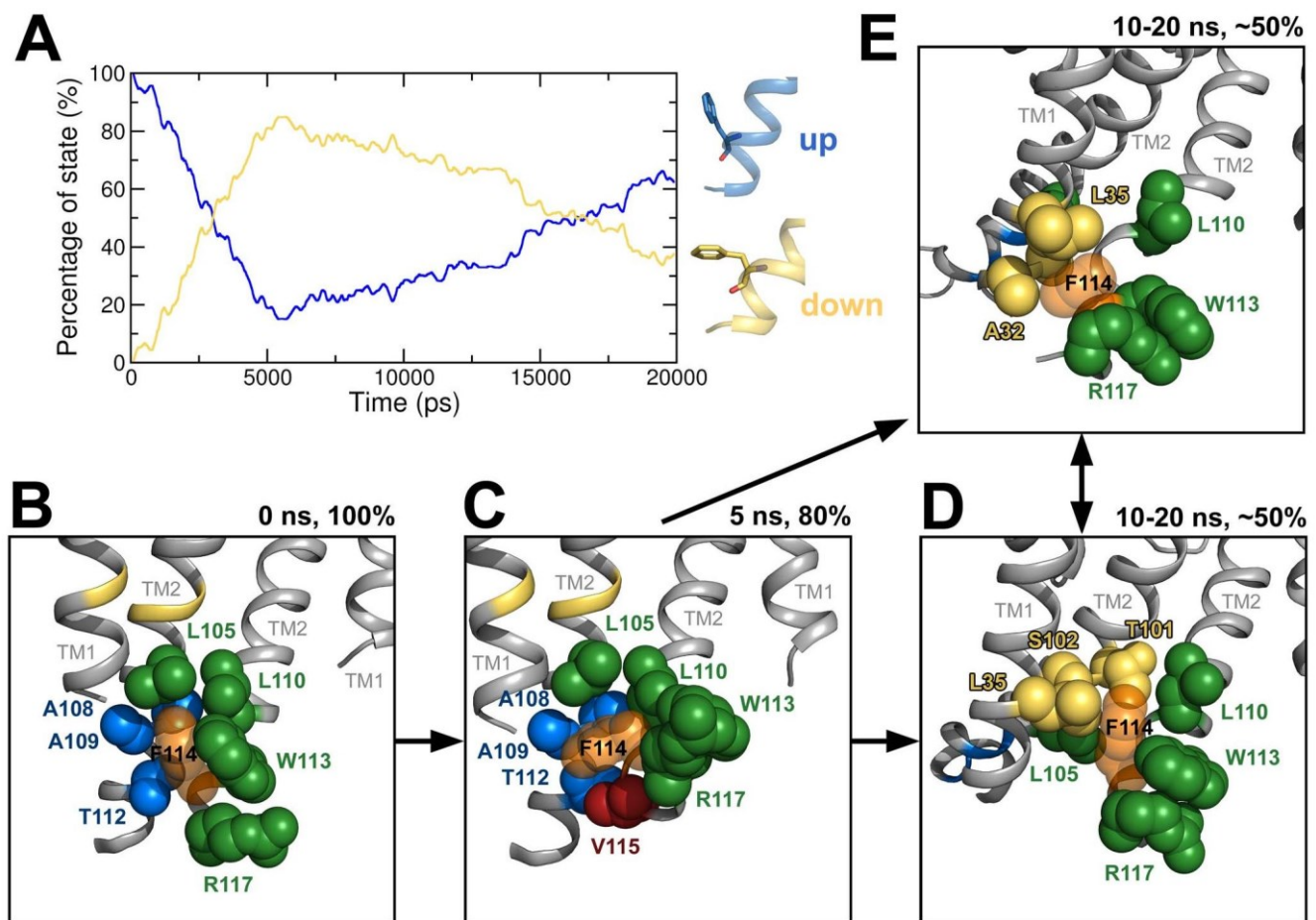


**Figure 5. Analysis of  $\chi_1$  angle dynamics of F114 and influence on packing.** A) Percentage of F114 in the up (blue) and down (yellow) state over time. Packing of the F114 (transparent orange spheres) in the closed conformation (B), the transition state (C), the open states with F114 in the up (D) and the down state (E). Amino acids interacting in all states are shown in green. Interacting amino acids in the closed/open/transition state are represented in blue/yellow/red.  
doi:10.1371/journal.pcbi.1003058.g005

(Figure S3). These findings are in line with previous computational studies, which showed that the main opening of the gate occurs after an initial unlock from the closed state by structural rearrangements of amino acids [18,21]. Additionally, simulations in the reverse direction showed similar local and global structural rearrangements in inverse order supporting the validity of the simulations.

#### Relation to experimental data

The transition pathways obtained by the ED simulations are in good agreement with experimental data. First, the simulations are able to sample the intermediate crystal structure (pdb identifier: 3f7v; green shaded energy well in Figure 4A) [12], which was not included in our ED simulation protocol. Secondly, as expected [13], KcsA crystal structures 1k4c, 3f7v, and 3fb6 occupy energy wells in our calculated energy profile (Figure 4A). Thirdly, the energy profile indicates that the pore is intrinsically more stable in the closed conformation. This observation is supported by experimental studies on potassium channels [39–41], although it should be noted that the latter two studies were carried out on shaker-like channels, rendering the comparison indirect. Further, residues involved in pH sensing of KcsA were not included in the simulated system, which may also affect stability.

Simulations support the hypothesis that the F114 conformational changes are crucial to trigger initial activation gating.

Mutational studies have shown the important role of the tightly packed helix bundle crossing region including F114. Several mutations in this region revealed a destabilization of the closed conformation [39,42]. The fact that F114 is conserved in many K<sup>+</sup> channels additionally underlines the importance of this aromatic amino acid for channel function [40,43–46]. Mutational analysis of interacting amino acids in the open state like L35, T101, and T102 (analyzed in Shaker [40,47]) or A32 would be of great interest and may lead to new insights into the packing of F114 in the open state.

#### Lipid interactions of TM2 helices during activation gating

Since the C-terminus of the TM2 helices moves from a water environment towards the lipid/water interface during activation gating, interactions between the TM2 helices and lipids were investigated. Analyses revealed that the number of hydrogen bonds between the hydrogen bond forming residues W113 and R117 and the lipid head groups increased during gate opening (Figure 6). This indicates that the C-terminus of TM2 moved towards the inner leaflet of the bilayer membrane while hydrogen bonds are mainly formed between R117 and the phosphate groups of the lipids. A decrease of hydrogen bonds was found for the closing simulations (Figure S4) while TM2 moves back from the lipid environment to the water environment.

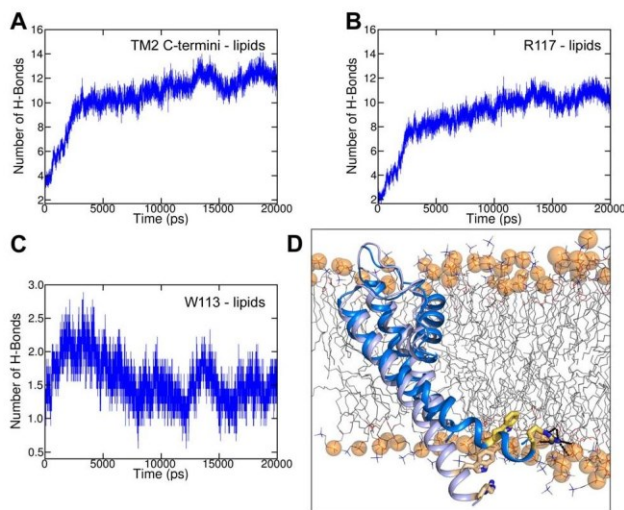


**Figure 6. Lipid interactions of TM2 helices during activation gate opening.** A) Average number of H-bonds between H-bond forming residues (W113 and R117) of the C-terminal TM2 helices and lipid head groups was measured over time. B) Average number of H-bonds of R117 with lipids. C) Average number of H-bonds of W113 with lipids. D) Representation of one SU in the closed (light blue) and open (marine blue) conformation with lipids. H-bond forming residues W113 and R117 are shown as yellow sticks. Lipids are depicted as gray lines while phosphate groups are shown as orange spheres. Dashed black lines represent H-bonds.

doi:10.1371/journal.pcbi.1003058.g006

### Cooperativity of activation gating

ED simulations were applied on one, two, and three SUs, respectively, while the other SUs were allowed to move freely. Simulations revealed that at least three SUs are necessary to open the activation gate. RMSD analyses of simulations with the ED method applied on one and two SUs showed that there was only a slight decrease in RMSD over time suggesting that the channel remained in the closed state. However, simulations with the ED method applied on three SUs revealed that the end structures deviated 2.5 Å from the target structure (Figure 7). Cooperativity analyses of ED simulations presented in this study support previous studies on cooperativity of potassium channels in general [48–51] and of the pore domain in particular [19,21,52,53]. Our simulations indicate that movement of one SU or two SUs is insufficient to open the gate. However, opening of three SUs is sufficient to obtain an open gate structure. Comprehensive investigations on cooperativity are subject of further studies.

### Conclusion

The results presented here show that the ED simulation approach successfully sampled transition pathways between closed and open states of an ion channel on the nanosecond time scale and allowed investigations on activation gating. There is good agreement between our investigations and previous experimental and computational studies, supporting the validity of this approach. The simulations provided new insights into conformational changes during gating and revealed that activation gating occurs as a two phase process. Additionally, investigation of the energy landscape allowed the correlation of conformational changes to energy barriers at the atomistic level. The first phase, in which local structural rearrangements in the helix bundle crossing region take place, correlates to a small energy barrier. The second phase was found to correlate with a large second energy barrier. During this phase, the main conformational

changes of the TM2 helices, which occur upon gating, were observed.

In addition, we showed the feasibility of the ED approach to study the cooperativity of activation gating. The simulations suggest that individual SUs cannot open the activation gate. Rather, several SUs have to move in a cooperative manner in order to open the gate.

We expect that ED simulations will be useful for further investigations including the analysis of gating sensitive mutations. This is of special interest with regard to inherited channelopathies. Furthermore, we expect that these simulations will be valuable for studies on drug binding with different channel states.

## Methods

### Simulation setup

The closed (pdb identifier: 1k4c) [54] and open (pdb identifier: 3f7v) [12] crystal structures were used as starting conformations for the ED simulations. Additionally, they were subject to free MD simulations to assess the stability and the side chain dynamics. Free MD simulations of the intermediate conformation (pdb identifier: 3fb6) [12] were performed to investigate the sampling region of the structure along the transition pathway. Since the helices of the open conformation were not crystallized to the same extent as in the closed state (seven amino acids are missing at the beginning of TM1 and six amino acids at the end of TM2), the helix-lengths of the closed crystal structure were adapted by deleting these amino acids. The Q117 in the crystal structure of the open conformation was mutated to arginine in order to obtain the wild type structure using Swiss-PdbViewer [55]. For the intermediate state, one helical turn on the C-terminus was added in PdbViewer to obtain the same length of the helices as for the closed and open conformation. The protein was embedded in an equilibrated membrane consisting of 280 dioleoylphosphatidylcholine (DOPC) lipids using the *g\_membed* tool [56], which is part of the *gromacs* package.  $K^+$  ions were placed in the SF, as described previously [57], at  $K^+$  sites S0, S2, and S4, with waters placed at S1 and S3 of the SF [38].  $Cl^-$  ions were added randomly within the solvent to neutralize the system. All simulations were carried out using the *gromacs* simulation software v.4.5.4 [58]. The *amber99sb* force field [59] and the *TIP3P* model [60] were employed for the protein and water, respectively. Lipid parameter for the DOPC membrane were taken from Siu et al [61]. During all simulations, the area per lipid was at 0.72 nm<sup>2</sup> which is in good agreement with experimental values [62]. Electrostatic interactions were calculated at every step with the particle-mesh Ewald method [63] with a short-range electrostatic interaction cut off of 1.4 nm. Lennard-Jones interactions were calculated with a cut off of 1.4 nm. The LINCS algorithm [64] was used to constrain bonds, allowing for an integration step of 2 fs. The Nose-Hoover thermostat was used to keep simulation temperature constant by coupling ( $\tau = 0.5$  ps for equilibration simulations and  $\tau = 0.2$  ps during unrestrained simulations) the protein, lipids and solvent (water and ions) separately to a temperature bath of 310 K. Likewise, the pressure was kept constant at 1 bar by using the Parrinello-Rahman barostat algorithm with a coupling constant of 1 ps. Prior to simulation, 1000 conjugate gradient energy-minimization steps were performed, followed by 5 ns of equilibrium simulation in which the protein atoms were restrained by a force constant of 1000 kJ mol<sup>-1</sup> nm<sup>-2</sup> to their initial position. Lipids, ions, and water were allowed to move freely during equilibration.

### Molecular dynamics simulations

In order to assess the stability of the open, intermediate, and closed conformation of the KcsA channel, three 50 ns unrestrained MD simulations were carried out for each structure.

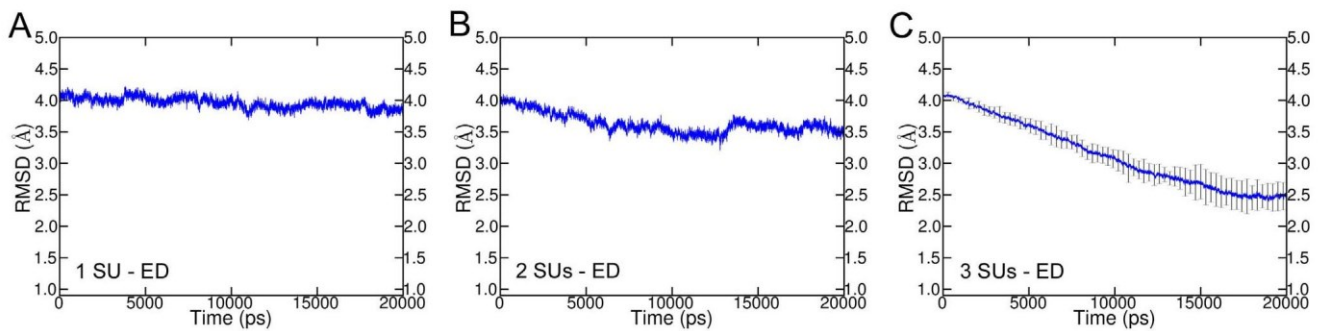


**Figure 7. RMSD of cooperativity simulations.** ED was applied on one (A), two (B), and three (C) SUs. The open structure was used as reference. For simulations with ED applied on one SU and two SUs, only one simulation each was performed. For ED simulations on three SUs, the average of the backbone RMSD without loops of ten simulations was measured. Standard deviation is indicated by the error bars. doi:10.1371/journal.pcbi.1003058.g007

### Principal component analysis

The basic method of the PCA is described in detail elsewhere [65]. A trajectory consisting of the closed and the open conformation was built and used for PCA. Subsequently, the covariance matrix of the positional fluctuations of the TM1, P-helix, and TM2 backbone atoms was built up and diagonalized (loops were excluded from analysis). For the PCA, all four SUs (one, two, and three SUs for cooperativity investigations) of the homotetrameric channel were taken into account. Only one EV with a non-zero eigenvalue results from this PCA, which represents the difference vector between the open and the closed crystal conformation. This vector was used as reaction coordinate for ED simulations.

### Essential dynamics simulations

The ED technique [23,24] can be used to simulate the conformational pathway between two crystal structures [26]. During simulation, the distance along the first EV was increased in fixed increments to drive the system from the closed to the open state and vice versa. It is important to emphasize that the EVs were obtained by PCA of the backbone atoms only and therefore did not contain any information on the side chains. For simulations, the equilibrated closed and open systems, respectively, consisting of the channel, lipid-membrane, ions, and water, were used as start positions. Helical restraints were applied to the last four C-terminal amino acids of the TM2 helix of each SU in order to prevent unwinding. All parameters were set as described above. Simulations were performed on the 20 ns timescale. Fixed increment linear expansion for each simulation step (2 fs) was set to  $1.28 \times 10^{-6}$  nm in order that the target structure was reached after two thirds of the simulation time. For cooperativity investigations, fixed increment linear expansion was set to  $1.89 \times 10^{-7}$  nm,  $6.27 \times 10^{-7}$  nm,  $9.24 \times 10^{-7}$  nm per step (2 fs) and was applied to one SU, two SUs, and three SUs, respectively.

### Umbrella sampling

The windows for the umbrella sampling simulation were taken from the ED simulation with the lowest RMSD. The first EV, which was derived from a PCA of the ED simulation, was used as a reaction coordinate. As this EV is dominant (its eigenvalue is more than an order of magnitude larger than the second largest), we assume that the transition pathway is sufficiently accurately covered by this mode. Along this reaction coordinate, 39 windows with the corresponding structures from the first ED simulation were chosen for umbrella sampling and simulated for 100 ns (Figure S5). 33 windows were simulated with a force constant of

$1 \text{ kJ mol}^{-1} \text{ nm}^{-2}$ . For six windows, the force constant was set to  $100 \text{ kJ mol}^{-1} \text{ nm}^{-2}$  in order to obtain sufficient sampling of the energy barriers. In total, umbrella sampling was performed for 3.9  $\mu\text{s}$ . The first 50 ns of each window were discarded for equilibration. The potential of mean force and the statistical errors of the activation gating energy profile were estimated by making use of the g\_wham tool of gromacs and the integrated bootstrap analysis method [66]. The number of bootstraps was set to 50.

### Supporting Information

**Figure S1 Stability of KcsA channel states.** Backbone RMSD (without loops) of three independent MD simulations of closed (A), intermediate (B), and open state (C) was measured as a function of time. (TIF)

**Figure S2 Analysis of ED closing simulations.** A) Average of the backbone RMSD without loops of seven closing ED simulations. The closed crystal structure was used as reference. The standard deviation is indicated by error bars. B) Conformational changes of F103 during activation gate closing. Analysis of  $\chi_1$  angle dynamics of F103 of the seven ED simulations was performed. Changes of the F103 orientation was measured as  $\chi_1$  angle over time. An angle of  $-70^\circ$  indicates the “up” state (blue) while an angle of  $-180^\circ$  represents the “down” state (yellow). C)  $\chi_1$  angle dynamics of F114 are shown as percentage of F114 in the up (blue) and down (yellow) states over time. (TIF)

**Figure S3 Average of the C $\alpha$ -C $\alpha$  T112-distances of all ten ED simulations.** The standard deviation is indicated by error bars. (TIF)

**Figure S4 Lipid interactions of TM2 helices during activation gate closing.** A) Average number of H-bonds between H-bond forming residues (W113 and R117) of the C-terminal TM2 helices and lipid head groups was measured over time. B) Average number of H-bonds of R117 with lipids. C) Average number of H-bonds of W113 with lipids. (TIF)

**Figure S5 Histograms of the 39 umbrella sampling windows.** The six windows with peaks above 40000 were derived from umbrella sampling with a force constant of  $100 \text{ kJ mol}^{-1} \text{ nm}^{-2}$  (default:  $1 \text{ kJ mol}^{-1} \text{ nm}^{-2}$ ). (TIF)

## Acknowledgments

The computational results presented have been achieved in part using the Vienna Scientific Cluster (VSC). The authors would like to thank Song Ke, Eva-Maria Zangerl, and Julia Praxmarer for critical reading of the manuscript.

## References

- Pollard CE, Abi Gerges N, Bridgland-Taylor MH, Easter A, Hammond TG, et al. (2010) An introduction to QT interval prolongation and non-clinical approaches to assessing and reducing risk. *Br J Pharmacol* 159: 12–21. doi:10.1111/j.1476-5381.2009.00207.x.
- Jehle J, Schweizer PA, Katus HA, Thomas D (2011) Novel roles for hERG K(+) channels in cell proliferation and apoptosis. *Cell Death Dis* 2: e193. doi:10.1038/cddis.2011.77.
- Nichols CG (2006) KATP channels as molecular sensors of cellular metabolism. *Nature* 440: 470–476. doi:10.1038/nature04711.
- Hodgkin AL, Huxley AF (1952) A quantitative description of membrane current and its application to conduction and excitation in nerve. *J Physiol* 117: 500–544.
- Hille B (2001) Ion channels of excitable membranes. 3rd edition. Sunderland: Sinauer.
- Doyle DA, Morais Cabral J, Pfuetzner RA, Kuo A, Gulbis JM, et al. (1998) The structure of the potassium channel: molecular basis of K<sup>+</sup> conduction and selectivity. *Science* 280: 69–77. doi:10.1126/science.280.5360.69.
- Perozo E, Cortes DM, Cuello LG (1999) Structural rearrangements underlying K<sup>+</sup>-channel activation gating. *Science* 285: 73–78. doi:10.1126/science.285.5424.73.
- Kelly BL, Gross A (2003) Potassium channel gating observed with site-directed mass tagging. *Nat Struct Biol* 10: 280–284. doi:10.1038/nsb908.
- Zimmer J, Doyle DA, Grossmann JG (2006) Structural characterization and pH-induced conformational transition of full-length KcsA. *Biophys J* 90: 1752–1766. doi:10.1529/biophysj.105.071175.
- Shimizu H, Iwamoto M, Konno T, Nihei A, Sasaki YC, et al. (2008) Global twisting motion of single molecular KcsA potassium channel upon gating. *Cell* 132: 67–78. doi:10.1016/j.cell.2007.11.040.
- Uysal S, Vázquez V, Tereshko V, Esaki K, Fellouse FA, et al. (2009) Crystal structure of full-length KcsA in its closed conformation. *Proc Natl Acad Sci U S A* 106: 6644–6649. doi:10.1073/pnas.0810663106.
- Cuello LG, Jogini V, Cortes DM, Perozo E (2010) Structural mechanism of C-type inactivation in K(+) channels. *Nature* 466: 203–208. doi:10.1038/nature09153.
- Henzler-Wildman K, Kern D (2007) Dynamic personalities of proteins. *Nature* 450: 964–972. doi:10.1038/nature06522.
- Biggin PC, Sansom MSP (2002) Open-state models of a potassium channel. *Biophys J* 83: 1867–1876. doi:10.1016/S0006-3495(02)73951-9.
- Tikhonov DB, Zhorov BS (2004) In silico activation of KcsA K<sup>+</sup> channel by lateral forces applied to the C-termini of inner helices. *Biophys J* 87: 1526–1536. doi:10.1529/biophysj.103.037770.
- Compoin M, Picard F, Ramseyer C, Girardet C (2005) Targeted molecular dynamics of an open-state KcsA channel. *J Chem Phys* 122: 134707. doi:10.1063/1.1869413.
- Shrivastava IH, Bahar I (2006) Common mechanism of pore opening shared by five different potassium channels. *Biophys J* 90: 3929–3940. doi:10.1529/biophysj.105.080093.
- Enosh A, Raviv B, Furman-Schueler O, Halperin D, Ben-Tal N (2008) Generation, comparison, and merging of pathways between protein conformations: gating in K-channels. *Biophys J* 95: 3850–3860. doi:10.1529/biophysj.108.135285.
- Haliloglu T, Ben-Tal N (2008) Cooperative transition between open and closed conformations in potassium channels. *PLoS Comput Biol* 4: e1000164. doi:10.1371/journal.pcbi.1000164.
- Mashl RJ, Jakobsson E (2008) End-point targeted molecular dynamics: large-scale conformational changes in potassium channels. *Biophys J* 94: 4307–4319. doi:10.1529/biophysj.107.118778.
- Denning EJ, Woolf TB (2010) Cooperative nature of gating transitions in K(+) channels as seen from dynamic importance sampling calculations. *Proteins* 78: 1105–1119. doi:10.1002/prot.22632.
- Miloshevsky G V, Jordan PC (2007) Open-state conformation of the KcsA K<sup>+</sup> channel: Monte Carlo normal mode following simulations. *Structure* 15: 1654–1662. doi:10.1016/j.str.2007.09.022.
- Amadei A, Linssen AB, De Groot BL, Van Aalten DM, Berendsen HJ (1996) An efficient method for sampling the essential subspace of proteins. *J Biomol Struct Dyn* 13: 615–625. doi:10.1080/07391102.1996.10508874.
- De Groot BL, Amadei A, Van Aalten DM, Berendsen HJ (1996) Toward an exhaustive sampling of the configurational spaces of the two forms of the peptide hormone guanylin. *J Biomol Struct Dyn* 13: 741–751. doi:10.1080/07391102.1996.10508888.
- De Groot BL, Amadei A, Scheek RM, Van Nuland NA, Berendsen HJ (1996) AID-PROT7>3.0.CO;2-D.

## Author Contributions

Conceived and designed the experiments: TL BLdG ASW. Performed the experiments: TL. Analyzed the data: TL BLdG ASW. Wrote the paper: TL BLdG ASW.

- Van Aalten DM, Conn DA, De Groot BL, Berendsen HJ, Findlay JB, et al. (1997) Protein dynamics derived from clusters of crystal structures. *Biophys J* 73: 2891–2896. doi:10.1016/S0006-3495(97)78317-6.
- Narzi D, Daidone I, Amadei A, Di Nola A (2008) Protein Folding Pathways Revealed by Essential Dynamics Sampling. *J Chem Theory Comput* 4: 1940–1948. doi:10.1021/ct800157v.
- Anishkin A, Milac AL, Guy HR (2010) Symmetry-restrained molecular dynamics simulations improve homology models of potassium channels. *Proteins* 78: 932–949. doi:10.1002/prot.22618.
- Bernèche S, Roux B (2000) Molecular dynamics of the KcsA K(+) channel in a bilayer membrane. *Biophys J* 78: 2900–2917. doi:10.1016/S0006-3495(00)76831-7.
- Iwamoto M, Shimizu H, Inoue F, Konno T, Sasaki YC, et al. (2006) Surface structure and its dynamic rearrangements of the KcsA potassium channel upon gating and tetrabutylammonium blocking. *J Biol Chem* 281: 28379–28386. doi:10.1074/jbc.M602018200.
- Iwamoto M, Oiki S (2013) Amphipathic antenna of an inward rectifier K<sup>+</sup> channel responds to changes in the inner membrane leaflet. *Proc Natl Acad Sci U S A* 110: 749–754. doi:10.1073/pnas.1217323110.
- Smart OS, Neduvellil JG, Wang X, Wallace BA, Sansom MSP (1996) HOLE: A program for the analysis of the pore dimensions of ion channel structural models. *J Mol Graph* 14: 354–360. doi:10.1016/S0263-7855(97)00009-X.
- Cuello LG, Jogini V, Cortes DM, Pan AC, Gagnon DG, et al. (2010) Structural basis for the coupling between activation and inactivation gates in K(+) channels. *Nature* 466: 272–275. doi:10.1038/nature09136.
- Pan AC, Cuello LG, Perozo E, Roux B (2011) Thermodynamic coupling between activation and inactivation gating in potassium channels revealed by free energy molecular dynamics simulations. *J Gen Physiol* 138: 571–580. doi:10.1085/jgp.201110670.
- Cordero-Morales JF, Cuello LG, Zhao Y, Jogini V, Cortes DM, et al. (2006) Molecular determinants of gating at the potassium-channel selectivity filter. *Nat Struct Mol Biol* 13: 311–318. doi:10.1038/nsmb1069.
- Cordero-Morales JF, Jogini V, Lewis A, Vázquez V, Cortes DM, et al. (2007) Molecular driving forces determining potassium channel slow inactivation. *Nat Struct Mol Biol* 14: 1062–1069. doi:10.1038/nsmb1309.
- Bhate MP, McDermott AE (2012) Protonation state of E71 in KcsA and its role for channel collapse and inactivation. *Proc Natl Acad Sci U S A* 109: 1–6. doi:10.1073/pnas.1211900109.
- Aqvist J, Luzhkov V (2000) Ion permeation mechanism of the potassium channel. *Nature* 404: 881–884. doi:10.1038/35009114.
- Irizarry SN, Kutluay E, Drews G, Hart SJ, Heginbotham L (2002) Opening the KcsA K<sup>+</sup> Channel: Tryptophan Scanning and Complementation Analysis Lead to Mutants with Altered Gating. *Biochemistry* 41: 13653–13662. doi:10.1021/bi026393r.
- Yifrach O, MacKinnon R (2002) Energetics of Pore Opening in a Voltage-Gated K<sup>+</sup> Channel. *Cell* 111: 231–239. doi:10.1016/S0092-8674(02)01013-9.
- Sadovsky E, Yifrach O (2007) Principles underlying energetic coupling along an allosteric communication trajectory of a voltage-activated K<sup>+</sup> channel. *Proc Natl Acad Sci U S A* 104: 19813–19818. doi:10.1073/pnas.0708120104.
- Paynter J, Sarkies P, Andres-Enguix I, Tucker SJ (2008) Genetic selection of activatory mutations in KcsA. *Channels* 2: 413–418. doi:10.4161/chan.2.6.6874.
- Lee S-Y, Banerjee A, MacKinnon R (2009) Two separate interfaces between the voltage sensor and pore are required for the function of voltage-dependent K(+) channels. *PLoS Biol* 7: e47. doi:10.1371/journal.pbio.1000047.
- Jiang Y, Lee A, Chen J, Ruta V, Cadene M, et al. (2003) X-ray structure of a voltage-dependent K<sup>+</sup> channel. *Nature* 423: 33–41. doi:10.1038/nature01580.
- Long SB, Campbell EB, MacKinnon R (2005) Crystal structure of a mammalian voltage-dependent Shaker family K<sup>+</sup> channel. *Science* 309: 897–903. doi:10.1126/science.1116269.
- Hackos DH (2002) Scanning the Intracellular S6 Activation Gate in the Shaker K<sup>+</sup> Channel. *J Gen Physiol* 119: 521–532. doi:10.1085/jgp.20028569.
- Li-Smerin Y, Hackos DH, Swartz KJ (2000) A Localized Interaction Surface for Voltage-Sensing Domains on the Pore Domain of a K<sup>+</sup> Channel. *Neuron* 25: 411–423. doi:10.1016/S0896-6273(00)80904-6.
- Tytgat J, Hess P (1992) Evidence for cooperative interactions in potassium channel gating. *Nature* 359: 420–423. doi:10.1038/359420a0.
- Smith-Maxwell CJ, Ledwell JL, Aldrich RW (1998) Role of the S4 in cooperativity of voltage-dependent potassium channel activation. *J Gen Physiol* 111: 399–420. doi:10.1085/jgp.111.3.399.
- Ledwell JL, Aldrich RW (1999) Mutations in the S4 region isolate the final voltage-dependent cooperative step in potassium channel activation. *J Gen Physiol* 113: 389–414. doi:10.1085/jgp.113.3.389.

51. Pathak M, Kurtz L, Tombola F, Isacoff E (2005) The cooperative voltage sensor motion that gates a potassium channel. *J Gen Physiol* 125: 57–69. doi:10.1085/jgp.200409197.
52. Blunck R, McGuire H, Hyde HC, Bezannila F (2008) Fluorescence detection of the movement of single KcsA subunits reveals cooperativity. *Proc Natl Acad Sci U S A* 105: 20263–20268. doi:10.1073/pnas.0807056106.
53. Zandany N, Ovadia M, Orr I, Yifrach O (2008) Direct analysis of cooperativity in multisubunit allosteric proteins. *Proc Natl Acad Sci U S A* 105: 11697–11702. doi:10.1073/pnas.0804104105.
54. Zhou Y, Morais-Cabral JH, Kaufman A, MacKinnon R (2001) Chemistry of ion coordination and hydration revealed by a K<sup>+</sup> channel-Fab complex at 2.0 Å resolution. *Nature* 414: 43–48. doi:10.1038/35102009.
55. Guex N, Peitsch MC (1997) SWISS-MODEL and the Swiss-PdbViewer: an environment for comparative protein modeling. *Electrophoresis* 18: 2714–2723. doi:10.1002/elps.1150181505.
56. Wolf MG, Hoefling M, Aponte-Santamaria C, Grubmüller H, Groenhof G (2010) g\_membed: Efficient insertion of a membrane protein into an equilibrated lipid bilayer with minimal perturbation. *J Comput Chem* 31: 2169–2174. doi:10.1002/jcc.21507.
57. Knappe K, Linder T, Wolschann P, Beyer A, Stary-Weinzinger A (2011) In silico Analysis of Conformational Changes Induced by Mutation of Aromatic Binding Residues: Consequences for Drug Binding in the hERG K<sup>+</sup> Channel. *PloS one* 6: e28778. doi:10.1371/journal.pone.0028778.
58. Hess B, Kutzner C, Van der Spoel D, Lindahl E (2008) GROMACS 4: Algorithms for Highly Efficient, Load-Balanced, and Scalable Molecular Simulation. *J Chem Theory Comput* 4: 435–447. doi:10.1021/ct700301q.
59. Hornak V, Abel R, Okur A, Strockbine B, Roitberg A, et al. (2006) Comparison of multiple Amber force fields and development of improved protein backbone parameters. *Proteins* 65: 712–725. doi:10.1002/prot.21123.
60. Jorgensen WL, Chandrasekhar J, Madura JD, Impey RW, Klein ML (1983) Comparison of simple potential functions for simulating liquid water. *J Chem Phys* 79: 926. doi:10.1063/1.445869.
61. Siu SWI, Vácha R, Jungwirth P, Böckmann R a (2008) Biomolecular simulations of membranes: physical properties from different force fields. *J Chem Phys* 128: 125103. doi:10.1063/1.2897760.
62. Liu Y, Nagle JF (2004) Diffuse scattering provides material parameters and electron density profiles of biomembranes. *Phys Rev E: Stat, Nonlinear, Soft Matter Phys* 69: 040901. doi:10.1103/PhysRevE.69.040901.
63. Darden T, York D, Pedersen L (1993) Particle mesh Ewald: An N log(N) method for Ewald sums in large systems. *J Chem Phys* 98: 10089. doi:10.1063/1.464397.
64. Hess B, Bekker H, Berendsen HJC, Fraaije JGEM (1997) AID-JCC4>3.0.CO;2-H.
65. Amadei A, Linssen AB, Berendsen HJ (1993) Essential dynamics of proteins. *Proteins* 17: 412–425. doi:10.1002/prot.340170408.
66. Hub JS, De Groot BL, Van der Spoel D (2010) g\_wham—A Free Weighted Histogram Analysis Implementation Including Robust Error and Autocorrelation Estimates. *J Chem Theory Comput* 6: 3713–3720. doi:10.1021/ct100494z.

## Supplemental material

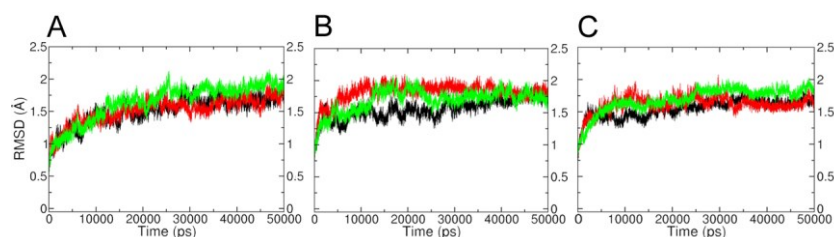


**Figure S1. Stability of KcsA channel states.** Backbone RMSD (without loops) of three independent MD simulations of closed (A), intermediate (B), and open state (C) was measured as a function of time.

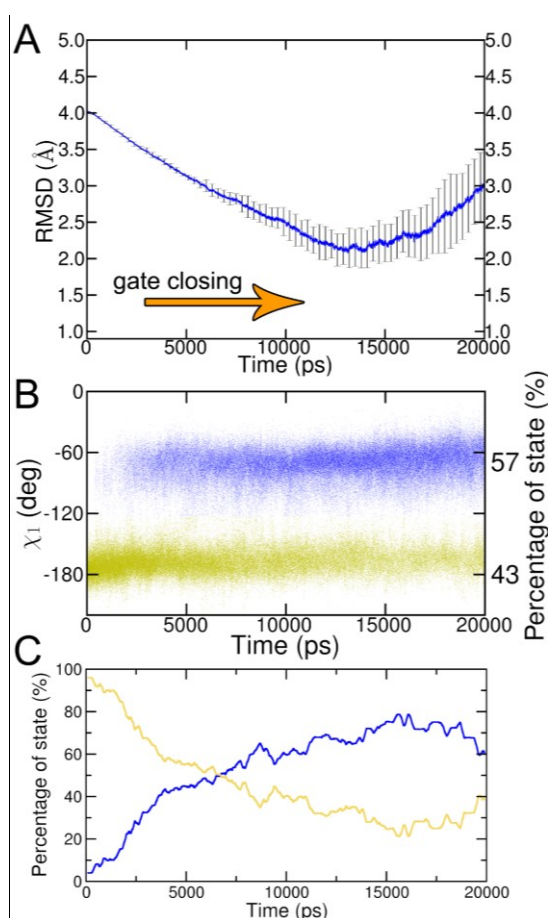


**Figure S2. Analysis of ED closing simulations.** A) Average of the backbone RMSD without loops of seven closing ED simulations. The closed crystal structure was used as reference. The standard deviation is indicated by error bars. B) Conformational changes of F103 during activation gate closing. Analysis of  $\chi_1$  angle dynamics of F103 of the seven ED simulations was performed. Changes of the F103 orientation was measured as  $\chi_1$  angle over time. An angle of  $-70^\circ$  indicates the “up” state (blue) while an angle of  $-180^\circ$  represents the “down” state (yellow). C)  $\chi_1$  angle dynamics of F114 are shown as percentage of F114 in the up (blue) and down (yellow) states over time.

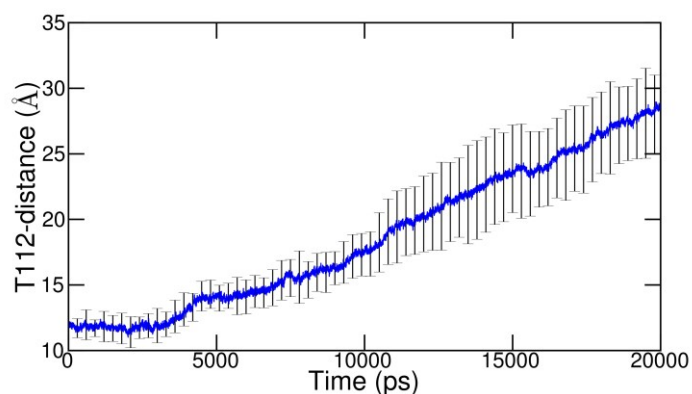


**Figure S3. Average of the C $\alpha$ -C $\alpha$  T112-distances of all ten ED simulations.** The standard deviation is indicated by error bars.

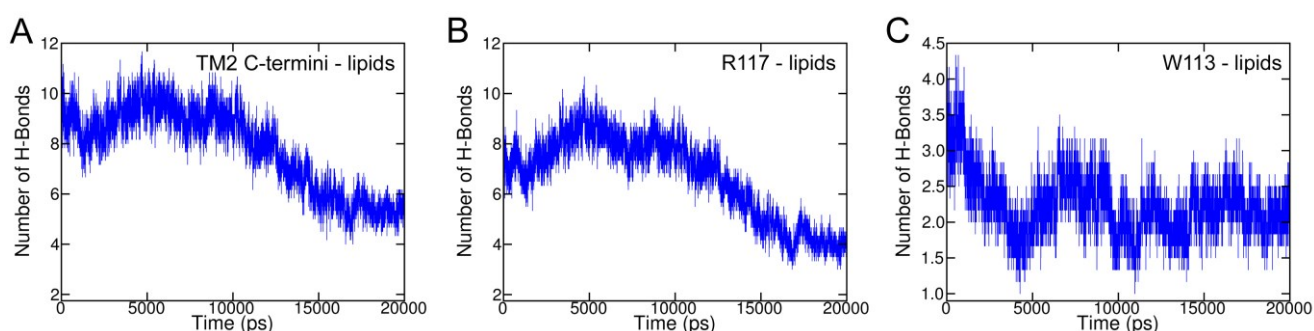


**Figure S4. Lipid interactions of TM2 helices during activation gate closing.** A) Average number of H-bonds between H-bond forming residues (W113 and R117) of the C-terminal TM2 helices and lipid head groups was measured over time. B) Average number of H-bonds of R117 with lipids. C) Average number of H-bonds of W113 with lipids.

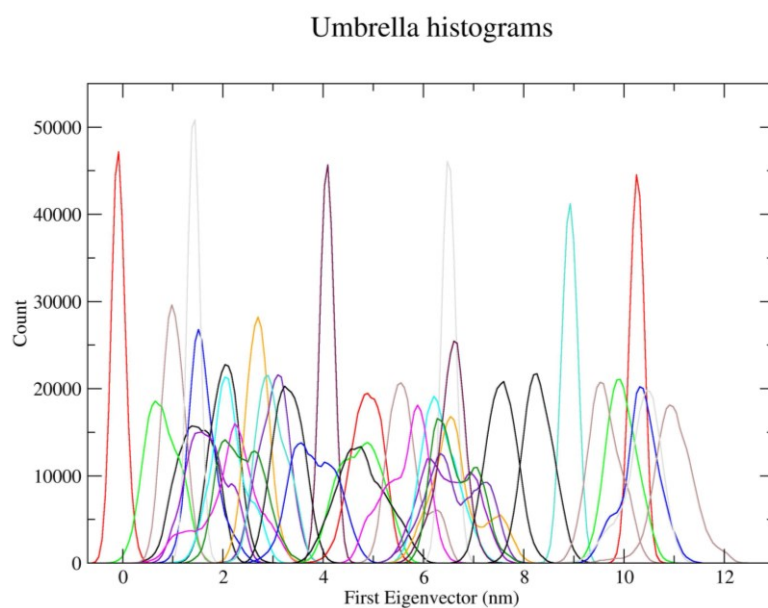


**Figure S5. Histograms of the 39 umbrella sampling windows.** The six windows with peaks above 40000 were derived from umbrella sampling with a force constant of 100 kJ mol<sup>-1</sup> nm<sup>-2</sup> (default: 1 kJ mol<sup>-1</sup> nm<sup>-2</sup>).

## **4.2 Molecular dynamics simulations of KirBac1.1 mutants reveal global gating changes of Kir channels**

---

Stary-Weinzinger A\*, Linder T\*, Zangerl E-M

*\* These authors contributed equally*

*The findings of this study are currently subject to experimental validation*

# Molecular dynamics simulations of KirBac1.1 mutants reveal global gating changes of Kir channels

*Anna Stry-Weinzinger<sup>‡\*</sup>, Tobias Linder<sup>‡</sup>, Eva-Maria Zangerl*

Department of Pharmacology and Toxicology, University of Vienna, Vienna, Austria.

<sup>‡</sup>These authors contributed equally

Running title: MD simulations of KirBac1.1 gating

Keywords: inward rectifier potassium channel, prokaryotic, cytoplasmic domain rotation, water flux, pore gating

## ABSTRACT

Prokaryotic inwardly rectifying (KirBac) potassium channels are homologous to mammalian Kir channels. Their activity is controlled by dynamical conformational changes that regulate ion flow through a central pore. Understanding the dynamical rearrangements of Kir channels during gating requires high-resolution structure information from channels crystallized in different conformations and insight into the transition steps, which are difficult to access experimentally. In this study, we use MD simulations on wild type KirBac1.1 and an activatory mutant to investigate activation gating of KirBac channels. Full atomistic MD simulations revealed that introducing glutamate in position 143 causes significant widening at the helix bundle crossing gate, enabling water flux into the cavity. Further, global rearrangements including a twisting motion as well as local rearrangements at the subunit interface in the cytoplasmic domain were observed. These structural rearrangements are similar to recently reported KirBac3.1 crystal structures in closed and open conformation, suggesting that our simulations capture major conformational changes during KirBac1.1 opening. In addition, an important role of protein-lipid interactions during gating was observed. Slide-helix and C-linker interactions with lipids were strengthened during activation gating.

## INTRODUCTION

Inwardly rectifying potassium (Kir) channels are intrinsic membrane proteins that control the selective permeation of potassium ions across otherwise ion impermeable cell membranes. The primary role of Kir channels is the regulation of outward directed  $K^+$  current. Under physiological conditions, Kir channels generate a large inward  $K^+$  conductance at potentials negative to the equilibrium potential of potassium ( $E_K$ ), but permit less outward current flow at potentials positive to  $E_K$ . These channels are regulated by many different cellular factors such as ATP, intracellular pH, phosphatidylinositol-4,5-bisphosphate ( $PIP_2$ ) and nonspecific secondary anionic phospholipids (Bichet *et al*, 2003; Hibino *et al*, 2010; Lee *et al*, 2013).

Over the last 10 years, several Kir crystal structures of the cytoplasmic domain as well as several full length structures of prokaryotic and eukaryotic channels have been published (Nishida & MacKinnon, 2002; Kuo *et al*, 2003; Pegan *et al*, 2005; Nishida *et al*, 2007; Tao *et al*, 2009; Clarke *et al*, 2010; Hansen *et al*, 2011; Whorton & MacKinnon, 2011; Bavro *et al*, 2012; Whorton & MacKinnon, 2013; Zubcevic *et al*, 2014). Interestingly, prokaryotic homologues, despite moderate sequence conservation on the amino acid level, share similar architecture and behave functionally similar as eukaryotic channels (Cheng *et al*, 2009). All Kir channels undergo dynamical changes to regulate ion flow. This process, referred to as “gating”, involves large structural rearrangements of the transmembrane (TM) as well as the cytoplasmic domains (CTD). In the closed conformation, ion flux is prevented by a narrowing of the inner TM2 helices, which form a constriction site at the helix bundle crossing (HBC) gate close to the intracellular side (see Figure 1). Computational modeling studies on TM KirBac1.1 channel models provided insights into ion selectivity and gating dynamics (Domene *et al*, 2004; Grottesi *et al*, 2005; Hellgren *et al*, 2006; Domene *et al*, 2006, 2008). A limitation of all these studies was the lack of open state x-ray structures. In 2012, the first X-ray structure of a bacterial homolog of Kir channels was crystallized in a presumably open conformation, using a known activatory “gain-of-function” mutant (Bavro *et al*, 2012). Comparison of this open structure with various Kir channels in closed conformation (Clarke *et al*, 2010) provides insights into gating induced changes of these channels. In the open structure, global conformational changes are observed, including a rotational movement of the CTD relative to the plane of the membrane; in addition, a bending of the TM2 at a highly conserved glycine opens the HBC gate. The sequential process of gating events remains a major open question. Especially, the cross-talk between TM and CT domains and how this leads to channel opening is still unknown. To investigate these events, we performed MD

simulations on the KirBac1.1 channel, for which only closed state x-ray structures are available (Clarke *et al*, 2010).

## METHODS

### *Molecular dynamics simulations*

The closed (pdb identifier: 2WLL) crystal structure (Clarke *et al*, 2010), comprising residues 38 to 308, was used as starting point for the MD simulations. The G143E mutant in protonated and deprotonated conformations and the R153A mutant were generated with the software Swiss-PdbViewer (Guex & Peitsch, 1997). The structures were embedded in an equilibrated membrane consisting of 256 palmitoylcholine (POPC) lipids using the *g\_membed* tool (Wolf *et al*, 2010), which is part of the *gromacs* package.  $K^+$  ions were placed in the SF at  $K^+$  sites S0, S2, and S4 with waters placed at S1 and S3 (Aqvist & Luzhkov, 2000).  $Cl^-$  ions were added randomly within the solvent to neutralize the system. All simulations were carried out using the *gromacs* simulation software v.4.5.4 (Hess *et al*, 2008). The *amber99sb* force field (Hornak *et al*, 2006) and the SPC/E (Berendsen *et al*, 1987) and TIP3P (Jorgensen *et al*, 1983) model were employed for the protein and water, respectively. Lipid parameters for the POPC membrane were taken from Berger *et al*. (Berger *et al*, 1997). The corrected monovalent ion Lennard-Jones parameters for the *amber* forcefield were used (Joung & Cheatham, 2008). Electrostatic interactions were calculated at a distance smaller than 1.0 nm, long-range electrostatic interactions were treated by the particle-mesh Ewald method at every step (Darden *et al*, 1993). Lennard-Jones interactions were calculated with a cut off of 1.0 nm. The LINCS algorithm (Hess *et al*, 1997) was used to constrain bonds. Modeling hydrogens as virtual sites (Feenstra *et al*, 1999) allowed for an integration step of 4 fs. The Nose-Hoover thermostat (Nosé, 1984; Hoover, 1985) was used to keep simulation temperature constant by coupling ( $\tau = 0.2$  ps) the protein, lipids and solvent (water and ions) separately to a temperature bath of 310 K. Likewise, the pressure was kept constant at 1 bar by using the Parrinello-Rahman barostat algorithm (Parrinello & Rahman, 1981) with a coupling constant of 1 ps. Prior to simulation, 1000 conjugate gradient energy-minimization steps were performed, followed by 5 ns of equilibrium simulation in which the protein atoms were restrained by a force constant of  $1000 \text{ kJ mol}^{-1} \text{ nm}^{-2}$  to their initial position. Lipids, ions, and water were allowed to move freely during equilibration. Four times

200 ns MD simulations were performed for the full length WT channel as well as the G143E<sub>d</sub>, G143E<sub>p</sub> and G143E<sub>d</sub>-R153A mutant channels.

### *Salt bridge analysis*

Electrostatic interactions were analyzed by measuring the center of mass distances between positively and negatively charged functional groups of amino acids. A distance cut off of 6 Å was set which represents three different types of ion pair interactions, namely salt bridge, N-O bridge, and long range ion pair (Kumar & Nussinov, 2002) which are named “salt bridges” in this study. The occurrence of interaction is normalized to the most prominent electrostatic interaction in the protein (R193 and E187 of adjacent SU in WT simulations). Interaction partners that contributed more than 1 % to the total electrostatic interactions in the protein are plotted in the star graphs.

### *Energy profile calculations*

Potential of mean force (PMF) calculations were performed as described previously (Linder *et al*, 2013). Briefly, the main conformational changes in the most prominent G143E<sub>d</sub> opening simulation were obtained by principal component analysis and were used as the reaction coordinate. Along this reaction coordinate, 45 windows were chosen for umbrella sampling and simulated for 50 ns. Umbrella sampling simulations were performed by applying a harmonic restraint force along the transition pathway with force constants between 1 and 100 kJ mol<sup>-1</sup> nm<sup>-2</sup>. The first 30 ns of each window were discarded for equilibration. The potential of mean force and the statistical errors of the activation gating energy profile were estimated by making use of the g\_wham tool of gromacs and the integrated bootstrap analysis method (Hub *et al*, 2010). The number of bootstraps was set to 100.

## RESULTS

To probe the mechanism of KirBac1.1 gating, we made use of the known activatory (“gain-of function”) mutant G143E (Paynter *et al*, 2010). This mutant was selected due to its equivalent position to activatory mutant S129R in KirBac3.1, which was used to obtain open state crystals of this channel (Bavro *et al*, 2012). G143E is located in transmembrane helix 2 (TM2) at a hydrophobic interface between two adjacent TM2 helices (see Figure 1A, B). The activatory effect of this mutant was investigated using four times 200 ns unbiased full

atomistic MD simulations of the full length KirBac1.1 WT crystal structure and mutant G143E in deprotonated (denoted as G143E<sub>d</sub>) and protonated (G143E<sub>p</sub>) form.

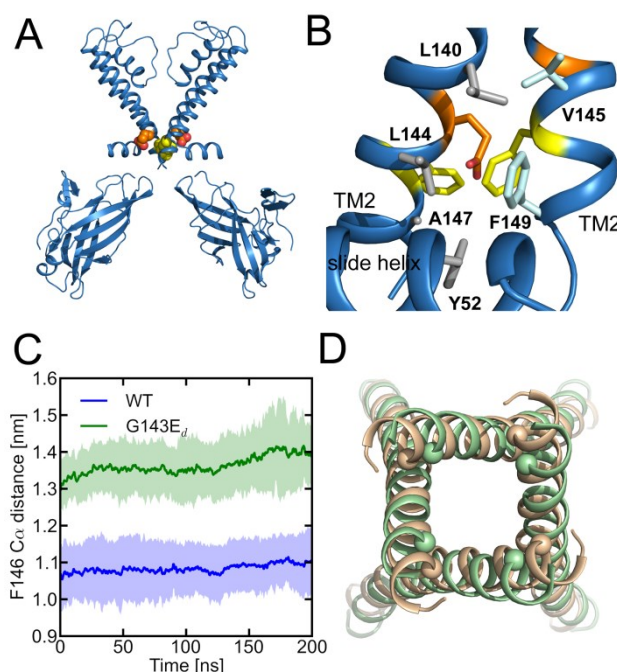


**Figure 1. G143E<sub>d</sub> location and induced channel opening.** A) Position of F146 (yellow) forming the helix bundle crossing gate and the introduced G143E<sub>d</sub> mutant (orange). For clarity, only two opposing subunits are shown. B) G143E is located in a tightly packed hydrophobic pocket formed by Y52 (slide-helix), F146 (yellow), L140, L144, and A147 (all four located in the TM2) of the same subunit (SU, colored gray) and V145, F146 (yellow), and F149 of the adjacent TM2 (colored light blue). C) Averages of F146 C $\alpha$ -C $\alpha$  distances in WT and G143E<sub>d</sub> simulations are shown as blue and green lines, respectively. Standard deviations are depicted as light shades accordingly. D) Superposition of the TM2 helices of the open KirBac3.1 structure (pdb identifier: 3ZRS, shown in ochre) and the G143E<sub>d</sub> mutant (final state, shown in green). The C $\alpha$  atoms of F146 (KirBac1.1) and the equivalent Y132 (KirBac3.1) are shown as green and ochre spheres.

### *Mutant G143E<sub>d</sub> induces opening of the HBC gate*

MD simulations show that mutant G143E<sub>d</sub> induces global conformational rearrangements of the protein. Bending at a highly conserved glycine hinge (G134) in TM2, leading to opening at the HBC, was observed in all four simulations. To monitor the changes at the gate, we measured the C $\alpha$ -C $\alpha$  distance between opposing F146 residues, lining the narrowest point of this gate. As shown in Figure 1C, the distance rapidly increased to  $13.8 \pm 0.9$  Å, compared to WT simulations, where the gate remained fully closed (C $\alpha$ -C $\alpha$  distance at F146:  $11.0 \pm 0.9$  Å). The end state of the G143E<sub>d</sub> mutant was compared with the S129R mutant KirBac3.1

x-ray structure in open conformation. Figure 1D shows a structural superposition of the TM2 helices of the two structures, revealing good overlay between the structures. Next, the  $\chi_1$  angle distribution of the F146 side chain over time was analyzed. As shown in Figure 2A-C, the  $\chi_1$  angle switched from  $\sim 160^\circ$  (cavity facing) to  $\sim 270^\circ$  (cavity lining).

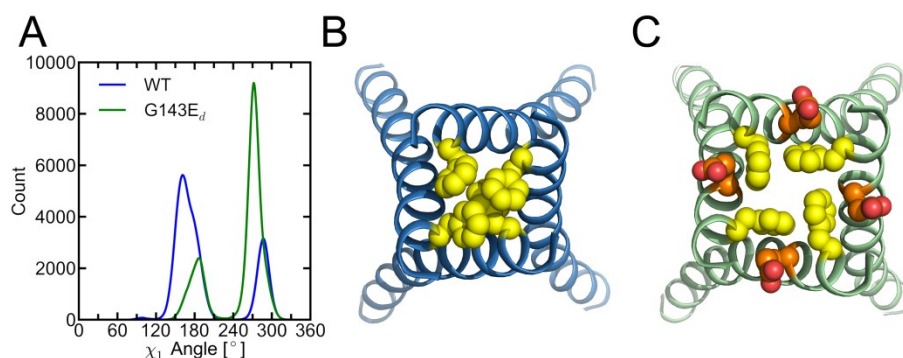


**Figure 2. Conformational changes of F146 during gate opening.** A)  $\chi_1$  angle distribution of the F146 side chain in WT (blue) and G143E<sub>d</sub> (green) simulations. B) Bottom view of the closed helix bundle crossing gate in WT simulations with F146 (yellow spheres) in the cavity facing conformation ( $\chi_1$  angle of  $\sim 160^\circ$ ). C) Bottom view of an open helix bundle crossing gate in G143E<sub>d</sub> simulations with F146 in the cavity lining rotameric state ( $\chi_1$  angle of  $\sim 270^\circ$ ). G143E<sub>d</sub> are shown as orange spheres.

To further investigate the consequence of these structural changes on the HBC gate, we monitored the water flux through the gate in WT and G143E<sub>d</sub> simulations. While water flux was not observed in the WT simulations (see Figure 3A, C), considerable water migration through the gate occurred in the G143E<sub>d</sub> mutant (Figure 3B, C).

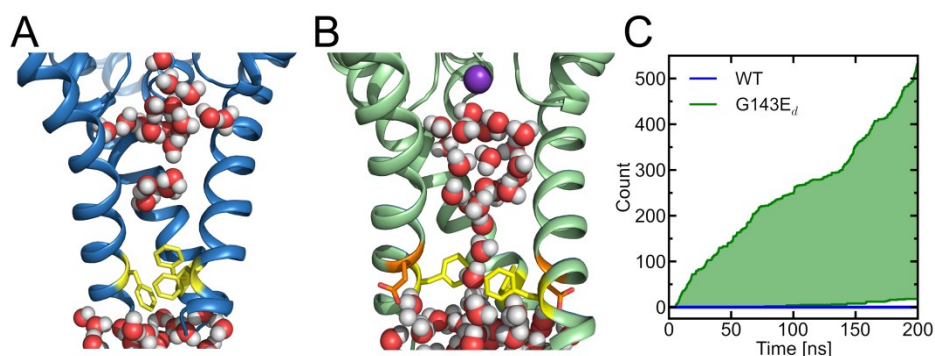


**Figure 3. Water flux through the HBC gate.** A) Water impermeable gate in the WT simulation. Three SUs are shown for clarity. F146 residues are shown as yellow sticks. Water molecules are represented as spheres. B) Water flux through the open gate in G143E<sub>d</sub> simulations. G143E<sub>d</sub> is depicted as orange sticks and the K<sup>+</sup> ion as purple sphere. C) Water count of permeation events in the WT (blue line) and G143E<sub>d</sub> (green shade) simulations.

### *Global conformational changes in the cytoplasmic domain*

Additionally, to the rearrangements at the HBC, our simulations revealed large conformational changes at the CTD. A rotational movement of the CTD relative to the plane of the membrane was seen in all four G143E<sub>d</sub> mutant simulations. The degree of this twisting motion amounted to 15° on average, with maximum values of 23° in one run (see Figure 4A). These values are in good agreement with data obtained from several KirBac3.1 x-ray structures (Clarke *et al*, 2010; Bavro *et al*, 2012), suggesting that the rotational movements of these two channels are conserved.

Moreover, rearrangements at the subunit interface, especially salt bridge formations, were analyzed. In this study, the term "salt bridge" denotes non-bonded, N-O bridged and long range electrostatic interactions between acidic carboxyl groups and basic amino groups in the same subunit (sSU) or adjacent SUs (aSUs) as described by Kumar *et al* (Kumar & Nussinov, 2002). In the WT closed structure, R271, located in the  $\beta_I$  strand (see Figure 4B, D), forms a salt bridge with E262 (G-loop of the adjacent subunit). Further, E187 interacts with K191 and R193 from the  $\beta_D$  strand of the aSU. Moreover, hydrogen bonds between R193 and E218 from the adjacent CD-loop were observed.

In the G143E<sub>d</sub> mutant, global conformational rearrangements of the CTD led to an additional salt bridge between R271 and E187 of the aSU (Figure 4 B, E). This salt bridge formation occurred within the first 80 ns in all four simulations between all four interfaces. Due to the R271-E187 salt bridge formation, interactions between K191 and E187 were weakened.

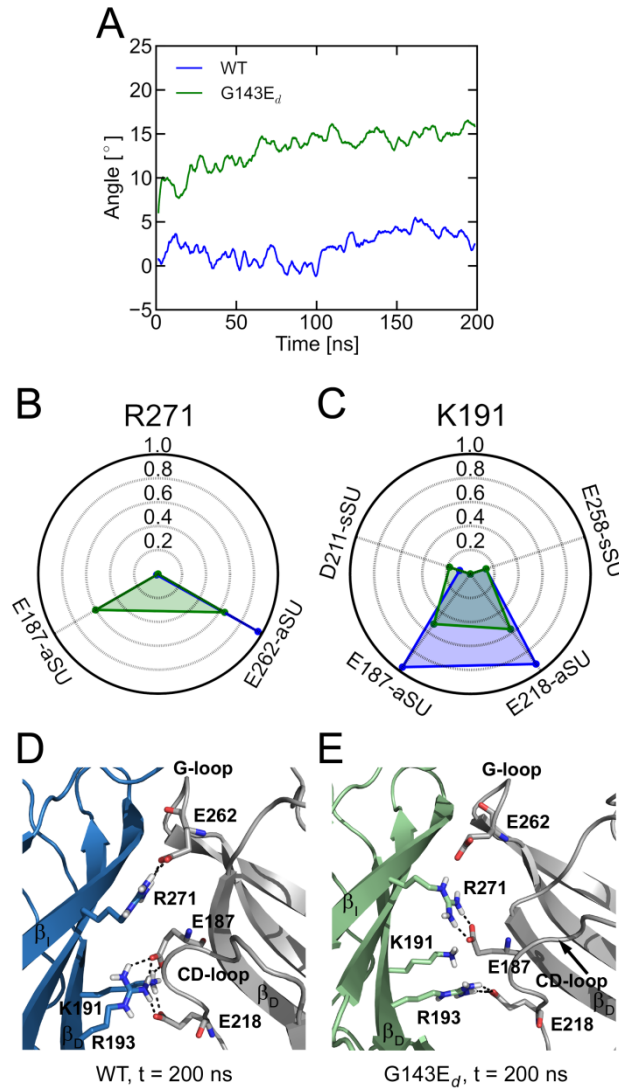


**Figure 4. Changes in the interaction network of the CTD.** A) Average of the CTD rotation angle in WT (blue) and G143E<sub>d</sub> simulations (green). B) Star graph of salt bridges between R271 and neighboring amino acids of adjacent SUs (aSU) and the same SU (sSU). Interactions in WT and G143E<sub>d</sub> simulations are depicted as blue and green shades, respectively. The magnitude of interaction is normalized to the most prominent salt bridge in the protein. C) Star graph of salt bridges between K191 and neighboring amino acids of aSUs and the sSU. D) SU-interface of CTD conformation in WT simulation. The two aSUs are colored blue and gray. Salt bridges are depicted as dashed lines. E) SU-interface of CTD conformation in G143E<sub>d</sub> simulation. The two aSUs are colored green and gray. Salt bridges are depicted as dashed lines.

### *Salt bridge formation between G143E<sub>d</sub> and R153*

Further, the structural changes at the TM-CTD interface were examined. Our analysis revealed that the G143E<sub>d</sub> side chains form a stable salt bridge (see Figure 5A, C and Figure 8D) with residue R153, located in the C-linker of the neighboring subunit, within the first half of the simulations. To investigate the importance of this salt bridge for the cross-talk between TM and CTD, R153A was introduced in the background of the G143E<sub>d</sub> mutant in all four subunits. In these simulations, the HBC gate opens on average to 13 Å (not shown), but the observed rotation of the CTD was rather small with  $\sim 5^\circ$  (Figure 6). This suggests that the strong electrostatic interactions between G143E<sub>d</sub> and R153 are important for the twisting motion observed in the G143E<sub>d</sub> mutant.

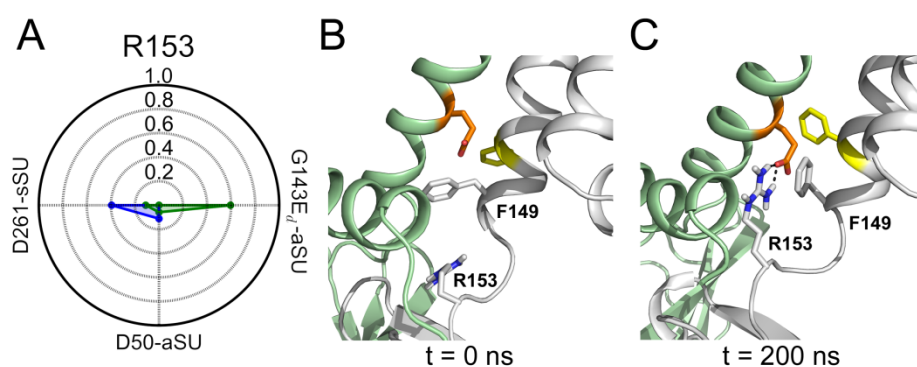


**Figure 5. Salt bridge interactions of R153.** A) Star graph of salt bridges between R153 and neighboring amino acids of aSUs and the sSU. Interactions in WT and G143E<sub>d</sub> simulations are depicted as blue and green shades, respectively. The magnitude of interaction is normalized to the most prominent salt bridge in the protein. B) Starting conformation of G143E<sub>d</sub> simulations. aSUs are colored green and gray. G143E<sub>d</sub> and F146 are shown as orange and yellow sticks. C) G143E<sub>d</sub>-R153 salt bridge (dashed line) after 200 ns.

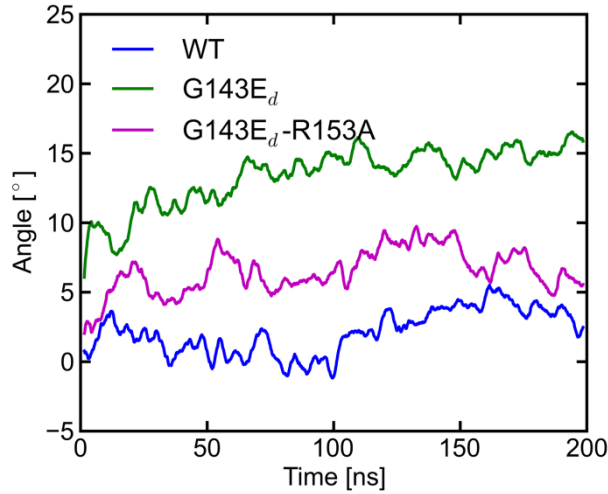


**Figure 6. Average of the CTD rotation angle.** Average rotation angle as a function of time in WT (blue), G143E<sub>d</sub> (green), and G143E<sub>d</sub>-R153A double mutant (magenta) simulations.

#### *Influence of protonation state on channel conformation*

The above described observations indicate that opening involves a two-step process. First, strong repulsion between G143E<sub>d</sub> and the surrounding hydrophobic residues triggers opening at the bundle crossing region. In a second step, electrostatic interactions between G143E<sub>d</sub> and R153 of the adjacent C-linker induce rotation of the CTD. It was previously reported that the activity of a close homolog of KirBac1.1 is strongly pH-dependent (Zubcevic *et al*, 2014), thus we investigated the influence of the protonation state of G143E on channel gating. In repeated simulations with G143E<sub>p</sub> (protonated), neither opening at the HBC nor twisting at the CTD were observed (see Figure 7A, B). Moreover, no water flux was observed within 200 ns (not shown).

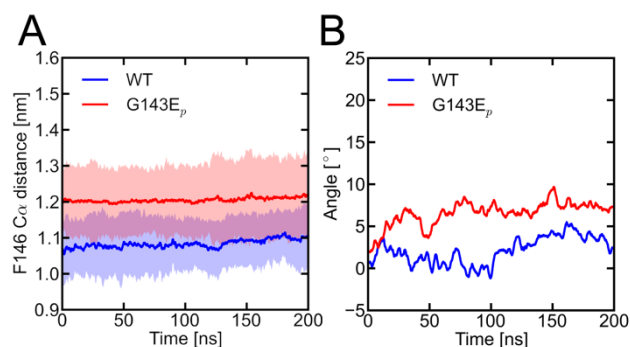


**Figure 7. Analysis of G143E<sub>p</sub> simulations.** A) Averages of F146 Cα-Cα distances in WT and G143E<sub>p</sub> simulations are shown as blue and red lines, respectively. Standard deviations are depicted as light shades accordingly. B) Average CTD rotation angle as a function of time in WT (blue) and G143E<sub>p</sub> (red) simulations.

### *Energetics of the G143E<sub>d</sub> mutant channel opening*

To investigate the coupling between the HBC gate and the CTD twisting motion in more detail, we calculated the free energy landscape of activation gating (Figure 8). The main conformational changes in the most prominent G143E<sub>d</sub> opening simulation (CTD rotation of 23°) were obtained by principal component analysis and used as reaction coordinate for umbrella sampling calculations. At the beginning of the simulation a steep energy decrease of ~ 7 kcal/mol was observed. During this phase, the HBC gate opened and the rotameric state of the F146 side chain changed from a cavity facing to a cavity lining conformation. Further, a first rotational movement of the CTD of ~ 12° occurred. In addition, monitoring of the G143E<sub>d</sub>-R153 salt bridge along the reaction coordinate revealed that in 3 of the 4 subunits a salt bridge between TM2 and the linker of the adjacent subunit was formed during this phase. From 6 to 7 nm, a plateau phase (Figure 8A) was observed, where no rotational movement of the CTD occurred (Figure 8C). Subsequently, a second rotational movement of the CTD led to a total rotation of 23° compared to the starting structure and a further decrease in energy of ~ 3 kcal/mol.

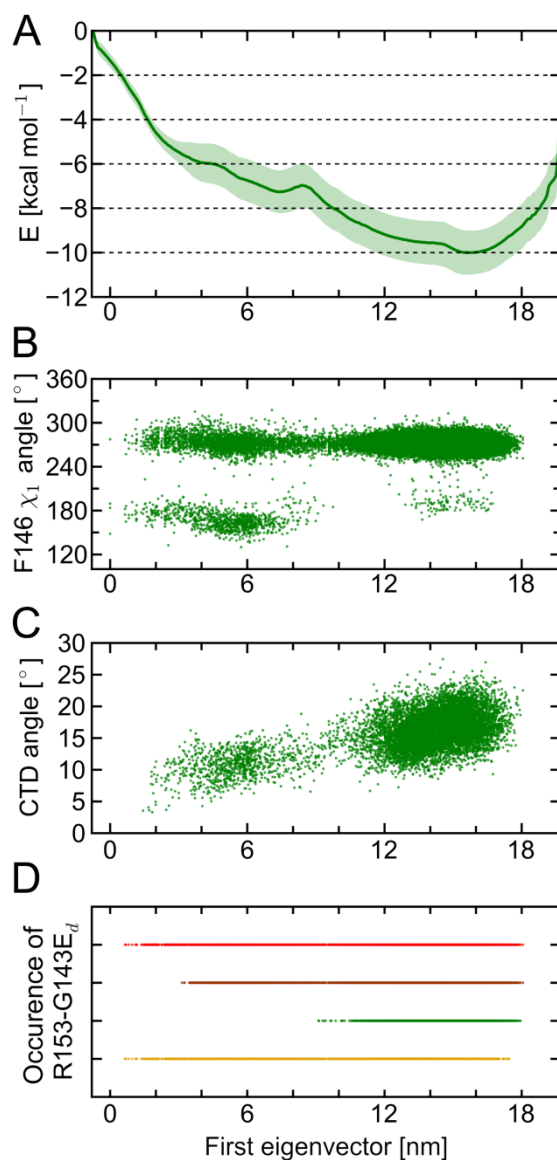


**Figure 8. Free energy profile and corresponding gating changes of KirBac1.1 channel opening.** A) Energy profile along the main conformational changes of opening represented by the first eigenvector. Statistical error is depicted as green shade. B)  $\chi_1$  angle dynamics of F146 during gate opening. C) Rotational angle of the CTD along the first eigenvector. D) Occurrence of the salt bridge between R153 and G143E<sub>d</sub> in all four SUs.

### *Protein-lipid interactions during gating*

The interaction of KirBac1.1 with phospholipids at the TM-CTD interface was reported previously (Enkvetchakul et al, 2007; Clarke et al, 2010). Thus, we investigated the protein-lipid contacts in this region. Figure 9 shows the number of hydrogen bonds to the lipid head groups over time. While for R49 no gating dependent effect was seen, the number of hydrogen bonds increased for K57 (slide-helix) and R151 (C-linker) during channel opening.

Downward movement of the slide-helix at the C-terminal end and a subtle outward movement repositions K57, leading to increased lipid exposure of this residue. Further, repositioning of the C-linker induced by the G143Ed-R153 salt bridge, led to an upward movement of the R151 side chain, and strengthened lipid contacts as shown in Figure 9C.

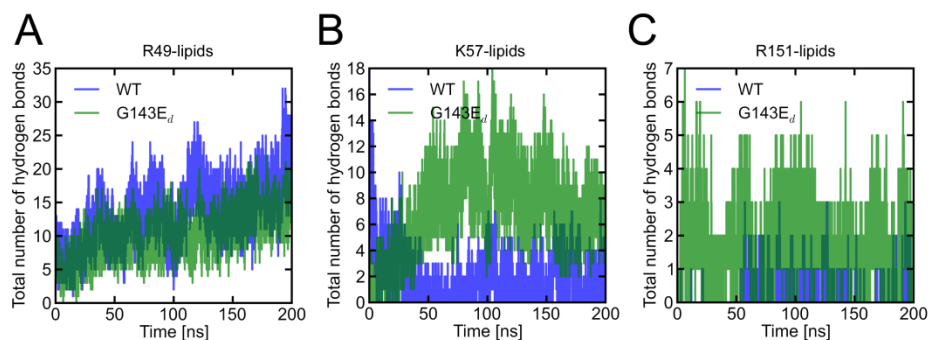


**Figure 9. Protein-lipid interactions during gating.** The total number of hydrogen bonds formed between lipids and R49 (A), K57 (B), and R151 (C) in all four WT and G143Ed simulations are depicted as blue and green lines, respectively.

#### *Comparison to experimental evidence for KirBac gating motions*

The transition pathways obtained by our MD simulations are in good agreement with experimental data. Recent FRET experiments on KirBac1.1 channels revealed major molecular motions in the CTD induced by PIP<sub>2</sub> binding (Wang et al, 2012). Remarkably, during our 200 ns simulations with the G143Ed mutant, we observed tilting motions of the  $\beta_1$  sheet, as reported from FRET experiments. Additionally, x-ray structure analyses on the homolog KirBac3.1 channel revealed a twisting motion of the CTD of 23° relative to the plane of the membrane (Clarke et al, 2010). The final KirBac1.1 state obtained by simulating the G143Ed mutant is in excellent agreement with the twisted conformation described for the homologous KirBac3.1 channel (Clarke et al, 2010; Bavro et al, 2012). The structural changes observed for the HBC gate (bending at a glycine hinge) are consistent with data on other K<sup>+</sup> channels. However, the extent of channel opening varies among crystallized structures (Cuello et al, 2010; Magidovich & Yifrach, 2004; Jin et al, 2002; Domene et al, 2005; Sackin et al, 2006).

## DISCUSSION

In this study, we investigated conformational changes of KirBac1.1 gating by taking advantage of the known activatory mutant G143E<sub>d</sub> in TM2. Simulations with this mutant revealed detailed mechanistic insights into the gating of Kir channels.

In all G143E<sub>d</sub> mutant simulations, HBC opening occurred prior to conformational changes at the CTD. The introduction of a negatively charged glutamic acid in a hydrophobic pocket between TM2 helices led to strong repulsion, which enabled opening of the HBC (Figure 1 and 2). This finding is supported by a previous MD simulation on a KirBac6.1 homology model (Paynter *et al*, 2010). Further, this region has previously been shown to have dramatic effects on gating. For example, a KirBac3.1 open state x-ray structure was crystallized by mutating the equivalent position S129 to an arginine (Bavro *et al*, 2012). Interestingly, an activatory mutant (A108T/S) was also identified at this site in the bacterial K<sup>+</sup> channel KcsA (Irizarry *et al*, 2002; Paynter *et al*, 2008). Moreover, we recently showed that the equivalent position is conserved in voltage gated calcium channels (Depil *et al*, 2011) and mutation of this position has substantial effects on channel gating. We and others have indicated that the small size at this position seems critical for stabilizing the closed gate (Irizarry *et al*, 2002; Hardman *et al*, 2007; Nagaoka *et al*, 2008; Shang & Tucker, 2008). Comparing G143E simulations in protonated and deprotonated state (Figure 1 and 7), revealed that the effect of the mutant in KirBac1.1 on gating is primarily resulting from the negative charge of the side chain and to a lesser extent a size effect. This suggests that several factors contribute to the effects of mutants close to the HBC gate.

The limited simulation time of 200 ns makes it difficult to assess, whether the HBC gate is fully or only partially opened in our simulations. However, water flux observed in all G143E<sub>d</sub> mutant simulations indicates an open state (Figure 3). Substantial conformational variation of the open HBC gate have been reported in x-ray structures (Jiang *et al*, 2002; Kuo *et al*, 2003; Uysal *et al*, 2011; Bavro *et al*, 2012) indicating that subtle variations between channel species might exist. For example, structural differences in CTDs might influence gating. Additionally, there is accumulating evidence that several open states for each channel exist as reported for KirBac1.1 (Cheng *et al*, 2009).

In previous x-ray structures of KirBac3.1 channel, twisted and non-twisted CTD conformations were obtained only with a closed HBC gate (Clarke *et al*, 2010). This led to the conclusion that the CTD rearrangements trigger HBC opening. Contrary to this previously

suggested gating model (Bavro *et al*, 2012; Zubcevic *et al*, 2014), our simulations revealed that the CTD conformational changes occurred after HBC gate opening (Figure 1 and 8). This indicates that the coupling between TM and CTD might operate bidirectionally. The mutant might influence the cross-talk between the two domains. Nevertheless, the importance of electrostatic interactions for stabilizing the twisted conformation, as predicted in our simulations (Figure 5), is in excellent agreement with previous data on KirBac3.1 (Clarke *et al*, 2010). In the G143E<sub>d</sub> mutant, these interactions are mainly accomplished by salt bridge formation of the mutant side chain with R153. The significance of this contact is further stressed by results from the R153A mutant simulations, where only subtle twisting motions were observed (Figure 6). Although this interaction can only occur in the G143E<sub>d</sub> mutant, end states obtained from simulations closely resemble native twisting motions of the CTD as inferred from KirBac3.1 structures. Moreover, subunit interface rearrangements predicted by our simulations (Figure 4) are similar to KirBac3.1 (Clarke *et al*, 2010).

Another important prediction from our simulations concerns the pH-dependence of mutant G143E. Only the deprotonated glutamic acid induced global conformational changes on the nanosecond time scale, suggesting that gating of this mutant might be pH dependent (Figure 1 and 7). Similar observations were reported for a F168E mutant in the HBC gate of the mammalian Kir6.2 channel (Khurana *et al*, 2011). Taken together, our data provide structural details how protonatable side chains can be used to induce channel gating by pH titration.

It is remarkable that nanosecond simulations are sufficient to observe global gating rearrangements in both the HBC gate and the CTD with the G143E<sub>d</sub> mutant. This suggests that the mutant might significantly decrease the energetic barrier for channel opening, since all WT x-ray structures to date were captured with a closed HBC gate. Indeed, our PMF calculations revealed an energy difference of ~ 10 kcal/mol between closed and open state, with no energy barriers present (Figure 8). It is conceivable that an energetic barrier needs to be overcome in WT for channel opening as shown in a previous simulation study on KcsA (Linder *et al*, 2013).

There is accumulating evidence highlighting the importance of lipid components for regulating Kir channels (for recent reviews see (Levitan *et al*, 2010; Logothetis *et al*, 2010; D'Avanzo *et al*, 2010; Rosenhouse-Dantsker *et al*, 2012; Fürst *et al*, 2014)). Analysis of protein lipid interactions in WT and G143E<sub>d</sub> mutant simulations revealed gating-dependent hydrogen bond formation. Especially, interactions of K57 located in the slide-helix and R151

from the C-linker to the lipid head groups are significantly increased upon channel opening (Figure 9). These observations are in excellent agreement with a study by Enkvetchakul et al. (Enkvetchakul *et al*, 2007) which reported the importance of lipid head groups in regulating KirBac1.1 gating. Interestingly, nonspecific anionic lipid interactions have been recently shown to be required for Kir2 channel gating (Lee *et al*, 2013). This indicates that all Kir channels are strongly lipid regulated. This is further supported by a recent MD study on a Kir3.1 chimera (Meng *et al*, 2012).

In conclusion, the presented simulations clearly unravel the progression of conformational changes during gate opening. Contrary to previous hypotheses based on static crystal structures, opening of the HBC gate triggers twisting of the CTD. This process is mediated by electrostatic interactions between TM and CT domains. Additionally, lipid contacts with the slide-helix facilitate channel opening and presumably stabilize this conformation.

## FUNDING SOURCES

This work was supported by the Austrian Science Fund (FWF; Grant W1232; <http://www.fwf.ac.at>). Tobias Linder was supported by a research fellowship 2013 from the University of Vienna.

## ACKNOWLEDGMENTS

The computational results presented have been achieved using the Vienna Scientific Cluster (VSC).

## REFERENCES

- Aqvist J & Luzhkov V (2000) Ion permeation mechanism of the potassium channel. *Nature* **404**: 881–4
- Bavro VN, De Zorzi R, Schmidt MR, Muniz JRC, Zubcevic L, Sansom MSP, Vénien-Bryan C & Tucker SJ (2012) Structure of a KirBac potassium channel with an open bundle crossing indicates a mechanism of channel gating. *Nat. Struct. Mol. Biol.* **19**: 158–63

- Berendsen HJC, Grigera JR & Straatsma TP (1987) The missing term in effective pair potentials. *J. Phys. Chem.* **91**: 6269–6271
- Berger O, Edholm O & Jahnig F (1997) Molecular Dynamics Simulations of a Fluid Bilayer of Dipalmitoylphosphatidylcholine at Full Hydration, Constant Pressure, and Constant Temperature. *Biophys. J.* **72**: 2002–2013
- Bichet D, Haass FA & Jan LY (2003) Merging functional studies with structures of inward-rectifier K(+) channels. *Nat. Rev. Neurosci.* **4**: 957–67
- Cheng WWL, Enkvetchakul D & Nichols CG (2009) KirBac1.1: it's an inward rectifying potassium channel. *J. Gen. Physiol.* **133**: 295–305
- Clarke OB, Caputo AT, Hill AP, Vandenberg JI, Smith BJ & Gulbis JM (2010) Domain Reorientation and Rotation of an Intracellular Assembly Regulate Conduction in Kir Potassium Channels. *Cell* **141**: 1018–1029
- Cuello LG, Jogini V, Cortes DM & Perozo E (2010) Structural mechanism of C-type inactivation in K(+) channels. *Nature* **466**: 203–8
- D'Avanzo N, Cheng WWL, Wang S, Enkvetchakul D & Nichols CG (2010) Lipids driving protein structure? Evolutionary adaptations in Kir channels. *Channels* **4**: 139–41
- Darden T, York D & Pedersen L (1993) Particle mesh Ewald: An N log(N) method for Ewald sums in large systems. *J. Chem. Phys.* **98**: 10089
- Depil K, Beyl S, Stary-Weinzinger A, Hohaus A, Timin E & Hering S (2011) Timothy mutation disrupts the link between activation and inactivation in Ca(V)1.2 protein. *J. Biol. Chem.* **286**: 31557–64
- Domene C, Doyle D a & Vénien-Bryan C (2005) Modeling of an ion channel in its open conformation. *Biophys. J.* **89**: L01–3
- Domene C, Grottesi A & Sansom MSP (2004) Filter flexibility and distortion in a bacterial inward rectifier K<sup>+</sup> channel: simulation studies of KirBac1.1. *Biophys. J.* **87**: 256–67
- Domene C, Vemparala S, Furini S, Sharp K & Klein ML (2008) The role of conformation in ion permeation in a K<sup>+</sup> channel. *J. Am. Chem. Soc.* **130**: 3389–98

- Domene C, Vemparala S, Klein ML, Vénien-Bryan C & Doyle DA (2006) Role of aromatic localization in the gating process of a potassium channel. *Biophys. J.* **90**: L01–3
- Enkvetchakul D, Jeliaskova I, Bhattacharyya J & Nichols CG (2007) Control of inward rectifier K channel activity by lipid tethering of cytoplasmic domains. *J. Gen. Physiol.* **130**: 329–34
- Feenstra KA, Hess B & Berendsen HJC (1999) Improving efficiency of large time-scale molecular dynamics simulations of hydrogen-rich systems. *J. Comput. Chem.* **20**: 786–798
- Fürst O, Mondou B & D’Avanzo N (2014) Phosphoinositide regulation of inward rectifier potassium (Kir) channels. *Front. Physiol.* **4**: 404
- Grottesi A, Domene C, Hall B & Sansom MSP (2005) Conformational dynamics of M2 helices in KirBac channels: helix flexibility in relation to gating via molecular dynamics simulations. *Biochemistry* **44**: 14586–94
- Guex N & Peitsch MC (1997) SWISS-MODEL and the Swiss-PdbViewer: an environment for comparative protein modeling. *Electrophoresis* **18**: 2714–23
- Hansen SB, Tao X & MacKinnon R (2011) Structural basis of PIP<sub>2</sub> activation of the classical inward rectifier K<sup>+</sup> channel Kir2.2. *Nature* **477**: 495–8
- Hardman RM, Stansfeld PJ, Dalibalta S, Sutcliffe MJ & Mitcheson JS (2007) Activation gating of hERG potassium channels: S6 glycines are not required as gating hinges. *J. Biol. Chem.* **282**: 31972–81
- Hellgren M, Sandberg L & Edholm O (2006) A comparison between two prokaryotic potassium channels (KirBac1.1 and KcsA) in a molecular dynamics (MD) simulation study. *Biophys. Chem.* **120**: 1–9
- Hess B, Bekker H, Berendsen HJC & Fraaije JGEM (1997) LINCS: A linear constraint solver for molecular simulations. *J. Comput. Chem.* **18**: 1463–1472

- Hess B, Kutzner C, van der Spoel D & Lindahl E (2008) GROMACS 4: Algorithms for Highly Efficient, Load-Balanced, and Scalable Molecular Simulation. *J. Chem. Theory Comput.* **4**: 435–447
- Hibino H, Inanobe A, Furutani K, Murakami S, Findlay I & Kurachi Y (2010) Inwardly rectifying potassium channels: their structure, function, and physiological roles. *Physiol. Rev.* **90**: 291–366
- Hoover W (1985) Canonical dynamics: Equilibrium phase-space distributions. *Phys. Rev. A* **31**: 1695–1697
- Hornak V, Abel R, Okur A, Strockbine B, Roitberg A & Simmerling C (2006) Comparison of multiple Amber force fields and development of improved protein backbone parameters. *Proteins* **65**: 712–25
- Hub JS, de Groot BL & van der Spoel D (2010) g\_wham—A Free Weighted Histogram Analysis Implementation Including Robust Error and Autocorrelation Estimates. *J. Chem. Theory Comput.* **6**: 3713–3720
- Irizarry SN, Kutluay E, Drews G, Hart SJ & Heginbotham L (2002) Opening the KcsA K<sup>+</sup> Channel: Tryptophan Scanning and Complementation Analysis Lead to Mutants with Altered Gating. *Biochemistry* **41**: 13653–13662
- Jiang Y, Lee A, Chen J, Cadene M, Chait BT & MacKinnon R (2002) Crystal structure and mechanism of a calcium-gated potassium channel. *Nature* **417**: 515–22
- Jin T, Peng L, Mirshahi T, Rohacs T, Chan KW, Sanchez R & Logothetis DE (2002) The (beta)gamma subunits of G proteins gate a K<sup>(+)</sup> channel by pivoted bending of a transmembrane segment. *Mol. Cell* **10**: 469–81
- Jorgensen WL, Chandrasekhar J, Madura JD, Impey RW & Klein ML (1983) Comparison of simple potential functions for simulating liquid water. *J. Chem. Phys.* **79**: 926
- Joung IS & Cheatham TE (2008) Determination of alkali and halide monovalent ion parameters for use in explicitly solvated biomolecular simulations. *J. Phys. Chem. B* **112**: 9020–41

- Khurana A, Shao ES, Kim RY, Vilin YY, Huang X, Yang R & Kurata HT (2011) Forced gating motions by a substituted titratable side chain at the bundle crossing of a potassium channel. *J. Biol. Chem.* **286**: 36686–93
- Kumar S & Nussinov R (2002) Close-range electrostatic interactions in proteins. *Chembiochem* **3**: 604–17
- Kuo A, Gulbis JM, Antcliff JF, Rahman T, Lowe ED, Zimmer J, Cuthbertson J, Ashcroft FM, Ezaki T & Doyle DA (2003) Crystal structure of the potassium channel KirBac1.1 in the closed state. *Science* **300**: 1922–6
- Lee S-J, Wang S, Borschel W, Heyman S, Gyore J & Nichols CG (2013) Secondary anionic phospholipid binding site and gating mechanism in Kir2.1 inward rectifier channels. *Nat. Commun.* **4**: 2786
- Levitan I, Fang Y, Rosenhouse-Dantsker A & Romanenko V (2010) Cholesterol and ion channels. *Subcell. Biochem.* **51**: 509–49
- Linder T, de Groot BL & Stary-Weinzinger A (2013) Probing the energy landscape of activation gating of the bacterial potassium channel KcsA. *PLoS Comput. Biol.* **9**: e1003058
- Logothetis DE, Petrou VI, Adney SK & Mahajan R (2010) Channelopathies linked to plasma membrane phosphoinositides. *Pflügers Arch.* **460**: 321–41
- Magidovich E & Yifrach O (2004) Conserved gating hinge in ligand- and voltage-dependent K<sup>+</sup> channels. *Biochemistry* **43**: 13242–7
- Meng X-Y, Zhang H-X, Logothetis DE & Cui M (2012) The molecular mechanism by which PIP(2) opens the intracellular G-loop gate of a Kir3.1 channel. *Biophys. J.* **102**: 2049–59
- Nagaoka Y, Shang L, Banerjee A, Bayley H & Tucker SJ (2008) Peptide backbone mutagenesis of putative gating hinges in a potassium ion channel. *Chembiochem* **9**: 1725–8
- Nishida M, Cadene M, Chait BT & MacKinnon R (2007) Crystal structure of a Kir3.1-prokaryotic Kir channel chimera. *EMBO J.* **26**: 4005–15

- Nishida M & MacKinnon R (2002) Structural basis of inward rectification: cytoplasmic pore of the G protein-gated inward rectifier GIRK1 at 1.8 Å resolution. *Cell* **111**: 957–65
- Nosé S (1984) A unified formulation of the constant temperature molecular dynamics methods. *J. Chem. Phys.* **81**: 511
- Parrinello M & Rahman A (1981) Polymorphic transitions in single crystals: A new molecular dynamics method. *J. Appl. Phys.* **52**: 7182
- Paynter J, Sarkies P, Andres-Enguix I & Tucker SJ (2008) Genetic selection of activatory mutations in KcsA. *Channels* **2**: 413–418
- Paynter JJ, Andres-Enguix I, Fowler PW, Tottey S, Cheng W, Enkvetchakul D, Bavro VN, Kusakabe Y, Sansom MSP, Robinson NJ, Nichols CG & Tucker SJ (2010) Functional complementation and genetic deletion studies of KirBac channels: activatory mutations highlight gating-sensitive domains. *J. Biol. Chem.* **285**: 40754–61
- Pegan S, Arrabit C, Zhou W, Kwiatkowski W, Collins A, Slesinger P A & Choe S (2005) Cytoplasmic domain structures of Kir2.1 and Kir3.1 show sites for modulating gating and rectification. *Nat. Neurosci.* **8**: 279–87
- Rosenhouse-Dantsker A, Mehta D & Levitan I (2012) Regulation of ion channels by membrane lipids. *Compr. Physiol.* **2**: 31–68
- Sackin H, Nanazashvili M, Palmer LG & Li H (2006) Role of conserved glycines in pH gating of Kir1.1 (ROMK). *Biophys. J.* **90**: 3582–9
- Shang L & Tucker SJ (2008) Non-equivalent role of TM2 gating hinges in heteromeric Kir4.1/Kir5.1 potassium channels. *Eur. Biophys. J.* **37**: 165–71
- Tao X, Avalos JL, Chen J & MacKinnon R (2009) Crystal structure of the eukaryotic strong inward-rectifier K<sup>+</sup> channel Kir2.2 at 3.1 Å resolution. *Science* **326**: 1668–74
- Uysal S, Cuello LG, Cortes DM, Koide S, Kossiakoff AA & Perozo E (2011) Mechanism of activation gating in the full-length KcsA K<sup>+</sup> channel. *Proc. Natl. Acad. Sci. U. S. A.* **108**: 11896–9

- Wang S, Lee S-J, Heyman S, Enkvetchakul D & Nichols CG (2012) Structural rearrangements underlying ligand-gating in Kir channels. *Nat. Commun.* **3**: 617
- Whorton MR & MacKinnon R (2011) Crystal structure of the mammalian GIRK2 K<sup>+</sup> channel and gating regulation by G proteins, PIP<sub>2</sub>, and sodium. *Cell* **147**: 199–208
- Whorton MR & MacKinnon R (2013) X-ray structure of the mammalian GIRK2-βγ G-protein complex. *Nature* **498**: 190–7
- Wolf MG, Hoefling M, Aponte-Santamaría C, Grubmüller H & Groenhof G (2010) g\_membed: Efficient insertion of a membrane protein into an equilibrated lipid bilayer with minimal perturbation. *J. Comput. Chem.* **31**: 2169–74
- Zubcevic L, Bavro VN, Muniz JRC, Schmidt MR, Wang S, De Zorzi R, Venien-Bryan C, Sansom MSP, Nichols CG & Tucker SJ (2014) Control of KirBac3.1 Potassium Channel Gating at the Interface between Cytoplasmic Domains. *J. Biol. Chem.* **289**: 143–51

### **4.3 Structural insights into trapping and dissociation of small molecules in K<sup>+</sup> channels**

---

Linder T, Saxena P, Timin E, Hering S, Stry-Weinzinger A.

*Journal of Chemical Information and Modeling*

Under revision since 16 June, 2014

# Structural insights into trapping and dissociation of small molecules in K<sup>+</sup> channels

*Tobias Linder, Priyanka Saxena, Eugen Timin, Steffen Hering, Anna Stary-Weinzinger\**

Department for Pharmacology and Toxicology, University of Vienna, Althanstraße 14, 1090  
Vienna

**KEYWORDS:** molecular dynamics simulations, tetrabutylammonium, hERG, KcsA, two-electrode voltage clamp.

**ABSTRACT.** K<sup>+</sup> channels play a critical role in numerous physiological and pathophysiological processes rendering them an attractive target for therapeutic intervention. However, the hERG K<sup>+</sup> channel poses a special challenge in drug discovery, since block of this channel by a plethora of diverse chemical entities can lead to long QT syndrome and sudden death. Of particular interest is the so called trapping phenomenon, characterized by capture of a drug behind closed channel gates, which harbors an increased pro-arrhythmic risk. In this study we investigated the influence of trapped blockers on the gating dynamics and probed the state dependence of dissociation in K<sup>+</sup> channels by making use of the quaternary tetrabutylammonium. By applying essential dynamics simulations and two-electrode voltage clamp we obtained detailed insights into the dynamics of trapping in KcsA and hERG. Our simulations suggest that the trapped TBA influences the F656 flexibility during gate closure. Based on these findings, we provide a structural hypothesis for drug trapping. Further our simulations reveal the extent of gate opening necessary for drug dissociation.

## INTRODUCTION

Voltage gated  $K^+$  channels play a critical role in numerous physiological and pathophysiological processes such as nerve and muscle excitation, sensory transduction and cell proliferation. With a wide range of human diseases linked to voltage gated  $K^+$  channels, so called “channelopathies”, they represent an attractive target for therapeutic intervention (Bagal *et al*, 2013). The human ether-à-go-go related gene (hERG)  $K^+$  channel poses a special challenge in drug discovery, since it can be blocked by a plethora of structurally diverse drugs including antiarrhythmics, antihistamines, antipsychotics and antibiotics (Fermini & Fossa, 2003). This often unwanted inhibition can lead to acquired long QT syndrome (LQTS) and sudden cardiac death (Chiang & Roden, 2000; Keating & Sanguinetti, 2001). Consequently, several pharmaceuticals such as cisapride or terfenadine were withdrawn from the market. Further, reduced hERG channel function caused by inherited mutation leads to congenital LQTS. Recent research indicates that hERG channels are frequently overexpressed in certain human cancers and that long-term treatment with blockers could have therapeutic potential in cancer treatment (Jehle *et al*, 2011; Pier *et al*, 2014). Thus, pharmacological intervention could potentially be useful for cancer treatment and clinical management of LQTS.

Great efforts have been directed toward a better understanding of the molecular and structural mechanisms of hERG channel gating and block. Substantial progress has been made by identifying the amino acids essential for drug block. They include T623, S624 and V625, from the pore helix, and residues G648, Y652 and F656, located on the TM2 segments (Mitcheson *et al*, 2000a; Lees-Miller *et al*, 2000; Kamiya *et al*, 2001; Sánchez-Chapula *et al*, 2002; Sánchez-Chapula *et al*, 2003; Sánchez-Chapula *et al*, 2004; Ridley *et al*, 2004; Perry *et al*, 2004; Witchel *et al*, 2004; Fernandez *et al*, 2004; Sanguinetti & Mitcheson, 2005; Kamiya *et al*, 2006; Guo *et al*, 2006; Kamiya *et al*, 2008). However, a key unresolved question in hERG channel block is how drug dissociation is influenced by channel closure. There is

evidence that hERG channel blockers can be trapped in the inner cavity of the closed channel (Carmeliet, 1992; Mitcheson *et al*, 2000b; Perry *et al*, 2004; Witchel *et al*, 2004; Kamiya *et al*, 2006; Stork *et al*, 2007; Kamiya *et al*, 2008; Windisch *et al*, 2011). The importance of this phenomenon is emphasized by a recent study highlighting a connection between pro-arrhythmic risk and trapping (di Veroli *et al*, 2013).

The trapping phenomenon in  $K^+$  channels was first described for quaternary ammonium (QA) blockers by Armstrong in 1971 (Armstrong, 1971). Since then, QA compounds have been widely used as structural probes to identify the binding site of ion channel blockers (Armstrong & Hille, 1972; MacKinnon & Yellen, 1990; Luzhkov & Aqvist, 2001; Zhou *et al*, 2001a), investigate gating processes (Holmgren *et al*, 1997; Posson *et al*, 2013) and to shed light on the structure of ion channels (Yellen *et al*, 1991; Choi *et al*, 1993; Crouzy *et al*, 2001; Lenaeus *et al*, 2005).

Herein, we set out to investigate the influence of trapped blockers on the gating dynamics and probe the state dependence of dissociation in  $K^+$  channels by making use of the QA blocker tetrabutylammonium (TBA). The crystal structure complex of the prototypical  $K^+$  channel KcsA with a TBA bound in the closed channel pore (Faraldo-Gómez *et al*, 2007; Yohannan *et al*, 2007) provides an excellent starting point to analyze trapping dynamics and drug dissociation pathways in  $K^+$  channels. We utilized essential dynamics (ED) simulations and two-electrode voltage clamp to obtain detailed insights into the dynamics of trapping in KcsA and hERG. Further, free energy calculations were performed to examine state dependent dissociation of a trapped channel blocker.

## METHODS

**MD simulations.** The crystal structure (pdb identifier: 2HVK), comprising of the closed KcsA channel from residue 22 to 124 and the co-crystallized trapped TBA (Yohannan *et al*, 2007), was used as starting point for MD simulations. The open (pdb identifier: 3f7v) and the intermediate (pdb identifier: 3fb6) channel state were obtained from Cuello *et al*. (Cuello *et al*, 2010) Due to crystallization of shorter fragments of the latter two structures, the missing amino acids at the N- and C-termini below the bundle crossing gate were added using Discovery Studio 3.5 (Accelrys Software Inc., San Diego, CA, USA) to obtain channel states of the same length. In addition, the introduced cysteine at position 90 in the crystal structures was mutated back to the WT leucine. TBA was added to the open and intermediate channels by placing it in the cavity according to the closed channel binding site. Further, TBA was docked to the open hERG homology model (Stary *et al*, 2010) using FlexX which is part of the LeadIT software package version 2.0.1 (BioSolveIT, Sankt Augustin, Germany). The sphere center of the binding site was placed in the middle of the cavity and the radius was set to 10 Å. General amber force field parameters (Wang *et al*, 2004) for TBA were generated by making use of Gaussian09 (Frisch *et al*, 2009) and antechamber (Wang *et al*, 2006) which is part of the amber package (Case *et al*, 2010). Protein-ligand complexes were embedded in an equilibrated palmitoylcholinephosphatidylcholine (POPC) membrane consisting of 256 lipids using the g\_membed tool (Wolf *et al*, 2010). K<sup>+</sup> ions were placed in the selectivity filter (SF) at sites S0, S2, S4 and water was added at S1, S3 (Aqvist & Luzhkov, 2000). The system was neutralized by randomly adding Cl<sup>-</sup> within the solvent. All simulations were carried out using the MD simulation software Gromacs v.4.5.4 (Hess *et al*, 2008). The amber99sb force field (Hornak *et al*, 2006) and the TIP3P water model (Jorgensen *et al*, 1983) were employed. Lipid parameters were taken from Berger *et al*. (Berger *et al*, 1997). The cutoff for Lennard-Jones interactions was set to 1.0 nm and parameters were corrected for monovalent ions

(Joung & Cheatham, 2008). Electrostatic interactions were calculated with a cutoff of 1.0 nm, long-range electrostatic interactions were treated by the particle-mesh Ewald method at every step (Darden *et al*, 1993). The LINCS algorithm (Hess *et al*, 1997) was used to constrain bonds, allowing for an integration step of 2 fs. The Nose-Hoover thermostat (Nosé, 1984; Hoover, 1985) was used keeping the simulation temperature constant at 310 K. Coupling groups were defined as the protein-ligand complex, lipids and solvent with a time constant of 0.2 ps. The Parrinello-Rahman barostat algorithm (Parrinello & Rahman, 1981) with a coupling constant of 1 ps was used for a constant pressure of 1 bar. Prior to simulation, 1000 conjugate gradient energy-minimization steps and a 5 ns equilibration run by restraining the protein-ligand complex by a force constant of 1000 kJ/mol/nm<sup>2</sup> were performed. Subsequent free MD simulations were carried out for 20 ns in KcsA and for 100 ns in hERG.

**Essential dynamics simulations.** The ED technique was employed as described previously (Linder *et al*, 2013). Briefly, an eigenvector representing the transition between open and closed channel state was obtained from principal component analysis. For this analysis, the backbone of the helices between the two states was compared. Fixed increment linear expansion was set to  $-1.69 \times 10^{-6}$  nm per simulation step (2 fs). 20 closing ED simulations, lasting for 20 ns each, were performed in the absence and presence of TBA for KcsA and the hERG channel, respectively.

**Force probe MD simulations and umbrella sampling.** To probe different dissociation pathways of TBA, a harmonic potential with a force constant of 1000 kJ/mol/nm<sup>2</sup> was applied on TBA. The compound was pulled for 20 ns with a rate of 0.00025 nm/ps along z-axis to investigate dissociation through the activation gate. The first turn of the extracellular side of the P-helix was restrained with a force constant of 1000 kJ/mol/nm<sup>2</sup> during pulling to prohibit movement of the protein. For dissociation simulations of the open KcsA and hERG channel, ions were restrained with a force constant of 10000 kJ/mol/nm<sup>2</sup> to prevent ion migration through the gate and minimize the ion influence on drug dissociation. In case of dissociation

experiments on KcsA, 65, 67, and 56 snapshots from closed, intermediate, and open state simulations were extracted, respectively, and subject to 20 ns umbrella sampling with force constants of either 1000 or 10000 kJ/mol/nm<sup>2</sup>. For hERG dissociation, 57 snapshots from open simulations were obtained and used for umbrella sampling accordingly (histograms of umbrella sampling simulations are shown in the supporting information). The first 10 ns of each window were discarded for equilibration. The potential of mean force and the statistical errors were estimated by the g\_wham tool and the integrated bootstrap analysis method using 100 bootstraps (Hub *et al*, 2010).

**Experimental procedure.** cDNAs of hERG (accession number NP000229) were kindly provided by Prof. Sanguinetti (University of Utah, UT, USA). Synthesis of capped runoff complementary ribonucleic acid (cRNA) transcripts from linearized complementary deoxyribonucleic acid (cDNA) templates and injection of cRNA were performed as described in detail by Sanguinetti *et al*. (Sanguinetti *et al*, 1995). Oocytes from the South African clawed frog, *Xenopus laevis*, (NASCO, Fort Atkinson, WI, USA) were prepared as follows: After 15 min exposure of female *Xenopus laevis* to the anaesthetic (0.2 % solution of MS-222; the methane sulfonate salt of 3-aminobenzoic acid ethyl ester; Sigma), parts of the ovary tissue were surgically removed. Defolliculation was achieved by enzymatical treatment with 2 mg/mL collagenase type 1A (Sigma) and mechanical removal of follicular layer using forceps. Stage V–VI oocytes were selected and injected with the WT and mutant hERG-encoding cRNA. Injected oocytes were stored at 18 °C in ND96 bath solution (96 mM sodium chloride, 2 mM potassium chloride, 1 mM magnesium chloride, 5 mM HEPES, 1.8 mM CaCl<sub>2</sub>; pH 7.5, titrated with NaOH) containing 1% penicillin-streptomycin solution. All chemicals used were purchased from Sigma-Aldrich Chemie GmbH, Taufkirchen, Germany.

Currents through hERG channels were studied 1 to 4 days after microinjection of the cRNA using the two-microelectrode voltage clamp technique. ND96 was used as extracellular recording solution. Voltage-recording and current-injecting microelectrodes were filled with 3

M KCl, and had resistances between 0.3 and 2 M $\Omega$ . Endogenous currents (estimated in oocytes injected with DEPC water) did not exceed 0.15  $\mu$ A. Currents > 5  $\mu$ A were discarded to minimize voltage clamp errors. Ionic currents were recorded with a Turbo Tec 03X Amplifier (npi electronic, GmbH, Tamm, Germany) and digitized with a Digidata 1322A (Axon Instruments Inc., Union City, CA, USA). The pClamp software package version 9.2 (Axon Instruments Inc.) was used for data acquisition. Microcal Origin 7.0 was employed for analysis and curve fitting.

A precondition for all measurements was the achievement of stable peak current amplitudes over periods of 10 min after an initial run-up period. A frequency of 0.3 Hz was used for all voltage clamp experiments. Drugs were applied by means of a perfusion system enabling solution exchange within 100 ms (Baburin *et al*, 2006). The oocytes were kept for 5 min at a holding potential of -100 mV to equilibrate drug diffusion. The tail current was measured at -50 mV, after a step to +20 mV. Use-dependent hERG channel block was estimated as peak tail current inhibition. Data are presented as means  $\pm$  s.e. from at least four oocytes from  $\geq 2$  batches; statistical significance of differences was defined as  $P < 0.0001$  in Student's unpaired *t*-test. The studied compound TBA was obtained from Sigma and was dissolved in ND96 extracellular recording solution to prepare a 1 M stock on the day of experiments. Drug stock solution was further diluted to the required concentration.

## RESULTS

**TBA trapping simulations in KcsA.** Using MD simulations, we have previously identified key residues in KcsA essential for gating (Linder *et al*, 2013). In particular, we found that the TBA binding determinant F103 changes its rotameric state during channel gating. Thus, to investigate the influence of TBA on conformational changes upon channel closure, 20 ED simulations with and without TBA present in the cavity were performed which enable

simulating channel closure on the ns time scale (Linder *et al*, 2013). Each closing simulation was conducted for 20 ns. ED is a free MD simulation method, with all coordinates equilibrating, except for one coordinate, which is derived from a linear interpolation between the open and closed helix backbone structures and is biased to drive gating. All other degrees of freedom are explicitly allowed to relax continuously, enabling investigation of side chain conformational changes during drug trapping.

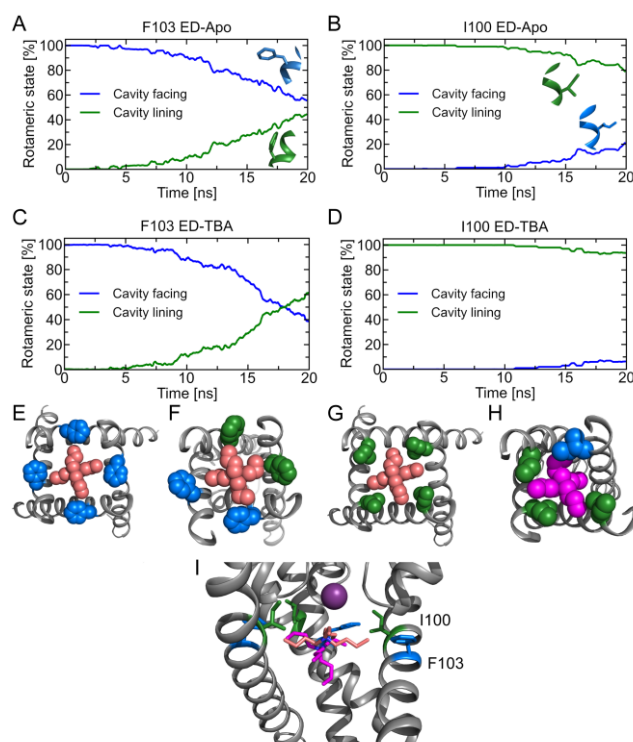


**Figure 1. Rotameric states of F103 and I100 during KcsA gate closure.** Conformational changes of F103 (A and C) and I100 (B and D) in the absence (A and B) and presence (C and D) of TBA during gating. The cavity facing ( $\chi_1$  angle  $< -123^\circ$ ) and cavity lining ( $\chi_1$  angle  $> -123^\circ$ ) states are shown as blue and green line, respectively. Panels E and F show the rotameric states of F103 as spheres at the beginning and end of gate closure in top view, respectively. In panels G and H, I100 is shown as spheres accordingly. Panel I represent the xy-plane (pink sticks) and tilted (magenta sticks) orientation of TBA in the side view. For clarity, only three SUs are shown in gray. The K<sup>+</sup> ion in the SF is represented as a violet sphere. The color code of the amino acids corresponds to the rotameric states.

Specifically, the  $\chi_1$  angle of the binding site forming F103 and I100 was monitored and separated into the two possible rotameric states, namely cavity lining ( $\chi_1$  angle  $> -123^\circ$ ) and cavity facing ( $\chi_1$  angle  $< -123^\circ$ ) state. Subsequently, the percentage of the two states was calculated for each time step and plotted over time (Figure 1). In the absence of TBA (Figure 1A), nearly equal distribution between the two states was observed at the end of gate closure for F103, which is in good agreement with our previous work (Linder *et al*, 2013). In the presence of TBA, only a slightly faster rotameric switch from cavity facing to the cavity lining was observed over time leading to a preference of the cavity lining conformation at the end of gate closure (Figure 1C). The second important binding determinant, I100, displayed high stability during gating. Only rare changes from the cavity lining to the cavity facing conformation were detected with negligible impact by the bound TBA (Figure 1B and D).

Crystallographic data in combination with MD simulations revealed that TBA can adopt two different orientations in the KcsA binding site linked to the ion configuration in the SF (Faraldo-Gómez *et al*, 2007).

Throughout gate closure, TBA remained in the high affinity binding site formed by F103 and I100 (Figure 1E-H). TBA is either in a xy-plane orientation which is parallel to the membrane plane and is centered on the channel symmetry axis. In this orientation, the butyl side chains project into the grooves formed by I100 and F103. Alternatively, TBA adopts a tilted, vertical orientation which is indicated by an off-axis center of TBA (Figure 1I). In the gating simulations, sampling of the xy-plane and the tilted orientation was observed independent of the ion configuration in the SF. No specific pattern between F103 switch and TBA orientation was found indicating that F103 can either face or line the cavity and still allow both TBA orientations. In the rare observations where I100 faced the cavity, spatial displacement led to the tilted orientation of TBA (Figure 1H).

TBA primarily exists in two conformations. The energetically more favorable D<sub>2d</sub> conformation exhibit a cross-shaped structure with all four butyl chains in a planar

arrangement while the S<sub>4</sub> conformation exhibits the shape of an inverted tetrahedron. Quantum-mechanical calculations of the QA analogue tetraethylammonium (TEA) have shown that the D<sub>2d</sub> state is separated from the S<sub>4</sub> conformation by energy barriers of around 10 kcal/mol and a total energy difference of around 1 kcal/mol (Luzhkov *et al*, 2002). The energy difference between the two states is similar for TBA (Faraldo-Gómez & Roux, 2007). Throughout the closing process, TBA stayed in the D<sub>2d</sub> conformation (see supplemental Figure S1), which is in good agreement with previous TBA simulations in the closed channel (Faraldo-Gómez *et al*, 2007). Only rare transitions to the S<sub>4</sub> conformation were observed. This suggests that TBA does not have to change its conformation in order to allow rotation of the F103 side chain. In addition, this observation indicates that the TBA conformation is independent of the rotameric state of F103. Taken together, our data suggests that TBA does not interfere with side chain rearrangements necessary for gating in KcsA.

**Experimental characterization of hERG channel block by TBA.** Despite the crucial role of drug trapping in hERG channels (di Veroli *et al*, 2013), the structural interplay between drug and channel during closure are not well understood. Again, we resorted to the well-studied model drug TBA to investigate trapping in hERG. It was previously shown by Choi *et al*. (Choi *et al*, 2011) that externally applied TBA presumably blocks hERG from the intracellular side by permeating through the cell membrane in CHO cells. However, the characteristics of TBA block were not investigated in detail. Therefore, we set out to test whether TBA is trapped in hERG channels expressed in *Xenopus* oocytes by using the two-electrode voltage-clamp technique.

hERG channels were activated and subsequently inactivated by 300 ms depolarization to +20 mV (Figure 2A). Upon repolarization to -50 mV, channels undergo rapid recovery from inactivation inducing a large tail current. In order to analyze state-dependent block, currents were measured in the absence of TBA (control, Figure 2A) and after preincubation for 330 s

with 20 mM TBA while holding at -100 mV. Subsequently, 0.3 Hz pulse trains were applied until steady state block was reached. The ratio between tail current amplitude in the presence of TBA and tail current amplitude in the control solution was taken as a measure of block. Channel block developed in a “use-dependent” manner. The first current after the 330 s equilibrium in TBA displayed a pronounced decay during the 300 ms prepulse to +20 mV (Figure 2A, p1) with a significant tail current inhibition. Prepulse and tail currents were further inhibited during the 0.3 Hz pulse train. The steady state block was achieved rapidly within the first 2 pulses (Figure 2A; p2, p13). The development of block during channel activation at +20 mV suggests that TBA blocks hERG channels in an open channel conformation. 20 mM TBA blocked hERG channels by  $68.3 \pm 2.0 \%$  (Figure 2D).

To identify amino acids essential for TBA block, we performed alanine mutation studies on Y652 and F656 which have been shown to play a key role for binding of different chemical entities (Fernandez *et al*, 2004). The WT channel voltage protocol was utilized for Y652A, while tail currents were measured at -140 mV for F656A as reported by Witchel *et al*. (Witchel *et al*, 2004). Y652A and F656A significantly reduced channel inhibition to  $19.6 \pm 2.7 \%$  and  $11.7 \pm 3.2 \%$ , respectively (Figure 2B-D). This is in line with data shown in Figure 2A suggesting that TBA accesses a binding site inside the cavity comprising of the two prominent aromatic residues.

Next, we probed if TBA is trapped inside the hERG cavity as suggested for KcsA (Zhou *et al*, 2001a; Faraldo-Gómez *et al*, 2007; Yohannan *et al*, 2007). The hallmark of drug trapping is an ultra-slow recovery or lack of recovery at rest (Mitcheson *et al*, 2000b; Kamiya *et al*, 2006; Stork *et al*, 2007; Windisch *et al*, 2011). Recovery of hERG from TBA block during a 0.3 Hz train was monitored after a 330 s period at holding potential of -100 mV where the channels are in a closed resting state. During this rest period, the oocytes were perfused with TBA-free solution (Figure 2E). The first current amplitudes after this rest period recovered from block only by  $5 \pm 1.1 \%$  indicating that TBA is trapped in the closed channel

conformation. Subsequent frequent opening of the channel during continuous stimulation at 0.3 Hz induced mono-exponential recovery from TBA block to  $41.3 \pm 8.3 \%$  in 330 s (Figure 2E) suggesting that trapped TBA leaves the channel during activation when the channels are in an open conformation.

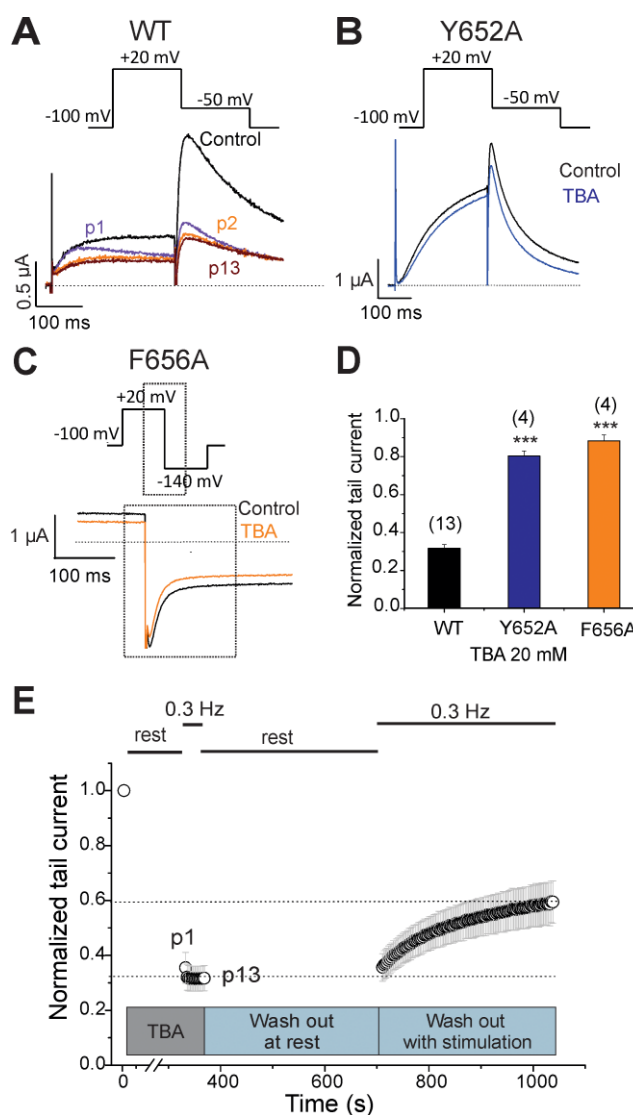


**Figure 2. WT and mutant hERG channel inhibition by TBA.** A) Superimposed current traces in the absence of TBA (control, black) and after a 330 s preincubation period in 20 mM TBA (p1, magenta). Steady state block occurred within the first 2 pulses (p2, orange and p13, brown). The voltage protocol is shown on top of the current traces. B and C) Representative current traces and corresponding voltage protocols for current measurements of mutants Y652A and F656A in the absence (Control, black trace) and presence of 20 mM TBA (blue and orange trace, respectively). Tail currents of F656A were recorded at -140 mV. D) Normalized peak tail currents of WT, Y652A, and F656A channels after steady state block by 20 mM TBA (n=4-13, error bars,  $\pm$ SEM; unpaired *t*-test,  $P < 0.0001$ ). E) State dependent recovery of hERG channels from TBA block. Peak tail

currents were normalized to control currents and plotted against time. After 330 s incubation of WT hERG channels with 20 mM TBA, steady state block was reached within the first 2 pulses of a 0.3 Hz pulse train (p1 - p13). During the following 330 s wash period, channels were kept closed at resting potential of -100 mV. Recovery from block at rest was probed by subsequent pulsing at 0.3 Hz.

**Structural insights of TBA block in hERG.** To further explore TBA hERG channel interactions, we docked TBA into the hERG cavity using the program FlexX and the open hERG homology model (Stary *et al*, 2010). In the docking simulations, the tilted orientation is favored over the xy-plane orientation thereby maximizing hydrophobic interactions of TBA with Y652 and F656 (Figure 3A and B). In a subsequent 100 ns MD simulation starting from the best ranked docking pose, TBA sampled both planar and tilted orientations equally, closely interacting with the two aromatic amino acids Y652 and F656. In Figure 3C, the shortest distances between a TBA side chain and the aromatic rings of Y652 and F656 are plotted over time. Distances between 4 and 6 Å indicate that TBA side chains favorably interact with the aromatic amino acids. Measured distances between the quaternary nitrogen of TBA and Y652 and F656 were always above 5.5 Å in our simulation. At such distances the potential energies of cation-pi interactions become insignificant (Marshall *et al*, 2009). Therefore, it is unlikely that cation-pi stacking contribute to binding. Throughout the simulations TBA remained in the energetically favorable D<sub>2d</sub> conformation.

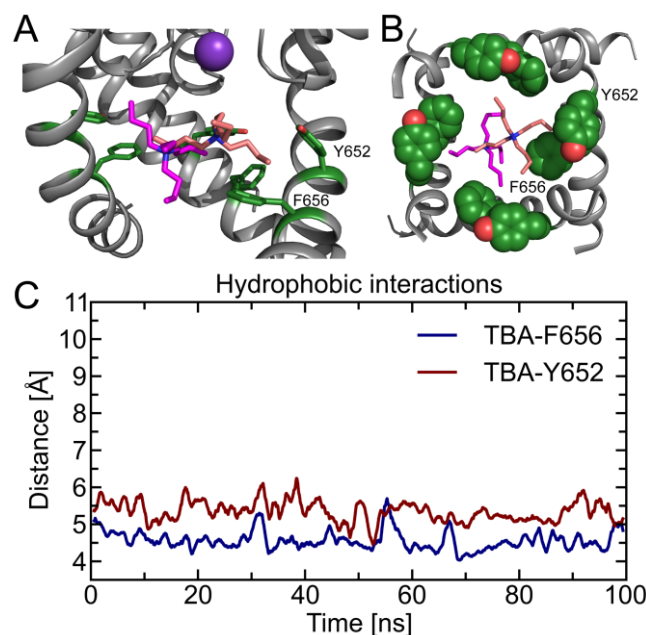


**Figure 3. Orientation of TBA in hERG and distances between TBA side chains and Y652 and F656.** A) TBA in the xy-plane (pink sticks) and tilted (magenta sticks) orientation in side view. For clarity, only three SUs are shown in gray. The  $K^+$  ion in the SF is represented as a violet sphere. Y652 and F656 are shown as green sticks. B) Top view of TBA in the xy-plane (pink sticks) and tilted (magenta sticks) orientation. Y652 and F656 in the cavity facing state are shown as green spheres. C) Distances between TBA side chains and Y652 and F656. The distance between the three outermost carbon atoms of each butyl side chain and the aromatic rings was calculated. The closest distance at each time step is plotted.

**Dynamics of TBA trapping in hERG.** To investigate possible conformational changes during hERG gating, we performed 20 ED simulations in the absence and presence of TBA. The apo simulations revealed that the conformation of Y652 remains in the cavity facing orientation, independent of channel state (Figure 4A). In contrast the rotameric state of the second aromatic amino acid forming the binding site, F656 changed dramatically during gate closure. While preferably in the cavity facing conformation in the open channel state, F656 switched rapidly to the cavity lining conformation in the apo simulations, reaching equal distribution between the two states after 8 ns (Figure 4B). Interestingly, a third, rare rotameric state of F656 was observed during gating. F656 can rotate to a state orthogonally to the S6

helix since two adjacent S6 helices approach each other during closing and therefore decrease the space in this region. These findings show that Y652 remains rigid during gating while F656 undergoes gating specific rotameric changes.

Next, we probed the influence of TBA on gating dependent rearrangements of binding residues. We observed no significant differences for Y652 (Figure 4C). However, TBA clearly influenced the dynamics of F656 during trapping. Figure 4D illustrates that TBA slows the transition from the cavity facing to the cavity lining conformation. In simulations without the blocker, equal distribution was reached after 8 ns while in the presence of TBA, 15 ns were necessary. This suggests that the trapped TBA stabilizes the F656 conformation in cavity facing orientation.

As observed in KcsA, TBA remains in the D<sub>2d</sub> conformation with rare observations of the S<sub>4</sub> state during hERG channel closure (supplemental Figure S2). Due to the larger cavity, TBA can adopt the tilted as well as the xy-plane orientation (Figure 4E and F).

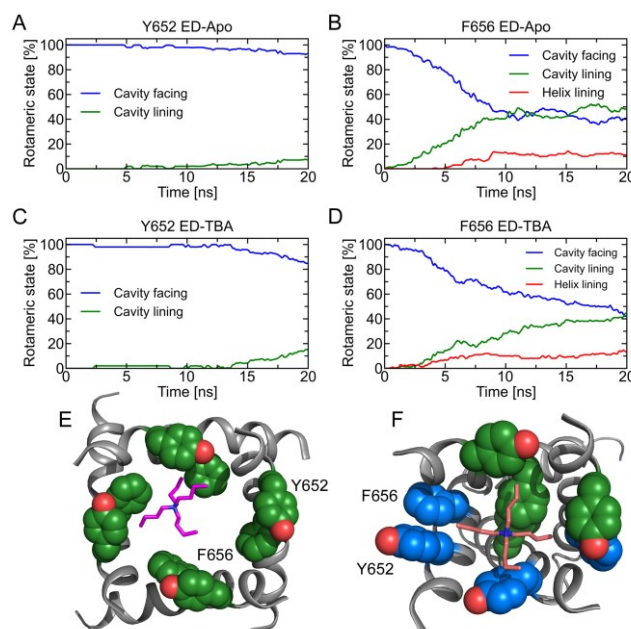


**Figure 4. Rotameric states of Y652 and F656 during hERG gate closure.** Conformational changes of Y652 (A and C) and F656 (B and D) in the absence (A and B) and presence (C and D) of TBA during gating. Cavity facing (blue line) and cavity lining (green line) states identified for KcsA also apply for hERG. For F656, an additional helix lining state ( $\chi_1$  angle in the range of  $80^\circ$ , red line) was observed. E and F) Rotameric states of

Y652 and F656 as spheres at the beginning and end of gate closure in top view, respectively. TBA is represented as sticks and colored magenta and pink in the tilted and xy-plane orientation, respectively. Y652 and F656 are colored according to their rotameric states.

**State dependence of TBA dissociation.** While it was shown that dissociation of trapped compounds is explicitly linked to an open gate, the extent of gate opening necessary for dissociation remains elusive. Crystal structures of KcsA in closed, intermediate and open states (Zhou *et al*, 2001b; Cuello *et al*, 2010), and a co-crystallized TBA (Faraldo-Gómez *et al*, 2007; Yohannan *et al*, 2007) provide an ideal set of structural information to probe state dependent dissociation. The closed channel with TBA, crystallized by Yohannan *et al*. (Yohannan *et al*, 2007), served as a starting point. TBA was placed to the same binding site in the intermediate and open channel state (Cuello *et al*, 2010) and all systems were subject to 20 ns free MD simulation to allow equilibration of TBA orientation. TBA remained in the xy-plane orientation as seen in the crystal structures (Faraldo-Gómez *et al*, 2007; Yohannan *et al*, 2007). Subsequently, force probe MD simulations were used to pull the compound along the channel axis through the gate region. Free energy calculations of the dissociation pathway by umbrella sampling provide qualitative insights into the probability of TBA dissociation from specific channel states. In the closed KcsA channel, TBA is tightly packed in the cavity formed by F103 and I100 as well as by T107 where the pore becomes constricted (see Figure 5B and C). The small energy well in the cavity and the large energy increase along the z-axis indicate that the cavity space in the closed state is very limited (Figure 5A). Squeezing TBA through the closed gate (Figure 5D-G) led to a total energy barrier of 50 kcal/mol rendering spontaneous dissociation through the closed gate very unlikely. During the force probe simulation, TBA adopted and remained in the S<sub>4</sub> conformation. This suggests that part of the applied energy, contributing to the energy barrier, is used to change the TBA conformation. In addition, up to 1 kcal/mol might be stored in the S<sub>4</sub> conformation.

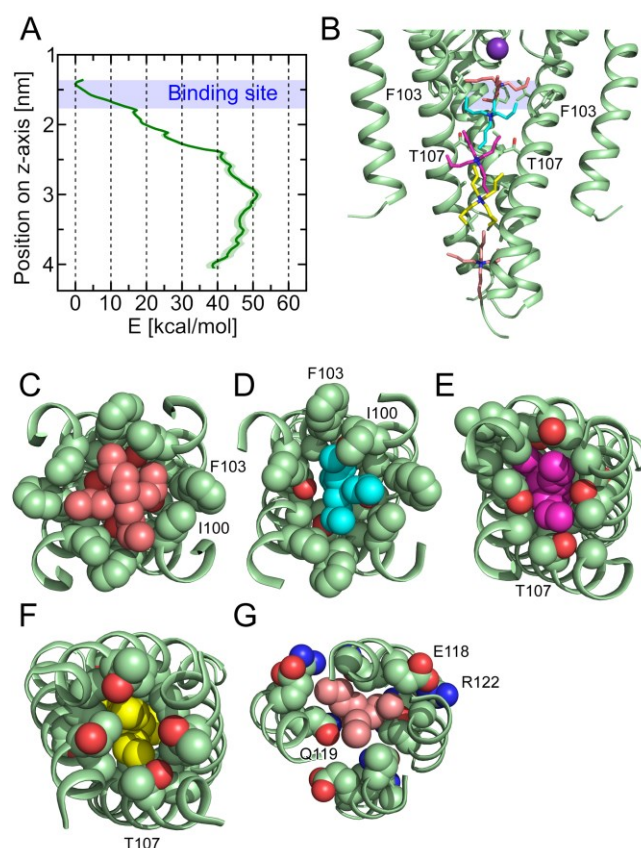


**Figure 5.** A) Free energy profile of TBA dissociation from the closed KcsA channel. The blue shade depicts the high affinity binding site. Statistical error is shown as green shade. B) TBA structures, represented as sticks, show the dissociation pathway through the gate. For clarity, only three SUs are shown in green. Interacting amino acids are depicted as green sticks. The  $K^+$  ion in the SF is represented as a violet sphere. TBA structures in panel B and C-G correspond to positions 1.45 nm (pink, C), 1.84 nm (cyan, D), 2.45 nm (magenta, E), 3.0 nm (yellow, F), and 4.0 nm (light pink, G). C-G) Top view of TBA and interacting amino acids during dissociation. TBA is colored according to its position and amino acids are shown as green spheres with one SU labeled.

Next, TBA was pulled through the intermediate channel gate (gate diameter of 8 Å). The opening of the gate increased the cavity size leading to a broader energy well of TBA in the binding site. However, an energy barrier of 40 kcal/mol was calculated for TBA dissociation (Figure 6A-F). Again, TBA adopted the  $S_4$  conformation during dissociation and stayed in that conformation.

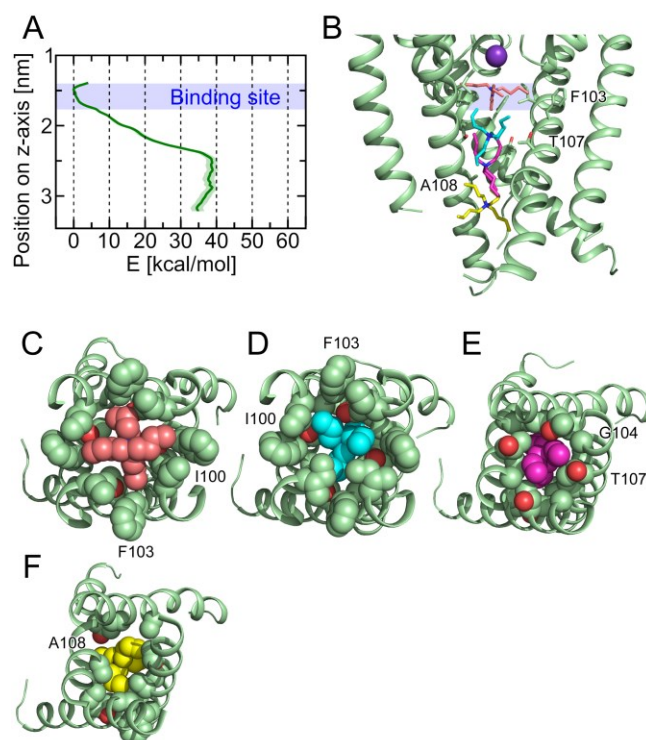


**Figure 6.** A) Free energy profile of TBA dissociation from the intermediate KcsA channel. The blue shade depicts the high affinity binding site. Statistical error is shown as green shade. B) TBA structures, represented as sticks, show the dissociation pathway through the gate. For clarity, only three SUs are shown in green. Interacting amino acids are depicted as green sticks. The  $K^+$  ion in the SF is represented as a violet sphere. TBA structures in panel B and C-F correspond to positions 1.5 nm (pink, C), 2.1 nm (cyan, D), 2.5 nm (magenta, E), and 3.2 nm (yellow, F). C-F) Top view of TBA and interacting amino acids during dissociation. TBA is colored according to its position and amino acids are shown as green spheres with one SU labeled.

In the open KcsA channel, the cavity (gate diameter of 14 Å) is directly accessible to the solvent. The force probe MD simulations revealed that TBA, due to its hydrophobic nature, moves along the TM2 and TM1 helices before it gets fully hydrated in the intracellular compartment. Free energy calculations showed that the open gate does not cause an energy barrier for TBA dissociation (Figure 7A). The increase in energy during dissociation is mainly caused by TBA leaving its high affinity binding site between 2 and 2.5 nm on the z-axis (Figure 7A, B-D). A total energy difference of 8 kcal/mol between the bound and the solvated TBA was measured. Throughout the dissociation simulation, TBA remained in the  $D_{2d}$

conformation further indicating that the gate is wide enough to allow dissociation of a planar TBA which has a diameter of 12 Å (Figure 7B-F).

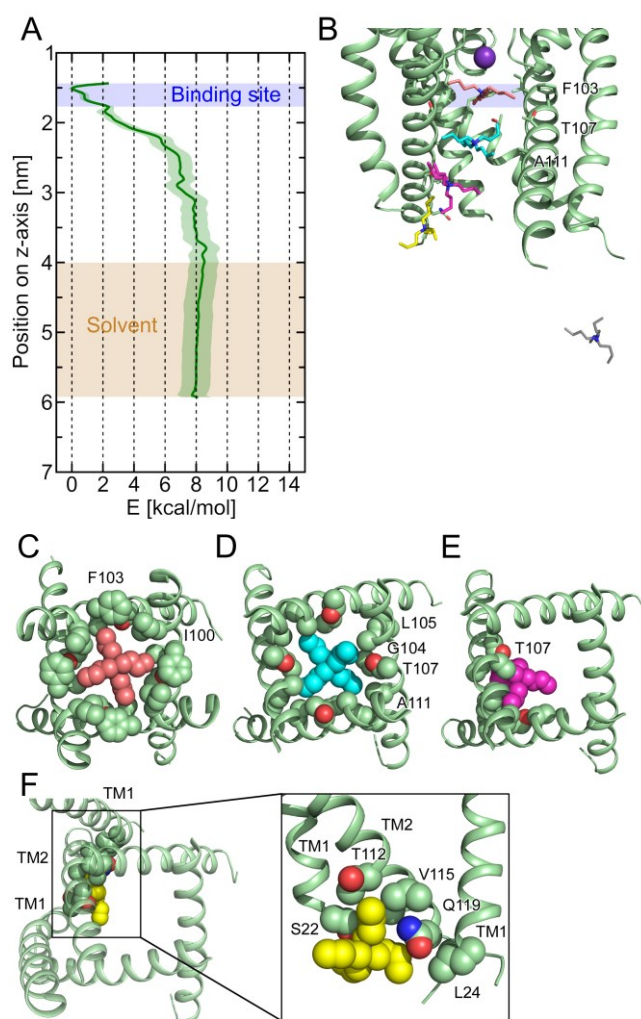


**Figure 7.** A) Free energy profile of TBA dissociation from the fully open KcsA channel state. The blue and beige shades depict the high affinity binding site and the solvent compartment, respectively. Statistical error is shown as green shade. B) TBA structures, represented as sticks, show the dissociation pathway through the gate. For clarity, only three SUs are shown in green. Interacting amino acids are depicted as green sticks. TBA structures in panel B and C-F correspond to positions 1.5 nm (pink, C), 2.3 nm (cyan, D), 2.9 nm (magenta, E), 3.6 nm (yellow, F), and 5.2 nm on z-axis. C-E) Top view of TBA and interacting amino acids during dissociation. F) Top and side view of TBA and interacting amino acids on TM1 and TM2 helices.

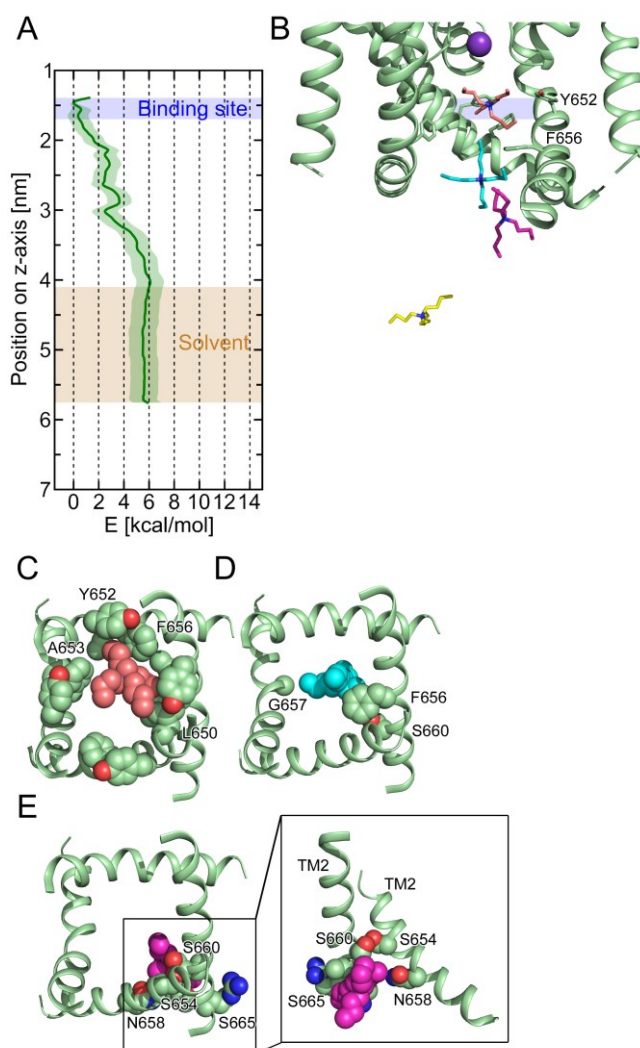


**Figure 8.** A) Free energy profile of TBA dissociation from the open hERG channel. The blue and beige shades depict the binding site and the solvent compartment, respectively. Statistical error is shown as green shade. B) TBA structures, represented as sticks, show the dissociation pathway through the gate. For clarity, only three SUs are shown in green. The binding determinants Y652 and F656 are depicted as green sticks. TBA structures in panel B and C-E correspond to positions 1.58 nm (pink, C), 2.5 nm (cyan, D), 3 nm (magenta, E), 4.5 nm (yellow) on z-axis. C-D) Top view of TBA and interacting amino acids during dissociation. E) Top and side view of TBA and interacting amino acids on two adjacent TM2 helices.

**TBA dissociation from the open hERG.** To explore dissociation of TBA from the hERG channel we applied force probe simulations and umbrella sampling, as described above for KcsA. TBA dissociation was only probed from the fully open hERG state since free energy calculations on KcsA suggest that dissociation solely occurs from an open channel state.

For hERG dissociation, a total energy difference of 6 kcal/mol was measured (Figure 8A-C). At position 2.2 to 2.4 nm on z-axis, an interacting F656 switched from the cavity facing to the cavity lining state; thereby allowing easier passage of TBA through the channel gate and causing an energy plateau phase. The subsequent energy barrier from 2.5 to 3 nm is caused by the first exposure of TBA to the solvent after the F656 passage (Figure 8D and E). At 3 nm on z-axis (Figure 8E), TBA packs to two adjacent TM2 helices before it gets fully hydrated shown by an energy increase to 6 kcal/mol. Throughout the dissociation simulation, TBA remained in the D<sub>2d</sub> conformation.

## DISCUSSION

In this study we addressed two important questions concerning drug trapping in K<sup>+</sup> channels. First, do trapped drugs influence gating? Second, is a fully open gate required for drug dissociation? To answer the first question, we performed MD simulations with the prototypical K<sup>+</sup> channel KcsA and a model of the hERG K<sup>+</sup> channel. Closing ED simulations with TBA in KcsA and hERG revealed that the drug influences structural rearrangements in hERG but not in KcsA. This is in agreement with crystal structures of TBA trapped in KcsA by Faraldo-Gómez et al. (Faraldo-Gómez *et al*, 2007) and Yohannan et al. (Yohannan *et al*, 2007) indicating a negligible effect of drug block on the channel structure.

In hERG, experimental characterization of TBA block was lacking so far. Thus, we first investigated the mechanism of TBA hERG interactions in detail. Open/inactivated channel dependence of block of TBA was indicated by fast current decrease upon channel activation (Figure 2A). This finding is in line with the well described state dependence of drug block in hERG (Perrin *et al*, 2008; Hill *et al*, 2014). Alanine mutations of Y652 and F656 revealed that both residues significantly reduce the potency of TBA (Figure 2D) indicating that these compounds bind to the cavity as has been shown for a multitude of other hERG blockers

(Mitcheson *et al*, 2000a; Lees-Miller *et al*, 2000; Kamiya *et al*, 2001; Sánchez-Chapula *et al*, 2002, 2004; Ridley *et al*, 2004; Perry *et al*, 2004; Guo *et al*, 2006; Kamiya *et al*, 2006, 2008).

TBA shares common features with trapped drugs. Block occurs from the intracellular side of the channel and requires prior channel opening. Further, the drug cannot be washed out during 330 s at resting state and repetitive stimulation during wash-out induces rapid recovery from block, suggesting that TBA is trapped in the hERG cavity (Figure 2E).

In agreement with experimental results, docking and MD simulations support the importance of Y652 and F656 for binding. According to our modeling studies, these interactions are primarily of hydrophobic nature. Cation- $\pi$  interactions were not observed, the quaternary nitrogen and aromatic rings of Y652 and F656 were too distant (Marshall *et al*, 2009) throughout the simulation. This fits to data by Xia *et al*, showing that higher exposure of the quaternary nitrogen and a decrease of hydrophobicity by shorter alkyl chains leads to reduced potency of QA compounds (Xia *et al*, 2011). The hERG channel closure simulations highlight the important role of F656 during channel closure. Fast transitions of F656 from cavity facing to cavity lining conformation were observed (Figure 4B). This finding is in agreement with a recent MD simulation study revealing innate flexibility of the F656 side chain (Knappe *et al*, 2011). Further, it is supported by a mutagenesis study by Fernandez *et al*. (Fernandez *et al*, 2004), suggesting an important role of this residue for normal deactivation. Their work clearly showed that replacement of the bulky side chain by smaller hydrophobic amino acids leads to faster channel closure. Therefore, it is conceivable that the bulkiness at this position contributes to the slow deactivation kinetics in hERG.

Remarkably, in the presence of TBA, F656 structural rearrangements are significantly perturbed during gating (Figure 4D), indicating that binding of TBA stabilizes the aromatic side chains in the cavity facing conformation. This finding is of particular interest since most hERG blockers bind to F656 (Mitcheson *et al*, 2000a; Lees-Miller *et al*, 2000; Kamiya *et al*, 2001; Sánchez-Chapula *et al*, 2002, 2004; Ridley *et al*, 2004; Perry *et al*, 2004; Guo *et al*,

2006; Kamiya *et al*, 2006, 2008). Interestingly, it has been suggested previously that F656 might act as physical barrier for drug dissociation of certain compounds (Karczewski *et al*, 2009). It is tempting to speculate that specific interactions with F656 determine if a compound is trapped or not. Based on our simulations, we propose that trapped compounds might stabilize the cavity facing state of F656, presenting a barrier for drug dissociation. Increased sampling of the cavity lining conformation might facilitate drug dissociation prior to complete channel closure. This hypothetical mechanism is illustrated in schematic Figure 9. One way to test the validity of this scenario would be the use of F656 mutants as described by Fernandez *et al*. (Fernandez *et al*, 2004), which still exhibit reasonable affinity for blockers while introducing different amino acid size and deactivation kinetics. This approach will be subject of further studies.

In hERG, not all blockers demonstrate slow recovery from block (Milnes *et al*, 2003; Stork *et al*, 2007; Mitcheson, 2008), but appear to quickly dissociate even when the channels are held at resting state. This might be explained by our findings, demonstrating the important role of F656 during gating. F656 might function as a second gate and prevent dissociation of trapped drugs via mutual interference.

The second important question that was addressed in this study concerns the extent of gate opening necessary for dissociation. Force probe MD simulations and energy calculations on 3 different KcsA crystal structures with pore diameters of up to 14 Å (fully open) revealed that dissociation is only possible when the gate is fully open. Similarly, no energy barrier was found for TBA dissociation from the open hERG state model. In both channels, TBA moves along the cavity wall maximizing hydrophobic contacts to the protein during dissociation. The exit scenario from closed and intermediate KcsA channel states is predicted to trigger conformational changes of TBA to the S<sub>4</sub> conformation. Despite this more compressed structure (diameter of 8 Å), large energy barriers render dissociation from these states highly

unlikely. Since, except for F103, only small residues line the cavity in KcsA, the observed high energy barriers (40 – 50 kcal/mol) result primarily from the conformational state, defined by the backbone coordinates. Although high energy barriers occurred during dissociation from these channel states, our force probe simulations did not cause changes in the protein secondary structure. Taken together, we propose that compounds cannot dissociate from closed or intermediate states, but require an open helix bundle crossing gate. This is supported by earlier findings from our lab (Beyl *et al*, 2007).

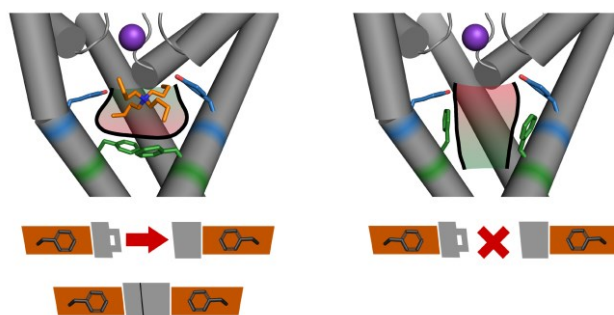


**Figure 9. Schematic figure of the importance of the F656 conformation on trapping.**

## ASSOCIATED CONTENT

**Supporting Information.** Distribution of dihedral angles of TBA monitored during closing ED simulations in KcsA and hERG and histograms of the umbrella sampling windows. This material is available free of charge via the Internet at <http://pubs.acs.org>.

## AUTHOR INFORMATION

### Corresponding Author

\*E-mail: [anna.stary@univie.ac.at](mailto:anna.stary@univie.ac.at)

## **Author Contributions**

Conceived and designed the experiments: TL, PS, ET, SH, ASW. Performed the experiments: TL, PS. Analyzed the data: TL, PS, ET, SH, ASW. Wrote the paper: TL, PS, ET, SH, ASW. All authors have given approval to the final version of the manuscript.

## **Funding Sources**

This work was supported by the Austrian Science Fund (FWF; Grants P22395 and W1232; <http://www.fwf.ac.at>). Tobias Linder was supported by a research fellowship from the University of Vienna and an EMBO short-term fellowship. Anna Stry-Weinzinger is supported by the Johanna Mahlke, geb. Obermann Stiftung.

## **Notes**

The authors declare no competing financial interest.

## **ACKNOWLEDGMENT**

The computational results presented have been achieved using the Vienna Scientific Cluster (VSC).

## **ABBREVIATIONS**

ED, essential dynamics; hERG, human ether-à-go-go related gene; LQTS, long QT syndrome; SF, selectivity filter; TBA, tetrabutylammonium; TEA, tetraethylammonium; QA, quaternary ammonium.

## REFERENCES

- Aqvist J & Luzhkov V (2000) Ion permeation mechanism of the potassium channel. *Nature* **404**: 881–4
- Armstrong CM (1971) Interaction of Tetraethylammonium Ion Derivatives with the Potassium Channels of Giant Axons. *J. Gen. Physiol.* **58**: 413–437
- Armstrong CM & Hille B (1972) The inner quaternary ammonium ion receptor in potassium channels of the node of Ranvier. *J. Gen. Physiol.* **59**: 388–400
- Baburin I, Beyl S & Hering S (2006) Automated fast perfusion of *Xenopus* oocytes for drug screening. *Pflugers Arch.* **453**: 117–23
- Bagal SK, Brown AD, Cox PJ, Omoto K, Owen RM, Pryde DC, Sidders B, Skerratt SE, Stevens EB, Storer RI & Swain NA (2013) Ion channels as therapeutic targets: a drug discovery perspective. *J. Med. Chem.* **56**: 593–624
- Berger O, Edholm O & Jahnig F (1997) Molecular Dynamics Simulations of a Fluid Bilayer of Dipalmitoylphosphatidylcholine at Full Hydration, Constant Pressure, and Constant Temperature. *Biophys. J.* **72**: 2002–2013
- Beyl S, Timin EN, Hohaus A, Stary A, Kudrnac M, Guy RH & Hering S (2007) Probing the architecture of an L-type calcium channel with a charged phenylalkylamine: evidence for a widely open pore and drug trapping. *J. Biol. Chem.* **282**: 3864–70
- Carmeliet E (1992) Voltage- and time-dependent block of the delayed K<sup>+</sup> current in cardiac myocytes by dofetilide. *J. Pharmacol. Exp. Ther.* **262**: 809–17
- Case DA, Darden TA, Cheatham TE, Simmerling CL, Wang J, Duke RE, Luo R, Crowley M, Walker RC, Zhang W, Merz KM, Wang B, Hayik S, Roitberg A, Seabra G, Kolossváry I, Wong KF, Paesani F, Vanicek J, Wu X, et al (2010) Amber 11.
- Chiang CE & Roden DM (2000) The long QT syndromes: genetic basis and clinical implications. *J. Am. Coll. Cardiol.* **36**: 1–12
- Choi K-H, Song C, Shin D & Park S (2011) hERG channel blockade by externally applied quaternary ammonium derivatives. *Biochim. Biophys. Acta* **1808**: 1560–6
- Choi KL, Mossman C, Aubé J & Yellen G (1993) The internal quaternary ammonium receptor site of Shaker potassium channels. *Neuron* **10**: 533–41
- Crouzy S, Bernèche S & Roux B (2001) Extracellular blockade of K(+) channels by TEA: results from molecular dynamics simulations of the KcsA channel. *J. Gen. Physiol.* **118**: 207–18
- Cuello LG, Jogini V, Cortes DM & Perozo E (2010) Structural mechanism of C-type inactivation in K(+) channels. *Nature* **466**: 203–8

- Darden T, York D & Pedersen L (1993) Particle mesh Ewald: An  $N \log(N)$  method for Ewald sums in large systems. *J. Chem. Phys.* **98**: 10089
- Di Veroli GY, Davies MR, Zhang H, Abi-Gerges N & Boyett MR (2013) hERG Inhibitors With Similar Potency But Different Binding Kinetics Do Not Pose the Same Proarrhythmic Risk: Implications for Drug Safety Assessment. *J. Cardiovasc. Electrophysiol.* **25**: 197–207
- Faraldo-Gómez JD, Kutluay E, Jogini V, Zhao Y, Heginbotham L & Roux B (2007) Mechanism of intracellular block of the KcsA K<sup>+</sup> channel by tetrabutylammonium: insights from X-ray crystallography, electrophysiology and replica-exchange molecular dynamics simulations. *J. Mol. Biol.* **365**: 649–62
- Faraldo-Gómez JD & Roux B (2007) Characterization of conformational equilibria through Hamiltonian and temperature replica-exchange simulations: assessing entropic and environmental effects. *J. Comput. Chem.* **28**: 1634–47
- Fermini B & Fossa AA (2003) The impact of drug-induced QT interval prolongation on drug discovery and development. *Nat. Rev. Drug Discov.* **2**: 439–47
- Fernandez D, Ghanta A, Kauffman GW & Sanguinetti MC (2004) Physicochemical features of the HERG channel drug binding site. *J. Biol. Chem.* **279**: 10120–7
- Frisch MJ, Trucks GW, Schlegel HB, Scuseria GE, Robb MA, Cheeseman JR, Scalmani G, Barone V, Mennucci B, Petersson GA, Nakatsuji H, Caricato M, Li X, Hratchian HP, Izmaylov AF, Bloino J, Zheng G, Sonnenberg JL, Hada M, Ehara M, et al (2009) Gaussian 09.
- Guo J, Gang H & Zhang S (2006) Molecular determinants of cocaine block of human ether-á-go-go-related gene potassium channels. *J. Pharmacol. Exp. Ther.* **317**: 865–74
- Hess B, Bekker H, Berendsen HJC & Fraaije JGEM (1997) LINCS: A linear constraint solver for molecular simulations. *J. Comput. Chem.* **18**: 1463–1472
- Hess B, Kutzner C, van der Spoel D & Lindahl E (2008) GROMACS 4: Algorithms for Highly Efficient, Load-Balanced, and Scalable Molecular Simulation. *J. Chem. Theory Comput.* **4**: 435–447
- Hill AP, Perrin MJ, Heide J, Campbell TJ, Mann SA & Vandenberg JI (2014) Kinetics of drug interaction with the Kv11.1 potassium channel. *Mol. Pharmacol.* **85**: 769–76
- Holmgren M, Smith PL & Yellen G (1997) Trapping of organic blockers by closing of voltage-dependent K<sup>+</sup> channels: evidence for a trap door mechanism of activation gating. *J. Gen. Physiol.* **109**: 527–35
- Hoover W (1985) Canonical dynamics: Equilibrium phase-space distributions. *Phys. Rev. A* **31**: 1695–1697
- Hornak V, Abel R, Okur A, Strockbine B, Roitberg A & Simmerling C (2006) Comparison of multiple Amber force fields and development of improved protein backbone parameters. *Proteins* **65**: 712–25

- Hub JS, de Groot BL & van der Spoel D (2010) g\_wham—A Free Weighted Histogram Analysis Implementation Including Robust Error and Autocorrelation Estimates. *J. Chem. Theory Comput.* **6**: 3713–3720
- Jehle J, Schweizer PA, Katus HA & Thomas D (2011) Novel roles for hERG K(+) channels in cell proliferation and apoptosis. *Cell Death Dis.* **2**: e193
- Jorgensen WL, Chandrasekhar J, Madura JD, Impey RW & Klein ML (1983) Comparison of simple potential functions for simulating liquid water. *J. Chem. Phys.* **79**: 926
- Joung IS & Cheatham TE (2008) Determination of alkali and halide monovalent ion parameters for use in explicitly solvated biomolecular simulations. *J. Phys. Chem. B* **112**: 9020–41
- Kamiya K, Mitcheson JS, Yasui K, Kodama I & Sanguinetti MC (2001) Open channel block of HERG K(+) channels by vesnarinone. *Mol. Pharmacol.* **60**: 244–53
- Kamiya K, Niwa R, Mitcheson JS & Sanguinetti MC (2006) Molecular determinants of HERG channel block. *Mol. Pharmacol.* **69**: 1709–16
- Kamiya K, Niwa R, Morishima M, Honjo H & Sanguinetti MC (2008) Molecular Determinants of hERG Channel Block by Terfenadine and Cisapride. *J. Pharmacol. Sci.* **108**: 301–307
- Karczewski J, Wang J, Kane SA, Kiss L, Koblan KS, Culberson JC & Spencer RH (2009) Analogs of MK-499 are differentially affected by a mutation in the S6 domain of the hERG K<sup>+</sup> channel. *Biochem. Pharmacol.* **77**: 1602–11
- Keating MT & Sanguinetti MC (2001) Molecular and Cellular Mechanisms of Cardiac Arrhythmias. *Cell* **104**: 569–580
- Knape K, Linder T, Wolschann P, Beyer A & Stry-Weinzinger A (2011) In silico Analysis of Conformational Changes Induced by Mutation of Aromatic Binding Residues: Consequences for Drug Binding in the hERG K<sup>+</sup> Channel. *PLoS One* **6**: e28778
- Lees-Miller JP, Duan Y, Teng GQ & Duff HJ (2000) Molecular determinant of high-affinity dofetilide binding to HERG1 expressed in *Xenopus* oocytes: involvement of S6 sites. *Mol. Pharmacol.* **57**: 367–74
- Lenaus MJ, Vamvouka M, Focia PJ & Gross A (2005) Structural basis of TEA blockade in a model potassium channel. *Nat. Struct. Mol. Biol.* **12**: 454–9
- Linder T, de Groot BL & Stry-Weinzinger A (2013) Probing the energy landscape of activation gating of the bacterial potassium channel KcsA. *PLoS Comput. Biol.* **9**: e1003058
- Luzhkov VB & Aqvist J (2001) Mechanisms of tetraethylammonium ion block in the KcsA potassium channel. *FEBS Lett.* **495**: 191–6

- Luzhkov VB, Österberg F, Acharya P, Chattopadhyaya J & Aqvist J (2002) Computational and NMR study of quaternary ammonium ion conformations in solution. *Phys. Chem. Chem. Phys.* **4**: 4640–4647
- MacKinnon R & Yellen G (1990) Mutations affecting TEA blockade and ion permeation in voltage-activated K<sup>+</sup> channels. *Science* **250**: 276–9
- Marshall MS, Steele RP, Thanthiriwatte KS & Sherrill CD (2009) Potential energy curves for cation- $\pi$  interactions: off-axis configurations are also attractive. *J. Phys. Chem. A* **113**: 13628–32
- Milnes JT, Crociani O, Arcangeli A, Hancox JC & Witchel HJ (2003) Blockade of HERG potassium currents by fluvoxamine: incomplete attenuation by S6 mutations at F656 or Y652. *Br. J. Pharmacol.* **139**: 887–98
- Mitcheson JS (2008) hERG potassium channels and the structural basis of drug-induced arrhythmias. *Chem. Res. Toxicol.* **21**: 1005–10
- Mitcheson JS, Chen J, Lin M, Culberson C & Sanguinetti MC (2000a) A structural basis for drug-induced long QT syndrome. *Proc. Natl. Acad. Sci. U. S. A.* **97**: 12329–33
- Mitcheson JS, Chen J & Sanguinetti MC (2000b) Trapping of a methanesulfonanilide by closure of the HERG potassium channel activation gate. *J. Gen. Physiol.* **115**: 229–40
- Nosé S (1984) A unified formulation of the constant temperature molecular dynamics methods. *J. Chem. Phys.* **81**: 511
- Parrinello M & Rahman A (1981) Polymorphic transitions in single crystals: A new molecular dynamics method. *J. Appl. Phys.* **52**: 7182
- Perrin MJ, Kuchel PW, Campbell TJ & Vandenberg JI (2008) Drug binding to the inactivated state is necessary but not sufficient for high-affinity binding to human ether-à-go-go-related gene channels. *Mol. Pharmacol.* **74**: 1443–52
- Perry M, de Groot MJ, Helliwell R, Leishman D, Tristani-Firouzi M, Sanguinetti MC & Mitcheson J (2004) Structural determinants of HERG channel block by clofilium and ibutilide. *Mol. Pharmacol.* **66**: 240–9
- Pier DM, Shehatou GS, Giblett S, Pullar CE, Tresize DJ, Pritchard CA, Challiss J & Mitcheson JS (2014) Long-term Channel Block is Required to Inhibit Cellular Transformation by Human Ether-a-go-go-related Gene (Herg1) Potassium Channels. *Mol. Pharmacol.* **86**: 211–221
- Posson DJ, McCoy JG & Nimigean CM (2013) The voltage-dependent gate in MthK potassium channels is located at the selectivity filter. *Nat. Struct. Mol. Biol.* **20**: 159–66
- Ridley JM, Dooley PC, Milnes JT, Witchel HJ & Hancox JC (2004) Lidoflazine is a high affinity blocker of the HERG K(+)channel. *J. Mol. Cell. Cardiol.* **36**: 701–5

- Sánchez-Chapula JA, Ferrer T, Navarro-Polanco RA & Sanguinetti MC (2003) Voltage-dependent profile of human ether-a-go-go-related gene channel block is influenced by a single residue in the S6 transmembrane domain. *Mol. Pharmacol.* **63**: 1051–8
- Sánchez-Chapula JA, Navarro-Polanco RA, Culberson C, Chen J & Sanguinetti MC (2002) Molecular determinants of voltage-dependent human ether-a-go-go related gene (HERG) K<sup>+</sup> channel block. *J. Biol. Chem.* **277**: 23587–95
- Sánchez-Chapula JA, Navarro-Polanco RA & Sanguinetti MC (2004) Block of wild-type and inactivation-deficient human ether-a-go-go-related gene K<sup>+</sup> channels by halofantrine. *Naunyn. Schmiedeberg's. Arch. Pharmacol.* **370**: 484–91
- Sanguinetti MC, Jiang C, Curran ME & Keating MT (1995) A mechanistic link between an inherited and an acquired cardiac arrhythmia: HERG encodes the IKr potassium channel. *Cell* **81**: 299–307
- Sanguinetti MC & Mitcheson JS (2005) Predicting drug-hERG channel interactions that cause acquired long QT syndrome. *Trends Pharmacol. Sci.* **26**: 119–24
- Stary A, Wacker SJ, Boukharta L, Zachariae U, Karimi-Nejad Y, Aqvist J, Vriend G & de Groot BL (2010) Toward a consensus model of the HERG potassium channel. *ChemMedChem* **5**: 455–67
- Stork D, Timin EN, Berjukow S, Huber C, Hohaus A, Auer M & Hering S (2007) State dependent dissociation of HERG channel inhibitors. *Br. J. Pharmacol.* **151**: 1368–76
- Wang J, Wang W, Kollman PA & Case DA (2006) Automatic atom type and bond type perception in molecular mechanical calculations. *J. Mol. Graph. Model.* **25**: 247–60
- Wang J, Wolf RM, Caldwell JW, Kollman PA & Case DA (2004) Development and testing of a general amber force field. *J. Comput. Chem.* **25**: 1157–74
- Windisch A, Timin E, Schwarz T, Stork-Riedler D, Erker T, Ecker G & Hering S (2011) Trapping and dissociation of propafenone derivatives in HERG channels. *Br. J. Pharmacol.* **162**: 1542–52
- Witchel HJ, Dempsey CE, Sessions RB, Perry M, Milnes JT, Hancox JC & Mitcheson JS (2004) The low-potency, voltage-dependent HERG blocker propafenone - molecular determinants and drug trapping. *Mol. Pharmacol.* **66**: 1201–12
- Wolf MG, Hoefling M, Aponte-Santamaría C, Grubmüller H & Groenhof G (2010) g\_membed: Efficient insertion of a membrane protein into an equilibrated lipid bilayer with minimal perturbation. *J. Comput. Chem.* **31**: 2169–74
- Xia M, Shahane SA, Huang R, Titus SA, Shum E, Zhao Y, Southall N, Zheng W, Witt KL, Tice RR & Austin CP (2011) Identification of quaternary ammonium compounds as potent inhibitors of hERG potassium channels. *Toxicol. Appl. Pharmacol.* **252**: 250–8
- Yellen G, Jurman ME, Abramson T & MacKinnon R (1991) Mutations affecting internal TEA blockade identify the probable pore-forming region of a K<sup>+</sup> channel. *Science* **251**: 939–42

- Yohannan S, Hu Y & Zhou Y (2007) Crystallographic study of the tetrabutylammonium block to the KcsA K<sup>+</sup> channel. *J. Mol. Biol.* **366**: 806–14
- Zhou M, Morais-Cabral JH, Mann S & MacKinnon R (2001a) Potassium channel receptor site for the inactivation gate and quaternary amine inhibitors. *Nature* **411**: 657–61
- Zhou Y, Morais-Cabral JH, Kaufman A & MacKinnon R (2001b) Chemistry of ion coordination and hydration revealed by a K<sup>+</sup> channel-Fab complex at 2.0 Å resolution. *Nature* **414**: 43–8

## Supporting Information

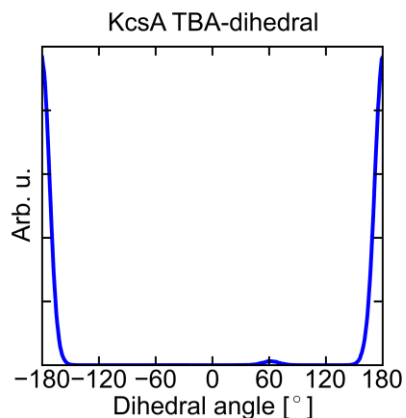


**Figure S1. Dihedral angle distribution of TBA during KcsA closure.** Dihedral angles were calculated as described in (Luzhkov *et al*, 2002). Dihedrals at  $-180^\circ$  and  $180^\circ$  represent the  $D_{2d}$  conformation while a dihedral angle at  $60^\circ$  stand for the  $S_4$  conformation.

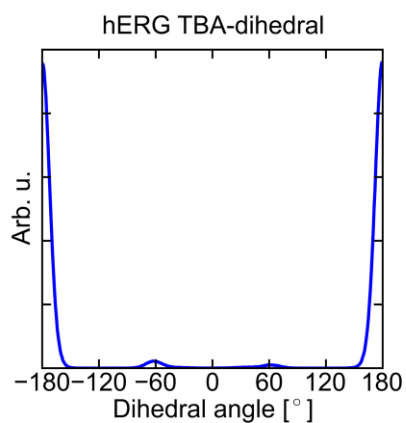


**Figure S2. Dihedral angle distribution of TBA during hERG closure.** Dihedral angles were calculated as described in (Luzhkov *et al*, 2002). Dihedrals at  $-180^\circ$  and  $180^\circ$  represent the  $D_{2d}$  conformation while dihedral angles at  $-60^\circ$  and  $60^\circ$  stand for the  $S_4$  conformation.

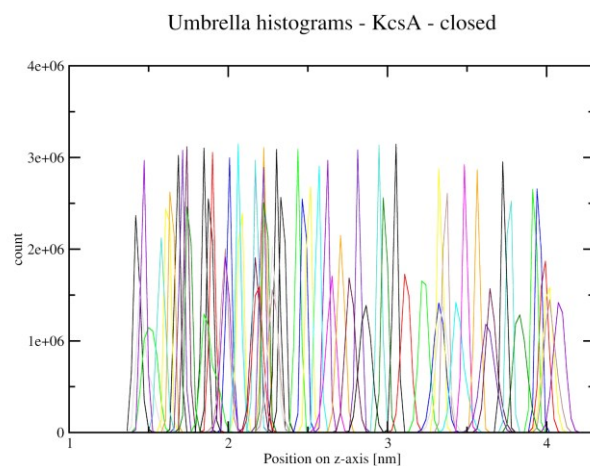


**Figure S3. Histograms of the 65 umbrella sampling windows in KcsA closed state.** Windows were simulated with 1000 or 10000 kJ/mol/nm<sup>2</sup> and can be distinguished by the peak height.

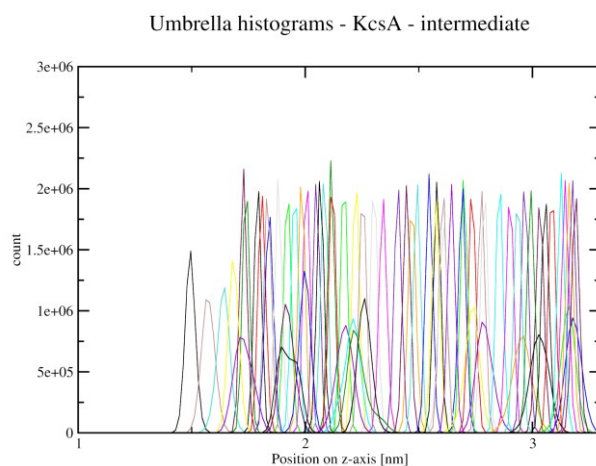


**Figure S4. Histograms of the 67 umbrella sampling windows in KcsA intermediate state.** Windows were simulated with 1000 or 10000 kJ/mol/nm<sup>2</sup> and can be distinguished by the peak height.

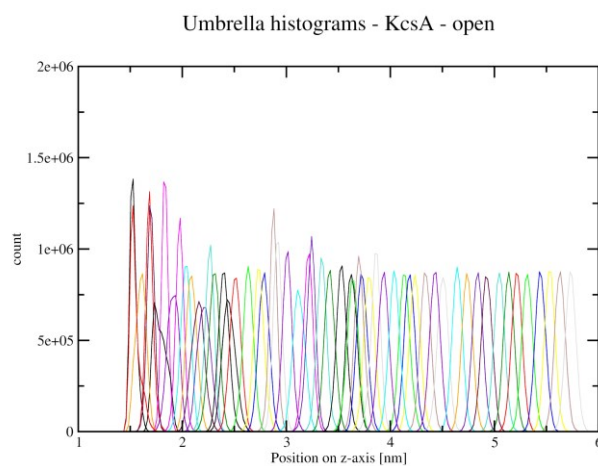


**Figure S5. Histograms of the 56 umbrella sampling windows in KcsA open state.** Windows were simulated with 1000 or 10000 kJ/mol/nm<sup>2</sup> and can be distinguished by the peak height.

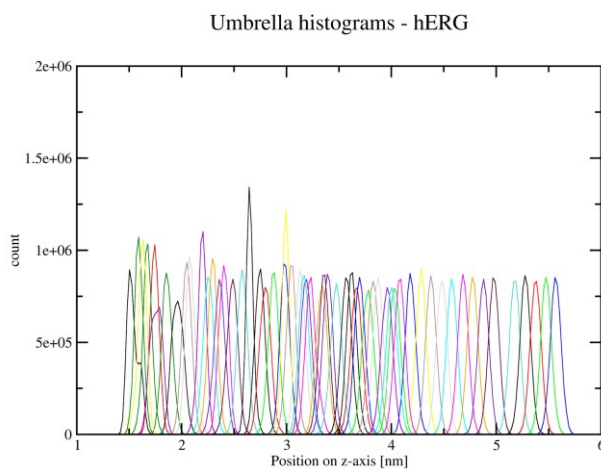


**Figure S6. Histograms of the 57 umbrella sampling windows in hERG open state.** Windows were simulated with 1000 or 10000 kJ/mol/nm<sup>2</sup> and can be distinguished by the peak height.

Luzhkov VB, Österberg F, Acharya P, Chattopadhyaya J & Aqvist J (2002) Computational and NMR study of quaternary ammonium ion conformations in solution. *Phys. Chem. Chem. Phys.* **4**: 4640–4647

## **4.4 Drug trapping in hERG channels – an experimental approach**

---

Linder T

Research stay at the Michael C. Sanguinetti laboratory at the Nora Eccles Harrison Cardiovascular Research and Training Institute, University of Utah, USA.

November - December 2013

Our findings of the above described MD simulations suggest that the gate does not have to close completely to trap a compound and prohibit dissociation. Additionally, trapped drugs might affect the conformational rearrangements of the channel during gating. Since the channel cavity is of limited size, a trapped drug might prevent complete closure of the channel. Therefore, we investigated if a trapped drug influences the extent of channel closure. To answer this question we made use of a new approach locking the hERG channel gate with disulfide bonds. The study was conducted during a research stay in the laboratory of Michael C. Sanguinetti at the Nora Eccles Harrison Cardiovascular Research and Training Institute, University of Utah, USA.

A hERG cysteine double mutant was successfully used by Ferrer *et al.* (Ferrer *et al.*, 2006) to confirm that the S4-S5 linker directly couples voltage sensor movement to the activation gate. By adding the membrane-permeable oxidizing agent  $\text{tbHO}_2$ , a disulfide bond between L666C of the S6 helix and D540C of the S4-S5 linker was formed which locked the channel in the closed state. Additionally, it was shown that this cysteine bridge can be reversed and normal channel function can be regained by adding the reducing agent DTT. Most importantly for our study, the formation of the disulfide bond was state dependent, meaning that the bond was only formed in the closed state. In order to build a cysteine bridge, the  $\beta$ -carbons of the two amino acids need to be located within 5 Å and oriented orthogonally to each other (Careaga & Falke, 1992). These specific distance requirements allow us to identify changes of gate closure in the presence of drugs. If the cysteine bridges can be formed, no currents will be observed at depolarized potentials. This result would strongly support drug binding and trapping without gate modification. In contrast, if drugs prevent full channel closure or modify the channel gate, cysteine bridge formation is prevented. Therefore, ionic currents would occur after washout of the drugs while keeping the channel open by membrane depolarization. This effect would strongly suggest that the tested hERG blockers influence gate closure. In this study, the two high-affinity hERG blockers cisapride and dofetilide were used representing a non-trapped (Stork *et al.*, 2007; Kamiya *et al.*, 2008) and a trapped drug (Kamiya *et al.*, 2006), respectively.

Before testing the disulfide formation with drugs, two important prerequisites need to be met. First, the used drugs should not be modified by the used oxidizing and reducing agents. To probe the stability of the drugs, thin layer chromatography (TLC) was performed with drugs exposed to three different solutions. Each solution contained a drug concentration of 100  $\mu\text{M}$ . The control solution contained 96 mM NaCl, 2 mM KCl, 1 mM  $\text{MgCl}_2$ , 1.8 mM  $\text{CaCl}_2$ , and 5 mM HEPES (pH 7.5, titrated with NaOH). For the second and third solution, 2 mM  $\text{tbHO}_2$  and 20 mM DTT were added to the control solution, respectively. Reduction or oxidation of functional groups would lead to differences in the attraction to the stationary

silica gel phase and in the solubility in solvent. Therefore, changes in the chemical structure would be observed by differences in the travel distance and in the retardation factor. In all three solutions, the compounds moved to the same extent indicating that the compounds were neither oxidized nor reduced.

Second, it is important to verify that the drug binding site is unaffected by the double mutant and thus does not influence the potency of the drugs. Therefore, half maximal inhibitory concentrations ( $IC_{50}$ ) for cisapride and dofetilide in the D540C-L666C mutant channel were measured (Figure 1). For cisapride, an  $IC_{50}$  value of  $1.079 \pm 0.05 \mu\text{M}$  was measured (Figure 1A). This is in good agreement with WT channel values reported in the literature (Mitcheson *et al*, 2000; Fernandez *et al*, 2004; Kamiya *et al*, 2008; Myokai *et al*, 2008). Dofetilide exhibited an  $IC_{50}$  of  $0.206 \pm 0.02 \mu\text{M}$  which is in line with WT  $IC_{50}$  values (Figure 1C) (Lees-Miller *et al*, 2000; Kamiya *et al*, 2006). Our data indicates that drug block is not affected by the two introduced cysteine mutants. However, the applied voltage protocol for drug block (Figure 1B) revealed an unusual gating property of the double mutant. The oocytes were kept at a holding potential of -90 mV, followed by a 1-s test pulse to +20 mV. Subsequent tail currents were recorded at -70 mV. A prepulse to -70 mV prior to depolarization can be of great use to determine the leak currents in oocytes since hERG channels are usually closed at this membrane potential. Conversely, in case of the cysteine double mutant, drug blocking effects were also observed during these prepulses indicating altered gating properties of D540C-L666C.

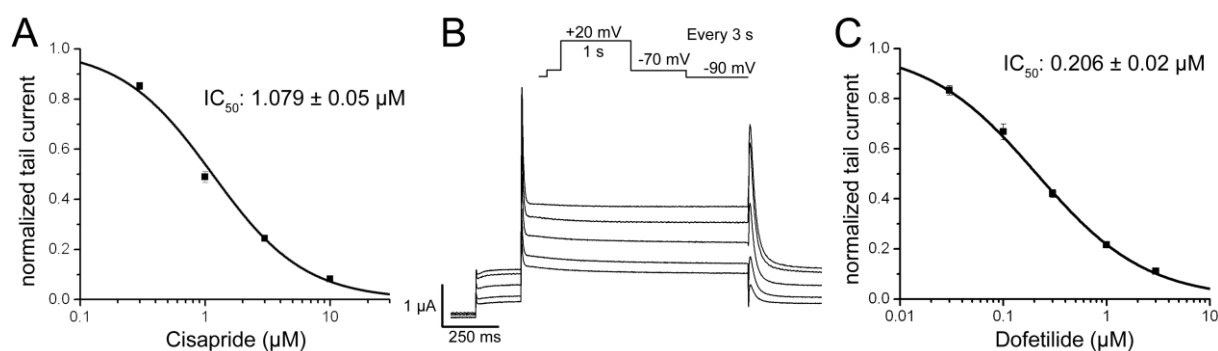


**Figure 1. Concentration dependent block of the D540C-L666C mutant channel by cisapride and dofetilide.** A) Concentration-effect relationship for cisapride block of hERG D540C-L666C channel current. The  $IC_{50}$  was  $1.079 \pm 0.10 \mu\text{M}$  with a Hill coefficient of 1.18 ( $n=5$ ). B) Voltage protocol and steady-state currents in the absence and presence of cisapride in  $0.3 \mu\text{M}$ ,  $0.1 \mu\text{M}$ ,  $3 \mu\text{M}$ , and  $10 \mu\text{M}$  concentrations (currents in descending order). C) Concentration-effect relationship for dofetilide. The  $IC_{50}$  value was  $0.206 \pm 0.05 \mu\text{M}$  with a Hill coefficient of 0.82 ( $n=4$ ). Points are means  $\pm$  SEM.

The gating properties were probed by investigating the current-voltage relationship (Figure 2). The oocytes were kept at the  $K^+$  reversal potential of -95 mV (in KCM211 solution, see methods). 2-s test pulses were applied in the range from -80 to +70 mV in 10 mV increments. Tail currents were recorded at -70 mV and normalized to the maximal tail current obtained at the +70 mV test pulse. A half-maximal activation ( $V_{1/2}$ ) of  $19.5 \pm 0.2$  mV was measured for the mutant. This corresponds to a shift of around 40 mV to more positive voltages compared to the WT hERG channel. Further, the I-V curve revealed that the channel exhibits a constitutive conductance at negative potentials although the pore gate is closely coupled with the voltage sensor as indicated by the steep voltage dependence of activation. The finding that D540C-L666C hERG channels display a standing conductance of 15 % even at negative potentials was not reported in the original work and has great consequences for our investigations of trapping as described below.

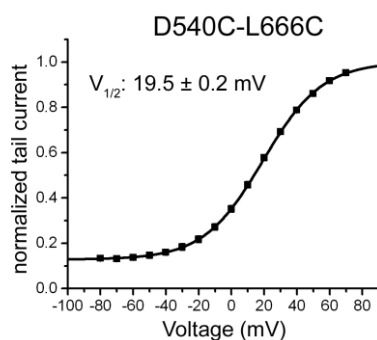


**Figure 2. Current-voltage relationship of the D540C-L666C hERG channel.** A  $V_{1/2}$  of  $19.5 \pm 0.2$  mV was measured. The I-V curve illustrates the steady-state current at negative potentials where hERG channels are usually closed. Points are means  $\pm$  SEM (n=6).

The following procedure was applied to investigate the extent of hERG channel closure upon drug trapping (Figure 3A). Either 10  $\mu$ M cisapride or 3  $\mu$ M dofetilide or no drug (control) were applied until steady-state block was reached (time < -600 s). Subsequently, the channels were kept at holding potential (-90 mV) and treated with 0.5 mM  $tbHO_2$  for 5 min to form the D540C-L666C disulfide bond and wash out unbound drug. This phase was followed by a 5 min washing period with the superfusing solution KCM211 at holding potential to wash out excessive oxidizing agent. Then, pulse trains were applied (time = 0) to elucidate currents through channels which did not form a disulfide bond due to probable modification of gate closure by a trapped drug. To verify the formation of a disulfide bond, 20 mM of the reducing agent DTT was subsequently applied and washed out by KCM211. In these experiments, the 1-s test pulse was set to +40 mV as described in the original work by Ferrer et al. while the rest of the protocol remained as described above. In both experiments with the trapped dofetilide and the non-trapped cisapride, a steady-state block of 90 % was reached. After treatment with  $tbHO_2$  and wash out, no difference in the currents could be

observed between cisapride and dofetilide during 15 min pulsing. Further, application of the reducing agent led to an increase in current indicating that the disulfide bond was formed in both cases. The wash out of DTT caused another increase in current which is probably caused by the dissociation of DTT from extracellular channel blocking sites. Currents did not recover completely which might result from long exposure of the channel to  $\text{tbHO}_2$  (personal communication with Michael C. Sanguinetti and Martin Tristani-Firouzi). Interestingly, no difference between trapped and non-trapped drugs in terms of disulfide formation was detected in our experiments which is in contrast to our proposed hypothesis. Therefore, we asked if dofetilide is really trapped during the 10 min period at holding potential. To probe dofetilide trapping in the D540C-L666C mutant, blocked channels were kept at holding potential for 10 min while superfusing with KCM211. Surprisingly, channels recovered almost completely from dofetilide block during this phase (Figure 3B). The lack of dofetilide trapping is caused by insufficient closure of the D540C-L666C mutant channel as described by the I-V relationship. Due to the activated channels at holding potential, dofetilide can dissociate during the wash phase. Thus, unfortunately, the D540C-L666C mutant is not suitable to study trapping as this phenomenon is greatly affected by the mutant.

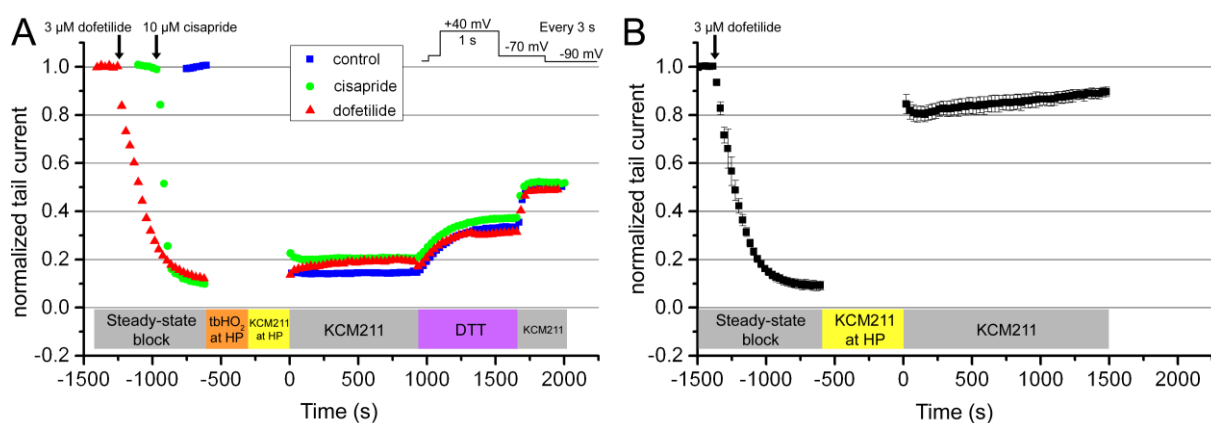


**Figure 3. Disulfide bond forming experiment with the D540C-L666C channel.** A) Application of 3  $\mu\text{M}$  dofetilide and 10  $\mu\text{M}$  cisapride until steady-state block was reached (time < 600 s). Steady-state block was followed by application of 0.5 mM  $\text{tbHO}_2$  and KCM211 for 5 min each at holding potential. Subsequent pulsing elucidates the amount of channels locked by disulfide bonds. After 15 min, disulfide bonds were reduced by 20 mM DTT. Subsequent washout led to dissociation of DTT from extracellular blocking sites. For clarity, the number of plotted data points per experiment was reduced to 100. B) Dissociation experiment with 3  $\mu\text{M}$  dofetilide. After steady-state block, channels were kept at holding potential for 10 min and were superfused with KCM211. Subsequent pulsing showed that channels recovered almost completely from dofetilide block indicating that dofetilide can dissociate from the mutant channel at holding potential. Points are means  $\pm$  SEM ( $n=3$ ). For clarity, the number of plotted data points was reduced to 100.

As the above described cysteine double mutant greatly affected drug trapping, we set out to identify other disulfide forming hERG mutations that allow investigations on hERG trapping. Based on our hERG homology model of the closed channel state (Garg *et al*, 2011), we proposed that cysteine residues located at the S660 amino acid in the TM2 would be in close proximity ( $C_{\beta}$ - $C_{\beta}$  distance: 5-6 Å) in the closed channel state and might form disulfide bonds with each other (Figure 4A). Indeed, TEVC recordings showed that the S660C mutant exhibited sensitivity to application of 1 mM  $tbHO_2$  during repetitive pulsing and led to current reduction of 50 % which could be reversed by 20 mM DTT application (not depicted). The formation of the disulfide bond in S660C was significantly slower than in the double-mutant. This effect might be caused by a reduced accessibility of  $tbHO_2$  to the S660C in the pore gate region. I-V relationship recordings showed that  $V_{1/2}$  is unaffected by the mutant which is in agreement with a previous study (Wynia-Smith *et al*, 2008). Additionally, complete closure of the channels was achieved at potentials below -60 mV (Figure 4B). However, as illustrated in Figure 4C, the necessary long holding potential period had great implications for the channel behavior. In an experiment without hERG blockers, the channels showed a current inhibition of 80 % after a holding period of 25 min at -90 mV. Subsequent repetitive pulsing caused complete recovery of the current. This behavior probably results from the initiation of an additional closed state by the S660C mutant. The mutant channels might adopt this state by long time periods at negative membrane potentials. This state appears to be less sensitive to depolarized membrane potentials. During repetitive pulsing, the channels slowly recover from this additional closed state and participate in the normal gating process induced by the voltage protocol. The unique channel state behavior of the S660C mutant renders trapping studies with this mutant impossible.

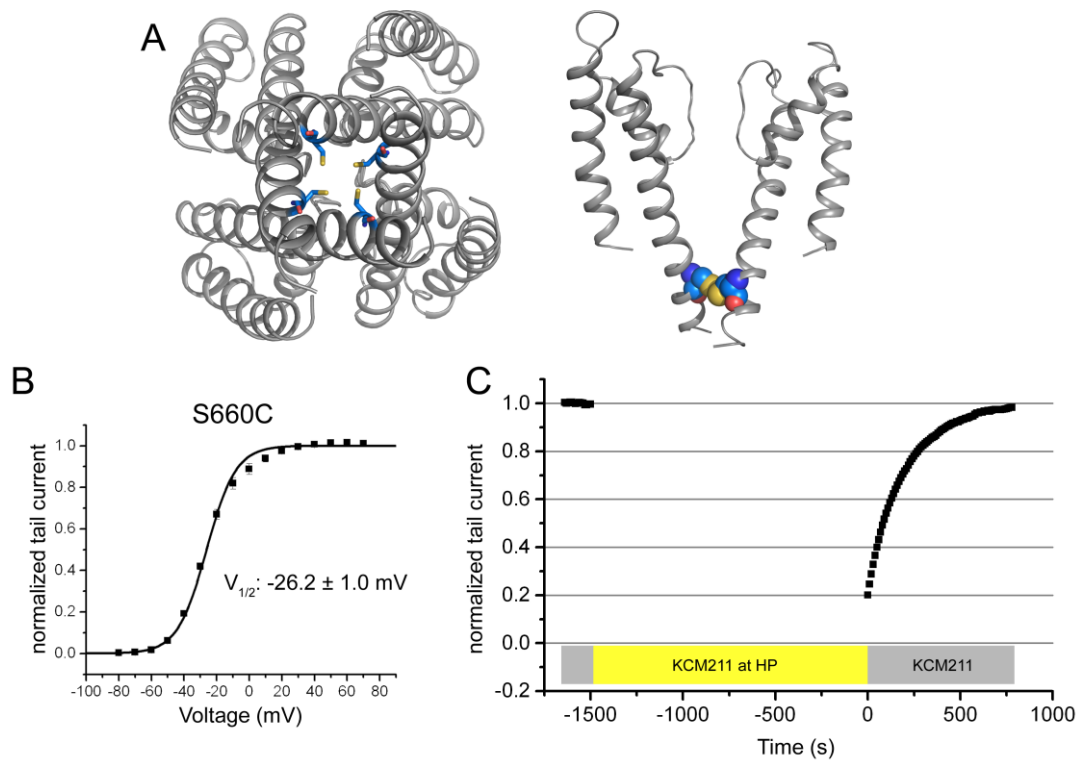


**Figure 4. Current-voltage relationship and pulsing behavior of the S660C channel.** A) Bottom (left) and side (right) view of the proposed S660C location in the closed hERG channel state. SUs are shown as gray cartoon while the S660C residue is depicted as blue sticks (bottom view) and spheres (side view). For clarity, only two opposing SUs are shown in the side view. B) A  $V_{1/2}$  of  $-26.2 \pm 1.0$  mV was measured. Points are means  $\pm$  SEM ( $n=6$ ). C) Reduced current after 25 min at holding potential in the absence of blocking drugs. Currents completely recovered during 10 min repetitive pulsing. For clarity, the number of plotted data points was reduced to 100.

Summarizing, the herein used cysteine mutant channels influenced trapping of drugs or changed the gating properties of the respective channels. Thus, the mutants are not applicable to investigate our research question. Nevertheless, as disulfide bond experiments add high resolution information to electrophysiology studies, this approach might ultimately shed light on drug trapping. However, identifying suitable mutations that do not influence the biophysical properties of the channel which are crucial for trapping, such as channel closure and gating behavior, might be challenging.

## REFERENCES

- Careaga CL & Falke JJ (1992) Thermal motions of surface alpha-helices in the D-galactose chemosensory receptor. Detection by disulfide trapping. *J. Mol. Biol.* **226**: 1219–35
- Fernandez D, Ghanta A, Kauffman GW & Sanguinetti MC (2004) Physicochemical features of the HERG channel drug binding site. *J. Biol. Chem.* **279**: 10120–7
- Ferrer T, Rupp J, Piper DR & Tristani-Firouzi M (2006) The S4-S5 linker directly couples voltage sensor movement to the activation gate in the human ether-à-go-go-related gene (hERG) K<sup>+</sup> channel. *J. Biol. Chem.* **281**: 12858–64
- Garg V, Stary-Weinzinger A, Sachse F & Sanguinetti MC (2011) Molecular determinants for activation of human ether-à-go-go-related gene 1 potassium channels by 3-nitro-n-(4-phenoxyphenyl) benzamide. *Mol. Pharmacol.* **80**: 630–7
- Kamiya K, Niwa R, Mitcheson JS & Sanguinetti MC (2006) Molecular determinants of HERG channel block. *Mol. Pharmacol.* **69**: 1709–16
- Kamiya K, Niwa R, Morishima M, Honjo H & Sanguinetti MC (2008) Molecular Determinants of hERG Channel Block by Terfenadine and Cisapride. *J. Pharmacol. Sci.* **108**: 301–307
- Lees-Miller JP, Duan Y, Teng GQ & Duff HJ (2000) Molecular determinant of high-affinity dofetilide binding to HERG1 expressed in *Xenopus* oocytes: involvement of S6 sites. *Mol. Pharmacol.* **57**: 367–74
- Mitcheson JS, Chen J, Lin M, Culberson C & Sanguinetti MC (2000) A structural basis for drug-induced long QT syndrome. *Proc. Natl. Acad. Sci. U. S. A.* **97**: 12329–33
- Myokai T, Ryu S, Shimizu H & Oiki S (2008) Topological mapping of the asymmetric drug binding to the human ether-à-go-go-related gene product (HERG) potassium channel by use of tandem dimers. *Mol. Pharmacol.* **73**: 1643–51
- Stork D, Timin EN, Berjukow S, Huber C, Hohaus A, Auer M & Hering S (2007) State dependent dissociation of HERG channel inhibitors. *Br. J. Pharmacol.* **151**: 1368–76
- Wynia-Smith SL, Gillian-Daniel AL, Satyshur KA & Robertson GA (2008) hERG gating microdomains defined by S6 mutagenesis and molecular modeling. *J. Gen. Physiol.* **132**: 507–20

## 5 Discussion

In this thesis, comprehensive investigations of the gating behavior of K<sup>+</sup> channels were performed. Although the herein studied prototypical bacterial K<sup>+</sup> channel KcsA, the bacterial Kir channel KirBac1.1, and the human Kv channel hERG are only distantly related and exhibit a low sequence identity (full length: ~ 1 %; TM domain: ~ 7 %), they share a similar TM domain architecture. Likewise, the global rearrangements of the three channels occurring in our gating simulations display common gating motions. In all three cases, the TM2 helix bended and straightened at the conserved glycine hinge<sup>47</sup> in opening and closing simulations, respectively (G99 in KcsA, G134 in KirBac1.1, G648 in hERG). However, the extent of channel opening at the pore gate varied in the studies of KcsA and KirBac1.1. Gating simulations in KcsA resulted in an open channel state that closely resembles the 23 Å open KcsA crystal structure<sup>38</sup> (Figure 1 and 2 in chapter 4.1, page 40). Simulations in KirBac1.1 with the activatory mutant G143E led to smaller gate opening movements (Figure 2 and 3 in chapter 4.2, page 55) which fit to the open 17 Å crystal structure.<sup>38</sup> If this state represents a fully open conformation of KirBac1.1 is unknown as much wider openings of the pore gate of up to 32 Å were reported with truncated crystal structures of KcsA.<sup>38</sup> However, full-length crystal structures of KcsA<sup>446</sup> suggested that the C-terminal domain restricts the gate opening to about 21 Å. Thus, it seems likely that the large CTD of Kir channels imposes structural constraints on the maximal extent of gate opening. The important role of intracellular domains on gating is further emphasized by the fact that for some channels such as NaK, open state crystal structures could be only obtained when intracellular facing parts were removed.<sup>447</sup>

In Kir channels, the CTD not only affects the maximal opening of the HBC gate but also critically regulates gating of the channel. While previous studies on KirBac suggested that a rotational movement of the CTD has to occur prior to HBC gate opening,<sup>42,371</sup> our simulations indicate that the HBC gate can trigger twisting of the CTD. This would imply that the coupling between the TM domain and the CTD might operate bidirectionally. Studies on the prokaryotic Kir channels have provided invaluable insights into the atomistic rearrangements of these channels during gating. However, it is important to note that eukaryotic Kir channel gating is regulated by various different ligands such as nucleotides or GPCR SUs. Therefore, our current understanding of Kir channel gating might be restricted to the basic elements. Future studies focusing on the channel subtype specific structural rearrangements might lead to a more sophisticated knowledge of the differences and similarities of gating movements of Kir channels.

Beside the global conformational changes during gating, local structural rearrangements of amino acids were monitored in the different channel gating studies. Strikingly, in all three channels, KcsA, KirBac1.1, and hERG, aromatic amino acids play a crucial role during gating and their side chain conformational changes have great impact on gating. In KcsA, F103 and F114 located on the TM2 helices show gating specific patterns. During opening ED simulations, F103 switched from a “cavity lining” to a “cavity facing” state. This rotameric switch was linked to inactivation of the SF and it was proposed that F103 mechanically couples activation and inactivation in KcsA.<sup>55,448</sup> Although the rotameric changes of F103 were observed in our gating simulations, the SF remained in an activated state (Figure 3 in chapter 4.1, page 40), closely resembling the high K<sup>+</sup> crystal structure of Zhou et al.<sup>33</sup> This suggests that the SF state is not implicitly coupled to the F103 conformation. Instead, the hydrogen bond network<sup>136,137,449</sup> on the backside of the SF with the P-helix and, as recently shown, water molecules between these two segments<sup>56</sup> appear to be more critical for inactivation. Interestingly, while the conformational state of F103 in KcsA was tightly coupled to pore gating, the equivalent position in hERG, Y652, displayed high stability in the cavity facing orientation irrespective of the gating state (Figure 4A in chapter 4.3, page 87). The difference in flexibility of the aromatic amino acids might also reflect the observation that F103 is important for KcsA inactivation as the F103A mutant exhibited impaired inactivation kinetics<sup>55</sup> while the Y652A mutant in hERG does not influence inactivation.<sup>166</sup> However, the influence of the used hERG homology model remains elusive and warrants further investigations. Nevertheless, it was shown that Y652 plays a crucial role for the effect of hERG activators on inactivation<sup>450,451</sup> suggesting that Y652 is involved in a yet unresolved inactivation coupling process. Inactivation processes of K<sup>+</sup> channels appear to be of complex and diverse nature as the above described observations indicate. It was proposed by Clarke et al.<sup>367</sup> that SF changes related to inactivation are coupled to the distant rotational movements of the CTD in Kir channels which further emphasizes the diversity of inactivation mechanisms among channels.

The second aromatic amino acid in KcsA, F114, appears to be important for the initial local rearrangements to “unlock” the channel from the closed state and allow subsequent global gating changes. In the KirBac1.1 channel, F146 located on the TM2 helices is part of the HBC gate. Our simulations indicate that the orientation of F146 greatly contributes to the regulation of gating as only subtle TM2 bending motions but distinct rotameric changes of F146 resulted in a water permeable gate (Figure 2 and 3 in chapter 4.2, page 55). This suggests that the gating state is in part defined by the side chain orientation of the conserved aromatic amino acid in the HBC gate of Kir channels (F181 in Kir3.1 and F187 in Kir3.4, F146 in KirBac1.1, Y132 in KirBac3.1). Taken together, the herein presented studies emphasize the importance of aromatic amino acids for channel gating by affecting the

coupling between the pore gate and the SF, by unlocking channels from a specific state, or by forming the HBC gate.

In recent years, there is accumulating evidence that the membrane lipid composition is of great importance for channel regulation.<sup>19,381</sup> In KirBac1.1, the positively charged amino acids of the slide helix, R49 and K57, were reported to interact with the negative head groups of phospholipids.<sup>452</sup> Since it was suggested that Kir channel gating is coupled to the movement of the slide-helix,<sup>42,365,367</sup> the slide-helix lipid interactions might mediate gating and stabilize channels states. Analysis of these interactions in our KirBac study revealed that a tilting downward movement of the slide-helix at the C-terminus during gating leads to a repositioning of K57 and thereby to a stronger hydrogen bond network with the lipids (Figure 9 in chapter 4.2, page 62). R49 also formed a tight hydrogen bond network throughout our simulations; however, no gating specific differences could be observed. It is worth mentioning that the studied system comprised only of one type of lipid and does not resemble the native membrane composition. Thus, future studies will be needed to provide more detailed insights into the lipid specific interactions with the protein which mediate channel gating. Additionally, studies on the distinct response of prokaryotic<sup>400,402</sup> and eukaryotic<sup>372,373,379</sup> channels to PIP2 and the involvement of the C-linker in the respective gating behavior would be of great interest and might reveal further details of Kir channel gating.

While the structural basis of channel gating is now well described and was comprehensively studied in this thesis, the direct link between the conformational changes and the underlying energies remained an unaddressed research topic. Consequently, the energy landscapes of gating in KcsA and KirBac1.1 were investigated and described herein. In KcsA, free energy calculations of ED gating simulations showed that the open and closed states are separated by two energy barriers (Figure 4 in chapter 4.1, page 41). The first, smaller energy barrier could be directly correlated to local structural rearrangements at the pore gate which unlock the closed channel state. The subsequent global movement of the TM2 helices results in a second, larger energy barrier before the channel reaches the open state. Interestingly, the energy well between the two barriers is sampled by an intermediate crystal structure of KcsA which was not included in the gating simulations. This finding emphasizes the validity of ED simulations to derive native gating structures. The overall shape of the energy profile showed that KcsA is intrinsically more stable in the closed conformation. This is in contrast to a simultaneously published study on the pore domain of Kv1.2. Fowler et al.<sup>453</sup> showed that forces need to be applied to close the channel pore. A major difference between these two channels is the presence of a PVP motif in the TM2 helices of Kv1.2, which was shown to contribute to an increased open probability of K<sup>+</sup>

channels.<sup>47,48,50</sup> Indeed, mutating PVP to a PVA motif shifted the energy well toward the closed channel state suggesting that the PVP motif contributes to the energy discrepancy between the two channels. However, the lack of closed crystal structures of Kv1.2 makes it challenging to estimate the position of the closed channel state on the energy landscape. In our KcsA study and in the Kv1.2 work of Fowler et al.<sup>453</sup>, energy calculations were performed on the pore domain only. The C-terminus in KcsA and the VSD in Kv1.2 presumably affect the energy landscape of channel gating and thus will result in altered energy profiles. Nevertheless, the studies show that, although the channels share similar architecture, the fine tuning of channels greatly influences the energetically favorable states.

The ED simulation approach allowed the calculation of the WT energy profile of native KcsA states. In case of KirBac1.1, the activatory mutant G143E was employed to simulate gating. Therefore, it is not surprising that energy calculations displayed an energetically more favorable open state. While it is very likely that the energy profile does not resemble the native WT gating profile of KirBac1.1, it provides insights into the mutant specific energies of gating movements. The profile revealed that a steep energy decrease is caused by the G143E induced HBC gate opening as the negatively charged glutamic acid is located in a hydrophobic pocket in the closed state which results in strong repulsion. Additionally, it showed that the rotational movement of the CTD occurs in two steps. First, an initial movement is induced by the HBC gate opening and correlates to a steep energy decrease. Second, the CTD conformation is relaxed by a further rotation causing an additional energy decrease. The final rotational state of the CTD closely resembles the open twisted CTD conformation of the KirBac3.1 crystal structures.<sup>42</sup> Another recent open crystal structure of KirBac3.1 obtained by a different activatory mutant suggests that each mutant results in a different open state. Therefore, it would be of great interest to derive a complete energy map of channel gating and identify mutant specific transition pathways and energy wells on this map.

A major part of this thesis focused on the drug trapping phenomenon in KcsA and hERG. Although a recent study highlighted the increased pro-arrhythmic risk of trapped drugs in hERG,<sup>445</sup> it is unknown which characteristics render a drug trapped. We stated three main questions which might help to obtain detailed insights into the trapping process. First, do specific amino acids in the channel cause trapping? Second, when does the drug get trapped during gate closure? And third, does the trapped drug influence the global gating movements of the channel? To study the first question, we investigated if a trapped compound affects structural rearrangements of binding site lining amino acids during channel closure. Tetrabutylammonium (TBA) was used as a trapped compound since this ligand was co-crystallized in the closed KcsA structure.<sup>454,455</sup> These structures provide invaluable insights

into conformational states of binding site forming amino acids. Additionally, the possible conformational states and the underlying energies are known for this compound.<sup>456,457</sup> As TBA is a symmetrical compound, the orientation of the ligand in the binding site and during dissociation is of minor relevance and thereby reduces the necessary sampling in MD simulations. These features render TBA an ideal trapped model ligand for trapping investigations.

Investigations on the impact of TBA trapping on cavity lining amino acids were performed in KcsA and hERG by making use of ED closure simulations. While the two binding determinants in KcsA I100 and F103 were relatively unaffected by TBA (Figure 1 in chapter 4.3, page 80), the rotameric reorientation of F656 in hERG was significantly impaired by the trapped TBA (Figure 4 in chapter 4.3, page 87). In the apo simulation, F656 switched from a cavity facing to a cavity lining orientation upon channel closure. However, in the presence of TBA, the side chain was stabilized in the cavity facing conformation and thereby displays a physical barrier for dissociation. This finding might provide a structural explanation for the trapping phenomenon as most hERG blockers, non-trapped and trapped, bind to F656.<sup>166–169,171–174,176,177,458</sup> It would be of great importance to investigate the probable distinct effect on the F656 orientation of trapped and non-trapped drugs in future MD studies. To probe this hypothesis experimentally, F656 mutations described by Fernandez et al.<sup>175</sup> might be employed which still exhibit reasonable affinity for blockers but introduce different amino acid size and deactivation kinetics.

The second question concerned the extent of gate closure necessary for trapping. This was examined by calculating the energy barriers of drug dissociation from different channel states (Figures 5, 6, 7, and 8 in chapter 4.3, page 89). Our stimulations suggest that dissociation is only possible when the gate is fully open indicating that TBA is already trapped in the early beginning of gate closure. Thirdly, the applicability of an experimental TEVC approach for investigations of the drug trapping impact on the global hERG gating behavior was probed (chapter 4.4, page 107). More specifically, we asked if a trapped drug influences the extent of channel closure. We made use of disulfide bond forming hERG cysteine mutants. The stringent structural prerequisites for the formation of a cysteine bridge add high resolution structural information to electrophysiology recordings. Thus, the presence or absence of such a bond in trapping experiments allows the identification of drug induced changes of gate closure. Unfortunately, the herein studied mutants greatly influenced the trapping of drugs or the gating properties of the respective channels, rendering this approach not applicable for trapping studies so far.

Summarizing, this thesis provides novel insights into the channel specific movements during pore gating. Although the three investigated channels, KcsA, KirBac1.1, and hERG, share similar global gating rearrangements in terms of TM2 movements, they exhibit uniquely fine-tuned local gating changes of amino acids. Specifically aromatic amino acids were shown to adopt crucial roles in shaping the drug binding site, causing drug trapping and forming the pore gate during channel gating. As  $K^+$  channels are important drug targets to treat a plethora of pathophysiological conditions, the knowledge of specific local structural rearrangements might contribute to the development of drugs which target specific channel states. This might help to avoid the trapping characteristic found in various hERG blocking drugs and thereby provide safer medications in the future.

## 6 References

- (1) Meer, G. Van; Voelker, D.; Feigenson, G. Membrane Lipids: Where They Are and How They Behave. *Nat. Rev. Mol. Cell Biol.* **2008**, 9, 112–124.
- (2) Yu, F. H.; Yarov-Yarovoy, V.; Gutman, G. A.; Catterall, W. A. Overview of Molecular Relationships in the Voltage-Gated Ion Channel Superfamily. *Pharmacol. Rev.* **2005**, 57, 387–395.
- (3) Clapham, D. E.; Julius, D.; Montell, C.; Schultz, G. International Union of Pharmacology. XLIX. Nomenclature and Structure-Function Relationships of Transient Receptor Potential Channels. *Pharmacol. Rev.* **2005**, 57, 427–450.
- (4) Hofmann, F.; Biel, M.; Kaupp, U. B. International Union of Pharmacology. LI. Nomenclature and Structure-Function Relationships of Cyclic Nucleotide-Regulated Channels. *Pharmacol. Rev.* **2005**, 57, 455–462.
- (5) Collingridge, G. L.; Olsen, R. W.; Peters, J.; Spedding, M. A Nomenclature for Ligand-Gated Ion Channels. *Neuropharmacology* **2009**, 56, 2–5.
- (6) Catterall, W. A.; Goldin, A. L.; Waxman, S. G. International Union of Pharmacology. XLVII. Nomenclature and Structure-Function Relationships of Voltage-Gated Sodium Channels. *Pharmacol. Rev.* **2005**, 57, 397–409.
- (7) Catterall, W. A.; Perez-Reyes, E.; Snutch, T. P.; Striessnig, J. International Union of Pharmacology. XLVIII. Nomenclature and Structure-Function Relationships of Voltage-Gated Calcium Channels. *Pharmacol. Rev.* **2005**, 57, 411–425.
- (8) Gutman, G. A.; Chandy, K. G.; Grissmer, S.; Lazdunski, M.; McKinnon, D.; Pardo, L. A.; Robertson, G. A.; Rudy, B.; Sanguinetti, M. C.; Stühmer, W.; Wang, X. International Union of Pharmacology. LIII. Nomenclature and Molecular Relationships of Voltage-Gated Potassium Channels. *Pharmacol. Rev.* **2005**, 57, 473–508.
- (9) Alexander, S. P. H.; Benson, H. E.; Faccenda, E.; Pawson, A. J.; Sharman, J. L.; Catterall, W. A.; Spedding, M.; Peters, J. A.; Harmar, A. J. The Concise Guide to PHARMACOLOGY 2013/14: Ion Channels. *Br. J. Pharmacol.* **2013**, 170, 1607–1651.
- (10) Yu, F. H.; Catterall, W. A. The VGL-Chanome: A Protein Superfamily Specialized for Electrical Signaling and Ionic Homeostasis. *Sci. STKE* **2004**, 2004, re15.
- (11) Hille, B. *Ion Channels of Excitable Membranes*; 3rd ed.; Sinauer, 2001.
- (12) Cahalan, M. D.; Wulff, H.; Chandy, K. G. Molecular Properties and Physiological Roles of Ion Channels in the Immune System. *J. Clin. Immunol.* **2001**, 21, 235–252.
- (13) Wang, W.; Hebert, S. C.; Giebisch, G. Renal K<sup>+</sup> Channels: Structure and Function. *Annu. Rev. Physiol.* **1997**, 59, 413–436.
- (14) Wangemann, P. K<sup>+</sup> Cycling and the Endocochlear Potential. *Hear. Res.* **2002**, 165, 1–9.
- (15) Babenko, A. P.; Aguilar-Bryan, L.; Bryan, J. A View of sur/KIR6.X, KATP Channels. *Annu. Rev. Physiol.* **1998**, 60, 667–687.
- (16) Ashcroft, F. M.; Gribble, F. M. ATP-Sensitive K<sup>+</sup> Channels and Insulin Secretion: Their Role in Health and Disease. *Diabetologia* **1999**, 42, 903–919.

- (17) Bichet, D.; Haass, F. A.; Jan, L. Y. Merging Functional Studies with Structures of Inward-Rectifier K(+) Channels. *Nat. Rev. Neurosci.* **2003**, *4*, 957–967.
- (18) Hibino, H.; Inanobe, A.; Furutani, K.; Murakami, S.; Findlay, I.; Kurachi, Y. Inwardly Rectifying Potassium Channels: Their Structure, Function, and Physiological Roles. *Physiol. Rev.* **2010**, *90*, 291–366.
- (19) Rosenhouse-Dantsker, A.; Mehta, D.; Levitan, I. Regulation of Ion Channels by Membrane Lipids. *Compr. Physiol.* **2012**, *2*, 31–68.
- (20) Wei, A. D.; Gutman, G. A.; Aldrich, R.; Chandy, K. G.; Grissmer, S.; Wulff, H. International Union of Pharmacology. LII. Nomenclature and Molecular Relationships of Calcium-Activated Potassium Channels. *Pharmacol. Rev.* **2005**, *57*, 463–472.
- (21) Kaupp, U. B.; Seifert, R. Cyclic Nucleotide-Gated Ion Channels. *Physiol. Rev.* **2002**, *82*, 769–824.
- (22) Biel, M.; Wahl-Schott, C.; Michalakakis, S.; Zong, X. Hyperpolarization-Activated Cation Channels: From Genes to Function. *Physiol. Rev.* **2009**, *89*, 847–885.
- (23) Goldstein, S. A. N.; Bayliss, D. A.; Kim, D.; Lesage, F.; Plant, L. D.; Rajan, S. International Union of Pharmacology. LV. Nomenclature and Molecular Relationships of Two-P Potassium Channels. *Pharmacol. Rev.* **2005**, *57*, 527–540.
- (24) Enyedi, P.; Czirják, G. Molecular Background of Leak K<sup>+</sup> Currents: Two-Pore Domain Potassium Channels. *Physiol. Rev.* **2010**, *90*, 559–605.
- (25) Hodgkin, A. L.; Huxley, A. F. A Quantitative Description of Membrane Current and Its Application to Conduction and Excitation in Nerve. *J. Physiol.* **1952**, *117*, 500–544.
- (26) Armstrong, C.; Binstock, L. Anomalous Rectification in the Squid Giant Axon Injected with Tetraethylammonium Chloride. *J. Gen. Physiol.* **1965**, *48*, 859–872.
- (27) Armstrong, C. M. Time Course of TEA(+)-Induced Anomalous Rectification in Squid Giant Axons. *J. Gen. Physiol.* **1966**, *50*, 491–503.
- (28) Hille, B. Ionic Channels in Excitable Membranes. Current Problems and Biophysical Approaches. *Biophys. J.* **1978**, *22*, 283–294.
- (29) Goldstein, S. A.; Bockenhauer, D.; O’Kelly, I.; Zilberberg, N. Potassium Leak Channels and the KCNK Family of Two-P-Domain Subunits. *Nat. Rev. Neurosci.* **2001**, *2*, 175–184.
- (30) French, R.; Wells, J. Sodium Ions as Blocking Agents and Charge Carriers in the Potassium Channel of the Squid Giant Axon. *J. Gen. Physiol.* **1977**, 707–724.
- (31) Doyle, D. A.; Morais Cabral, J.; Pfuetzner, R. A.; Kuo, A.; Gulbis, J. M.; Cohen, S. L.; Chait, B. T.; MacKinnon, R. The Structure of the Potassium Channel: Molecular Basis of K<sup>+</sup> Conduction and Selectivity. *Science* **1998**, *280*, 69–77.
- (32) Roderick MacKinnon - Facts  
[http://www.nobelprize.org/nobel\\_prizes/chemistry/laureates/2003/mackinnon-facts.html](http://www.nobelprize.org/nobel_prizes/chemistry/laureates/2003/mackinnon-facts.html)  
(accessed Jun 15, 2014).
- (33) Zhou, Y.; Morais-Cabral, J. H.; Kaufman, A.; MacKinnon, R. Chemistry of Ion Coordination and Hydration Revealed by a K<sup>+</sup> Channel-Fab Complex at 2.0 Å Resolution. *Nature* **2001**, *414*, 43–48.

- (34) Gouaux, E.; Mackinnon, R. Principles of Selective Ion Transport in Channels and Pumps. *Science* **2005**, *310*, 1461–1465.
- (35) Morais-Cabral, J. H.; Zhou, Y.; MacKinnon, R. Energetic Optimization of Ion Conduction Rate by the K<sup>+</sup> Selectivity Filter. *Nature* **2001**, *414*, 37–42.
- (36) Aqvist, J.; Luzhkov, V. Ion Permeation Mechanism of the Potassium Channel. *Nature* **2000**, *404*, 881–884.
- (37) Treptow, W.; Tarek, M. K<sup>+</sup> Conduction in the Selectivity Filter of Potassium Channels Is Monitored by the Charge Distribution along Their Sequence. *Biophys. J.* **2006**, *91*, L81–3.
- (38) Cuello, L. G.; Jogini, V.; Cortes, D. M.; Perozo, E. Structural Mechanism of C-Type Inactivation in K(+) Channels. *Nature* **2010**, *466*, 203–208.
- (39) Jiang, Y.; Lee, A.; Chen, J.; Cadene, M.; Chait, B. T.; MacKinnon, R. Crystal Structure and Mechanism of a Calcium-Gated Potassium Channel. *Nature* **2002**, *417*, 515–522.
- (40) Jiang, Y.; Lee, A.; Chen, J.; Ruta, V.; Cadene, M.; Chait, B. T.; MacKinnon, R. X-Ray Structure of a Voltage-Dependent K<sup>+</sup> Channel. *Nature* **2003**, *423*, 33–41.
- (41) Long, S. B.; Campbell, E. B.; Mackinnon, R. Crystal Structure of a Mammalian Voltage-Dependent Shaker Family K<sup>+</sup> Channel. *Science* **2005**, *309*, 897–903.
- (42) Bavro, V. N.; De Zorzi, R.; Schmidt, M. R.; Muniz, J. R. C.; Zubcevic, L.; Sansom, M. S. P.; Vénien-Bryan, C.; Tucker, S. J. Structure of a KirBac Potassium Channel with an Open Bundle Crossing Indicates a Mechanism of Channel Gating. *Nat. Struct. Mol. Biol.* **2012**, *19*, 158–163.
- (43) Perozo, E.; Cortes, D. M.; Cuello, L. G. Structural Rearrangements Underlying K<sup>+</sup>-Channel Activation Gating. *Science* **1999**, *285*, 73–78.
- (44) Liu, Y. S.; Sompornpisut, P.; Perozo, E. Structure of the KcsA Channel Intracellular Gate in the Open State. *Nat. Struct. Biol.* **2001**, *8*, 883–887.
- (45) Kelly, B. L.; Gross, A. Potassium Channel Gating Observed with Site-Directed Mass Tagging. *Nat. Struct. Biol.* **2003**, *10*, 280–284.
- (46) Shimizu, H.; Iwamoto, M.; Konno, T.; Nihei, A.; Sasaki, Y. C.; Oiki, S. Global Twisting Motion of Single Molecular KcsA Potassium Channel upon Gating. *Cell* **2008**, *132*, 67–78.
- (47) Magidovich, E.; Yifrach, O. Conserved Gating Hinge in Ligand- and Voltage-Dependent K<sup>+</sup> Channels. *Biochemistry* **2004**, *43*, 13242–13247.
- (48) Hackos, D. H.; Chang, T.-H.; Swartz, K. J. Scanning the Intracellular S6 Activation Gate in the Shaker K<sup>+</sup> Channel. *J. Gen. Physiol.* **2002**, *119*, 521–532.
- (49) Labro, A. J.; Raes, A. L.; Bellens, I.; Ottschytsch, N.; Snyders, D. J. Gating of Shaker-Type Channels Requires the Flexibility of S6 Caused by Prolines. *J. Biol. Chem.* **2003**, *278*, 50724–50731.
- (50) Labro, A. J.; Grottesi, A.; Sansom, M. S. P.; Raes, A. L.; Snyders, D. J. A Kv Channel with an Altered Activation Gate Sequence Displays Both “Fast” and “Slow” Activation Kinetics. *Am. J. Physiol. Cell Physiol.* **2008**, *294*, C1476–84.
- (51) Levy, D. I.; Deutsch, C. Recovery from C-Type Inactivation Is Modulated by Extracellular Potassium. *Biophys. J.* **1996**, *70*, 798–805.

- (52) Kiss, L.; Korn, S. J. Modulation of C-Type Inactivation by K<sup>+</sup> at the Potassium Channel Selectivity Filter. *Biophys. J.* **1998**, *74*, 1840–1849.
- (53) Ogielska, E. M.; Aldrich, R. W. Functional Consequences of a Decreased Potassium Affinity in a Potassium Channel Pore. Ion Interactions and C-Type Inactivation. *J. Gen. Physiol.* **1999**, *113*, 347–358.
- (54) Lu, Z.; Klem, A. M.; Ramu, Y. Ion Conduction Pore Is Conserved among Potassium Channels. *Nature* **2001**, *413*, 809–813.
- (55) Cuello, L. G.; Jogini, V.; Cortes, D. M.; Pan, A. C.; Gagnon, D. G.; Dalmas, O.; Cordero-Morales, J. F.; Chakrapani, S.; Roux, B.; Perozo, E. Structural Basis for the Coupling between Activation and Inactivation Gates in K(+) Channels. *Nature* **2010**, *466*, 272–275.
- (56) Ostmeyer, J.; Chakrapani, S.; Pan, A. C.; Perozo, E.; Roux, B. Recovery from Slow Inactivation in K<sup>+</sup> Channels Is Controlled by Water Molecules. *Nature* **2013**, *501*, 121–124.
- (57) Warmke, J. W.; Ganetzky, B. A Family of Potassium Channel Genes Related to Eag in *Drosophila* and Mammals. *Proc. Natl. Acad. Sci. U. S. A.* **1994**, *91*, 3438–3442.
- (58) Curran, M. E.; Splawski, I.; Timothy, K. W.; Vincen, G. M.; Green, E. D.; Keating, M. T. A Molecular Basis for Cardiac Arrhythmia: HERG Mutations Cause Long QT Syndrome. *Cell* **1995**, *80*, 795–803.
- (59) Recanatini, M.; Poluzzi, E.; Masetti, M.; Cavalli, A.; De Ponti, F. QT Prolongation through hERG K(+) Channel Blockade: Current Knowledge and Strategies for the Early Prediction during Drug Development. *Med. Res. Rev.* **2005**, *25*, 133–166.
- (60) Mitcheson, J. S. hERG Potassium Channels and the Structural Basis of Drug-Induced Arrhythmias. *Chem. Res. Toxicol.* **2008**, *21*, 1005–1010.
- (61) Kuryshhev, Y. A.; Ficker, E.; Wang, L.; Hawryluk, P.; Dennis, A. T.; Wible, B. A.; Brown, A. M.; Kang, J.; Chen, X.; Sawamura, K.; Reynolds, W.; Rampe, D. Pentamidine-Induced Long QT Syndrome and Block of hERG Trafficking. *J. Pharmacol. Exp. Ther.* **2005**, *312*, 316–323.
- (62) Eckhardt, L. L.; Rajamani, S.; January, C. T. Protein Trafficking Abnormalities: A New Mechanism in Drug-Induced Long QT Syndrome. *Br. J. Pharmacol.* **2005**, *145*, 3–4.
- (63) Wible, B. A.; Hawryluk, P.; Ficker, E.; Kuryshhev, Y. A.; Kirsch, G.; Brown, A. M. HERG-Lite: A Novel Comprehensive High-Throughput Screen for Drug-Induced hERG Risk. *J. Pharmacol. Toxicol. Methods* **2005**, *52*, 136–145.
- (64) Viskin, S. Long QT Syndromes and Torsade de Pointes. *Lancet* **1999**, *354*, 1625–1633.
- (65) Chiang, C. E.; Roden, D. M. The Long QT Syndromes: Genetic Basis and Clinical Implications. *J. Am. Coll. Cardiol.* **2000**, *36*, 1–12.
- (66) Keating, M. T.; Sanguinetti, M. C. Molecular and Cellular Mechanisms of Cardiac Arrhythmias. *Cell* **2001**, *104*, 569–580.
- (67) Sanguinetti, M. C.; Mitcheson, J. S. Predicting Drug-hERG Channel Interactions That Cause Acquired Long QT Syndrome. *Trends Pharmacol. Sci.* **2005**, *26*, 119–124.
- (68) Redfern, W. S.; Carlsson, L.; Davis, A. S.; Lynch, W. G.; MacKenzie, I.; Palethorpe, S.; Siegl, P. K. S.; Strang, I.; Sullivan, A. T.; Wallis, R.; Camm, A. J.; Hammond, T. G. Relationships between Preclinical Cardiac Electrophysiology, Clinical QT Interval Prolongation and Torsade de Pointes for a Broad Range of Drugs: Evidence for a Provisional Safety Margin in Drug Development. *Cardiovasc. Res.* **2003**, *58*, 32–45.

- (69) De Bruin, M. L.; Pettersson, M.; Meyboom, R. H. B.; Hoes, A. W.; Leufkens, H. G. M. Anti-HERG Activity and the Risk of Drug-Induced Arrhythmias and Sudden Death. *Eur. Heart J.* **2005**, *26*, 590–597.
- (70) Huffaker, S. J.; Chen, J.; Nicodemus, K. K.; Sambataro, F.; Yang, F.; Mattay, V.; Lipska, B. K.; Hyde, T. M.; Song, J.; Rujescu, D.; Giegling, I.; Mayilyan, K.; Proust, M. J.; Soghoyan, A.; Caforio, G.; Callicott, J. H.; Bertolino, A.; Meyer-Lindenberg, A.; Chang, J.; Ji, Y.; Egan, M. F.; Goldberg, T. E.; Kleinman, J. E.; Lu, B.; Weinberger, D. R. A Primate-Specific, Brain Isoform of KCNH2 Affects Cortical Physiology, Cognition, Neuronal Repolarization and Risk of Schizophrenia. *Nat. Med.* **2009**, *15*, 509–518.
- (71) Shoeb, F.; Malykhina, A. P.; Akbarali, H. I. Cloning and Functional Characterization of the Smooth Muscle Ether-a-Go-Go-Related Gene K<sup>+</sup> Channel. Potential Role of a Conserved Amino Acid Substitution in the S4 Region. *J. Biol. Chem.* **2003**, *278*, 2503–2514.
- (72) Parr, E.; Pozo, M. J.; Horowitz, B.; Nelson, M. T.; Mawe, G. M. ERG K<sup>+</sup> Channels Modulate the Electrical and Contractile Activities of Gallbladder Smooth Muscle. *Am. J. Physiol. Gastrointest. Liver Physiol.* **2003**, *284*, G392–8.
- (73) Farrelly, A. M.; Ro, S.; Callaghan, B. P.; Khoi, M. A.; Fleming, N.; Horowitz, B.; Sanders, K. M.; Keef, K. D. Expression and Function of KCNH2 (HERG) in the Human Jejunum. *Am. J. Physiol. Gastrointest. Liver Physiol.* **2003**, *284*, G883–95.
- (74) Rosati, B.; Marchetti, P.; Crociani, O.; Lecchi, M.; Lupi, R.; Arcangeli, A.; Olivetto, M.; Wanke, E. Glucose- and Arginine-Induced Insulin Secretion by Human Pancreatic Beta-Cells: The Role of HERG K(+) Channels in Firing and Release. *FASEB J.* **2000**, *14*, 2601–2610.
- (75) Noble, D.; Tsien, R. W. Outward Membrane Currents Activated in the Plateau Range of Potentials in Cardiac Purkinje Fibres. *J. Physiol.* **1969**, *200*, 205–231.
- (76) Noble, D.; Tsien, R. W. Reconstruction of the Repolarization Process in Cardiac Purkinje Fibres Based on Voltage Clamp Measurements of Membrane Current. *J. Physiol.* **1969**, *200*, 233–254.
- (77) Sanguinetti, M. C.; Jurkiewicz, N. K. Two Components of Cardiac Delayed Rectifier K<sup>+</sup> Current. Differential Sensitivity to Block by Class III Antiarrhythmic Agents. *J. Gen. Physiol.* **1990**, *96*, 195–215.
- (78) Nattel, S. Delayed-Rectifier Potassium Currents and the Control of Cardiac Repolarization: Noble and Tsien 40 Years After. *J. Physiol.* **2008**, *586*, 5849–5852.
- (79) Sanguinetti, M. C.; Jiang, C.; Curran, M. E.; Keating, M. T. A Mechanistic Link between an Inherited and an Acquired Cardiac Arrhythmia: HERG Encodes the IKr Potassium Channel. *Cell* **1995**, *81*, 299–307.
- (80) Trudeau, M. C.; Warmke, J. W.; Ganetzky, B.; Robertson, G. A. HERG, a Human Inward Rectifier in the Voltage-Gated Potassium Channel Family. *Science* **1995**, *269*, 92–95.
- (81) Hancox, J. C.; Levi, A. J.; Witchel, H. J. Time Course and Voltage Dependence of Expressed HERG Current Compared with Native “Rapid” Delayed Rectifier K Current during the Cardiac Ventricular Action Potential. *Pflügers Arch.* **1998**, *436*, 843–853.
- (82) Jervell, A.; Lange-Nielsen, F. Congenital Deaf-Mutism, Functional Heart Disease with Prolongation of the QT Interval, and Sudden Death. *Am. Heart J.* **1957**, *54*, 59–68.
- (83) Dessertenne, F. Ventricular Tachycardia with 2 Variable Opposing Foci. *Arch. Mal. Coeur Vaiss.* **1966**, *59*, 263–272.

- (84) Motté, G.; Coumel, P.; Abitbol, G.; Dessertenne, F.; Slama, R. The Long QT Syndrome and Syncope Caused by Spike Torsades. *Arch. Mal. Coeur Vaiss.* **1970**, *63*, 831–853.
- (85) Pollard, C. E.; Abi Gerges, N.; Bridgland-Taylor, M. H.; Easter, A.; Hammond, T. G.; Valentin, J.-P. An Introduction to QT Interval Prolongation and Non-Clinical Approaches to Assessing and Reducing Risk. *Br. J. Pharmacol.* **2010**, *159*, 12–21.
- (86) Sanguinetti, M. C.; Tristani-Firouzi, M. hERG Potassium Channels and Cardiac Arrhythmia. *Nature* **2006**, *440*, 463–469.
- (87) Wang, Q.; Curran, M. E.; Splawski, I.; Burn, T. C.; Millholland, J. M.; VanRaay, T. J.; Shen, J.; Timothy, K. W.; Vincent, G. M.; de Jager, T.; Schwartz, P. J.; Toubin, J. A.; Moss, A. J.; Atkinson, D. L.; Landes, G. M.; Connors, T. D.; Keating, M. T. Positional Cloning of a Novel Potassium Channel Gene: KVLQT1 Mutations Cause Cardiac Arrhythmias. *Nat. Genet.* **1996**, *12*, 17–23.
- (88) Romano, C.; Gemme, G.; Pongiglione, R. Rare Cardiac Arrhythmias of the Pediatric Age. II. Syncopal Attack due to Paroxysmal Ventricular Fibrillation. (presentation of 1st Case in Italian Pediatric Literature). *Clin. Pediatr. (Bologna)*. **1963**, *45*, 656–683.
- (89) Ward, O. C. A New Familial Cardiac Syndrome in Children. *J. Ir. Med. Assoc.* **1964**, *54*, 103–106.
- (90) Furutani, M.; Trudeau, M. C.; Hagiwara, N.; Seki, A.; Gong, Q.; Zhou, Z.; Imamura, S.; Nagashima, H.; Kasanuki, H.; Takao, A.; Momma, K.; January, C. T.; Robertson, G. A.; Matsuoka, R. Novel Mechanism Associated with an Inherited Cardiac Arrhythmia: Defective Protein Trafficking by the Mutant HERG (G601S) Potassium Channel. *Circulation* **1999**, *99*, 2290–2294.
- (91) Delisle, B. P.; Anson, B. D.; Rajamani, S.; January, C. T. Biology of Cardiac Arrhythmias: Ion Channel Protein Trafficking. *Circ. Res.* **2004**, *94*, 1418–1428.
- (92) Anderson, C. L.; Delisle, B. P.; Anson, B. D.; Kilby, J. A.; Will, M. L.; Tester, D. J.; Gong, Q.; Zhou, Z.; Ackerman, M. J.; January, C. T. Most LQT2 Mutations Reduce Kv11.1 (hERG) Current by a Class 2 (trafficking-Deficient) Mechanism. *Circulation* **2006**, *113*, 365–373.
- (93) Gong, Q.; Keeney, D. R.; Molinari, M.; Zhou, Z. Degradation of Trafficking-Defective Long QT Syndrome Type II Mutant Channels by the Ubiquitin-Proteasome Pathway. *J. Biol. Chem.* **2005**, *280*, 19419–19425.
- (94) Brugada, R.; Hong, K.; Dumaine, R.; Cordeiro, J.; Gaita, F.; Borggrefe, M.; Menendez, T. M.; Brugada, J.; Pollevick, G. D.; Wolpert, C.; Burashnikov, E.; Matsuo, K.; Wu, Y. S.; Guerchicoff, A.; Bianchi, F.; Giustetto, C.; Schimpf, R.; Brugada, P.; Antzelevitch, C. Sudden Death Associated with Short-QT Syndrome Linked to Mutations in HERG. *Circulation* **2004**, *109*, 30–35.
- (95) Gussak, I.; Brugada, P.; Brugada, J.; Wright, R. S.; Kopecky, S. L.; Chaitman, B. R.; Bjerregaard, P. Idiopathic Short QT Interval: A New Clinical Syndrome? *Cardiology* **2000**, *94*, 99–102.
- (96) Schimpf, R.; Wolpert, C.; Gaita, F.; Giustetto, C.; Borggrefe, M. Short QT Syndrome. *Cardiovasc. Res.* **2005**, *67*, 357–366.
- (97) Jehle, J.; Schweizer, P. A.; Katus, H. A.; Thomas, D. Novel Roles for hERG K(+) Channels in Cell Proliferation and Apoptosis. *Cell Death Dis.* **2011**, *2*, e193.
- (98) Bianchi, L.; Wible, B.; Arcangeli, A.; Taglialatela, M.; Morra, F.; Castaldo, P.; Crociani, O.; Rosati, B.; Faravelli, L.; Olivotto, M.; Wanke, E. Herg Encodes a K<sup>+</sup> Current Highly Conserved

- in Tumors of Different Histogenesis: A Selective Advantage for Cancer Cells? *Cancer Res.* **1998**, *58*, 815–822.
- (99) Arcangeli, A.; Bianchi, L.; Becchetti, A.; Faravelli, L.; Coronello, M.; Mini, E.; Olivotto, M.; Wanke, E. A Novel Inward-Rectifying K<sup>+</sup> Current with a Cell-Cycle Dependence Governs the Resting Potential of Mammalian Neuroblastoma Cells. *J. Physiol.* **1995**, *489*, 455–471.
  - (100) Smith, G. A. M.; Tsui, H.-W.; Newell, E. W.; Jiang, X.; Zhu, X.; Tsui, F. W. L.; Schlichter, L. C. Functional up-Regulation of HERG K<sup>+</sup> Channels in Neoplastic Hematopoietic Cells. *J. Biol. Chem.* **2002**, *277*, 18528–18534.
  - (101) Chen, S.; Jiang, M.; Zhen, Y. HERG K<sup>+</sup> Channel Expression-Related Chemosensitivity in Cancer Cells and Its Modulation by Erythromycin. *Cancer Chemother. Pharmacol.* **2005**, *56*, 212–220.
  - (102) Lastraioli, E.; Guasti, L.; Crociani, O.; Polvani, S.; Hofmann, G.; Witchel, H.; Bencini, L.; Calistri, M.; Messerini, L.; Scatizzi, M.; Moretti, R.; Wanke, E.; Olivotto, M.; Mugnai, G.; Arcangeli, A. herg1 Gene and HERG1 Protein Are Overexpressed in Colorectal Cancers and Regulate Cell Invasion of Tumor Cells. *Cancer Res.* **2004**, *64*, 606–611.
  - (103) Roy, J.; Vantol, B.; Cowley, E. A.; Blay, J.; Linsdell, P. Pharmacological Separation of hEAG and hERG K<sup>+</sup> Channel Function in the Human Mammary Carcinoma Cell Line MCF-7. *Oncol. Rep.* **2008**, *19*, 1511–1516.
  - (104) Wang, H.; Zhang, Y.; Cao, L.; Han, H.; Wang, J.; Yang, B.; Nattel, S.; Wang, Z. HERG K<sup>+</sup> Channel, a Regulator of Tumor Cell Apoptosis and Proliferation. *Cancer Res.* **2002**, *62*, 4843–4848.
  - (105) Cherubini, A.; Hofmann, G.; Pillozzi, S.; Guasti, L.; Crociani, O.; Cilia, E.; Di Stefano, P.; Degani, S.; Balzi, M.; Olivotto, M.; Wanke, E.; Becchetti, A.; Defilippi, P.; Wymore, R.; Arcangeli, A. Human Ether-a-Go-Go-Related Gene 1 Channels Are Physically Linked to beta1 Integrins and Modulate Adhesion-Dependent Signaling. *Mol. Biol. Cell* **2005**, *16*, 2972–2983.
  - (106) Sanguinetti, M. C. HERG1 Channelopathies. *Pflugers Arch.* **2010**, *460*, 265–276.
  - (107) Vandenberg, J. I.; Perry, M. D.; Perrin, M. J.; Mann, S. A.; Ke, Y.; Hill, A. P. hERG K<sup>+</sup> Channels: Structure, Function, and Clinical Significance. *Physiol. Rev.* **2012**, *92*, 1393–1478.
  - (108) Long, S. B.; Campbell, E. B.; Mackinnon, R. Voltage Sensor of Kv1.2: Structural Basis of Electromechanical Coupling. *Science* **2005**, *309*, 903–908.
  - (109) Smith, P. L.; Yellen, G. Fast and Slow Voltage Sensor Movements in HERG Potassium Channels. *J. Gen. Physiol.* **2002**, *119*, 275–293.
  - (110) Piper, D. R.; Varghese, A.; Sanguinetti, M. C.; Tristani-Firouzi, M. Gating Currents Associated with Intramembrane Charge Displacement in HERG Potassium Channels. *Proc. Natl. Acad. Sci. U. S. A.* **2003**, *100*, 10534–10539.
  - (111) Wang, S.; Liu, S.; Morales, M. J.; Strauss, H. C.; Rasmusson, R. L. A Quantitative Analysis of the Activation and Inactivation Kinetics of HERG Expressed in *Xenopus* Oocytes. *J. Physiol.* **1997**, *502* ( Pt 1), 45–60.
  - (112) Spector, P. S.; Curran, M. E.; Zou, A.; Keating, M. T.; Sanguinetti, M. C. Fast Inactivation Causes Rectification of the IKr Channel. *J. Gen. Physiol.* **1996**, *107*, 611–619.
  - (113) Smith, P. L.; Baukrowitz, T.; Yellen, G. The Inward Rectification Mechanism of the HERG Cardiac Potassium Channel. *Nature* **1996**, *379*, 833–836.

- (114) Schönherr, R.; Heinemann, S. H. Molecular Determinants for Activation and Inactivation of HERG, a Human Inward Rectifier Potassium Channel. *J. Physiol.* **1996**, *493*, 635–642.
- (115) Shibasaki, T. Conductance and Kinetics of Delayed Rectifier Potassium Channels in Nodal Cells of the Rabbit Heart. *J. Physiol.* **1987**, *387*, 227–250.
- (116) Lu, Y.; Mahaut-Smith, M. P.; Varghese, A.; Huang, C. L.; Kemp, P. R.; Vandenberg, J. I. Effects of Premature Stimulation on HERG K(+) Channels. *J. Physiol.* **2001**, *537*, 843–851.
- (117) Pond, A. L.; Scheve, B. K.; Benedict, A. T.; Petrecca, K.; Van Wagoner, D. R.; Shrier, A.; Nerbonne, J. M. Expression of Distinct ERG Proteins in Rat, Mouse, and Human Heart. Relation to Functional I(Kr) Channels. *J. Biol. Chem.* **2000**, *275*, 5997–6006.
- (118) Jones, E. M. C.; Roti Roti, E. C.; Wang, J.; Delfosse, S. A.; Robertson, G. A. Cardiac IKr Channels Minimally Comprise hERG 1a and 1b Subunits. *J. Biol. Chem.* **2004**, *279*, 44690–44694.
- (119) Sale, H.; Wang, J.; O'Hara, T. J.; Tester, D. J.; Phartiyal, P.; He, J.-Q.; Rudy, Y.; Ackerman, M. J.; Robertson, G. A. Physiological Properties of hERG 1a/1b Heteromeric Currents and a hERG 1b-Specific Mutation Associated with Long-QT Syndrome. *Circ. Res.* **2008**, *103*, e81–95.
- (120) Blaustein, R. O.; Miller, C. Ion Channels: Shake, Rattle or Roll? *Nature* **2004**, *427*, 499–500.
- (121) Catterall, W. A. Ion Channel Voltage Sensors: Structure, Function, and Pathophysiology. *Neuron* **2010**, *67*, 915–928.
- (122) Guy, H. R.; Seetharamulu, P. Molecular Model of the Action Potential Sodium Channel. *Proc. Natl. Acad. Sci. U. S. A.* **1986**, *83*, 508–512.
- (123) Jensen, M. Ø.; Jogini, V.; Borhani, D. W.; Leffler, A. E.; Dror, R. O.; Shaw, D. E. Mechanism of Voltage Gating in Potassium Channels. *Science* **2012**, *336*, 229–233.
- (124) Subbiah, R. N.; Kondo, M.; Campbell, T. J.; Vandenberg, J. I. Tryptophan Scanning Mutagenesis of the HERG K<sup>+</sup> Channel: The S4 Domain Is Loosely Packed and Likely to Be Lipid Exposed. *J. Physiol.* **2005**, *569*, 367–379.
- (125) Liu, J.; Zhang, M.; Jiang, M.; Tseng, G. Negative Charges in the Transmembrane Domains of the HERG K Channel Are Involved in the Activation- and Deactivation-Gating Processes. *J. Gen. Physiol.* **2003**, *121*, 599–614.
- (126) Tristani-Firouzi, M.; Chen, J.; Sanguinetti, M. C. Interactions between S4-S5 Linker and S6 Transmembrane Domain Modulate Gating of HERG K<sup>+</sup> Channels. *J. Biol. Chem.* **2002**, *277*, 18994–19000.
- (127) Ferrer, T.; Rupp, J.; Piper, D. R.; Tristani-Firouzi, M. The S4-S5 Linker Directly Couples Voltage Sensor Movement to the Activation Gate in the Human Ether-À-Go-Go-Related Gene (hERG) K<sup>+</sup> Channel. *J. Biol. Chem.* **2006**, *281*, 12858–12864.
- (128) Ng, C. A.; Perry, M. D.; Tan, P. S.; Hill, A. P.; Kuchel, P. W.; Vandenberg, J. I. The s4-s5 Linker Acts as a Signal Integrator for HERG K Channel Activation and Deactivation Gating. *PLoS One* **2012**, *7*, e31640.
- (129) Wang, J.; Trudeau, M. C.; Zappia, A. M.; Robertson, G. A. Regulation of Deactivation by an Amino Terminal Domain in Human Ether-À-Go-Go-Related Gene Potassium Channels. *J. Gen. Physiol.* **1998**, *112*, 637–647.

- (130) Hardman, R. M.; Stansfeld, P. J.; Dalibalta, S.; Sutcliffe, M. J.; Mitcheson, J. S. Activation Gating of hERG Potassium Channels: S6 Glycines Are Not Required as Gating Hinges. *J. Biol. Chem.* **2007**, *282*, 31972–31981.
- (131) Knape, K.; Linder, T.; Wolschann, P.; Beyer, A.; Stary-Weinzinger, A. In Silico Analysis of Conformational Changes Induced by Mutation of Aromatic Binding Residues: Consequences for Drug Binding in the hERG K<sup>+</sup> Channel. *PLoS One* **2011**, *6*, e28778.
- (132) Zou, A.; Xu, Q. P.; Sanguinetti, M. C. A Mutation in the Pore Region of HERG K<sup>+</sup> Channels Expressed in *Xenopus* Oocytes Reduces Rectification by Shifting the Voltage Dependence of Inactivation. *J. Physiol.* **1998**, *509*, 129–137.
- (133) Herzberg, I. M.; Trudeau, M. C.; Robertson, G. A. Transfer of Rapid Inactivation and Sensitivity to the Class III Antiarrhythmic Drug E-4031 from HERG to M-Eag Channels. *J. Physiol.* **1998**, *511*, 3–14.
- (134) Ficker, E.; Jarolimek, W.; Kiehn, J.; Baumann, A.; Brown, A. M. Molecular Determinants of Dofetilide Block of HERG K<sup>+</sup> Channels. *Circ. Res.* **1998**, *82*, 386–395.
- (135) Stansfeld, P. J.; Grottesi, A.; Sands, Z. A.; Sansom, M. S. P.; Gedeck, P.; Gosling, M.; Cox, B.; Stanfield, P. R.; Mitcheson, J. S.; Sutcliffe, M. J. Insight into the Mechanism of Inactivation and pH Sensitivity in Potassium Channels from Molecular Dynamics Simulations. *Biochemistry* **2008**, *47*, 7414–7422.
- (136) Cordero-Morales, J. F.; Jogini, V.; Lewis, A.; Vásquez, V.; Cortes, D. M.; Roux, B.; Perozo, E. Molecular Driving Forces Determining Potassium Channel Slow Inactivation. *Nat. Struct. Mol. Biol.* **2007**, *14*, 1062–1069.
- (137) Cordero-Morales, J. F.; Cuello, L. G.; Zhao, Y.; Jogini, V.; Cortes, D. M.; Roux, B.; Perozo, E. Molecular Determinants of Gating at the Potassium-Channel Selectivity Filter. *Nat. Struct. Mol. Biol.* **2006**, *13*, 311–318.
- (138) Bhate, M. P.; McDermott, A. E. Protonation State of E71 in KcsA and Its Role for Channel Collapse and Inactivation. *Proc. Natl. Acad. Sci. U. S. A.* **2012**, *109*, 15265–15270.
- (139) Liu, J.; Zhang, M.; Jiang, M.; Tseng, G. Structural and Functional Role of the Extracellular s5-P Linker in the HERG Potassium Channel. *J. Gen. Physiol.* **2002**, *120*, 723–737.
- (140) Torres, A. M.; Bansal, P. S.; Sunde, M.; Clarke, C. E.; Bursill, J. A.; Smith, D. J.; Bauskin, A.; Breit, S. N.; Campbell, T. J.; Alewood, P. F.; Kuchel, P. W.; Vandenberg, J. I. Structure of the HERG K<sup>+</sup> Channel S5P Extracellular Linker: Role of an Amphipathic Alpha-Helix in C-Type Inactivation. *J. Biol. Chem.* **2003**, *278*, 42136–42148.
- (141) Jiang, M.; Zhang, M.; Maslennikov, I. V.; Liu, J.; Wu, D.; Korolkova, Y. V.; Arseniev, A. S.; Grishin, E. V.; Tseng, G. Dynamic Conformational Changes of Extracellular S5-P Linkers in the hERG Channel. *J. Physiol.* **2005**, *569*, 75–89.
- (142) Pardo-Lopez, L.; Zhang, M.; Liu, J.; Jiang, M.; Possani, L. D.; Tseng, G.-N. Mapping the Binding Site of a Human Ether-a-Go-Go-Related Gene-Specific Peptide Toxin (ErgTx) to the Channel's Outer Vestibule. *J. Biol. Chem.* **2002**, *277*, 16403–16411.
- (143) Dun, W.; Jiang, M.; Tseng, G. N. Allosteric Effects of Mutations in the Extracellular S5-P Loop on the Gating and Ion Permeation Properties of the hERG Potassium Channel. *Pflugers Arch.* **1999**, *439*, 141–149.
- (144) Morais Cabral, J. H.; Lee, A.; Cohen, S. L.; Chait, B. T.; Li, M.; Mackinnon, R. Crystal Structure and Functional Analysis of the HERG Potassium Channel N Terminus: A Eukaryotic PAS Domain. *Cell* **1998**, *95*, 649–655.

- (145) Chen, J.; Zou, A.; Splawski, I.; Keating, M. T.; Sanguinetti, M. C. Long QT Syndrome-Associated Mutations in the Per-Arnt-Sim (PAS) Domain of HERG Potassium Channels Accelerate Channel Deactivation. *J. Biol. Chem.* **1999**, *274*, 10113–10118.
- (146) Wang, J.; Myers, C. D.; Robertson, G. A. Dynamic Control of Deactivation Gating by a Soluble Amino-Terminal Domain in HERG K(+) Channels. *J. Gen. Physiol.* **2000**, *115*, 749–758.
- (147) Ng, C. A.; Hunter, M. J.; Perry, M. D.; Mobli, M.; Ke, Y.; Kuchel, P. W.; King, G. F.; Stock, D.; Vandenberg, J. I. The N-Terminal Tail of hERG Contains an Amphipathic  $\alpha$ -Helix That Regulates Channel Deactivation. *PLoS One* **2011**, *6*, e16191.
- (148) Ke, Y.; Hunter, M. J.; Ng, C. A.; Perry, M. D.; Vandenberg, J. I. Role of the Cytoplasmic N-Terminal Cap and Per Arnt Sim (PAS) Domain in Trafficking and Stabilization of Kv11.1 Channels. *J. Biol. Chem.* **2014**.
- (149) Cui, J.; Melman, Y.; Palma, E.; Fishman, G. I.; McDonald, T. V. Cyclic AMP Regulates the HERG K(+) Channel by Dual Pathways. *Curr. Biol.* **2000**, *10*, 671–674.
- (150) Gustina, A. S.; Trudeau, M. C. hERG Potassium Channel Gating Is Mediated by N- and C-Terminal Region Interactions. *J. Gen. Physiol.* **2011**, *137*, 315–325.
- (151) Osterberg, F.; Aqvist, J. Exploring Blocker Binding to a Homology Model of the Open hERG K<sup>+</sup> Channel Using Docking and Molecular Dynamics Methods. *FEBS Lett.* **2005**, *579*, 2939–2944.
- (152) Farid, R.; Day, T.; Friesner, R. A.; Pearlstein, R. A. New Insights about HERG Blockade Obtained from Protein Modeling, Potential Energy Mapping, and Docking Studies. *Bioorg. Med. Chem.* **2006**, *14*, 3160–3173.
- (153) Stansfeld, P. J.; Gedeck, P.; Gosling, M.; Cox, B.; Mitcheson, J. S.; Sutcliffe, M. J. Drug Block of the hERG Potassium Channel: Insight from Modeling. *Proteins* **2007**, *68*, 568–580.
- (154) Tseng, G.; Sonawane, K. D.; Korolkova, Y. V.; Zhang, M.; Liu, J.; Grishin, E. V.; Guy, H. R. Probing the Outer Mouth Structure of the hERG Channel with Peptide Toxin Footprinting and Molecular Modeling. *Biophys. J.* **2007**, *92*, 3524–3540.
- (155) Masetti, M.; Cavalli, A.; Recanatini, M. Modeling the hERG Potassium Channel in a Phospholipid Bilayer: Molecular Dynamics and Drug Docking Studies. *J. Comput. Chem.* **2008**, *29*, 795–808.
- (156) Imai, Y. N.; Ryu, S.; Oiki, S. Docking Model of Drug Binding to the Human Ether- $\Delta$ -Go-Go Potassium Channel Guided by Tandem Dimer Mutant Patch-Clamp Data: A Synergic Approach. *J. Med. Chem.* **2009**, *52*, 1630–1638.
- (157) Stary, A.; Wacker, S. J.; Boukharta, L.; Zachariae, U.; Karimi-Nejad, Y.; Aqvist, J.; Vriend, G.; de Groot, B. L. Toward a Consensus Model of the HERG Potassium Channel. *ChemMedChem* **2010**, *5*, 455–467.
- (158) Du-Cuny, L.; Chen, L.; Zhang, S. A Critical Assessment of Combined Ligand- and Structure-Based Approaches to HERG Channel Blocker Modeling. *J. Chem. Inf. Model.* **2011**, *51*, 2948–2960.
- (159) Durdagi, S.; Deshpande, S.; Duff, H. J.; Noskov, S. Y. Modeling of Open, Closed, and Open-Inactivated States of the hERG1 Channel: Structural Mechanisms of the State-Dependent Drug Binding. *J. Chem. Inf. Model.* **2012**, *52*, 2760–2774.
- (160) Singh, B. N.; Vaughan Williams, E. M. A Third Class of Anti-Arrhythmic Action. Effects on Atrial and Ventricular Intracellular Potentials, and Other Pharmacological Actions on Cardiac Muscle, of MJ 1999 and AH 3474. *Br. J. Pharmacol.* **1970**, *39*, 675–687.

- (161) Roden, D. M. Ibutilide and the Treatment of Atrial Arrhythmias. *Circulation* **1996**, *94*, 1499–1502.
- (162) Vitola, J.; Vukanovic, J.; Roden, D. M. Cisapride-Induced Torsades de Pointes. *J. Cardiovasc. Electrophysiol.* **1998**, *9*, 1109–1113.
- (163) ICH. ICH (International Conference on Harmonization of Technical Requirement for Registration of Pharmaceuticals for Human Use) Guideline S7B: The Non-Clinical Evaluation of the Potential for Delayed Ventricular Repolarization (QT Interval Prolongation) by Hum. **2005**.
- (164) Fermini, B.; Fossa, A. A. The Impact of Drug-Induced QT Interval Prolongation on Drug Discovery and Development. *Nat. Rev. Drug Discov.* **2003**, *2*, 439–447.
- (165) Fenichel, R. R.; Malik, M.; Antzelevitch, C.; Sanguinetti, M.; Roden, D. M.; Priori, S. G.; Ruskin, J. N.; Lipicky, R. J.; Cantilena, L. R. Drug-Induced Torsades de Pointes and Implications for Drug Development. *J. Cardiovasc. Electrophysiol.* **2004**, *15*, 475–495.
- (166) Mitcheson, J. S.; Chen, J.; Lin, M.; Culberson, C.; Sanguinetti, M. C. A Structural Basis for Drug-Induced Long QT Syndrome. *Proc. Natl. Acad. Sci. U. S. A.* **2000**, *97*, 12329–12333.
- (167) Lees-Miller, J. P.; Duan, Y.; Teng, G. Q.; Duff, H. J. Molecular Determinant of High-Affinity Dofetilide Binding to HERG1 Expressed in *Xenopus* Oocytes: Involvement of S6 Sites. *Mol. Pharmacol.* **2000**, *57*, 367–374.
- (168) Kamiya, K.; Mitcheson, J. S.; Yasui, K.; Kodama, I.; Sanguinetti, M. C. Open Channel Block of HERG K(+) Channels by Vesnarinone. *Mol. Pharmacol.* **2001**, *60*, 244–253.
- (169) Sánchez-Chapula, J. A.; Navarro-Polanco, R. A.; Culberson, C.; Chen, J.; Sanguinetti, M. C. Molecular Determinants of Voltage-Dependent Human Ether-a-Go-Go Related Gene (HERG) K<sup>+</sup> Channel Block. *J. Biol. Chem.* **2002**, *277*, 23587–23595.
- (170) Sánchez-Chapula, J. A.; Ferrer, T.; Navarro-Polanco, R. A.; Sanguinetti, M. C. Voltage-Dependent Profile of Human Ether-a-Go-Go-Related Gene Channel Block Is Influenced by a Single Residue in the S6 Transmembrane Domain. *Mol. Pharmacol.* **2003**, *63*, 1051–1058.
- (171) Sánchez-Chapula, J. A.; Navarro-Polanco, R. A.; Sanguinetti, M. C. Block of Wild-Type and Inactivation-Deficient Human Ether-a-Go-Go-Related Gene K<sup>+</sup> Channels by Halofantrine. *Naunyn. Schmiedeberg's Arch. Pharmacol.* **2004**, *370*, 484–491.
- (172) Ridley, J. M.; Dooley, P. C.; Milnes, J. T.; Witchel, H. J.; Hancox, J. C. Lidoflazine Is a High Affinity Blocker of the HERG K(+)channel. *J. Mol. Cell. Cardiol.* **2004**, *36*, 701–705.
- (173) Perry, M.; de Groot, M. J.; Helliwell, R.; Leishman, D.; Tristani-Firouzi, M.; Sanguinetti, M. C.; Mitcheson, J. Structural Determinants of HERG Channel Block by Clofilium and Ibutilide. *Mol. Pharmacol.* **2004**, *66*, 240–249.
- (174) Witchel, H. J.; Dempsey, C. E.; Sessions, R. B.; Perry, M.; Milnes, J. T.; Hancox, J. C.; Mitcheson, J. S. The Low-Potency, Voltage-Dependent HERG Blocker Propafenone - Molecular Determinants and Drug Trapping. *Mol. Pharmacol.* **2004**, *66*, 1201–1212.
- (175) Fernandez, D.; Ghanta, A.; Kauffman, G. W.; Sanguinetti, M. C. Physicochemical Features of the HERG Channel Drug Binding Site. *J. Biol. Chem.* **2004**, *279*, 10120–10127.
- (176) Kamiya, K.; Niwa, R.; Mitcheson, J. S.; Sanguinetti, M. C. Molecular Determinants of HERG Channel Block. *Mol. Pharmacol.* **2006**, *69*, 1709–1716.
- (177) Guo, J.; Gang, H.; Zhang, S. Molecular Determinants of Cocaine Block of Human Ether-Á-Go-Go-Related Gene Potassium Channels. *J. Pharmacol. Exp. Ther.* **2006**, *317*, 865–874.

- (178) Shealy, R. T.; Murphy, A. D.; Ramarathnam, R.; Jakobsson, E.; Subramaniam, S. Sequence-Function Analysis of the K<sup>+</sup>-Selective Family of Ion Channels Using a Comprehensive Alignment and the KcsA Channel Structure. *Biophys. J.* **2003**, *84*, 2929–2942.
- (179) Ficker, E.; Jarolimek, W.; Brown, A. M. Molecular Determinants of Inactivation and Dofetilide Block in Ether  $\alpha$ -Go-Go (EAG) Channels and EAG-Related K<sup>+</sup> Channels. *Mol. Pharmacol.* **2001**, *60*, 1343–1348 ST – Molecular determinants of inactivation.
- (180) Gessner, G.; Heinemann, S. H. Inhibition of hEAG1 and hERG1 Potassium Channels by Clofilium and Its Tertiary Analogue LY97241. *Br. J. Pharmacol.* **2003**, *138*, 161–171.
- (181) Gessner, G.; Zacharias, M.; Bechstedt, S.; Schönherr, R.; Heinemann, S. H. Molecular Determinants for High-Affinity Block of Human EAG Potassium Channels by Antiarrhythmic Agents. *Mol. Pharmacol.* **2004**, *65*, 1120–1129.
- (182) Numaguchi, H.; Mullins, F. M.; Johnson, J. P.; Johns, D. C.; Po, S. S.; Yang, I. C.; Tomaselli, G. F.; Balser, J. R. Probing the Interaction between Inactivation Gating and Dd-Sotalol Block of HERG. *Circ. Res.* **2000**, *87*, 1012–1018.
- (183) Wang, S.; Morales, M. J.; Liu, S.; Strauss, H. C.; Rasmusson, R. L. Modulation of HERG Affinity for E-4031 by [K<sup>+</sup>]<sub>o</sub> and C-Type Inactivation. *FEBS Lett.* **1997**, *417*, 43–47.
- (184) Perrin, M. J.; Kuchel, P. W.; Campbell, T. J.; Vandenberg, J. I. Drug Binding to the Inactivated State Is Necessary but Not Sufficient for High-Affinity Binding to Human Ether- $\alpha$ -Go-Go-Related Gene Channels. *Mol. Pharmacol.* **2008**, *74*, 1443–1452.
- (185) Chen, J.; Seeböhm, G.; Sanguinetti, M. C. Position of Aromatic Residues in the S6 Domain, Not Inactivation, Dictates Cisapride Sensitivity of HERG and Eag Potassium Channels. *Proc. Natl. Acad. Sci. U. S. A.* **2002**, *99*, 12461–12466.
- (186) Spector, P. S.; Curran, M. E.; Keating, M. T.; Sanguinetti, M. C. Class III Antiarrhythmic Drugs Block HERG, a Human Cardiac Delayed Rectifier K<sup>+</sup> Channel. Open-Channel Block by Methanesulfonanilides. *Circ. Res.* **1996**, *78*, 499–503.
- (187) Stork, D.; Timin, E. N.; Berjukow, S.; Huber, C.; Hohaus, A.; Auer, M.; Hering, S. State Dependent Dissociation of HERG Channel Inhibitors. *Br. J. Pharmacol.* **2007**, *151*, 1368–1376.
- (188) Dennis, A.; Wang, L.; Wan, X.; Ficker, E. hERG Channel Trafficking: Novel Targets in Drug-Induced Long QT Syndrome. *Biochem. Soc. Trans.* **2007**, *35*, 1060–1063.
- (189) Ficker, E.; Kuryshv, Y. A.; Dennis, A. T.; Obejero-Paz, C.; Wang, L.; Hawryluk, P.; Wible, B. A.; Brown, A. M. Mechanisms of Arsenic-Induced Prolongation of Cardiac Repolarization. *Mol. Pharmacol.* **2004**, *66*, 33–44.
- (190) Cordes, J. S.; Sun, Z.; Lloyd, D. B.; Bradley, J. A.; Opsahl, A. C.; Tengowski, M. W.; Chen, X.; Zhou, J. Pentamidine Reduces hERG Expression to Prolong the QT Interval. *Br. J. Pharmacol.* **2005**, *145*, 15–23.
- (191) Guo, J.; Massaeli, H.; Li, W.; Xu, J.; Luo, T.; Shaw, J.; Kirshenbaum, L. A.; Zhang, S. Identification of IKr and Its Trafficking Disruption Induced by Probucol in Cultured Neonatal Rat Cardiomyocytes. *J. Pharmacol. Exp. Ther.* **2007**, *321*, 911–920.
- (192) Rajamani, S.; Eckhardt, L. L.; Valdivia, C. R.; Klemens, C. A.; Gillman, B. M.; Anderson, C. L.; Holzem, K. M.; Delisle, B. P.; Anson, B. D.; Makielski, J. C.; January, C. T. Drug-Induced Long QT Syndrome: hERG K<sup>+</sup> Channel Block and Disruption of Protein Trafficking by Fluoxetine and Norfluoxetine. *Br. J. Pharmacol.* **2006**, *149*, 481–489.

- (193) Takemasa, H.; Nagatomo, T.; Abe, H.; Kawakami, K.; Igarashi, T.; Tsurugi, T.; Kabashima, N.; Tamura, M.; Okazaki, M.; Delisle, B. P.; January, C. T.; Otsuji, Y. Coexistence of hERG Current Block and Disruption of Protein Trafficking in Ketoconazole-Induced Long QT Syndrome. *Br. J. Pharmacol.* **2008**, *153*, 439–447.
- (194) Wang, L.; Dennis, A. T.; Trieu, P.; Charron, F.; Ethier, N.; Hebert, T. E.; Wan, X.; Ficker, E. Intracellular Potassium Stabilizes Human Ether-À-Go-Go-Related Gene Channels for Export from Endoplasmic Reticulum. *Mol. Pharmacol.* **2009**, *75*, 927–937.
- (195) Ficker, E.; Dennis, A. T.; Wang, L.; Brown, A. M. Role of the Cytosolic Chaperones Hsp70 and Hsp90 in Maturation of the Cardiac Potassium Channel HERG. *Circ. Res.* **2003**, *92*, e87–100.
- (196) Zhou, Z.; Gong, Q.; January, C. T. Correction of Defective Protein Trafficking of a Mutant HERG Potassium Channel in Human Long QT Syndrome. Pharmacological and Temperature Effects. *J. Biol. Chem.* **1999**, *274*, 31123–31126.
- (197) Ficker, E.; Obejero-Paz, C. a; Zhao, S.; Brown, A. M. The Binding Site for Channel Blockers That Rescue Misprocessed Human Long QT Syndrome Type 2 Ether-a-Gogo-Related Gene (HERG) Mutations. *J. Biol. Chem.* **2002**, *277*, 4989–4998.
- (198) Rajamani, S.; Anderson, C. L.; Anson, B. D.; January, C. T. Pharmacological Rescue of Human K(+) Channel Long-QT2 Mutations: Human Ether-a-Go-Go-Related Gene Rescue without Block. *Circulation* **2002**, *105*, 2830–2835.
- (199) Varkevisser, R.; Houtman, M. J. C.; Linder, T.; de Git, K. C. G.; Beekman, H. D. M.; Tidwell, R. R.; Ijzerman, a P.; Stary-Weinzinger, A.; Vos, M. A.; van der Heyden, M. A. G. Structure-Activity Relationships of Pentamidine-Affected Ion Channel Trafficking and Dofetilide Mediated Rescue. *Br. J. Pharmacol.* **2013**, *169*, 1322–1334.
- (200) Carmeliet, E. Voltage- and Time-Dependent Block of the Delayed K<sup>+</sup> Current in Cardiac Myocytes by Dofetilide. *J. Pharmacol. Exp. Ther.* **1992**, *262*, 809–817.
- (201) Mitcheson, J. S.; Chen, J.; Sanguinetti, M. C. Trapping of a Methanesulfonanilide by Closure of the HERG Potassium Channel Activation Gate. *J. Gen. Physiol.* **2000**, *115*, 229–240.
- (202) Windisch, A.; Timin, E.; Schwarz, T.; Stork-Riedler, D.; Erker, T.; Ecker, G.; Hering, S. Trapping and Dissociation of Propafenone Derivatives in HERG Channels. *Br. J. Pharmacol.* **2011**, *162*, 1542–1552.
- (203) Armstrong, C. M. Interaction of Tetraethylammonium Ion Derivatives with the Potassium Channels of Giant Axons. *J. Gen. Physiol.* **1971**, *58*, 413–437.
- (204) Sanguinetti, M. C.; Xu, Q. P. Mutations of the S4-S5 Linker Alter Activation Properties of HERG Potassium Channels Expressed in *Xenopus* Oocytes. *J. Physiol.* **1999**, *514*, 667–675.
- (205) Noble, D. Electrical Properties of Cardiac Muscle Attributable to Inward Going (anomalous) Rectification. *J. Cell. Comp. Physiol.* **1965**, *66*, 127–135.
- (206) Hagiwara, S.; Takahashi, K. The Anomalous Rectification and Cation Selectivity of the Membrane of a Starfish Egg Cell. *J. Membr. Biol.* **1974**, *18*, 61–80.
- (207) Miyazaki, S. I.; Takahashi, K.; Tsuda, K.; Yoshii, M. Analysis of Non-Linearity Observed in the Current-Voltage Relation of the Tunicate Embryo. *J. Physiol.* **1974**, *238*, 55–77.
- (208) Sakmann, B.; Trube, G. Conductance Properties of Single Inwardly Rectifying Potassium Channels in Ventricular Cells from Guinea-Pig Heart. *J. Physiol.* **1984**, *347*, 641–657.

- (209) Kubo, Y.; Adelman, J. P.; Clapham, D. E.; Jan, L. Y.; Karschin, A.; Kurachi, Y.; Lazdunski, M.; Nichols, C. G.; Seino, S.; Vandenberg, C. A. International Union of Pharmacology. LIV. Nomenclature and Molecular Relationships of Inwardly Rectifying Potassium Channels. *Pharmacol. Rev.* **2005**, *57*, 509–526.
- (210) Kurachi, Y. Voltage-Dependent Activation of the Inward-Rectifier Potassium Channel in the Ventricular Cell Membrane of Guinea-Pig Heart. *J. Physiol.* **1985**, *366*, 365–385.
- (211) Gähwiler, B. H.; Brown, D. A. GABAB-Receptor-Activated K<sup>+</sup> Current in Voltage-Clamped CA3 Pyramidal Cells in Hippocampal Cultures. *Proc. Natl. Acad. Sci. U. S. A.* **1985**, *82*, 1558–1562.
- (212) Williams, J. T.; Colmers, W. F.; Pan, Z. Z. Voltage- and Ligand-Activated Inwardly Rectifying Currents in Dorsal Raphe Neurons in Vitro. *J. Neurosci.* **1988**, *8*, 3499–3506.
- (213) Takahashi, T. Inward Rectification in Neonatal Rat Spinal Motoneurons. *J. Physiol.* **1990**, *423*, 47–62.
- (214) McKinney, L. C.; Gallin, E. K. Inwardly Rectifying Whole-Cell and Single-Channel K Currents in the Murine Macrophage Cell Line J774.1. *J. Membr. Biol.* **1988**, *103*, 41–53.
- (215) Greger, R.; Bleich, M.; Schlatter, E. Ion Channels in the Thick Ascending Limb of Henle's Loop. *Ren. Physiol. Biochem.* **1990**, *13*, 37–50.
- (216) Hebert, S. C.; Desir, G.; Giebisch, G.; Wang, W. Molecular Diversity and Regulation of Renal Potassium Channels. *Physiol. Rev.* **2005**, *85*, 319–371.
- (217) Beeler, G. W.; Reuter, H. Voltage Clamp Experiments on Ventricular Myocardial Fibres. *J. Physiol.* **1970**, *207*, 165–190.
- (218) Plaster, N. M.; Tawil, R.; Tristani-Firouzi, M.; Canún, S.; Bendahhou, S.; Tsunoda, A.; Donaldson, M. R.; Iannaccone, S. T.; Brunt, E.; Barohn, R.; Clark, J.; Deymeer, F.; George, A. L.; Fish, F. A.; Hahn, A.; Nitu, A.; Ozdemir, C.; Serdaroglu, P.; Subramony, S. H.; Wolfe, G.; Fu, Y. H.; Ptácek, L. J. Mutations in Kir2.1 Cause the Developmental and Episodic Electrical Phenotypes of Andersen's Syndrome. *Cell* **2001**, *105*, 511–519.
- (219) Tawil, R.; Ptacek, L. J.; Pavlakis, S. G.; DeVivo, D. C.; Penn, A. S.; Ozdemir, C.; Griggs, R. C. Andersen's Syndrome: Potassium-Sensitive Periodic Paralysis, Ventricular Ectopy, and Dysmorphic Features. *Ann. Neurol.* **1994**, *35*, 326–330.
- (220) Priori, S. G.; Pandit, S. V.; Rivolta, I.; Berenfeld, O.; Ronchetti, E.; Dhamoon, A.; Napolitano, C.; Anumonwo, J.; di Barletta, M. R.; Gudapakkam, S.; Bosi, G.; Stramba-Badiale, M.; Jalife, J. A Novel Form of Short QT Syndrome (SQT3) Is Caused by a Mutation in the KCNJ2 Gene. *Circ. Res.* **2005**, *96*, 800–807.
- (221) Nilius, B.; Droogmans, G. Ion Channels and Their Functional Role in Vascular Endothelium. *Physiol. Rev.* **2001**, *81*, 1415–1459.
- (222) Day, M.; Carr, D. B.; Ulrich, S.; Ilijic, E.; Tkatch, T.; Surmeier, D. J. Dendritic Excitability of Mouse Frontal Cortex Pyramidal Neurons Is Shaped by the Interaction among HCN, Kir2, and K<sub>leak</sub> Channels. *J. Neurosci.* **2005**, *25*, 8776–8787.
- (223) Nilius, B.; Schwarz, G.; Droogmans, G. Modulation by Histamine of an Inwardly Rectifying Potassium Channel in Human Endothelial Cells. *J. Physiol.* **1993**, *472*, 359–371.
- (224) Adams, D. J.; Hill, M. A. Potassium Channels and Membrane Potential in the Modulation of Intracellular Calcium in Vascular Endothelial Cells. *J. Cardiovasc. Electrophysiol.* **2004**, *15*, 598–610.

- (225) Knot, H. J.; Zimmermann, P. A.; Nelson, M. T. Extracellular K(+)-Induced Hyperpolarizations and Dilatations of Rat Coronary and Cerebral Arteries Involve Inward Rectifier K(+) Channels. *J. Physiol.* **1996**, 492, 419–430.
- (226) Knot, H. J.; Nelson, M. T. Regulation of Arterial Diameter and Wall [Ca<sup>2+</sup>] in Cerebral Arteries of Rat by Membrane Potential and Intravascular Pressure. *J. Physiol.* **1998**, 508, 199–209.
- (227) Frindt, G.; Palmer, L. G. Low-Conductance K Channels in Apical Membrane of Rat Cortical Collecting Tubule. *Am. J. Physiol.* **1989**, 256, F143–51.
- (228) Wang, W. H.; Schwab, A.; Giebisch, G. Regulation of Small-Conductance K<sup>+</sup> Channel in Apical Membrane of Rat Cortical Collecting Tubule. *Am. J. Physiol.* **1990**, 259, F494–502.
- (229) Lu, M.; Wang, W. H. Nitric Oxide Regulates the Low-Conductance K<sup>+</sup> Channel in Basolateral Membrane of Cortical Collecting Duct. *Am. J. Physiol.* **1996**, 270, C1336–42.
- (230) Le Maout, S.; Brejon, M.; Olsen, O.; Merot, J.; Welling, P. A. Basolateral Membrane Targeting of a Renal-Epithelial Inwardly Rectifying Potassium Channel from the Cortical Collecting Duct, CCD-IRK3, in MDCK Cells. *Proc. Natl. Acad. Sci. U. S. A.* **1997**, 94, 13329–13334.
- (231) Welling, P. A. Primary Structure and Functional Expression of a Cortical Collecting Duct Kir Channel. *Am. J. Physiol.* **1997**, 273, F825–36.
- (232) Romanenko, V. G.; Rothblat, G. H.; Levitan, I. Modulation of Endothelial Inward-Rectifier K<sup>+</sup> Current by Optical Isomers of Cholesterol. *Biophys. J.* **2002**, 83, 3211–3222.
- (233) Romanenko, V. G.; Fang, Y.; Byfield, F.; Travis, A. J.; Vandenberg, C. A.; Rothblat, G. H.; Levitan, I. Cholesterol Sensitivity and Lipid Raft Targeting of Kir2.1 Channels. *Biophys. J.* **2004**, 87, 3850–3861.
- (234) Fang, Y.; Mohler, E. R.; Hsieh, E.; Osman, H.; Hashemi, S. M.; Davies, P. F.; Rothblat, G. H.; Wilensky, R. L.; Levitan, I. Hypercholesterolemia Suppresses Inwardly Rectifying K<sup>+</sup> Channels in Aortic Endothelium in Vitro and in Vivo. *Circ. Res.* **2006**, 98, 1064–1071.
- (235) Kunkel, M. T.; Peralta, E. G. Identification of Domains Conferring G Protein Regulation on Inward Rectifier Potassium Channels. *Cell* **1995**, 83, 443–449.
- (236) Krapivinsky, G.; Krapivinsky, L.; Wickman, K.; Clapham, D. E. G Beta Gamma Binds Directly to the G Protein-Gated K<sup>+</sup> Channel, IKACH. *J. Biol. Chem.* **1995**, 270, 29059–29062.
- (237) Huang, C. L.; Slesinger, P. A.; Casey, P. J.; Jan, Y. N.; Jan, L. Y. Evidence That Direct Binding of G Beta Gamma to the GIRK1 G Protein-Gated Inwardly Rectifying K<sup>+</sup> Channel Is Important for Channel Activation. *Neuron* **1995**, 15, 1133–1143.
- (238) Slesinger, P. A.; Reuveny, E.; Jan, Y. N.; Jan, L. Y. Identification of Structural Elements Involved in G Protein Gating of the GIRK1 Potassium Channel. *Neuron* **1995**, 15, 1145–1156.
- (239) Chan, K. W.; Sui, J. L.; Vivaudou, M.; Logothetis, D. E. Specific Regions of Heteromeric Subunits Involved in Enhancement of G Protein-Gated K<sup>+</sup> Channel Activity. *J. Biol. Chem.* **1997**, 272, 6548–6555.
- (240) Huang, C.; Jan, Y.; Jan, L. Binding of the G Protein By Subunit to Multiple Regions of G Protein-Gated Inward-Rectifying K<sup>+</sup> Channels. *FEBS Lett.* **1997**, 405, 291–298.
- (241) He, C.; Zhang, H.; Mirshahi, T.; Logothetis, D. E. Identification of a Potassium Channel Site That Interacts with G Protein Subunits to Mediate Agonist-Induced Signaling. *J. Biol. Chem.* **1999**, 274, 12517–12524.

- (242) Ivanina, T.; Rishal, I.; Varon, D.; Mullner, C.; Frohnwieser-Steinecke, B.; Schreibmayer, W.; Dessauer, C. W.; Dascal, N. Mapping the Gbetagamma-Binding Sites in GIRK1 and GIRK2 Subunits of the G Protein-Activated K<sup>+</sup> Channel. *J. Biol. Chem.* **2003**, *278*, 29174–29183.
- (243) Logothetis, D. E.; Kurachi, Y.; Galper, J.; Neer, E. J.; Clapham, D. E. The Beta Gamma Subunits of GTP-Binding Proteins Activate the Muscarinic K<sup>+</sup> Channel in Heart. *Nature* **1987**, *325*, 321–326.
- (244) Ito, H.; Tung, R. T.; Sugimoto, T.; Kobayashi, I.; Takahashi, K.; Katada, T.; Ui, M.; Kurachi, Y. On the Mechanism of G Protein Beta Gamma Subunit Activation of the Muscarinic K<sup>+</sup> Channel in Guinea Pig Atrial Cell Membrane. Comparison with the ATP-Sensitive K<sup>+</sup> Channel. *J. Gen. Physiol.* **1992**, *99*, 961–983.
- (245) Clapham, D. E.; Neer, E. J. New Roles for G-Protein Beta Gamma-Dimers in Transmembrane Signalling. *Nature* **1993**, *365*, 403–406.
- (246) Reuveny, E.; Slesinger, P. A.; Inglese, J.; Morales, J. M.; Iñiguez-Lluhi, J. A.; Lefkowitz, R. J.; Bourne, H. R.; Jan, Y. N.; Jan, L. Y. Activation of the Cloned Muscarinic Potassium Channel by G Protein Beta Gamma Subunits. *Nature* **1994**, *370*, 143–146.
- (247) Wickman, K. D.; Iñiguez-Lluhi, J. A.; Davenport, P. A.; Taussig, R.; Krapivinsky, G. B.; Linder, M. E.; Gilman, A. G.; Clapham, D. E. Recombinant G-Protein Beta Gamma-Subunits Activate the Muscarinic-Gated Atrial Potassium Channel. *Nature* **1994**, *368*, 255–257.
- (248) Peleg, S.; Varon, D.; Ivanina, T.; Dessauer, C. W.; Dascal, N. Gai Controls the Gating of the G Protein-Activated K<sup>+</sup> Channel, GIRK. *Neuron* **2002**, *33*, 87–99.
- (249) Ivanina, T.; Varon, D.; Peleg, S.; Rishal, I.; Porozov, Y.; Dessauer, C. W.; Keren-Raifman, T.; Dascal, N. Gai1 and Gai3 Differentially Interact With, and Regulate, the G Protein-Activated K<sup>+</sup> Channel. *J. Biol. Chem.* **2004**, *279*, 17260–17268.
- (250) Lacey, M. G.; Mercuri, N. B.; North, R. A. On the Potassium Conductance Increase Activated by GABAB and Dopamine D2 Receptors in Rat Substantia Nigra Neurones. *J. Physiol.* **1988**, *401*, 437–453.
- (251) Saugstad, J. A.; Segerson, T. P.; Westbrook, G. L. Metabotropic Glutamate Receptors Activate G-Protein-Coupled Inwardly Rectifying Potassium Channels in *Xenopus* Oocytes. *J. Neurosci.* **1996**, *16*, 5979–5985.
- (252) Sharon, D.; Vorobiov, D.; Dascal, N. Positive and Negative Coupling of the Metabotropic Glutamate Receptors to a G Protein-Activated K<sup>+</sup> Channel, GIRK, in *Xenopus* Oocytes. *J. Gen. Physiol.* **1997**, *109*, 477–490.
- (253) Krapivinsky, G.; Gordon, E. A.; Wickman, K.; Velimirović, B.; Krapivinsky, L.; Clapham, D. E. The G-Protein-Gated Atrial K<sup>+</sup> Channel IKACH Is a Heteromultimer of Two Inwardly Rectifying K(+) -Channel Proteins. *Nature* **1995**, *374*, 135–141.
- (254) Noma, A.; Trautwein, W. Relaxation of the ACh-Induced Potassium Current in the Rabbit Sinoatrial Node Cell. *Pflugers Arch.* **1978**, *377*, 193–200.
- (255) Sakmann, B.; Noma, A.; Trautwein, W. Acetylcholine Activation of Single Muscarinic K<sup>+</sup> Channels in Isolated Pacemaker Cells of the Mammalian Heart. *Nature* **1983**, *303*, 250–253.
- (256) Del Castillo, J.; Katz, B. Production of Membrane Potential Changes in the Frog's Heart by Inhibitory Nerve Impulses. *Nature* **1955**, *175*, 1035.
- (257) Hutter, O. F.; Trautwein, W. Vagal and Sympathetic Effects on the Pacemaker Fibers in the Sinus Venosus of the Heart. *J. Gen. Physiol.* **1956**, *39*, 715–733.

- (258) Wickman, K.; Nemec, J.; Gendler, S. J.; Clapham, D. E. Abnormal Heart Rate Regulation in GIRK4 Knockout Mice. *Neuron* **1998**, *20*, 103–114.
- (259) Thompson, S. M.; Gähwiler, B. H. Comparison of the Actions of Baclofen at Pre- and Postsynaptic Receptors in the Rat Hippocampus in Vitro. *J. Physiol.* **1992**, *451*, 329–345.
- (260) Thompson, S. M.; Haas, H. L.; Gähwiler, B. H. Comparison of the Actions of Adenosine at Pre- and Postsynaptic Receptors in the Rat Hippocampus in Vitro. *J. Physiol.* **1992**, *451*, 347–363.
- (261) Kurachi, Y.; Ishii, M. Cell Signal Control of the G Protein-Gated Potassium Channel and Its Subcellular Localization. *J. Physiol.* **2004**, *554*, 285–294.
- (262) Lüscher, C.; Jan, L. Y.; Stoffel, M.; Malenka, R. C.; Nicoll, R. A. G Protein-Coupled Inwardly Rectifying K<sup>+</sup> Channels (GIRKs) Mediate Postsynaptic but Not Presynaptic Transmitter Actions in Hippocampal Neurons. *Neuron* **1997**, *19*, 687–695.
- (263) Williams, J. T.; Egan, T. M.; North, R. A. Enkephalin Opens Potassium Channels on Mammalian Central Neurones. *Nature* **1982**, *299*, 74–77.
- (264) Williams, J. T.; North, R. A. Opiate-Receptor Interactions on Single Locus Coeruleus Neurones. *Mol. Pharmacol.* **1984**, *26*, 489–497.
- (265) Koyrakh, L.; Luján, R.; Colón, J.; Karschin, C.; Kurachi, Y.; Karschin, A.; Wickman, K. Molecular and Cellular Diversity of Neuronal G-Protein-Gated Potassium Channels. *J. Neurosci.* **2005**, *25*, 11468–11478.
- (266) Morishige, K.; Inanobe, A.; Yoshimoto, Y.; Kurachi, H.; Murata, Y.; Tokunaga, Y.; Maeda, T.; Maruyama, Y.; Kurachi, Y. Secretagogue-Induced Exocytosis Recruits G Protein-Gated K<sup>+</sup> Channels to Plasma Membrane in Endocrine Cells. *J. Biol. Chem.* **1999**, *274*, 7969–7974.
- (267) Rorsman, P.; Bokvist, K.; Ammälä, C.; Arkhammar, P.; Berggren, P. O.; Larsson, O.; Wählander, K. Activation by Adrenaline of a Low-Conductance G Protein-Dependent K<sup>+</sup> Channel in Mouse Pancreatic B Cells. *Nature* **1991**, *349*, 77–79.
- (268) Abel, K.-B.; Lehr, S.; Ullrich, S. Adrenaline-, Not Somatostatin-Induced Hyperpolarization Is Accompanied by a Sustained Inhibition of Insulin Secretion in INS-1 Cells. Activation of Sulphonylurea K<sup>+</sup> + ATP Channels Is Not Involved. *Pflügers Arch. Eur. J. Physiol.* **1996**, *432*, 89–96.
- (269) Yoshimoto, Y.; Fukuyama, Y.; Horio, Y.; Inanobe, A.; Gotoh, M.; Kurachi, Y. Somatostatin Induces Hyperpolarization in Pancreatic Islet A Cells by Activating a G Protein-Gated K<sup>+</sup> Channel. *FEBS Lett.* **1999**, *444*, 265–269.
- (270) Sieg, A.; Su, J.; Muñoz, A.; Buchenau, M.; Nakazaki, M.; Aguilar-Bryan, L.; Bryan, J.; Ullrich, S. Epinephrine-Induced Hyperpolarization of Islet Cells without KATP Channels. *Am. J. Physiol. Endocrinol. Metab.* **2004**, *286*, E463–71.
- (271) Iwanir, S.; Reuveny, E. Adrenaline-Induced Hyperpolarization of Mouse Pancreatic Islet Cells Is Mediated by G Protein-Gated Inwardly Rectifying Potassium (GIRK) Channels. *Pflügers Arch.* **2008**, *456*, 1097–1108.
- (272) Ashcroft, F. M.; Harrison, D. E.; Ashcroft, S. J. H. Glucose Induces Closure of Single Potassium Channels in Isolated Rat Pancreatic B-Cells. *Nature* **1984**, *312*, 446–448.
- (273) Cook, D. L.; Hales, N. Intracellular ATP Directly Blocks K<sup>+</sup> Channels in Pancreatic B-Cells. *Nature* **1984**, *311*, 271–273.
- (274) Noma, A. ATP-Regulated K<sup>+</sup> Channels in Cardiac Muscle. *Nature* **1983**, *305*, 147–148.

- (275) Spruce, A. E.; Standen, N. B.; Stanfield, P. R. Voltage-Dependent ATP-Sensitive Potassium Channels of Skeletal Muscle Membrane. *Nature* **1985**, *316*, 736–738.
- (276) Standen, N. B.; Quayle, J. M.; Davies, N. W.; Brayden, J. E.; Huang, Y.; Nelson, M. T. Hyperpolarizing Vasodilators Activate ATP-Sensitive K<sup>+</sup> Channels in Arterial Smooth Muscle. *Science* **1989**, *245*, 177–180.
- (277) Beech, D. J.; Zhang, H.; Nakao, K.; Bolton, T. B. K Channel Activation by Nucleotide Diphosphates and Its Inhibition by Glibenclamide in Vascular Smooth Muscle Cells. *Br. J. Pharmacol.* **1993**, *110*, 573–582.
- (278) Ashford, M. L.; Boden, P. R.; Treherne, J. M. Glucose-Induced Excitation of Hypothalamic Neurones Is Mediated by ATP-Sensitive K<sup>+</sup> Channels. *Pflugers Arch.* **1990**, *415*, 479–483.
- (279) Ashcroft, F. M. Adenosine 5'-Triphosphate-Sensitive Potassium Channels. *Annu. Rev. Neurosci.* **1988**, *11*, 97–118.
- (280) Nichols, C. G. KATP Channels as Molecular Sensors of Cellular Metabolism. *Nature* **2006**, *440*, 470–476.
- (281) Inagaki, N.; Gonoi, T.; Clement, J. P.; Wang, C. Z.; Aguilar-Bryan, L.; Bryan, J.; Seino, S. A Family of Sulfonylurea Receptors Determines the Pharmacological Properties of ATP-Sensitive K<sup>+</sup> Channels. *Neuron* **1996**, *16*, 1011–1017.
- (282) McTaggart, J. S.; Clark, R. H.; Ashcroft, F. M. The Role of the KATP Channel in Glucose Homeostasis in Health and Disease: More than Meets the Islet. *J. Physiol.* **2010**, *588*, 3201–3209.
- (283) Franklin, I.; Gromada, J.; Gjinovci, A.; Theander, S.; Wollheim, C. B. Beta-Cell Secretory Products Activate Alpha-Cell ATP-Dependent Potassium Channels to Inhibit Glucagon Release. *Diabetes* **2005**, *54*, 1808–1815.
- (284) MacDonald, P. E.; De Marinis, Y. Z.; Ramracheya, R.; Salehi, A.; Ma, X.; Johnson, P. R. V.; Cox, R.; Eliasson, L.; Rorsman, P. A K ATP Channel-Dependent Pathway within Alpha Cells Regulates Glucagon Release from Both Rodent and Human Islets of Langerhans. *PLoS Biol.* **2007**, *5*, e143.
- (285) Gromada, J.; Franklin, I.; Wollheim, C. B. Alpha-Cells of the Endocrine Pancreas: 35 Years of Research but the Enigma Remains. *Endocr. Rev.* **2007**, *28*, 84–116.
- (286) Proks, P.; Antcliff, J. F.; Lippiat, J.; Gloyn, A. L.; Hattersley, A. T.; Ashcroft, F. M. Molecular Basis of Kir6.2 Mutations Associated with Neonatal Diabetes or Neonatal Diabetes plus Neurological Features. *Proc. Natl. Acad. Sci. U. S. A.* **2004**, *101*, 17539–17544.
- (287) Ashcroft, F. M. ATP-Sensitive Potassium Channelopathies: Focus on Insulin Secretion. *J. Clin. Invest.* **2005**, *115*, 2047–2058.
- (288) Ashcroft, F. M. From Molecule to Malady. *Nature* **2006**, *440*, 440–447.
- (289) Dunne, M. J.; Cosgrove, K. E.; Shepherd, R. M.; Aynsley-Green, A.; Lindley, K. J. Hyperinsulinism in Infancy: From Basic Science to Clinical Disease. *Physiol. Rev.* **2004**, *84*, 239–275.
- (290) Thomas, P. M.; Cote, G. J.; Wohlk, N.; Haddad, B.; Mathew, P. M.; Rabl, W.; Aguilar-Bryan, L.; Gagel, R. F.; Bryan, J. Mutations in the Sulfonylurea Receptor Gene in Familial Persistent Hyperinsulinemic Hypoglycemia of Infancy. *Science* **1995**, *268*, 426–429.

- (291) Huopio, H.; Reimann, F.; Ashfield, R.; Komulainen, J.; Lenko, H. L.; Rahier, J.; Vauhkonen, I.; Kere, J.; Laakso, M.; Ashcroft, F.; Otonkoski, T. Dominantly Inherited Hyperinsulinism Caused by a Mutation in the Sulfonylurea Receptor Type 1. *J. Clin. Invest.* **2000**, *106*, 897–906.
- (292) Thomas, P.; Ye, Y.; Lightner, E. Mutation of the Pancreatic Islet Inward Rectifier Kir6.2 Also Leads to Familial Persistent Hyperinsulinemic Hypoglycemia of Infancy. *Hum. Mol. Genet.* **1996**, *5*, 1809–1812.
- (293) Nestorowicz, A.; Inagaki, N.; Gono, T.; Schoor, K. P.; Wilson, B. A.; Glaser, B.; Landau, H.; Stanley, C. A.; Thornton, P. S.; Seino, S.; Permutt, M. A. A Nonsense Mutation in the Inward Rectifier Potassium Channel Gene, Kir6.2, Is Associated with Familial Hyperinsulinism. *Diabetes* **1997**, *46*, 1743–1748.
- (294) Reimann, F.; Huopio, H.; Dabrowski, M.; Proks, P.; Gribble, F. M.; Laakso, M.; Otonkoski, T.; Ashcroft, F. M. Characterisation of New KATP-Channel Mutations Associated with Congenital Hyperinsulinism in the Finnish Population. *Diabetologia* **2003**, *46*, 241–249.
- (295) Henwood, M. J.; Kelly, A.; Macmullen, C.; Bhatia, P.; Ganguly, A.; Thornton, P. S.; Stanley, C. A. Genotype-Phenotype Correlations in Children with Congenital Hyperinsulinism due to Recessive Mutations of the Adenosine Triphosphate-Sensitive Potassium Channel Genes. *J. Clin. Endocrinol. Metab.* **2005**, *90*, 789–794.
- (296) Gloyn, A. L.; Pearson, E. R.; Antcliff, J. F.; Proks, P.; Bruining, G. J.; Slingerland, A. S.; Howard, N.; Srinivasan, S.; Silva, J. M. C. L.; Molnes, J.; Edghill, E. L.; Frayling, T. M.; Temple, I. K.; Mackay, D.; Shield, J. P. H.; Sumnik, Z.; van Rhijn, A.; Wales, J. K. H.; Clark, P.; Gorman, S.; Aisenberg, J.; Ellard, S.; Njølstad, P. R.; Ashcroft, F. M.; Hattersley, A. T. Activating Mutations in the Gene Encoding the ATP-Sensitive Potassium-Channel Subunit Kir6.2 and Permanent Neonatal Diabetes. *N. Engl. J. Med.* **2004**, *350*, 1838–1849.
- (297) Ashcroft, F. M. The Walter B. Cannon Physiology in Perspective Lecture, 2007. ATP-Sensitive K<sup>+</sup> Channels and Disease: From Molecule to Malady. *Am. J. Physiol. Endocrinol. Metab.* **2007**, *293*, E880–9.
- (298) Hattersley, A. T.; Ashcroft, F. M. Activating Mutations in Kir6.2 and Neonatal Diabetes: New Clinical Syndromes, New Scientific Insights, and New Therapy. *Diabetes* **2005**, *54*, 2503–2513.
- (299) Nichols, C. G.; Lederer, W. J. Adenosine Triphosphate-Sensitive Potassium Channels in the Cardiovascular System. *Am. J. Physiol.* **1991**, *261*, H1675–86.
- (300) Kane, G. C.; Liu, X.-K.; Yamada, S.; Olson, T. M.; Terzic, A. Cardiac KATP Channels in Health and Disease. *J. Mol. Cell. Cardiol.* **2005**, *38*, 937–943.
- (301) Li, R. A.; Leppo, M.; Miki, T.; Seino, S.; Marbán, E. Molecular Basis of Electrocardiographic ST-Segment Elevation. *Circ. Res.* **2000**, *87*, 837–839.
- (302) Gross, G. J.; Auchampach, J. A. Blockade of ATP-Sensitive Potassium Channels Prevents Myocardial Preconditioning in Dogs. *Circ. Res.* **1992**, *70*, 223–233.
- (303) D'Alonzo, A. J.; Darbenzio, R. B.; Parham, C. S.; Grover, G. J. Effects of Intracoronary Cromakalim on Postischemic Contractile Function and Action Potential Duration. *Cardiovasc. Res.* **1992**, *26*, 1046–1053.
- (304) Yellon, D. M.; Downey, J. M. Preconditioning the Myocardium: From Cellular Physiology to Clinical Cardiology. *Physiol. Rev.* **2003**, *83*, 1113–1151.
- (305) Murry, C. E.; Jennings, R. B.; Reimer, K. A. Preconditioning with Ischemia: A Delay of Lethal Cell Injury in Ischemic Myocardium. *Circulation* **1986**, *74*, 1124–1136.

- (306) Zingman, L. V.; Hodgson, D. M.; Bast, P. H.; Kane, G. C.; Perez-Terzic, C.; Gumina, R. J.; Pucar, D.; Bienengraeber, M.; Dzeja, P. P.; Miki, T.; Seino, S.; Alekseev, A. E.; Terzic, A. Kir6.2 Is Required for Adaptation to Stress. *Proc. Natl. Acad. Sci. U. S. A.* **2002**, *99*, 13278–13283.
- (307) Kane, G. C.; Behfar, A.; Dyer, R. B.; O’Cochlain, D. F.; Liu, X.; Hodgson, D. M.; Reyes, S.; Miki, T.; Seino, S.; Terzic, A. KCNJ11 Gene Knockout of the Kir6.2 KATP Channel Causes Maladaptive Remodeling and Heart Failure in Hypertension. *Hum. Mol. Genet.* **2006**, *15*, 2285–2297.
- (308) Tong, X.; Porter, L. M.; Liu, G.; Dhar-Chowdhury, P.; Srivastava, S.; Pountney, D. J.; Yoshida, H.; Artman, M.; Fishman, G. I.; Yu, C.; Iyer, R.; Morley, G. E.; Gutstein, D. E.; Coetzee, W. A. Consequences of Cardiac Myocyte-Specific Ablation of KATP Channels in Transgenic Mice Expressing Dominant Negative Kir6 Subunits. *Am. J. Physiol. Heart Circ. Physiol.* **2006**, *291*, H543–51.
- (309) Isomoto, S.; Kondo, C.; Yamada, M.; Matsumoto, S.; Higashiguchi, O.; Horio, Y.; Matsuzawa, Y.; Kurachi, Y. A Novel Sulfonylurea Receptor Forms with BIR (Kir6.2) a Smooth Muscle Type ATP-Sensitive K<sup>+</sup> Channel. *J. Biol. Chem.* **1996**, *271*, 24321–24324.
- (310) Isomoto, S.; Kurachi, Y. Function, Regulation, Pharmacology, and Molecular Structure of ATP-Sensitive K<sup>+</sup> Channels in the Cardiovascular System. *J. Cardiovasc. Electrophysiol.* **1997**, *8*, 1431–1446.
- (311) Curley, M.; Cairns, M. T.; Friel, A. M.; McMeel, O. M.; Morrison, J. J.; Smith, T. J. Expression of mRNA Transcripts for ATP-Sensitive Potassium Channels in Human Myometrium. *Mol. Hum. Reprod.* **2002**, *8*, 941–945.
- (312) Sawada, K.; Morishige, K.; Hashimoto, K.; Tasaka, K.; Kurachi, H.; Murata, Y.; Kurachi, Y. Gestational Change of K<sup>+</sup> Channel Opener Effect Is Correlated with the Expression of Uterine KATP Channel Subunits. *Eur. J. Obstet. Gynecol. Reprod. Biol.* **2005**, *122*, 49–56.
- (313) Miki, T.; Liss, B.; Minami, K.; Shiuchi, T.; Saraya, A.; Kashima, Y.; Horiuchi, M.; Ashcroft, F.; Minokoshi, Y.; Roeper, J.; Seino, S. ATP-Sensitive K<sup>+</sup> Channels in the Hypothalamus Are Essential for the Maintenance of Glucose Homeostasis. *Nat. Neurosci.* **2001**, *4*, 507–512.
- (314) Yamada, K.; Ji, J. J.; Yuan, H.; Miki, T.; Sato, S.; Horimoto, N.; Shimizu, T.; Seino, S.; Inagaki, N. Protective Role of ATP-Sensitive Potassium Channels in Hypoxia-Induced Generalized Seizure. *Science* **2001**, *292*, 1543–1546.
- (315) Ballanyi, K. Protective Role of Neuronal KATP Channels in Brain Hypoxia. *J. Exp. Biol.* **2004**, *207*, 3201–3212.
- (316) Yamada, K.; Inagaki, N. Neuroprotection by KATP Channels. *J. Mol. Cell. Cardiol.* **2005**, *38*, 945–949.
- (317) Ho, K.; Nichols, C. G.; Lederer, W. J.; Lytton, J.; Vassilev, P. M.; Kanazirska, M. V.; Hebert, S. C. Cloning and Expression of an Inwardly Rectifying ATP-Regulated Potassium Channel. *Nature* **1993**, *362*, 31–38.
- (318) Giebisch, G.; Wang, W. Potassium Transport: From Clearance to Channels and Pumps. *Kidney Int.* **1996**, *49*, 1624–1631.
- (319) Simon, D. B.; Karet, F. E.; Rodriguez-Soriano, J.; Hamdan, J. H.; DiPietro, A.; Trachtman, H.; Sanjad, S. A.; Lifton, R. P. Genetic Heterogeneity of Bartter’s Syndrome Revealed by Mutations in the K<sup>+</sup> Channel, ROMK. *Nat. Genet.* **1996**, *14*, 152–156.

- (320) Károlyi, G. L.; Konrad, M.; Köckerling, A.; Ziegler, A.; Zimmermann, D. K.; Roth, B.; Wieg, C.; Grzeschik, K.; Koch, M. C.; Seyberth, H. W.; Vargas, G. R.; Forestier, L.; Jean, G.; Deschaux, M.; Rizzoni, G. F.; Niaudet, P.; Antignac, C.; Feldmann, G. D.; Lorrison, F.; Cougoureux, E.; Laroze, F.; Alessandri, J.; David, L. Mutations in the Gene Encoding the Inwardly-Rectifying Renal Potassium Channel, ROMK, Cause the Antenatal Variant of Bartter Syndrome: Evidence for Genetic Heterogeneity. *Hum. Mol. Genet.* **1997**, *6*, 17–26.
- (321) Károlyi, L.; Koch, M. C.; Grzeschik, K. H.; Seyberth, H. W. The Molecular Genetic Approach to “Bartter’s Syndrome”. *J. Mol. Med.* **1998**, *76*, 317–325.
- (322) Feldmann, D.; Alessandri, J. L.; Deschênes, G. Large Deletion of the 5’ End of the ROMK1 Gene Causes Antenatal Bartter Syndrome. *J. Am. Soc. Nephrol.* **1998**, *9*, 2357–2359.
- (323) Vollmer, M.; Koehrer, M.; Topaloglu, R.; Strahm, B.; Omran, H.; Hildebrandt, F. Two Novel Mutations of the Gene for Kir 1.1 (ROMK) in Neonatal Bartter Syndrome. *Pediatr. Nephrol.* **1998**, *12*, 69–71.
- (324) Asteria, C. Molecular Basis of Bartter’s Syndrome: New Insights into the Correlation between Genotype and Phenotype. *Eur. J. Endocrinol.* **1997**, *137*, 613–615.
- (325) Rodríguez-Soriano, J. Bartter and Related Syndromes: The Puzzle Is Almost Solved. *Pediatr. Nephrol.* **1998**, *12*, 315–327.
- (326) Lorenz, J. N.; Baird, N. R.; Judd, L. M.; Noonan, W. T.; Andringa, A.; Doetschman, T.; Manning, P. A.; Liu, L. H.; Miller, M. L.; Shull, G. E. Impaired Renal NaCl Absorption in Mice Lacking the ROMK Potassium Channel, a Model for Type II Bartter’s Syndrome. *J. Biol. Chem.* **2002**, *277*, 37871–37880.
- (327) Lu, M.; Wang, T.; Yan, Q.; Yang, X.; Dong, K.; Knepper, M. A.; Wang, W.; Giebisch, G.; Shull, G. E.; Hebert, S. C. Absence of Small Conductance K<sup>+</sup> Channel (SK) Activity in Apical Membranes of Thick Ascending Limb and Cortical Collecting Duct in ROMK (Bartter’s) Knockout Mice. *J. Biol. Chem.* **2002**, *277*, 37881–37887.
- (328) Bailey, M. A.; Cantone, A.; Yan, Q.; MacGregor, G. G.; Leng, Q.; Amorim, J. B. O.; Wang, T.; Hebert, S. C.; Giebisch, G.; Malnic, G. Maxi-K Channels Contribute to Urinary Potassium Excretion in the ROMK-Deficient Mouse Model of Type II Bartter’s Syndrome and in Adaptation to a High-K Diet. *Kidney Int.* **2006**, *70*, 51–59.
- (329) Tanemoto, M.; Kittaka, N.; Inanobe, A.; Kurachi, Y. In Vivo Formation of a Proton-Sensitive K<sup>+</sup> Channel by Heteromeric Subunit Assembly of Kir5.1 with Kir4.1. *J. Physiol.* **2000**, *525 Pt 3*, 587–592.
- (330) Tucker, S. J.; Imbrici, P.; Salvatore, L.; D’Adamo, M. C.; Pessia, M. pH Dependence of the Inwardly Rectifying Potassium Channel, Kir5.1, and Localization in Renal Tubular Epithelia. *J. Biol. Chem.* **2000**, *275*, 16404–16407.
- (331) Lourdel, S.; Paulais, M.; Cluzeaud, F.; Bens, M.; Tanemoto, M.; Kurachi, Y.; Vandewalle, A.; Teulon, J. An Inward Rectifier K(+) Channel at the Basolateral Membrane of the Mouse Distal Convoluted Tubule: Similarities with Kir4-Kir5.1 Heteromeric Channels. *J. Physiol.* **2002**, *538*, 391–404.
- (332) Fujita, A.; Horio, Y.; Higashi, K.; Mouri, T.; Hata, F.; Takeguchi, N.; Kurachi, Y. Specific Localization of an Inwardly Rectifying K(+) Channel, Kir4.1, at the Apical Membrane of Rat Gastric Parietal Cells; Its Possible Involvement in K(+) Recycling for the H(+)-K(+)-Pump. *J. Physiol.* **2002**, *540*, 85–92.
- (333) Kaufhold, M.-A.; Krabbenhöft, A.; Song, P.; Engelhardt, R.; Riederer, B.; Fährmann, M.; Klöcker, N.; Beil, W.; Manns, M.; Hagen, S. J.; Seidler, U. Localization, Trafficking, and

Significance for Acid Secretion of Parietal Cell Kir4.1 and KCNQ1 K<sup>+</sup> Channels. *Gastroenterology* **2008**, 134, 1058–1069.

- (334) Von Bekesy, G. DC Potentials and Energy Balance of the Cochlear Partition. *J. Acoust. Soc. Am.* **1951**, 23, 576.
- (335) Von Bekesy, G. Resting Potentials inside the Cochlear Partition of the Guinea Pig. *Nature* **1952**, 169, 241–242.
- (336) Hibino, H.; Kurachi, Y. Molecular and Physiological Bases of the K<sup>+</sup> Circulation in the Mammalian Inner Ear. *Physiology* **2006**, 21, 336–345.
- (337) Marcus, D. C.; Wu, T.; Wangemann, P.; Kofuji, P. KCNJ10 (Kir4.1) Potassium Channel Knockout Abolishes Endocochlear Potential. *Am. J. Physiol. Cell Physiol.* **2002**, 282, C403–7.
- (338) Wangemann, P.; Itza, E. M.; Albrecht, B.; Wu, T.; Jabba, S. V.; Maganti, R. J.; Lee, J. H.; Everett, L. A.; Wall, S. M.; Royaux, I. E.; Green, E. D.; Marcus, D. C. Loss of KCNJ10 Protein Expression Abolishes Endocochlear Potential and Causes Deafness in Pendred Syndrome Mouse Model. *BMC Med.* **2004**, 2, 30.
- (339) Newman, E. A. Regional Specialization of Retinal Glial Cell Membrane. *Nature* **2009**, 309, 155–157.
- (340) Bordey, A.; Sontheimer, H. Properties of Human Glial Cells Associated with Epileptic Seizure Foci. *Epilepsy Res.* **1998**, 32, 286–303.
- (341) Hinterkeuser, S.; Schröder, W.; Hager, G.; Seifert, G.; Blümcke, I.; Elger, C. E.; Schramm, J.; Steinhäuser, C. Astrocytes in the Hippocampus of Patients with Temporal Lobe Epilepsy Display Changes in Potassium Conductances. *Eur. J. Neurosci.* **2000**, 12, 2087–2096.
- (342) Gabriel, S.; Kivi, A.; Kovacs, R.; Lehmann, T. N.; Lanksch, W. R.; Meencke, H. J.; Heinemann, U. Effects of Barium on Stimulus-Induced Changes in [K<sup>+</sup>]<sub>o</sub> and Field Potentials in Dentate Gyrus and Area CA1 of Human Epileptic Hippocampus. *Neurosci. Lett.* **1998**, 249, 91–94.
- (343) Jauch, R.; Windmüller, O.; Lehmann, T.; Heinemann, U.; Gabriel, S. Effects of Barium, Furosemide, Ouabaine and 4,4'-Diisothiocyanatostilbene-2,2'-Disulfonic Acid (DIDS) on Ionophoretically-Induced Changes in Extracellular Potassium Concentration in Hippocampal Slices from Rats and from Patients with Epilepsy. *Brain Res.* **2002**, 925, 18–27.
- (344) Bockenhauer, D.; Feather, S.; Stanescu, H. C.; Bandulik, S.; Zdebik, A. A.; Reichold, M.; Tobin, J.; Lieberer, E.; Sterner, C.; Landouere, G.; Arora, R.; Sirimanna, T.; Thompson, D.; Cross, J. H.; van't Hoff, W.; Al Masri, O.; Tullus, K.; Yeung, S.; Anikster, Y.; Klootwijk, E.; Hubank, M.; Dillon, M. J.; Heitzmann, D.; Arcos-Burgos, M.; Knepper, M. A.; Dobbie, A.; Gahl, W. A.; Warth, R.; Sheridan, E.; Kleta, R. Epilepsy, Ataxia, Sensorineural Deafness, Tubulopathy, and KCNJ10 Mutations. *N. Engl. J. Med.* **2009**, 360, 1960–1970.
- (345) Scholl, U. I.; Choi, M.; Liu, T.; Ramaekers, V. T.; Häusler, M. G.; Grimmer, J.; Tobe, S. W.; Farhi, A.; Nelson-Williams, C.; Lifton, R. P. Seizures, Sensorineural Deafness, Ataxia, Mental Retardation, and Electrolyte Imbalance (SeSAME Syndrome) Caused by Mutations in KCNJ10. *Proc. Natl. Acad. Sci. U. S. A.* **2009**, 106, 5842–5847.
- (346) Nakamura, N.; Suzuki, Y.; Sakuta, H.; Ookata, K.; Kawahara, K.; Hirose, S. Inwardly Rectifying K<sup>+</sup> Channel Kir7.1 Is Highly Expressed in Thyroid Follicular Cells, Intestinal Epithelial Cells and Choroid Plexus Epithelial Cells: Implication for a Functional Coupling with Na<sup>+</sup>,K<sup>+</sup>-ATPase. *Biochem. J.* **1999**, 342, 329–336.

- (347) Kusaka, S.; Inanobe, A.; Fujita, A.; Makino, Y.; Tanemoto, M.; Matsushita, K.; Tano, Y.; Kurachi, Y. Functional Kir7.1 Channels Localized at the Root of Apical Processes in Rat Retinal Pigment Epithelium. *J. Physiol.* **2001**, *531*, 27–36.
- (348) Shimura, M.; Yuan, Y.; Chang, J. T.; Zhang, S.; Campochiaro, P. A.; Zack, D. J.; Hughes, B. A. Expression and Permeation Properties of the K(+) Channel Kir7.1 in the Retinal Pigment Epithelium. *J. Physiol.* **2001**, *531*, 329–346.
- (349) Ookata, K.; Tojo, A.; Suzuki, Y.; Nakamura, N.; Kimura, K.; Wilcox, C. S.; Hirose, S. Localization of Inward Rectifier Potassium Channel Kir7.1 in the Basolateral Membrane of Distal Nephron and Collecting Duct. *J. Am. Soc. Nephrol.* **2000**, *11*, 1987–1994.
- (350) Derst, C.; Hirsch, J. R.; Preisig-Müller, R.; Wischmeyer, E.; Karschin, A.; Döring, F.; Thomzig, A.; Veh, R. W.; Schlatter, E.; Kummer, W.; Daut, J. Cellular Localization of the Potassium Channel Kir7.1 in Guinea Pig and Human Kidney. *Kidney Int.* **2001**, *59*, 2197–2205.
- (351) Lee, M. M.; Ritter, R.; Hirose, T.; Vu, C. D.; Edwards, A. O. Snowflake Vitreoretinal Degeneration: Follow-up of the Original Family. *Ophthalmology* **2003**, *110*, 2418–2426.
- (352) Bendahhou, S.; Donaldson, M. R.; Plaster, N. M.; Tristani-Firouzi, M.; Fu, Y.; Ptáček, L. J. Defective Potassium Channel Kir2.1 Trafficking Underlies Andersen-Tawil Syndrome. *J. Biol. Chem.* **2003**, *278*, 51779–51785.
- (353) Decher, N.; Renigunta, V.; Zuzarte, M.; Soom, M.; Heinemann, S. H.; Timothy, K. W.; Keating, M. T.; Daut, J.; Sanguinetti, M. C.; Splawski, I. Impaired Interaction between the Slide Helix and the C-Terminus of Kir2.1: A Novel Mechanism of Andersen Syndrome. *Cardiovasc. Res.* **2007**, *75*, 748–757.
- (354) Tani, Y.; Miura, D.; Kurokawa, J.; Nakamura, K.; Ouchida, M.; Shimizu, K.; Ohe, T.; Furukawa, T. T75M-KCNJ2 Mutation Causing Andersen-Tawil Syndrome Enhances Inward Rectification by Changing Mg<sup>2+</sup> Sensitivity. *J. Mol. Cell. Cardiol.* **2007**, *43*, 187–196.
- (355) Jin, T.; Peng, L.; Mirshahi, T.; Rohacs, T.; Chan, K. W.; Sanchez, R.; Logothetis, D. E. The (beta)gamma Subunits of G Proteins Gate a K(+) Channel by Pivoted Bending of a Transmembrane Segment. *Mol. Cell* **2002**, *10*, 469–481.
- (356) Sadjia, R.; Smadja, K.; Alagem, N.; Reuveny, E. Coupling Gbetagamma-Dependent Activation to Channel Opening via Pore Elements in Inwardly Rectifying Potassium Channels. *Neuron* **2001**, *29*, 669–680.
- (357) Claydon, T. W.; Makary, S. Y.; Dibb, K. M.; Boyett, M. R. The Selectivity Filter May Act as the Agonist-Activated Gate in the G Protein-Activated Kir3.1/Kir3.4 K<sup>+</sup> Channel. *J. Biol. Chem.* **2003**, *278*, 50654–50663.
- (358) Nishida, M.; MacKinnon, R. Structural Basis of Inward Rectification: Cytoplasmic Pore of the G Protein-Gated Inward Rectifier GIRK1 at 1.8 Å Resolution. *Cell* **2002**, *111*, 957–965.
- (359) Pegan, S.; Arrabit, C.; Zhou, W.; Kwiatkowski, W.; Collins, A.; Slesinger, P. A.; Choe, S. Cytoplasmic Domain Structures of Kir2.1 and Kir3.1 Show Sites for Modulating Gating and Rectification. *Nat. Neurosci.* **2005**, *8*, 279–287.
- (360) Inanobe, A.; Matsuura, T.; Nakagawa, A.; Kurachi, Y. Structural Diversity in the Cytoplasmic Region of G Protein-Gated Inward Rectifier K<sup>+</sup> Channels. *Channels (Austin)*. **2007**, *1*, 39–45.
- (361) Nishida, M.; Cadene, M.; Chait, B. T.; MacKinnon, R. Crystal Structure of a Kir3.1-Prokaryotic Kir Channel Chimera. *EMBO J.* **2007**, *26*, 4005–4015.

- (362) Tristani-Firouzi, M.; Jensen, J. L.; Donaldson, M. R.; Sansone, V.; Meola, G.; Hahn, A.; Bendahhou, S.; Kwiecinski, H.; Fidzianska, A.; Plaster, N.; Fu, Y.; Ptacek, L. J.; Tawil, R. Functional and Clinical Characterization of KCNJ2 Mutations Associated with LQT7 (Andersen Syndrome). *J. Clin. Invest.* **2002**, *110*, 381–388.
- (363) Donaldson, M. R.; Jensen, J. L.; Tristani-Firouzi, M.; Tawil, R.; Bendahhou, S.; Suarez, W. A.; Cobo, A. M.; Poza, J. J.; Behr, E.; Wagstaff, J.; Szepletowski, P.; Pereira, S.; Mozaffar, T.; Escolar, D. M.; Fu, Y.-H.; Ptácek, L. J. PIP2 Binding Residues of Kir2.1 Are Common Targets of Mutations Causing Andersen Syndrome. *Neurology* **2003**, *60*, 1811–1816.
- (364) Antcliff, J. F.; Haider, S.; Proks, P.; Sansom, M. S. P.; Ashcroft, F. M. Functional Analysis of a Structural Model of the ATP-Binding Site of the KATP Channel Kir6.2 Subunit. *EMBO J.* **2005**, *24*, 229–239.
- (365) Kuo, A.; Gulbis, J. M.; Antcliff, J. F.; Rahman, T.; Lowe, E. D.; Zimmer, J.; Cuthbertson, J.; Ashcroft, F. M.; Ezaki, T.; Doyle, D. A. Crystal Structure of the Potassium Channel KirBac1.1 in the Closed State. *Science* **2003**, *300*, 1922–1926.
- (366) Tao, X.; Avalos, J. L.; Chen, J.; MacKinnon, R. Crystal Structure of the Eukaryotic Strong Inward-Rectifier K<sup>+</sup> Channel Kir2.2 at 3.1 Å Resolution. *Science* **2009**, *326*, 1668–1674.
- (367) Clarke, O. B.; Caputo, A. T.; Hill, A. P.; Vandenberg, J. I.; Smith, B. J.; Gulbis, J. M. Domain Reorientation and Rotation of an Intracellular Assembly Regulate Conduction in Kir Potassium Channels. *Cell* **2010**, *141*, 1018–1029.
- (368) Hansen, S. B.; Tao, X.; MacKinnon, R. Structural Basis of PIP2 Activation of the Classical Inward Rectifier K<sup>+</sup> Channel Kir2.2. *Nature* **2011**, *477*, 495–498.
- (369) Whorton, M. R.; MacKinnon, R. Crystal Structure of the Mammalian GIRK2 K<sup>+</sup> Channel and Gating Regulation by G Proteins, PIP2, and Sodium. *Cell* **2011**, *147*, 199–208.
- (370) Whorton, M. R.; MacKinnon, R. X-Ray Structure of the Mammalian GIRK2-By G-Protein Complex. *Nature* **2013**, *498*, 190–197.
- (371) Zubcevic, L.; Bavro, V. N.; Muniz, J. R. C.; Schmidt, M. R.; Wang, S.; De Zorzi, R.; Venien-Bryan, C.; Sansom, M. S. P.; Nichols, C. G.; Tucker, S. J. Control of KirBac3.1 Potassium Channel Gating at the Interface between Cytoplasmic Domains. *J. Biol. Chem.* **2014**, *289*, 143–151.
- (372) Fan, Z.; Makielski, J. C. Anionic Phospholipids Activate ATP-Sensitive Potassium Channels. *J. Biol. Chem.* **1997**, *272*, 5388–5395.
- (373) Huang, C. L.; Feng, S.; Hilgemann, D. W. Direct Activation of Inward Rectifier Potassium Channels by PIP2 and Its Stabilization by Gbetagamma. *Nature* **1998**, *391*, 803–806.
- (374) Shyng, S. L.; Nichols, C. G. Membrane Phospholipid Control of Nucleotide Sensitivity of KATP Channels. *Science* **1998**, *282*, 1138–1141.
- (375) Zhang, H.; He, C.; Yan, X.; Mirshahi, T.; Logothetis, D. E. Activation of Inwardly Rectifying K<sup>+</sup> Channels by Distinct PtdIns(4,5)P2 Interactions. *Nat. Cell Biol.* **1999**, *1*, 183–188.
- (376) Cukras, C. A.; Jeliaskova, I.; Nichols, C. G. Structural and Functional Determinants of Conserved Lipid Interaction Domains of Inward Rectifying Kir6.2 Channels. *J. Gen. Physiol.* **2002**, *119*, 581–591.
- (377) Lopes, C. M. B.; Zhang, H.; Rohacs, T.; Jin, T.; Yang, J.; Logothetis, D. E. Alterations in Conserved Kir Channel-PIP2 Interactions Underlie Channelopathies. *Neuron* **2002**, *34*, 933–944.

- (378) Haider, S.; Tarasov, A. I.; Craig, T. J.; Sansom, M. S. P.; Ashcroft, F. M. Identification of the PIP<sub>2</sub>-Binding Site on Kir6.2 by Molecular Modelling and Functional Analysis. *EMBO J.* **2007**, *26*, 3749–3759.
- (379) Suh, B.; Hille, B. PIP<sub>2</sub> Is a Necessary Cofactor for Ion Channel Function: How and Why? *Annu. Rev. Biophys.* **2008**, *37*, 175–195.
- (380) Logothetis, D. E.; Petrou, V. I.; Adney, S. K.; Mahajan, R. Channelopathies Linked to Plasma Membrane Phosphoinositides. *Pflugers Arch.* **2010**, *460*, 321–341.
- (381) D'Avanzo, N.; Cheng, W. W. L.; Wang, S.; Enkvetchakul, D.; Nichols, C. G. Lipids Driving Protein Structure? Evolutionary Adaptations in Kir Channels. *Channels* **2010**, *4*, 139–141.
- (382) Stansfeld, P. J.; Hopkinson, R.; Ashcroft, F. M.; Sansom, M. S. P. PIP<sub>2</sub>-Binding Site in Kir Channels: Definition by Multiscale Biomolecular Simulations. *Biochemistry* **2009**, *48*, 10926–10933.
- (383) Cheng, W. W. L.; D'Avanzo, N.; Doyle, D. A.; Nichols, C. G. Dual-Mode Phospholipid Regulation of Human Inward Rectifying Potassium Channels. *Biophys. J.* **2011**, *100*, 620–628.
- (384) Lee, S.-J.; Wang, S.; Borschel, W.; Heyman, S.; Gyore, J.; Nichols, C. G. Secondary Anionic Phospholipid Binding Site and Gating Mechanism in Kir2.1 Inward Rectifier Channels. *Nat. Commun.* **2013**, *4*, 2786.
- (385) Epshtein, Y.; Chopra, A. P.; Rosenhouse-Dantsker, A.; Kowalsky, G. B.; Logothetis, D. E.; Levitan, I. Identification of a C-Terminus Domain Critical for the Sensitivity of Kir2.1 to Cholesterol. *Proc. Natl. Acad. Sci. U. S. A.* **2009**, *106*, 8055–8060.
- (386) Levitan, I.; Fang, Y.; Rosenhouse-Dantsker, A.; Romanenko, V. Cholesterol and Ion Channels. *Subcell. Biochem.* **2010**, *51*, 509–549.
- (387) D'Avanzo, N.; Hyrc, K.; Enkvetchakul, D.; Covey, D. F.; Nichols, C. G. Enantioselective Protein-Sterol Interactions Mediate Regulation of Both Prokaryotic and Eukaryotic Inward Rectifier K<sup>+</sup> Channels by Cholesterol. *PLoS One* **2011**, *6*, e19393.
- (388) Matsuda, H.; Saigusa, A.; Irisawa, H. Ohmic Conductance through the Inwardly Rectifying K Channel and Blocking by Internal Mg<sup>2+</sup>. *Nature* **1987**, *325*, 156–159.
- (389) Lopatin, A. N.; Makhina, E. N.; Nichols, C. G. Potassium Channel Block by Cytoplasmic Polyamines as the Mechanism of Intrinsic Rectification. *Nature* **1994**, *372*, 366–369.
- (390) Lu, Z. Mechanism of Rectification in Inward-Rectifier K<sup>+</sup> Channels. *Annu. Rev. Physiol.* **2004**, *66*, 103–129.
- (391) Lu, Z.; MacKinnon, R. Electrostatic Tuning of Mg<sup>2+</sup> Affinity in an Inward-Rectifier K<sup>+</sup> Channel. *Nature* **1994**, *371*, 243–246.
- (392) Stanfield, P. R.; Davies, N. W.; Shelton, P. A.; Sutcliffe, M. J.; Khan, I. A.; Brammar, W. J.; Conley, E. C. A Single Aspartate Residue Is Involved in Both Intrinsic Gating and Blockage by Mg<sup>2+</sup> of the Inward Rectifier, IRK1. *J. Physiol.* **1994**, *478*, 1–6.
- (393) Wible, B. A.; Tagliatela, M.; Ficker, E.; Brown, A. M. Gating of Inwardly Rectifying K<sup>+</sup> Channels Localized to a Single Negatively Charged Residue. *Nature* **1994**, *371*, 246–249.
- (394) Ficker, E.; Tagliatela, M.; Wible, B. A.; Henley, C. M.; Brown, A. M. Spermine and Spermidine as Gating Molecules for Inward Rectifier K<sup>+</sup> Channels. *Science* **1994**, *266*, 1068–1072.

- (395) Fujiwara, Y.; Kubo, Y. Ser165 in the Second Transmembrane Region of the Kir2.1 Channel Determines Its Susceptibility to Blockade by Intracellular Mg<sup>2+</sup>. *J. Gen. Physiol.* **2002**, *120*, 677–693.
- (396) Taglialatela, M.; Ficker, E.; Wible, B. A.; Brown, A. M. C-Terminus Determinants for Mg<sup>2+</sup> and Polyamine Block of the Inward Rectifier K<sup>+</sup> Channel IRK1. *EMBO J.* **1995**, *14*, 5532–5541.
- (397) Yang, J.; Jan, Y. N.; Jan, L. Y. Control of Rectification and Permeation by Residues in Two Distinct Domains in an Inward Rectifier K<sup>+</sup> Channel. *Neuron* **1995**, *14*, 1047–1054.
- (398) Kubo, Y.; Murata, Y. Control of Rectification and Permeation by Two Distinct Sites after the Second Transmembrane Region in Kir2.1 K<sup>+</sup> Channel. *J. Physiol.* **2001**, *531*, 645–660.
- (399) Takanari, H.; Nalos, L.; Stary-Weinzinger, A.; de Git, K. C. G.; Varkevisser, R.; Linder, T.; Houtman, M. J. C.; Peschar, M.; de Boer, T. P.; Tidwell, R. R.; Rook, M. B.; Vos, M. A.; van der Heyden, M. A. G. Efficient and Specific Cardiac IK1 Inhibition by a New Pentamidine Analogue. *Cardiovasc. Res.* **2013**, *99*, 203–214.
- (400) Cheng, W. W. L.; Enkvetchakul, D.; Nichols, C. G. KirBac1.1: It's an Inward Rectifying Potassium Channel. *J. Gen. Physiol.* **2009**, *133*, 295–305.
- (401) Larkin, M. A.; Blackshields, G.; Brown, N. P.; Chenna, R.; McGettigan, P. A.; McWilliam, H.; Valentin, F.; Wallace, I. M.; Wilm, A.; Lopez, R.; Thompson, J. D.; Gibson, T. J.; Higgins, D. G. Clustal W and Clustal X Version 2.0. *Bioinformatics* **2007**, *23*, 2947–2948.
- (402) Enkvetchakul, D.; Jeliaskova, I.; Nichols, C. G. Direct Modulation of Kir Channel Gating by Membrane Phosphatidylinositol 4,5-Bisphosphate. *J. Biol. Chem.* **2005**, *280*, 35785–35788.
- (403) Robertson, J. L.; Palmer, L. G.; Roux, B. Long-Pore Electrostatics in Inward-Rectifier Potassium Channels. *J. Gen. Physiol.* **2008**, *132*, 613–632.
- (404) Zhou, W.; Jan, L. A Twist on Potassium Channel Gating. *Cell* **2010**, *141*, 920–922.
- (405) The Nobel Prize in Chemistry 2013 [http://www.nobelprize.org/nobel\\_prizes/chemistry/laureates/2013/](http://www.nobelprize.org/nobel_prizes/chemistry/laureates/2013/) (accessed Jun 15, 2014).
- (406) Karplus, M.; McCammon, J. A. Molecular Dynamics Simulations of Biomolecules. *Nat. Struct. Biol.* **2002**, *9*, 646–652.
- (407) Van Gunsteren, W. F.; Bakowies, D.; Baron, R.; Chandrasekhar, I.; Christen, M.; Daura, X.; Gee, P.; Geerke, D. P.; Glättli, A.; Hünenberger, P. H.; Kastenholz, M. A.; Oostenbrink, C.; Schenk, M.; Trzesniak, D.; van der Vegt, N. F. A.; Yu, H. B. Biomolecular Modeling: Goals, Problems, Perspectives. *Angew. Chem. Int. Ed. Engl.* **2006**, *45*, 4064–4092.
- (408) Scheraga, H. A.; Khalili, M.; Liwo, A. Protein-Folding Dynamics: Overview of Molecular Simulation Techniques. *Annu. Rev. Phys. Chem.* **2007**, *58*, 57–83.
- (409) Dror, R. O.; Dirks, R. M.; Grossman, J. P.; Xu, H.; Shaw, D. E. Biomolecular Simulation: A Computational Microscope for Molecular Biology. *Annu. Rev. Biophys.* **2012**, *41*, 429–452.
- (410) Cornell, W. D.; Cieplak, P.; Bayly, C. I.; Gould, I. R.; Merz, K. M.; Ferguson, D. M.; Spellmeyer, D. C.; Fox, T.; Caldwell, J. W.; Kollman, P. a. A Second Generation Force Field for the Simulation of Proteins, Nucleic Acids, and Organic Molecules. *J. Am. Chem. Soc.* **1995**, *117*, 5179–5197.
- (411) Hornak, V.; Abel, R.; Okur, A.; Strockbine, B.; Roitberg, A.; Simmerling, C. Comparison of Multiple Amber Force Fields and Development of Improved Protein Backbone Parameters. *Proteins* **2006**, *65*, 712–725.

- (412) Hess, B.; Bekker, H.; Berendsen, H. J. C.; Fraaije, J. G. E. M. LINCS: A Linear Constraint Solver for Molecular Simulations. *J. Comput. Chem.* **1997**, *18*, 1463–1472.
- (413) Darden, T.; York, D.; Pedersen, L. Particle Mesh Ewald: An  $N \log(N)$  Method for Ewald Sums in Large Systems. *J. Chem. Phys.* **1993**, *98*, 10089.
- (414) Feenstra, K. A.; Hess, B.; Berendsen, H. J. C. Improving Efficiency of Large Time-Scale Molecular Dynamics Simulations of Hydrogen-Rich Systems. *J. Comput. Chem.* **1999**, *20*, 786–798.
- (415) Berendsen, H. J. C.; Postma, J. P. M.; van Gunsteren, W. F.; DiNola, A.; Haak, J. R. Molecular Dynamics with Coupling to an External Bath. *J. Chem. Phys.* **1984**, *81*, 3684.
- (416) Bussi, G.; Donadio, D.; Parrinello, M. Canonical Sampling through Velocity Rescaling. *J. Chem. Phys.* **2007**, *126*, 014101.
- (417) Nosé, S. A Unified Formulation of the Constant Temperature Molecular Dynamics Methods. *J. Chem. Phys.* **1984**, *81*, 511.
- (418) Hoover, W. Canonical Dynamics: Equilibrium Phase-Space Distributions. *Phys. Rev. A* **1985**, *31*, 1695–1697.
- (419) Parrinello, M.; Rahman, A. Polymorphic Transitions in Single Crystals: A New Molecular Dynamics Method. *J. Appl. Phys.* **1981**, *52*, 7182.
- (420) Amadei, A.; Linssen, A. B.; Berendsen, H. J. Essential Dynamics of Proteins. *Proteins* **1993**, *17*, 412–425.
- (421) Grubmüller, H. Predicting Slow Structural Transitions in Macromolecular Systems: Conformational Flooding. *Phys. Rev. E. Stat. Phys. Plasmas. Fluids. Relat. Interdiscip. Topics* **1995**, *52*, 2893–2906.
- (422) Amadei, A.; Linssen, A. B.; de Groot, B. L.; van Aalten, D. M.; Berendsen, H. J. An Efficient Method for Sampling the Essential Subspace of Proteins. *J. Biomol. Struct. Dyn.* **1996**, *13*, 615–625.
- (423) De Groot, B. L.; Amadei, A.; van Aalten, D. M.; Berendsen, H. J. Toward an Exhaustive Sampling of the Configurational Spaces of the Two Forms of the Peptide Hormone Guanylin. *J. Biomol. Struct. Dyn.* **1996**, *13*, 741–751.
- (424) De Groot, B. L.; Amadei, A.; Scheek, R. M.; van Nuland, N. A.; Berendsen, H. J. An Extended Sampling of the Configurational Space of HPr from *E. Coli*. *Proteins* **1996**, *26*, 314–322.
- (425) Lange, O. F.; Schäfer, L. V.; Grubmüller, H. Flooding in GROMACS: Accelerated Barrier Crossings in Molecular Dynamics. *J. Comput. Chem.* **2006**, *27*, 1693–1702.
- (426) Hayward, S.; de Groot, B. L. Normal Modes and Essential Dynamics. *Methods Mol. Biol.* **2008**, *443*, 89–106.
- (427) Torrie, G. M.; Valleau, J. P. Nonphysical Sampling Distributions in Monte Carlo Free-Energy Estimation: Umbrella Sampling. *J. Comput. Phys.* **1977**, *23*, 187–199.
- (428) Frenkel, D.; Smit, B. Free Energy Calculations. In *Understanding Molecular Simulation (Second Edition): From Algorithms to Applications*; Elsevier Inc, 2002; p. 167.
- (429) Kumar, S.; Rosenberg, J. M.; Bouzida, D.; Swendsen, R. H.; Kollman, P. A. The Weighted Histogram Analysis Method for Free-Energy Calculations on Biomolecules. I. The Method. *J. Comput. Chem.* **1992**, *13*, 1011–1021.

- (430) Souaille, M.; Roux, B. Extension to the Weighted Histogram Analysis Method: Combining Umbrella Sampling with Free Energy Calculations. *Comput. Phys. Commun.* **2001**, *135*, 40–57.
- (431) Kästner, J. Umbrella Sampling. *Wiley Interdiscip. Rev. Comput. Mol. Sci.* **2011**, *1*, 932–942.
- (432) Hub, J. S.; de Groot, B. L.; van der Spoel, D. g\_wham—A Free Weighted Histogram Analysis Implementation Including Robust Error and Autocorrelation Estimates. *J. Chem. Theory Comput.* **2010**, *6*, 3713–3720.
- (433) Cole, K. S.; Moore, J. W. Ionic Current Measurements in the Squid Giant Axon Membrane. *J. Gen. Physiol.* **1960**, *44*, 123–167.
- (434) Bezanilla, F.; Vergara, J.; Taylor, R. E. Voltage Clamping of Excitable Membranes. *Methods Exp. Phys.* **1982**, *20*, 445–511.
- (435) Halliwell, J. V.; Plant, T. I. M. D.; Robbins, J. O. N.; Standen, N. B. Voltage Clamp Techniques. In *Microelectrode Techniques. The Plymouth Workshop Handbook (2nd ed.)*; edited by Ogden D. Cambridge, UK: The Company of Biologists Ltd., 1994; pp. 17–35.
- (436) Baumgartner, W.; Islas, L.; Sigworth, F. J. Two-Microelectrode Voltage Clamp of *Xenopus* Oocytes: Voltage Errors and Compensation for Local Current Flow. *Biophys. J.* **1999**, *77*, 1980–1991.
- (437) Cole, K. Dynamic Electrical Characteristics of the Squid Axon Membrane. *Arch. Sci. Physiol. (Paris)*. **1949**, *3*, 253–258.
- (438) Marmont, G. Studies on the Axon Membrane; a New Method. *J. Cell. Physiol.* **1949**, *34*, 351–382.
- (439) Huxley, A. From Overshoot to Voltage Clamp. *Trends Neurosci.* **2002**, *25*, 553–558.
- (440) The Nobel Prize in Physiology or Medicine 1963 [http://www.nobelprize.org/nobel\\_prizes/medicine/laureates/1963/](http://www.nobelprize.org/nobel_prizes/medicine/laureates/1963/) (accessed Jun 17, 2014).
- (441) Stühmer, W. Electrophysiological Recording from *Xenopus* Oocytes. *Methods Enzymol.* **1992**, *207*, 319–339.
- (442) White, S. H. Membrane proteins of known 3D structure [http://blanco.biomol.uci.edu/mpstruc/#id\\_TRANSMEMBRANE\\_PROTEINS\\_ALPHAHELICAL:C\\_hannels\\_Potassium\\_Sodium\\_Proton\\_IonSelective](http://blanco.biomol.uci.edu/mpstruc/#id_TRANSMEMBRANE_PROTEINS_ALPHAHELICAL:C_hannels_Potassium_Sodium_Proton_IonSelective) (accessed Jun 25, 2014).
- (443) Armstrong, C. M.; Hille, B. The Inner Quaternary Ammonium Ion Receptor in Potassium Channels of the Node of Ranvier. *J. Gen. Physiol.* **1972**, *59*, 388–400.
- (444) Paynter, J. J.; Andres-Enguix, I.; Fowler, P. W.; Tottey, S.; Cheng, W.; Enkvetchakul, D.; Bavro, V. N.; Kusakabe, Y.; Sansom, M. S. P.; Robinson, N. J.; Nichols, C. G.; Tucker, S. J. Functional Complementation and Genetic Deletion Studies of KirBac Channels: Activatory Mutations Highlight Gating-Sensitive Domains. *J. Biol. Chem.* **2010**, *285*, 40754–40761.
- (445) Di Veroli, G. Y.; Davies, M. R.; Zhang, H.; Abi-Gerges, N.; Boyett, M. R. hERG Inhibitors With Similar Potency But Different Binding Kinetics Do Not Pose the Same Proarrhythmic Risk: Implications for Drug Safety Assessment. *J. Cardiovasc. Electrophysiol.* **2013**, *25*, 197–207.
- (446) Uysal, S.; Cuello, L. G.; Cortes, D. M.; Koide, S.; Kossiakoff, A. A.; Perozo, E. Mechanism of Activation Gating in the Full-Length KcsA K<sup>+</sup> Channel. *Proc. Natl. Acad. Sci. U. S. A.* **2011**, *108*, 11896–11899.

- (447) Alam, A.; Jiang, Y. High-Resolution Structure of the Open NaK Channel. *Nat. Struct. Mol. Biol.* **2009**, *16*, 30–34.
- (448) Pan, A. C.; Cuello, L. G.; Perozo, E.; Roux, B. Thermodynamic Coupling between Activation and Inactivation Gating in Potassium Channels Revealed by Free Energy Molecular Dynamics Simulations. *J. Gen. Physiol.* **2011**, *138*, 571–580.
- (449) Cordero-Morales, J. F.; Jogini, V.; Chakrapani, S.; Perozo, E. A Multipoint Hydrogen-Bond Network Underlying KcsA C-Type Inactivation. *Biophys. J.* **2011**, *100*, 2387–2393.
- (450) Perry, M.; Sachse, F. B.; Sanguinetti, M. C. Structural Basis of Action for a Human Ether-a-Go-Go-Related Gene 1 Potassium Channel Activator. *Proc. Natl. Acad. Sci. U. S. A.* **2007**, *104*, 13827–13832.
- (451) Garg, V.; Stary-Weinzinger, A.; Sachse, F.; Sanguinetti, M. C. Molecular Determinants for Activation of Human Ether-Å-Go-Go-Related Gene 1 Potassium Channels by 3-Nitro-N-(4-Phenoxyphenyl) Benzamide. *Mol. Pharmacol.* **2011**, *80*, 630–637.
- (452) Enkvetchakul, D.; Jeliaskova, I.; Bhattacharyya, J.; Nichols, C. G. Control of Inward Rectifier K Channel Activity by Lipid Tethering of Cytoplasmic Domains. *J. Gen. Physiol.* **2007**, *130*, 329–334.
- (453) Fowler, P. W.; Sansom, M. S. P. The Pore of Voltage-Gated Potassium Ion Channels Is Strained When Closed. *Nat. Commun.* **2013**, *4*, 1872.
- (454) Faraldo-Gómez, J. D.; Kutluay, E.; Jogini, V.; Zhao, Y.; Heginbotham, L.; Roux, B. Mechanism of Intracellular Block of the KcsA K<sup>+</sup> Channel by Tetrabutylammonium: Insights from X-Ray Crystallography, Electrophysiology and Replica-Exchange Molecular Dynamics Simulations. *J. Mol. Biol.* **2007**, *365*, 649–662.
- (455) Yohannan, S.; Hu, Y.; Zhou, Y. Crystallographic Study of the Tetrabutylammonium Block to the KcsA K<sup>+</sup> Channel. *J. Mol. Biol.* **2007**, *366*, 806–814.
- (456) Luzhkov, V. B.; Österberg, F.; Acharya, P.; Chattopadhyaya, J.; Aqvist, J. Computational and NMR Study of Quaternary Ammonium Ion Conformations in Solution. *Phys. Chem. Chem. Phys.* **2002**, *4*, 4640–4647.
- (457) Faraldo-Gómez, J. D.; Roux, B. Characterization of Conformational Equilibria through Hamiltonian and Temperature Replica-Exchange Simulations: Assessing Entropic and Environmental Effects. *J. Comput. Chem.* **2007**, *28*, 1634–1647.
- (458) Kamiya, K.; Niwa, R.; Morishima, M.; Honjo, H.; Sanguinetti, M. C. Molecular Determinants of hERG Channel Block by Terfenadine and Cisapride. *J. Pharmacol. Sci.* **2008**, *108*, 301–307.

Ich habe mich bemüht, sämtliche Inhaber der Bildrechte ausfindig zu machen und ihre Zustimmung zur Verwendung der Bilder in dieser Arbeit eingeholt. Sollte dennoch eine Urheberrechtsverletzung bekannt werden, ersuche ich um Meldung bei mir.

## 7 Curriculum Vitae

### PERSONAL DATA

---

Name: Mag. pharm. Tobias Linder

Nationality: Austrian

Email: tobias.linder@univie.ac.at

### EDUCATION

---

02/2011 – 08/2014 **Doctoral studies Pharmacy**

Part of the Graduate Program MolTag

Part of the FWF-Project: “Dissociation of hERG channel inhibitors”

Molecular Modeling Laboratory, Department of Pharmacology and Toxicology, University of Vienna, Vienna, Austria

Supervisor: Dr. Anna Weinzinger

Co-Supervisor: Univ.-Prof. Dr. Gerhard Ecker

10/2004 – 11/2010 **Master studies Pharmacy**, Leopold-Franzens University, Innsbruck, Austria

Diploma thesis “Pharmacophore Modeling and Virtual Screening for Glucocorticoid Receptor Ligands: Unraveling Anti-Inflammatory or Endocrine Disrupting Effects of Chemicals”

Diploma advisors: Univ.-Prof. Dr. Helmut Schmidhammer

Dr. Daniela Schuster

11/1996 – 06/2004 **High school graduation** (with distinction)

Bundesrealgymnasium und Bundesoberstufenrealgymnasium, Dornbirn, Austria

## RESEARCH STAYS

---

- 11/2013 – 12/2013    **Michael C. Sanguinetti's laboratory** at the Cardiovascular Research and Training Institute, University of Utah, Salt Lake City, USA  
Research topic: Disulfide bond formation as a tool to investigate extent of hERG channel closure upon drug trapping
- 05/2012 – 06/2012    **Bert de Groot's laboratory** at the Max-Planck Institute for Biophysical Chemistry, Göttingen, Germany  
Research topic: Application of MD simulation methods for free energy calculations of ion channels

## HONORS

---

- 2013            EMBO short-term fellowship
- 2013            Research Fellowship of the University of Vienna
- 2011            Poster Award at the 15<sup>th</sup> International Congress Phytopharm, Nuremberg
- 2009            Merit fellowship of the University of Innsbruck

## CERTIFIED TRAININGS

---

- 02/2012    Excellence in Pharmacovigilance:  
Clinical Trials and Post-Marketing Training Course  
European Medicines Agency, London, UK

## TEACHING EXPERIENCE

---

- 2012            **Drug Interactions** (elective lecture, 0.5 ECTS)  
Interactive course of pharmacodynamic and pharmacokinetic drug interactions
- 2012            **Pharmacology, Pharmacotherapy and Toxicology** (seminar, 1 ECTS)  
Students learn to interpret clinical studies from renowned medical journals

## WORK EXPERIENCE

---

- 07/2010 – 01/2011    **Student scientific coworker**  
Application of pharmacophore-based searches for the identification of bioactive natural products  
Leopold-Franzens University, Innsbruck, Austria
- 2006 – 2009            **Internship (summers, 6 months in total)**  
Quality control of chemicals, reagents and intermediates for chemical and pharmaceutical industry  
Sigma-Aldrich Production GmbH, Buchs, Switzerland
- 08/2006 – 09/2006    **Internship**  
Production of original specialties  
Kreuzapotheke, Götzis, Austria

## PUBLICATIONS & POSTER

---

### Papers

- 8)      Structural insights into trapping and dissociation of small molecules in K<sup>+</sup> channels. Linder T, Saxena P, Timin E, Hering S, Stry-Weinzinger A. *Journal of Chemical Information and Modeling*. **2014** Under revision since 16 June, 2014
- 7)      Probing the energy landscape of activation gating of the bacterial potassium channel KcsA. Linder T, de Groot BL, Stry-Weinzinger A. *PLoS Computational Biology* **2013** May 9(5), e1003058
- 6)      Efficient and specific cardiac IK1 inhibition by a new pentamidine analogue. Takanari H, Nalos L, Stry-Weinzinger A, de Git KC, Varkevisser R, Linder T, Houtman MJ, Peschar M, de Boer TP, Tidwell RR, Rook MB, Vos MA, van der Heyden MAG. *Cardiovascular Research* **2013**, 99 (1), 203-214
- 5)      Structure-activity relationships of pentamidine-affected ion channel trafficking and dofetilide mediated rescue. Varkevisser R, Houtman MJ, Linder T, de Git KC, Beekman HD, Tidwell RR, Ijzerman AP, Stry-Weinzinger A, Vos MA, van der Heyden MAG. *British Journal of Pharmacology* **2013**, 169(6), 1322-1334
- 4)      Neutralization of a single voltage sensor affects gating determinants in all four pore forming S6 segments of CaV1.2: A cooperative gating model. Beyl S, Depil K, Hohaus A, Stry-Weinzinger A, Linder T, Timin E, Hering S. *Pflügers Archiv* **2012**, 464(4), 391-401

- 3) Catechol alkenyls from *Semecarpus anacardium*: acetylcholin esterase inhibition and binding mode predictions. Adhami HR, [Linder T](#), Kaehlig H, Schuster D, Zehl M, Krenn L. *Journal of Ethnopharmacology* **2012**, 139(1), 142-148
- 2) In silico Analysis of Conformational Changes Induced by Mutation of Aromatic Binding Residues: Consequences for Drug Binding in the hERG K<sup>+</sup> Channel. Knape K, [Linder T](#), Wolschann P, Beyer A, Stary-Weinzinger A. *PLoS One* **2011**, 6(12), e28778
- 1) Leoligin, the major lignan from Edelweiss, activates cholesteryl ester transfer protein. Duwensee K, Schwaiger S, Tancevski I, Eller K, van Eck M, Markt P, [Linder T](#), Stanzl U, Ritsch A, Patsch JR, Schuster D, Stuppner H, Bernhard D, Eller P. *Atherosclerosis* **2011**, 219(1), 109-115

## Posters

- 11) Insights into molecular basis of hERG inhibition by studying a library of dofetilide derivatives. Saxena P, [Linder T](#), Stary-Weinzinger A, Ijzerman AP, Timin E, Ecker GF, Hering S. 58th Annual Meeting of the Biophysical Society, February 15-19, **2014**, San Francisco, USA
- 10) F557L – a novel determinant of hERG channel inhibition: allosteric modulation or drug binding? Saxena P, [Linder T](#), Windisch A, Knape K, Timin E, Hering S, Stary-Weinzinger A. Joint Meeting of the Austrian Neuroscience Association (13th ANA Meeting) and the Austrian Pharmacological Society (19th Scientific Symposium of APHAR), September 16-19, **2013**, Vienna, Austria
- 9) Gating dynamics of ion channels and drug trapping investigated by MD simulations. [Linder T](#), Saxena P, Zangerl EM, Timin E, Hering S, Stary-Weinzinger A. Joint Meeting of the British and German Biophysical Society, March 21-23, **2013**, Hünfeld, Germany
- 8) Differences in activation gating of ion channels investigated by molecular dynamics simulations. Zangerl EM, [Linder T](#), Stary-Weinzinger A. Joint Meeting of the British and German Biophysical Society, March 21-23, **2013**, Hünfeld, Germany
- 7) Activation gating of KcsA: New insights into cooperativity and energy landscape from essential dynamics simulations. [Linder T](#), Stary-Weinzinger A. 57th Annual Meeting of the Biophysical Society, February 2-6, **2013**, Philadelphia, USA
- 6) Drug trapping in hERG channels does not require closure of the activation gate. Saxena P, Erker T, Bauer F, Stary-Weinzinger A, [Linder T](#), Hering S, Timin E. 57th Annual Meeting of the Biophysical Society, February 2-6, **2013**, Philadelphia, USA
- 5) Probing the dynamics of the bacterial K<sup>+</sup> channel KcsA during pore gating. [Linder T](#), Stary-Weinzinger A. 19th EuroQSAR, August 26-30, **2012**, Vienna, Austria

- 4) Development of a new and efficient IK1 inhibitor based on the pentamidine core structure. van der Heyden MAG, Takanari H, Nalos L, Stry-Weinzinger A, Varkevisser R, Linder T, Houtman, MJ, de Kort P, Peschar M, Rook MB, Vos MA. Heart Rhythm **2012**, May 9-12, 2012, Boston, USA
- 3) Pore gating of K<sup>+</sup> channels studied by essential dynamics simulations using the simplified bacterial K<sup>+</sup> channel KcsA. Linder T, Stry-Weinzinger A. 56th Annual Meeting of the Biophysical Society, February 25-29, **2012**, San Diego, USA
- 2) MD simulations reveal mutation induced reorientation of binding residues in the hERG K<sup>+</sup> channel. Knappe K, Linder T, Stry-Weinzinger A. EBSA 2011, August 23-27, **2011**, Budapest, Hungary
- 1) Binding mode predictions of catechol alkenyls for acetylcholinesterase inhibition. Adhami HR, Linder T, Kaehlig H, Zehl M, Schuster D, Krenn L. Phytopharm **2011**, July 25-27, 2011, Nuremberg, Germany